Micromagnetic models for high-temperature magnetization dynamics

Pablo Nieves Cordones

Advisor: Dr. Oksana Fesenko Morozova (Chubykalo-Fesenko)

Department Condensed Matter, Universidad Autonoma de Madrid

Tutor: Dr. Julio Camarero de Diego

A thesis submitted for the degree of

PhilosophiæDoctor (PhD), in Physics,

2015 April

This thesis was supported by the European Community's Seventh Framework Programme (FP7/2007-2013) under grant agreement No. 281043, FEMTOSPIN.

Resumen

Recientemente, se han descubierto sorprendentes fenómenos en materiales magnéticos como son la dinámica mágnetica ultrarrápida y el efecto spin Seebeck con un gran interés tecnológico que va desde la grabación magnética a la espintrónica. Para el desarrollo de aplicaciones tecnológicas basadas en estos nuevos procesos es necesario por un lado modelos micromagnéticos que permitan reproducir en simulaciones computacionales el comportamiento magnético a gran escala de dichos procesos y por otro lado es necesario también un mayor conocimiento sobre los mecanismos microscópicos responsables de los mismos.

Los modelos micromagnéticos basados en la ecuación de Landau-Lifshitz-Gilbert (LLG) son muy utilizados en la modelización de materiales magnéticos ya que en la mayoría de situaciones describen correctamente el comportamiento magnético de dichos materiales, y por tanto, estos modelos son una herramienta muy útil para el diseño de aplicaciones tecnológicas en las que se emplean materiales magnéticos. En la ecuación de LLG la magnitud de la magnetización promedio en un pequeño volumen del material (del orden de nm^3) es constante. Sin embargo, existen ciertos procesos como, por ejemplo, aquellos que tienen lugar a temperaturas cercanas a la temperatura de Curie en los que la ecuación de LLG no puede reproducir correctamente el comportamiento observado experimentalmente. Esto es debido a que a altas temperaturas las ondas de espín de alta frecuencia (baja longitud de onda) juegan un papel muy importante en el comportamiento mágnetico. Por otro lado, la magnitud de la magnetización promedio en un pequeño volumen de material no es constante a estas temperaturas. Generalmente, estos nuevos procesos tienen lugar a altas temperaturas, por tanto, es necesario el desarrollo de modelos micromagnéticos, alternativos a aquellos basados en la ecuación de LLG, que puedan describirlos correctamente.

Una posible alternativa a la ecuación de LLG es la ecuación de Landau-Lifshitz-Bloch (LLB) desarrollada por D. Garanin, ya que es más termodinámicamente consistente que la ecuación de LLG. La ecuación de LLB contiene un término que proviene del canje interno del material y describe la dinámica longitudinal magnética, y por tanto, puede describir correctamente los procesos magnéticos a altas temperaturas y tiempos cortos. En esta tesis proponemos un modelo micromagnético basado en la versión cuántica de la ecuación de LLB tanto para materiales ferromagnéticos como aleaciones magnéticas. Además esta

ecuación debido a su naturaleza cuántica permite analizar teóricamente como diferentes mecanismos microscópicos afectan a la dinámica magnética lo que podría ayudar a entender mejor el origen de estos nuevos procesos.

En resumen, los principales resultados que presentamos en esta tesis son los siguientes:

- Derivación de la ecuación cuántica de LLB para materiales ferromagnéticos a partir de un modelo de interacción del espín con electrones.

- Desarrollo de un modelo micromagnético basado en la ecuación cuántica de LLB y comparación con medidas experimentales de dinámica mágnetica ultrarrápida en láminas delgadas de FePt. Modelización de la dinámica de imanación inducida por la polarización circular del laser sobre láminas delgadas continuas y granulares de FePt.

- Desarrollo de un modelo cuántico y clásico macroscópico para aleaciones magnéticas de dos componentes. El modelo está derivado de forma similar a la ecuación LLB para materiales ferromagnéticos y verificado mediante simulaciones atomísticas.

- Análisis de los tiempos de relajación longitudinal mediante la ecuación de LLB en el material ferrimagnético GdFeCo en función de la temperatura y la concentración de Gd.

- Derivación de la energía libre para materiales magnéticos formados por dos subredes mediante dos métodos diferentes basados en la aproximación de campo medio.

Contents

1

Introduction and Motivation

1.1 Introduction

Advances in magnetism like designing of new magnetic materials, better theoretical understanding of magnetic phenomena and development of new experimental techniques have driven the progress of technology in general but specially in the data storage industry. Recently, novel high-temperature magnetic phenomena have been discovered and attracted a lot of research. One of them is the laser induced ultrafast magnetization dynamics[9, 144] where a subpicosecond dynamics is observed when a femtosecond laser pulse is applied to magnetic materials such as transition metals (Ni[21], Fe [29] or Co [147]). Another example is the spin Seebeck effect[141] where spin currents or spin accumulation are observed in a ferromagnet due to a temperature gradient. Apart from their fundamental interest, these phenomena are very appealing from technological perspectives that range from increasing the speed of the magnetization switching to the production of spin-voltage generators, which are crucial for driving spintronics. Moreover, it has been found that a good strategy to improve the performance of hard disk devices (HDD) and magnetic random-access memories (MRAMs) could be to increase the temperature of the magnetic thin film which contains the bits during the writing process. Therefore, it is necessary to search for models that can describe the magnetic behaviour in these novel high-temperature processes.

1.2 Ultrafast magnetization dynamics

Developments in magneto-optics with powerful pulsed lasers have lead to a new branch of magnetism which is the ultrafast magnetization dynamics. These experiments use pump-probe magneto-optical techniques [21] based on Kerr or Fadaray

effects. Similarly, second harmonic generation [59, 67, 119], photo-emission [2, 129] and more recently x-ray magnetic circular dichroism [133] contributed to the development of these new science. Due to the small time resolution (below 100 femtoseconds) that can be achieved in these experiments it was possible to observe a femtosecond demagnetization in a very wide range of magnetic materials such as transition metals (Ni[21], Fe [29] or Co [147]), magnetic semiconductors [148], dielectrics [85], half-metals[46] and ferrimagnetic alloys[134]. These short timescales corresponds to the interatomic exchange interaction through the time-energy correlation[138] $t = h/E$ which links the characteristic time t and energy E of a process (see Fig. 1.1 a)).

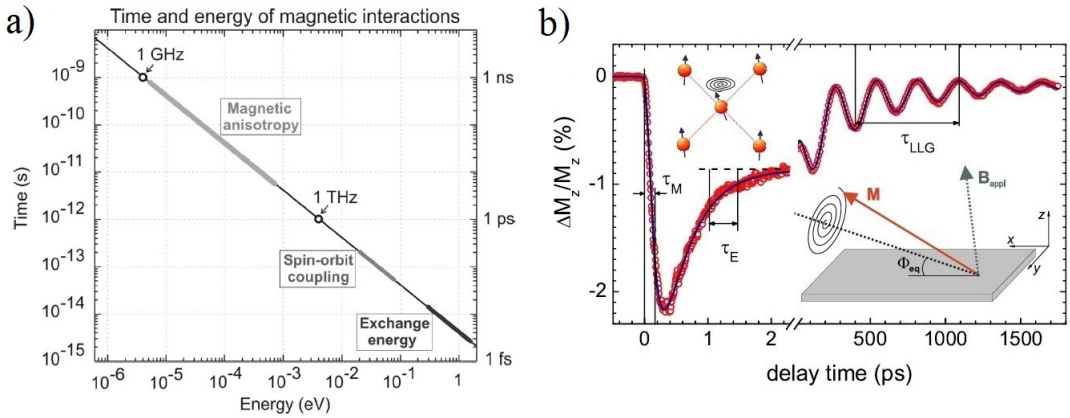

Figure 1.1: a) Time-energy correlation $t = h/E$ and typical time and energy scales associated to magnetic interactions. Figure taken from Ref.[138]. b) Experimental measurement of the dynamics in Ni after a femtosecond laser pulse is applied. Figure taken from Ref.[89].

In ultrafast magnetization dynamics one can identify three relevant time scales (see Fig. 1.1 b): i) fast demagnetization ii) magnetization recovery and iii) damped nanosecond timescale precession. Koopmans *et al.* [88] proposed to scale experimentally observed demagnetization time scales in different materials according to the ratio between the atomic magnetic moment and the Curie temperature μ_{at}/T_c of the material, leading to the classification of ferromangets in two types (see Fig. 1.2):

- *Type I:* ferromagnets with low value of μ_{at}/T_c exhibit demagnetization timescale of the order of 100 femtoseconds as transition metals like Ni, Fe or Co.

- *Type II:* ferromagnets with high value of μ_{at}/T_c exhibit a two-step demagnetization dynamics with a fast demagnetization in the first picosecond

followed by a slow demagnetization with larger characteristic times, e.g. Gd ∼100ps or Tb ∼10ps [149].

More recently it has been shown (see Chapter 4) that at high laser pulse fluency type I materials can also exhibit a type II like behaviour[107, 110, 120]. Ferrimagnetic alloys with a combination of fast (type I) and slow (type II) ferromagnets show not only ultrafast demagnetisation but also ultrafast magnetisation reversal[70].

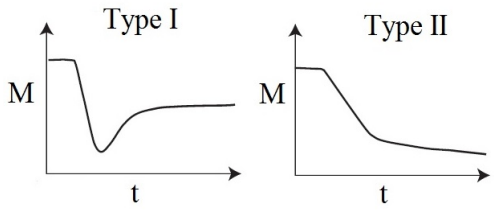

Figure 1.2: Magnetization dynamics profile of ferromagnets type I and II.

1.2.1 Experimental overview

In the last two decades a number of amazing and unexpected discoveries has been made in ultrafast magnetism. In order to give an idea of the advances in this new branch of magnetism we highlight the following experimental achievements.

1.2.1.1 Early discoveries

In 1996 Beaurepaire *et al.*[21] did the first measurement of the ultrafast magnetization dynamics in Ni (see Fig.1.3) using a pump-probe magneto-optical technique based on Kerr effect. The sub-picosecond magnetisation dynamics was completely unexpected since it was believed that the speed of magnetisation dynamics is limited by the spin-orbit coupling with a slower time scale.

A year later Hohlfeld *et al.*[67] using a second harmonic generation technique and Scholl *et al.*[129] using a two photon photoemission technique confirmed the ultrafast magnetization dynamics in Ni. In 1998 Ju *et al.*[73] and Beaurepaire *et al.*[20] observed an ultrafast magnetization dynamics in ferromagnetic $CoPt_3$ alloys film. In 1999 Koopmans *et al.*[87] proposed a new probe of the ultrafast spin dynamics called time-resolved magnetization modulation spectroscopy (TIMMS) which offers a high magnetic sensitivity. In 2000 Koopmans *et al.*[90] achieved a first identification of several magnetic and optical processes that contribute to the magneto-optical response of nickel thin films after excitation by a femtosecond

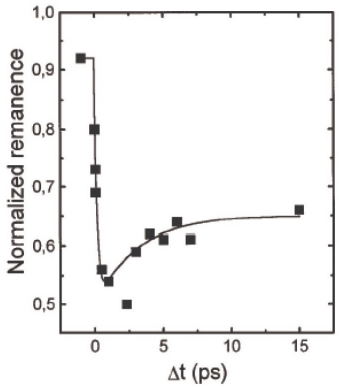

Figure 1.3: Ultrafast demagnetization in ferromagnetic Nickel induced by a 60 fs laser pulse. Figure taken from seminal work of Beaurepaire *et al.* [21].

laser pulse by explicitly measuring the time-resolved Kerr ellipticity and rotation, as well as its temperature and magnetic field dependence.

1.2.1.2 Measurements on ferrimagnetic alloys

In 2001 the intense research in ultrafast magentization dynamics was extended to ferrimagnetic alloys. Hohlfeld *et al.*[66] observed for the first time an ultrafast magnetization reversal of GdFeCo (a ferrimagnetic alloy) induced by femtosecond laser pulses. In 2007 Stanciu *et al.*[134] showed that the magnetization can be reversed in GdFeCo in a reproducible manner by a single 40 femtosecond circularly polarized laser pulse, without any applied magnetic field (see Fig. 1.4).

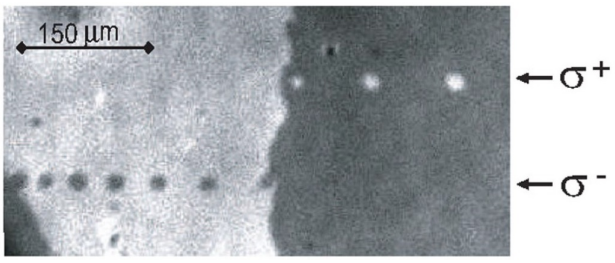

Figure 1.4: Experimental magneto-optical response to a 40 fs laser pulse of circularly polarized light on magnetic domains in $Gd_{22}Fe_{74.6}Co_{3.4}$. Figure taken from [134].

In 2011 Radu *et al.*[70] studied the magnetization dynamics of Fe and Gd in GdFeCo using the element-specific technique X-ray magnetic circular dichroism. They found that the ultrafast spin reversal in this material, where spins are coupled antiferromagnetically, occurs by way of a transient ferromagnetic-like

state. In 2012 Ostler *et al.*[115] demonstrated a novel mechanism of deterministic magnetization reversal in a ferrimagnet driven by an ultrafast heating of the medium resulting from the absorption of a sub-picosecond laser pulse without the presence of a magnetic field (see Fig. 1.5 a)). Vahaplar *et al.* [143] showed that for high laser fluences the ultrafast switching in GdFeCo doesn't depend on the light helicity confirming Ostler *et al.*[115] results that the ultrafast heating is a sufficient stimulus for this process (see Fig. 1.5 b)). Khorsand *et al.* [81] presented a quantitative explanation of the intensity window in which all-optical helicity-dependent switching (AO-HDS) occurs, based on magnetic circular dichroism (MCD).

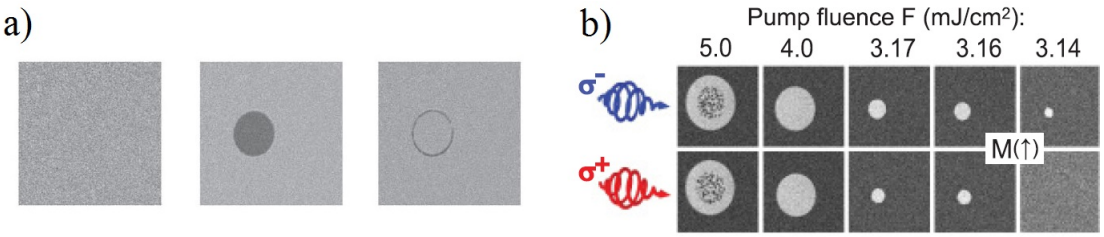

Figure 1.5: a) Magneto-optical images of a $Gd_{24}Fe_{66.5}Co_{9.5}$ continuous film, left image shows the initial homogeneously magnetized state, center image shows the magnetization after a 100 fs linearly polarized pulse is applied and right image shows the magnetization after another 100 fs pulse is applied to the same place than the previous one. Figure taken from Ref. [115]. b) Magneto-optical images of $Gd_{26}FeCo$ sample obtained after the action of single 100 fs circularly polarized laser pulse. Figure taken from Ref. [143].

In 2013 Graves *et al.*[56] presented ultrafast diffraction experiments with an X-ray laser that measured the spin dynamics after optical laser excitation in the ferrimagnetic alloy GdFeCo, which exhibits macroscopic all-optical switching. They observed Gd spin reversal in Gd-rich regions within the first picosecond driven by the non-local transfer of angular momentum from larger adjacent Fe-rich regions. In 2014 Bergeard *et al.*[22] reported the ultrafast transfer of angular momentum during the first hundred femtoseconds in ferrimagnetic CoGd and CoTb films using time-resolved X-ray magnetic circular dichroism. They showed that the demagnetization in ferrimagnetic alloys is driven by the local transfer of angular momenta between the two exchange-coupled sublattices while the total angular momentum stays constant.

1.2.1.3 Measurements on multilayer system

In order to clarify the role of transport phenomenon in ultrafast magnetization dynamics the research was also extended to multilayer systems. In 2012 Rudolf *et al.*[121] spatially separated the spin dynamics using Ni/Ru/Fe magnetic trilayers, where the Ni and Fe layers can be ferro or antiferromagnetically coupled. They found that optically induced demagnetization of the Ni layer transiently enhances the magnetization of the Fe layer when the two layer magnetizations are initially aligned parallel. Their observations could be explained by a laser-generated superdiffusive spin current between the layers. In 2013 Eschenlohr *et al.*[40] applied an ultrashort laser pulse to a multilayer system of Au/Ni/Pt/Al where the laser energy was mainly absorbed by the Au layer (see Fig. 1.6 a)). They observed an ultrafast demagnetization in the Ni layer showing that direct laser irradiation is in fact not essential for this process, and the electron cascades caused by hot electron currents (superdiffusive spin currents) accomplish it very efficiently (see Fig. 1.6 b)).

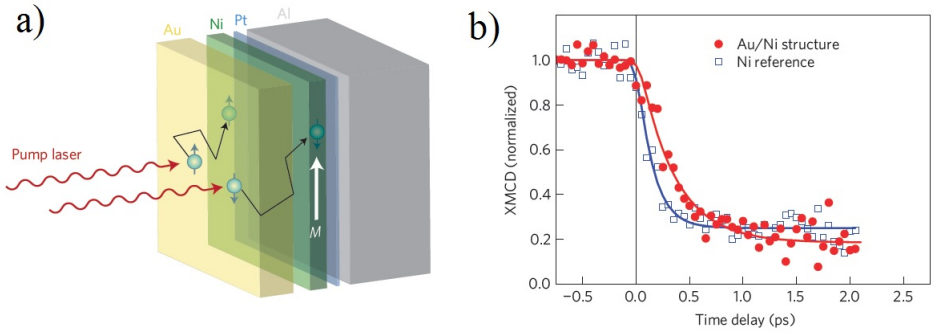

Figure 1.6: a) Sketch of the sample structure consisting of a 30nm Au layer on 15nm ferromagnetic Ni on an Al foil. b) Magnetization dynamics of the Ni layer, after excitation with a femtosecond laser pulse, as measured through the element-selective XMCD signal. Filled and open symbols denote the Au/Ni sample and the Ni reference sample, respectively. Figures taken from Ref. [40].

1.2.1.4 All optical switching

As we have mentioned the exploration of the magnetization dynamics in ultrashort timescales have lead to the discovery of amazing and unexpected magnetic behaviour. Probably, from a technological point of view, the most interesting one is what is called all optical switching (AOS), where the magnetization of a magnetic material is reversed in a picosecond timescale only using a femtosecond laser pulse.

Until a coupled of years AOS has been observed in GdFeCo[134] only, but more recently it was also reported in other amorphous rare-earth transition-metal ferrimagnetic alloys such as TbCo[4] and TbFe[61], TbFeCo [32], DyCo [102], HoFeCo [102], synthetic ferrimagnets [43, 102, 131] and possibly ferromagnets [93]. The influence of the optical excitation parameters on the AOS process has mainly been investigated, i.e., pulse chirp, pulse duration, wavelength, bandwidth, pulse repetition rate, and the combination of laser heating and circular polarization. We can distinguish two kinds of ultrafast switching: i) all-optical helicity-dependent switching (AO-HDS) where circularly polarized light is used (see Fig. 1.7 a)), and ii) thermally induced magnetic switching (TIMS) where the ultrafast switching is helicity-independent (see Fig. 1.7 b)). At low fluences GdFeCo exhibits AO-HDS and at high fluences it exhibits TIMS, but in both cases the effect is thermal and only depends on the total amount of energy absorbed in the sample[81]. Recently Hassdenteufel *et al.*[61] showed that circularly polarized light induces AOS in TbFe alloy films but linearly polarized light induces a domain wall depinning. On the other hand, the influence of the material parameters on the AOS process has also mainly been investigated, i.e., layer thickness, rare-earth concentration and initial magnetization state (room temperature). Probably, one of the most interesting question about AOS is the role played by the magnetization compensation point T_M, the temperature where the magnetization of both sublattices cancels each other, since AOS is mainly observed at room temperature close to T_M. Investigations of the formation speed of the transient ferromagnetic-like state as a function of T_M shows very pronounced variations suggesting that T_M could play an important role in AOS [60]. At the same time, AOS also occurs in systems without the magnetisation compensation point [115]. Recently. it has been shown that the most efficient switching occurs somewhere near this point [12].

In 2014 Lambert *et al.*[93] showed using the circularly polarized light (see Fig.1.8) that an all-optical control of the magnetization is a more broad phenomenon which can occur in variety of different materials including heterostructures such as CoPt multilayers and FePt magnetic recording thin film.

1.2.2 Theoretical overview

The question about the origin of ultrafast magnetization dynamics constitutes a subject of extensive on-going scientific debate. We highlight the following processes which could play an important role in this new phenomena.

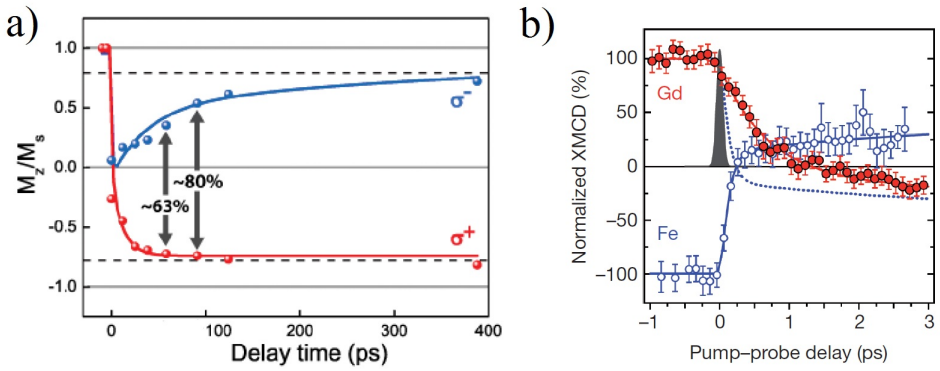

Figure 1.7: a) Experimental averaged magnetization after a laser pulse of circularly polarized light. Figure taken from [144]. b) Magnetization switching after a laser pulse of linearly polarized light. Figure taken from [70].

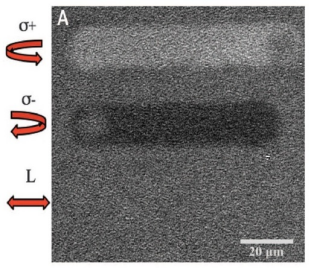

Figure 1.8: Experimental magneto-optical response without applied field of a 15-nm FePtAgC granular film sample starting with an initially demagnetized state. Figure taken from Ref. [93].

1.2.2.1 Inverse Faraday effect

When linearly polarized light is transmitted trough a magnetic material the polariztion plane of the light is rotated, this phenomena is the so-called Faraday effect which is used as a magnetization probe. The opposite effect where light can change the magnetization of a magnetic material is called inverse Faraday effect (IFE). The IFE has been observed in Eu^{+2}:$CaFe^2$[145], plasmas[68] and magnetic dielectrics[84]. However, in ferromagnetic metals like Ni and other transition-metals this effect could be very small[73, 92, 150]. As we have mentioned above in 2007 Stanciu *et al.*[134] showed that a 40 fs circularly polarized laser pulse can reverse the magnetization in GdFeCo (rare-earth transition-metal ferrimagnetic alloy) (see Figs. 1.4 and 1.9 a)). Since GdFeCo has strong magneto-optical properties [144] it was suggested that mechanism responsible for this ultrafast switching could be a strong magnetic field induced by the IFE [62, 146]. Khor-

sand *et al.* [81] demonstrated unambiguously that AO-HDS originates from MCD where right and left circularly polarized light absorption coefficients are different.

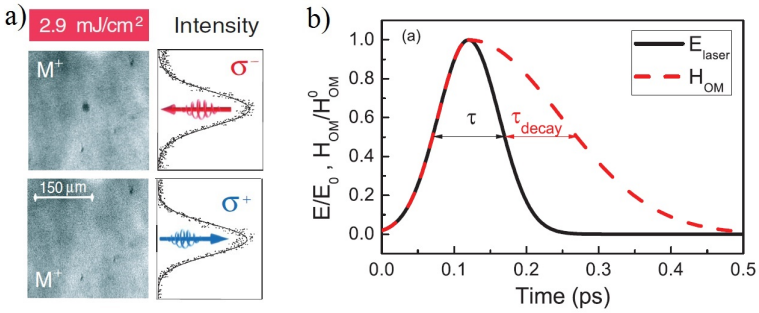

Figure 1.9: a) Experimental magneto-optical response to ultrashort laser pulses of circularly polarized light on magnetic domains in GdFeCo. Figure taken from [134]. b) Theoretical time evolution of the opto-magentic field $\mathbf{H}_{\mathrm{OM}}$ (red dash line) induced by the circularly polarized laser pulse calculated by Vahaplar *et al.*[143].

A complete theory of opto-magnetic effects induced in magnetic metals by ultrashort laser pulses has not been achieved[63, 156]. Vahaplar *et al.*[143] used an effective opto-magentic field $\mathbf{H}_{\mathrm{OM}}$ induced by the laser pulse derived for a transparent medium in thermodynamic equilibrium for modelling the IFE in GdFeCo (see Fig. 1.9 b)). In 2014 Battiato *et al.*[17] presented a quantum theory of IFE based on the density matrix formalism.

1.2.2.2 Ultrafast heating effect

As we have mentioned above in 2011 Radu *et al.*[70] showed an ultrafast switching in GdFeCo using an ultrashort linearly polarized laser pulse where the IFE is not expected to take place. In 2012 Ostler *et al.*[115] demonstrated experimentally and numerically that the ultrafast heating generated by the laser pulse can drive the magnetization reversal of GdFeCo in a deterministic way without the presence of a magnetic field, that is, an ultrafast heating is a sufficient stimulus for magnetization reversal in a ferrimagnet. This conclusion was confirmed by Vahaplar *et al.* [143] showing that at high fluences an ultrashort circularly polarized pulse also induces the ultrafast switching in GdFeCo independently of its polarization. Khorsand *et al.* [81], based on MCD, showed that the effective switching threshold, i.e., the actual absorbed energy density in GdFeCo layer at which switching occurs is independent of the polarization and the wavelength of the light pulse with a value of $F = 2.6 \pm 0.2$ mJ cm^{-2}.

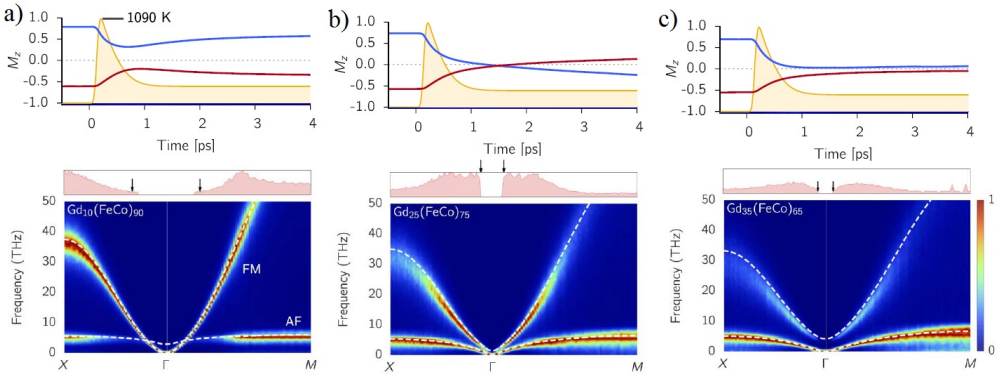

Figure 1.10: The upper panels present the computed magnetization dynamics of a) $Gd_{10}(FeCo)_{90}$ b) $Gd_{25}(FeCo)_{75}$ and c) $Gd_{35}(FeCo)_{65}$. The lower panels shows its corresponding magnon band structure. Figure taken from Ref. [12].

At this point an interesting question is raised: How does an increase in thermal energy can lead to a deterministic reversal of a vector? Atxitia *et al.*[11] studied numerically and theoretically the switching path followed by the magnetization in GdFeCo, they found that for switching to occur it is necessary that angular momentum is transferred from the longitudinal to transverse magnetization components in the transition metal. Mentink *et al.*[108] presented a general theoretical framework for ultrafast spin dynamics in multisublattice magnets using Onsager's relations, they predicted that exchange relaxation enhances the demagnetization speed of both sublattices when they are antiferromagnetically coupled like in GdFeCo. Recently, Barker *et al.*[12] identified the nature of the thermally induced magnetic switching (TIMS) in ferrimagnetic alloys as the excitation of two-magnon bound states where the energy is transferred from ferromagnetic to antiferromagnetic modes via non-linear interactions. As we see in Fig. 1.10 in situations where TIMS takes place, that is, for Gd concentration of 25%, there is a small gap between the antiferromagnetic and ferromagnetic magnon modes. In this thesis we focus mainly on TIMS as the mechanism of the ultra-fast magnetisation dynamics.

1.2.2.3 Superdiffusion

In 2010 Battiato *et al.*[18] suggested that when an ultrashort pulse heats a magnetic multilayer system a spin current through the layers called superdiffusion could take place. In order to describe superdiffusion they assumed that the photons coming from the laser pulse are absorbed by the d-band electrons which are excited to the sp-band above the Fermi level. Then they derived a transport

equation of these excited electrons showing a high depletion of majority carriers in the magnetic film and a transfer of magnetization away from the surface which could explain the femtosecond demagnetization measured in experiments. Fig. 1.11 a) shows a sketch of the superdiffusive processes caused by laser excitation and Fig. 1.11 b) shows the calculated spatial magnetization profile (black line) of Ni at three times caused by laser excitation, the Ni film extends up to 15 nm depth, the remaining is the Al film.

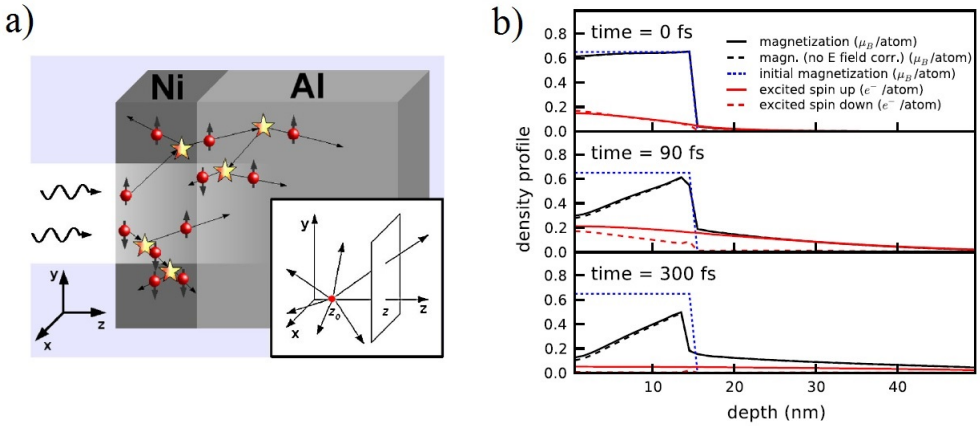

Figure 1.11: a) Sketch of the superdiffusive processes caused by laser excitation. b) Calculated spatial magnetization profile (black line) of Ni at t=0 fs, t=90 fs, t=300 fs caused by laser excitation, the Ni film extends up to 15 nm depth, the remaining is the Al film. Figures taken from Ref. [18].

As we have mentioned in the experimental overview a laser-generated superdiffusive spin current between the layers seems to be the most reasonable explanation for the observations of the magnetization dynamics in Ni/Ru/Fe magnetic trilayers[121] and in Au/Ni/Pt/Al multilayers[40] with enhanced transport properties. However, this seems not to be the case of other materials.

1.2.2.4 Microscopic scattering mechanisms

The heat-induced dynamics has an underlying quantum-mechanical origin with microscopic scattering mechanisms responsible for spin-flips. Some of the possible microscopic mechanisms that have been suggested are the following:

- *Elliott-Yafet like electron-phonon spin-flip:* Koopmans *et al.*[88] suggested this mechanism as the main one where spin-flips are mediated by electron-phonon momentum scattering events (see Fig. 1.12). Steiauf and Fahnle in Ref. [137] calculated the spin-flip probability mediated by Elliott-Yafet

mechanism using ab-initio density-functional electron theory, they found that this probability is high enough to explain the ultrafast magnetization dynamics observed in Ni. However, Karva *et al.* [30] recalculated this probability using a more sophisticated approach and they concluded that the Elliott-Yafet probability is insufficient to explain the femtosecond demagnetization. Later Schellekens and Koopmans[124] argued that the rigid band structure Stoner-like approach used by Karva *et al.* [30] will never be in quantitative agreement with experiments for any scattering mechanism (not only for Elliott-Yafet mechanism). Recently, Mueller *et al.*[109] improved the rigid band structure using a modified Stoner model with dynamic exchange splitting between majority and minority bands, they found that Elliott-Yafet mechanism could still play an important role in ultrafast magnetization dynamics. The role of the Elliott-Yafet mechanism is still a subject of an on-going debate.

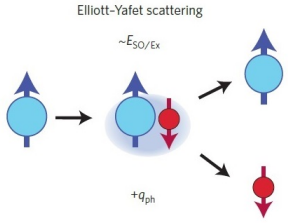

Figure 1.12: Sketch of the Elliot-Yafet scattering mechanism. Figure taken from Ref. [110].

- *Electron-electron Coulomb interaction:* Krauss *et al.*[91] suggested that an Elliott-Yafet like mechanism based on electron-electron Coulomb scattering could also explain the femtosecond demagnetization observed in Ni and Co thin films.

- *sp-d model:* Cywiński and Sham[38] suggested that the so-called sp-d model could be a good approach to describe the ultrafast magnetization dynamic of ferromagnetic (III,Mn)V semiconductors. In this approach, the d-shell spins contributes mainly to the macroscopic magnetization and they interact via exchange interaction with the s or p itinerant electrons.

- *Electron-magnon interaction:* Carpene *et al.*[29] suggested that the rapid ($\sim$ 100 fs) demagnetization is established at the electronic level through electron-magnon excitation, while the remagnetizacion is attributed to the Elliott-Yafet spin-flip scattering process on a time scale slightly shorter than a picosecond in Fe thin films.

- *Direct laser induced:* Zhang *et al.*[155] proposed that the femtosecond demagnetization could happen as a direct influence on the electronic structure by the laser field mediated by the presence spin-orbit coupling in Ni. Unfortunately, the calculations have been performed on very small clusters.

- *Relativistic electromagnetic-radiation-induced spin-flip:* since the ultrashort laser pulse couples efficiently to the magnetization of Ni and $CoPt_3$ thin films during the light propagation through the material, Bigot *et al.*[24] suggested the existence of a coherent coupling between the laser pulse and the magnetization. Moreover, they argued that the corresponding mechanism could have its origin in relativistic quantum electrodynamics, beyond the spin-orbit interaction involving the ionic potential.

1.2.3 More phenomenological models

Up to now the complete role of light, electrons, phonons and spins in the ultrafast magnetization dynamics has not been clarified. The quantum mechanical approaches based on the first principles were not able to reproduce magnetisation dynamics with correct demagnetisation size and time scale observed in experiment. However, more phenomenological models, based on the thermodynamical concepts were very successful in reproducing many experimental findings.

Beaurepaire *et al.*[21] proposed the phenomenological three temperature model (3TM) in order to describe the magnetization dynamics caused by the interaction of a laser pulse with Ni thin films. The 3TM considers that electrons, phonons and spins are described by a set of three coupled differential equations for the temperature of each system, that is, T_e, T_{ph} and T_s. Moreover, it assumes the energy deposited on the material by the laser pulse is absorbed mainly by the electron system and then it is redistributed into the phonon and spin systems.

However, since the spin system is not in the quasi-equilibrium on the femtosecond timescale then the description of the magnetization through a spin temperature is inadequate to describe the spin dynamics[80]. One way to solve this issue is to couple phenomenologically the two-temperature model (2TM) for phonon and electron temperatures to an equation of motion of the spin system. This approach is used by the atomistics spin dynamics (ASD)[79, 80] which is based on the Landau-Lifshitz-Gilbert equation (LLG) for atomistic spins. The 2TM coupled to ASD has been used to model the ultrafast magnetization dynamics of ferromagnets and ferrimagnets[12, 115] showing a good agreement with experiments.

Unfortunately, ASD can only be used to model the magnetic behaviour of small system due to the large consuming computer time of this approach. For

larger systems it was suggested to couple the 2TM to the Landau-Lifshitz-Bloch (LLB) equation[8, 9, 78] which can successfully describe the magnetization longitudinal dynamics during the first picoseconds and the subsequent transverse dynamics. In fact, comparison with experiments for Ni[9], Gd[139] and FePt[107] have shown a very good agreement. In this thesis we use ASD and LLB approaches to describe ultrafast magnetization dynamics.

Finally, Koopmans *et al.* [88] derived a microscopic version of the 3TM (M3TM) where the spin relaxation is mediated by Elliott-Yafet-like processes. M3TM successfully reproduces the diversity of ultrafast laser-induced magnetization dynamics observed in transition metals and rare-earth materials. Lately, it has been shown that the M3TM model is very similar to the LLB equation[6, 113].

1.3 Technological perspectives

1.3.1 Heat assisted magnetic recording (HAMR)

One of the greatest challenges in magnetic recording technology is to increase the areal density, that is, the number of bits per square inch. Fig. 1.13 a) shows the historical evolution of the bit density in magnetic recording media.

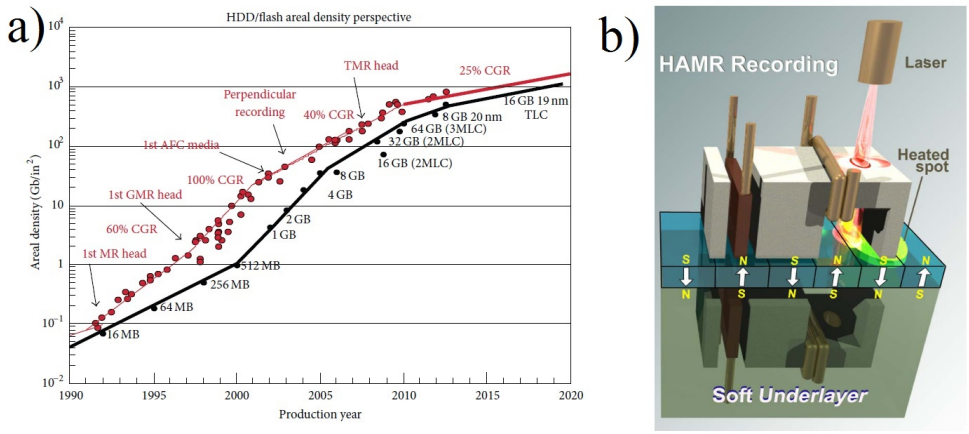

Figure 1.13: a) Areal density evolution of hard disc devices (HDD, red dots) and flash memories (black dots). Figure taken from Ref.[103]. b) Diagram showing a writing head in HAMR. Figure taken from Ref. [44].

Typically the medium in magnetic recording is a granular film where each bit consists of several ($\sim 10^2$) weakly interacting magnetic grains. The number of grains N included in a bit can not be reduced since one has to preserve the signal-to-noise ratio SNR$\sim \sqrt{N}$. Therefore, the areal density can only be increased by

a reduction of the grain volume V. However, the energy barrier separating two magnetization states is proportional to KV, where K is the magnetocrystalline anisotropy constant, hence if the grain volume is reduced then the bit becomes unstable and the inversion of the magnetization by thermal fluctuations is likely to occur. This effect is known as superparamagnetism and the corresponding limitation of the recording density as superparamagnetic limit. Generally, values of $KV/k_BT > 60$ (k_B is the Boltzmanns constant and $T = 300$ K is the temperature) are required to ensure the long-term stability of written information. Therefore, if a bit is written in very small grains then these grains must have a high K in order to be thermally stable. Unfortunately, a high magnetocrystalline anisotropy implies a high coercivity, and as consequence large external magnetic fields are required in the writing process. This constitutes a well known magnetic recording trilemma. One possible solution to this problem is the heat assisted magnetic recording (HAMR) where in the writing process, firstly a laser heats the magnetic grains reducing its coercivity and then an external magnetic field is applied which is enough to reverse the grain's magnetization (see Fig. 1.13 b)). In 2013 Western Digital demonstrated a working HAMR drive, although not yet ready for commercial sales. Recently, TDK company stated that HAMR drives up to around 15 Tbits per square inch would probably start to become available by 2016. Finally, the LLB equation has already been used successfully to model the magnetization switching dynamics in HAMR [104].

1.3.2 All optical magnetic recording

One of the most interesting technological application of the AOS could be storage data devices where only ultrashort laser pulses are used during the writing process, that is, an all optical magnetic recording (see Fig. 1.14) which will not require the recording head. Current hard-disk drives (HDD) make use of external magnetic fields in order to reverse the magnetization, that is, to write a "0" or "1" bit information. This process typically takes several nanoseconds via the Zeeman interaction. The situation is even worst in Flash solid state memories where the writing cycle is of the order of hundred of μs. Since the AOS last only several picoseconds then an all optical magnetic recording could improve drastically the writing speed of storage data devices. Moreover, the effective switching threshold in AOS is of the order of 3 mJcm^{-2} which is less than the writing fluence per bit of current HDD ($\sim 2\times10^4$ mJcm^{-2}) and Flash solid state memories, as a consequence all optical magnetic recording could have a lower power consumption than the other technologies. Unfortunately, the present switching area in AOS is quite large, in the order of micrometers, however it has been shown

that the switching area can be reduced using optical near-field microscopy[123] or plasmonic antennas[23].

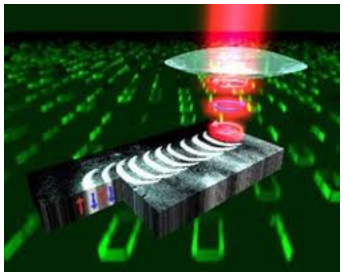

Figure 1.14: Demonstration of all-optical recording of magnetic bits. Figure taken from Ref. [134].

1.3.3 Spincaloritronics

Another technologically promising high-temperature magnetic application is the spin-Seebeck effect. In 1821 Thomas Johann Seebeck discovered that a temperature gradient generates an electromotive force, this phenomena is the so-called Seebeck effect. In 2008 Uchida *et al.*[141] discovered a spin analog of the Seebeck effect, they demonstrated that a temperature gradient in a ferromagnetic film creates a spin current injection from the ferromagnetic film into the attached nonmagnetic metal with the signal observed over a macroscopic scale of several millimeters. This spin current creates a transverse charge voltage in the nonmagnetic metal via the so-called inverse spin Hall effect[122] which is measured experimentally. Fig. 1.15a) shows the experimental setup for measuring the spin-Seebeck effect and Fig. 1.15b) shows the experimental results of the transverse charge voltage induced by the spin current as a function of temperature gradient. The spin-Seebeck effect has also been observed in magnetic semiconductors[72], non-magnetic semiconductors[71] and magnetic insulators[142]. Recently, it was shown that the magnon and phonon degrees of freedom play crucial roles in the spin Seebeck effect[1].

The spin-Seebeck effect is the keystone of the spincaloritronics. Very appealing technological possibilities are expected from this novel emerging new field [19]. The key problem of future electronics is that of Joule heating, where Ohmic losses can lead to intolerable power densities. From this point of view, it is important to realize that electrons can carry also heat in addition to charge and spin angular momentum. While the charge-spin transport is currently under exploitation, the heat transport investigations are only at an early stage. Nevertheless, it bears an important potential for energy saving: excess heat produced in microprocessors

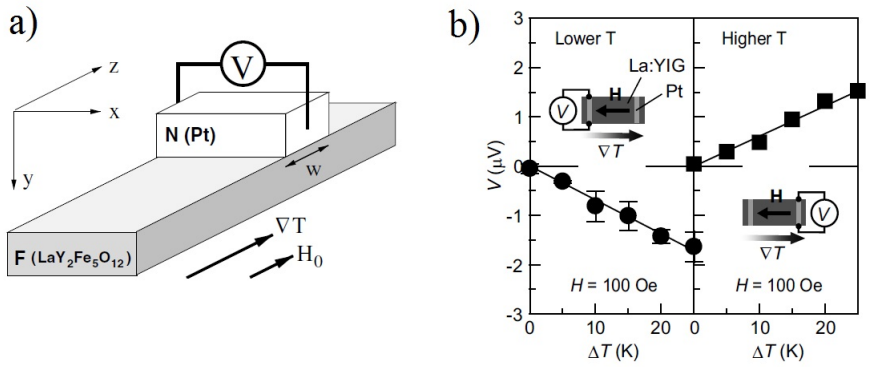

Figure 1.15: a) Experimental setup for measuring the spin-Seebeck effect. b) Experimental measurements of the transverse charge voltage induced by the spin current as a function of temperature gradient. Figures are taken from Ref. [1].

does not need to be released as waste energy into the environment, but can be recovered by generating thermoelectricity, for example, in spincaloritronics based waste-heat-to-electricity converters [76].

The LLB equation could be a good approach to model the spin-Seebeck effect at large scales. Hinzke *et al.*[65] used the LLB equation to show that magnonic spin currents caused by temperature gradients lead to spin transfer torque effects, which can drag a domain wall in a ferromagnetic nanostructure towards the hotter part of the wire. Schlickeiser *et al.*[127] calculated the domain wall velocity as well as the Walker breakdown induced by a temperature gradient using the LLB equation.

1.3.4 Thermally assisted MRAMs

Magnetic random-access memory (MRAM) is a non-volatile memory technology with a low voltage operation, fast write and read operation ($\sim$ 30 ns) and unlimited write and read endurance. The MRAM cell consists of a magnetic tunnel junction: two magnetic layers (one is always fixed and the other one can flip) separated by an insulator layer (tunnel barrier) where the antiparallel state (high resistence state) of both magnetic layers corresponds to the bit state "1" and the parallel state (low resistence state) corresponds to "0". Moreover, there are two electrical conductor lines (bit and digit lines) which are orthogonal to each other, and only when a charge current is flowing in both lines the magnetic field created by them is high enough to reverse the magnetization in one of the magnetic layers (see Fig. 1.16 a)). The scalability of MRAM to smaller bit sizes is faced with challenges like selectivity, thermal stability and power consumption[117]. It

is believed that thermally assisted MRAM (TA-MRAM) could solve these problems. The idea is that during the writing process an electrical current (writing current I_W) crosses the three layers increasing its temperature due to Joule effect and decreasing the coercivity of the magnetic layer, then only the magnetic field (switching field H_{SW}) created by one electrical conductor line is enough to reverse the magnetization in one of the magnetic layers (see Fig. 1.16 b)). Fig. 1.16 c) shows experimental measurements[151] of the switching field H_{SW} as function of the writing current I_W where the free magnetic layers are TbCo/CoFe, the fixed magnetic layers are CoFe/TbFeCo and the tunnel barrier is Cu, we see that as the writing current increases (which means higher temperatures at the magnetic layers due to the Joule effect) the switching field decreases.

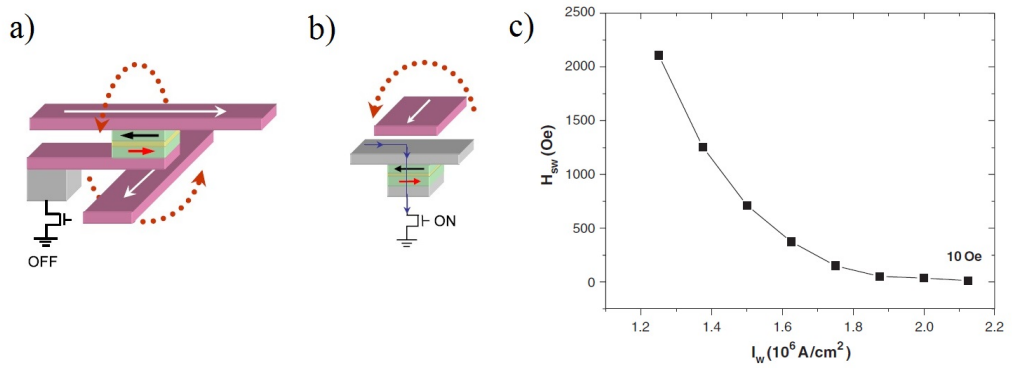

Figure 1.16: a) The writing procedure in a conventional MRAM architecture. b) The writing procedure in thermally assisted MRAM architecture. Figure taken from Ref. [117]. c) Experimental measurements of the switching field H_{SW} as function of the writing current I_W. Figure taken from Ref. [151].

1.4 The challenge of micromagnetic modeling at high-temperatures

In magnetism, micromagnetic modeling is a very useful complement to experimental measurements, especially for calculations of hysteresis and dynamics of magnetic nanostructures such as magnetic thin films, dots, stripes, etc[27, 31, 45]. The micromagnetics is essentially a macroscopic continuous theory. It uses a discretization of continous magnetisation function in finite elements or finite differences. The dynamics of each unit in standard micromagnetics is based on the integration of the classical Landau-Lifshitz-Gilbert (LLG) equation of motion

[55, 94]. It is essentially a zero-temperature equation, although the micromagnetic parameters could be taken as experimentally measured values at a given temperature T. Moreover, temperature effects can be included adding additional random fields acting on each discretization element [28, 34]. However, this approach is correct only for low temperatures [58] since the magnitude of the magnetization vector in each element is constant. At high temperatures, high-frequency spinwaves, responsible for longitudinal magnetization fluctuations near the Curie temperature T_c are cut and the value of the Curie temperature is strongly overestimated. To solve this issue an alternative micromagnetic approach for higher temperatures based on the Landau-Lifshitz-Bloch (LLB) equation has been proposed [35, 49] where the magnitude of the magnetization vector is not conserved at each discretization element and the longitudinal magnetisation fluctuations are introduced. Thus, micromagnetic modeling based on the LLB equation could be a good approach to study new phenomena such as the ultrafast magnetization dynamics, spincaloritronics and high-temperature magnetic recording processes. One of the aims of the this thesis is to study in more depth and to generalize the derivation of the quantum LLB equation in order to clarify its use for the ultrafast dynamics in ferromagnets and magnetic alloys.

1.5 About this thesis

The aim of the thesis is to further develop high-temperature micromagnetic models based on the LLB equation. Particularly, we focus our attention on the quantum LLB (qLLB) equation and the LLB equation for two-component alloys. The main application is to model ultra-fast magnetisation dynamics.

Chapter 2 Models for magnetization dynamics like atomistic and micromagnetic ones based on the LLG equation and the classical LLB equation are introduced in this chapter.

Chapter 3 A detailed derivation of the original qLLB equation based on spin-phonon interaction is presented. Moreover, a novel qLLB equation for spin-electron interaction is derived. The qLLB equation is written in the form, suitable for comparison with its classical counterpart. The temperature dependence of the macroscopic relaxation rates is discussed for both mechanisms. We demonstrate that the magnetization dynamics is slower in the quantum case than in the classical one.

Chapter 4 We apply the high-temperature micromagnetics based on the qLLB to investigate the femtosecond laser induced magnetization dynamics in ferromagnetic FePt thin films. We quantitatively compare our model and the experimental results which are provided by Prof. M. Münzenberg's group at the University of Göttingen (Germany). Both experimental and theoretical results are in a very good agreement giving proof of thermal magnetization mechanism based on spin-electron interaction. Furthermore, we investigate the possibility to switch FePt with the help of the inverse Farady effect.

Chapter 5 We present a novel classical and quantum LLB equation for two-component magnetic alloys.

Chapter 6 We study the magnetization dynamics of GdFeCo ferrimagnetic alloys using the previously derived ferrimagnetic LLB equation. The longitudinal relaxation times of materials constituting the alloy are investigated.

Chapter 7 The free energy for two-component alloys is derived using the variational procedure. We also present the free energy landscapes of GdFeCo and Permalloy ($Fe_{20}Ni_{80}$).

We also include four appendix sections.

Appendix A In this first appendix we introduce the density matrix formalism which the qLLB equation is based.

Appendix B This appendix presents a detailed derivation of the magnetization equation of motion in terms of the Hubbard operators for the spin-phonon and spin-electron interactions.

Appendix C Here a detailed evaluation of the qLLB relaxation parameters for the spin-phonon and spin-electron interactions is presented.

Appendix D The free energy for two-component alloys is derived using a standard mean-field formulation. We show that this approach can lead to non-physical free energy landscape.

2

Modeling methodology

2.1 Multiscale approach

A complete description of the material's magnetic behaviour requires very different spatial scales going from anstrong (like microscopic interactions at atomic level) to macroscale (magnetic domains usually have micrometer sizes), and also very different time scales going from femtoseconds (like ultrafast magnetization dynamics) to years (like thermal stability in magnetic storage media). One way to include the effects of the microscopic properties on the magnetic macroscopic behaviour is the multiscale approach. Namely, ab-initio calculations (the most widely used formalism is Density Functional Theory (DFT)) are used to calculate the intrinsic parameters as magnetic moment (μ), exchange constants (J), on-site magnetocrystalline anisotropy (d), etc..., then these parameters are used in atomistic classical (Heisenberg-like) models where the temperature dependence of the equilibrium magnetization $M_s(T)$, anisotropy $K(T)$ and exchange stiffness $A(T)$ among other properties can be calculated, and finally the temperature dependence of these parameters is included in the micromagnetic approach which can model the magnetic behaviour at large spatial scale (see Fig. 2.1).

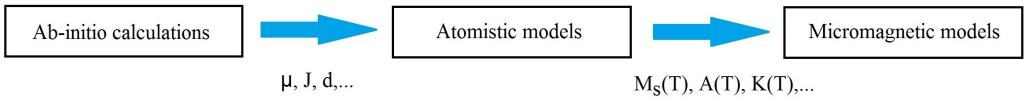

Figure 2.1: Diagram showing the multiscale approach.

2.2 Atomistic spin dynamics

The magnetic moments in the solid state can be localized or carried by the delocalized conduction electrons (itinerant magnetism) like in metals. However, models based on a classical Heisenberg Hamiltonian of localized spins are used to describe the main magnetic properties in both situations. Typically, the Hamiltonian in these atomistic models is given by

$$\mathcal{H} = -\sum_i \mathbf{H}\cdot\boldsymbol{\mu}_i - \sum_i d_i s_{i,z}^2 - \frac{1}{2}\sum_{i,j} J_{ij}\mathbf{s}_i\cdot\mathbf{s}_j \tag{2.1}$$

where $\mathbf{H}$ is the external magnetic field, $\boldsymbol{\mu}_i$ is the atomic magnetic moment at site i, $\mathbf{s}_i = \boldsymbol{\mu}_i/\mu_i$, d_i is the uniaxial anisotropy constant and J_{ij} is the exchange constant between the atoms i and j. The first term in Eq. (2.1) corresponds to the Zemann energy, the second term is the uniaxial anisotropy energy and the last one is the exchange energy. The dynamics of the each normalized classical atomic magnetic moment $\mathbf{s}_i$ in a solid can be described using the phenomenological Landau-Lifshitz-Gilbert equation (LLG) which is given by

$$\frac{d\mathbf{s}_i}{dt} = -\frac{\gamma}{1+\lambda^2}(\mathbf{s}_i\times\mathbf{H}_{\text{eff},i}) - \frac{\gamma\lambda}{(1+\lambda^2)}\mathbf{s}_i\times(\mathbf{s}_i\times\mathbf{H}_{\text{eff},i}) \tag{2.2}$$

where λ is called atomic coupling to the bath parameter, $\mathbf{H}_{\text{eff},i} = -\partial\mathcal{H}/\partial\boldsymbol{\mu}_i$ is the effective field and $\mathcal{H}$ is the Hamiltonian given by Eq. (2.1). Eq. (2.2) is a deterministic equation, it means that given the same initial conditions one obtains always exactly the same dynamics. However, the atomic magnetic moment in a solid follows a stochastic dynamic due to the interaction with its surroundings. This fact can be included in Eq. (2.2) adding a stochastic field $\boldsymbol{\zeta}_i$ to the effective field $\mathbf{H}_{\text{eff},i}$, that is,

$$\frac{d\mathbf{s}_i}{dt} = -\frac{\gamma}{1+\lambda^2}(\mathbf{s}_i\times(\mathbf{H}_{\text{eff},i}+\boldsymbol{\zeta}_i)) - \frac{\gamma\lambda}{(1+\lambda^2)}\mathbf{s}_i\times(\mathbf{s}_i\times(\mathbf{H}_{\text{eff},i}+\boldsymbol{\zeta}_i)) \tag{2.3}$$

where the stochastic field has the following time average properties

$$\langle\zeta_{i,k}\rangle_t = 0, \quad \langle\zeta_{i,k}(0)\zeta_{i,k'}(t)\rangle_t = 2\frac{\lambda k_B T}{\gamma\mu_i}\delta_{kk'}\delta(t), \quad k,k' = x,y,z \tag{2.4}$$

where k_B is the Boltzmann constant and T is the temperature. This approach is called atomistic spin dynamics (ASD)[41]. At thermal equilibrium each atomic magnetic moment follows Boltzmann statistic, that is, its time average is given by

$$\langle\boldsymbol{\mu}_i\rangle_t = \lim_{t_f\to\infty}\frac{1}{t_f-t_0}\int_{t_0}^{t_f} dt'\boldsymbol{\mu}_i(t') = \frac{\int\boldsymbol{\mu}_i e^{-\beta\mathcal{H}}d\boldsymbol{\mu}_1...d\boldsymbol{\mu}_N}{\int e^{-\beta\mathcal{H}}d\boldsymbol{\mu}_1...d\boldsymbol{\mu}_N}. \tag{2.5}$$

The macroscopic magnetization at time t is obtained as an average of the atomic magnetic moments over some volume V

$$\mathbf{M}(t) = \frac{1}{V}\sum_{i=1}^{N} \boldsymbol{\mu}_i(t), \tag{2.6}$$

where N is the total number of atomic magnetic moments inside the volume V.

2.3 Micromagnetics

Simulations based on ASD is a powerful tool to describe the magnetic behaviour of magnetic materials. Unfortunately, the size of a magnetic material that can be simulated using ASD is very limited (typically up to $(20 - 30 \text{ nm})^3$) due to large number of differential equations that must be numerically integrated which requires an enormous computer time. A suitable approach to study the magnetic behaviour of magnetic materials at large scale is micromagnetics. It is based on the continuum approximation where the length scales considered are large enough for the atomic structure of the material to be ignored and small enough to resolve magnetic structures such as domain walls or vortices. In the continuum approximation the macroscopic magnetization is assumed to be a spatial continuous function over the material

$$\mathbf{M}(\mathbf{r}) = M_s\mathbf{m}(\mathbf{r}), \tag{2.7}$$

where $|\mathbf{m}(\mathbf{r})| = 1$ and M_s is the saturation magnetization. In this approach the energy of the magnetic system reads[36]

$$E = \int_V d\mathbf{r}\{-\mathbf{M}\cdot\mathbf{H} - Km_z^2 + A(\nabla\mathbf{m})^2 - \frac{1}{2}\mathbf{M}\cdot\mathbf{H}_d\}, \tag{2.8}$$

where K is the macroscopic uniaxial anisotropy constant, A is the exchange stiffness parameter, $(\nabla\mathbf{m})^2 = (\nabla m_x)^2 + (\nabla m_y)^2 + (\nabla m_z)^2$, ∇ is the gradient operator and $\mathbf{H}_d$ is the demagnetizing field.

In order to solve micromagnetic problems numerically the system is divided in cells and then the average magnetization of the cell at position $\mathbf{r}_i$ is represented by vector called macrospin (see Fig. 2.2), $\mathbf{M}(\mathbf{r}_i) = \mathbf{M}_i = M_s\mathbf{m}_i$, so that the total energy becomes

$$E = \sum_i V_i\{-\mathbf{M}_i\cdot\mathbf{H}_i - K_i m_{i,z}^2 + A_i(\nabla\mathbf{m}_i)^2 - \frac{1}{2}\mathbf{M}_i\cdot\mathbf{H}_{d,i}\}, \tag{2.9}$$

where V_i is the volume of the discretization cell which typically is around few nm^3. In order to choose a suitable volume cell is important to take to account

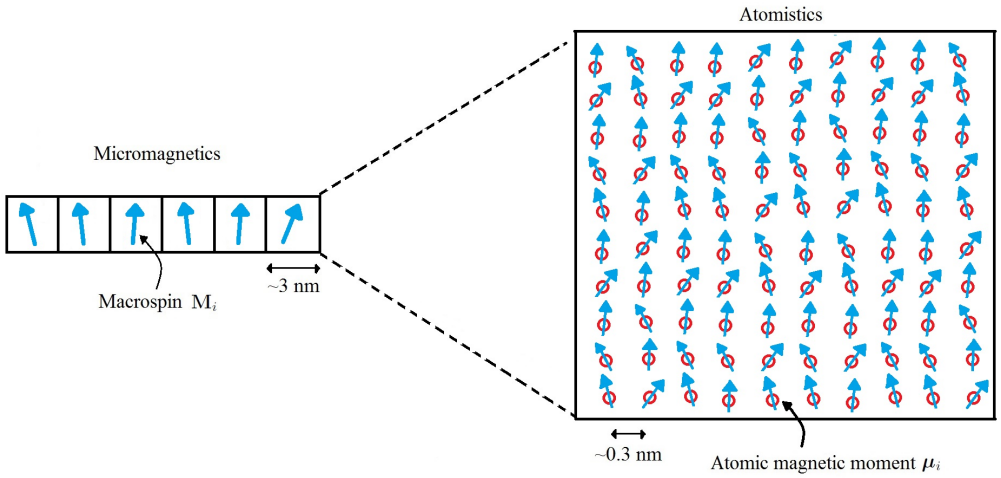

Figure 2.2: Illustration of the relation between atomistic model and micromagnetics.

the domain wall width parameter δ and the exchange length l_{ex} which are given by

$$\delta = \pi\sqrt{\frac{A}{K}}\ , \qquad l_{ex} = \sqrt{\frac{A}{M_s^2}}. \tag{2.10}$$

The domain wall width parameter corresponds to the width of a Bloch wall that is found in magnetic materials with a large magnetocrystalline anisotropy. The exchange length is the length below which atomic exchange interactions dominate typical magnetostatic fields and it is proportional to the Néel domain wall width. The discretization length must be less than the domain wall width but include enough atoms to be valid as the continuous approximation.

The standard dynamic micromagnetics is based on the LLG equation where the equation of motion for the macrospin $\mathbf{M}_i$ is given by

$$\frac{d\mathbf{M}_i}{dt} = -\frac{\gamma}{1+\alpha_{\mathrm{LLG}}^2}(\mathbf{M}_i \times \mathbf{H}_{\mathrm{eff},i}) - \frac{\gamma\alpha_{\mathrm{LLG}}}{(1+\alpha_{\mathrm{LLG}}^2)M_s}\mathbf{M}_i \times (\mathbf{M}_i \times \mathbf{H}_{\mathrm{eff},i}) \tag{2.11}$$

where α_{LLG} is called the LLG damping and $\mathbf{H}_{\mathrm{eff},i}$ is the effective field which is given by[36]

$$\mathbf{H}_{\mathrm{eff},i} = -\frac{1}{V_i}\frac{\partial E}{\partial \mathbf{M}_i} = \mathbf{H}_i + \frac{2K_i m_{i,z}}{M_s}\mathbf{e}_z + \frac{2A_i}{M_s}\nabla^2\mathbf{m}_i + \mathbf{H}_{d,i}. \tag{2.12}$$

2.3.1 Thermal micromagnetics at low-temperatures

The temperature effects in micromagnetism can be included in two ways:

i) *Via temperature-dependent parameters:* The parameters $M_s(T)$, $A(T)$ and $K(T)$ among others like susceptibilities $\chi(T)$ are temperature-dependent. As it was mentioned in section 2.1 their temperature dependence can be calculated numerically using ASD, a detailed explanation of this calculation can be found in Ref.[111] for FePt. They can also be obtained theoretically for example using the mean-field approximation (MFA) or experimentally.

ii) *Via thermal field:* In 1963 Brown suggested in his seminal work[28] to include thermal fluctuations in the Landau-Lifshitz (LL) dynamical equation as stochastic fields whose properties are defined by the equilibrium solution of the corresponding Fokker-Planck (FP) equation. In 1993 Lyberatos and Chantrell [99] studied the dynamics of two interacting magnetic dipoles including a fluctuating thermal field, the energy barriers obtained were in good agreement with the theory. This idea was further developed by many authors [33, 54, 112, 130] leading to Langevin dynamic micromagnetics where a fluctuating thermal field $\boldsymbol{\zeta}_i$ is added to the effective field given by Eq. (2.12) with the following time average properties

$$\langle \zeta_{i,k} \rangle_t = 0, \quad \langle \zeta_{i,k}(0)\zeta_{i,k'}(t) \rangle_t = 2\frac{\alpha_{\mathrm{LLG}} k_B T}{\gamma M_s(0) V_i}\delta_{kk'}\delta(t), \quad k,k' = x,y,z. \tag{2.13}$$

The main feature of this approach is that the magnitude of every macrospin is conserved in all dynamical processes, that is, $|\mathbf{M}_i|$ =const. However, the simulations of the magnetization dynamics based on the micromagnetic LLG equation are not suitable for high temperatures. This is due to the fact that micromagnetic simulations do not include the high-frequency spin waves and, thus, the Curie temperature is seriously overestimated [58] and the restriction $|\mathbf{M}_i|$ =const. Indeed, in recent ASD simulations [79] it has been demonstrated that at high temperatures several important effects occur which cannot be taken into account in the micromagnetic LLG approach. Namely, during the magnetization dynamics, (i) the magnetization vector magnitude is not conserved, (ii) longitudinal magnetization relaxation occurs with the longitudinal relaxation time increase approaching the Curie temperature (critical slowing down), and (iii) at the same time the transverse relaxation time decreases [35]. Therefore, a different micromagnetic approach is required at elevated temperatures.

2.3.2 Thermal micromagnetics at high-temperatures

As we have mentioned the micromagnetic LLG equation doesn't work properly at elevated temperatures. In 1997 an alternative approach was suggested by D. Garanin[49]. Based on the Fokker-Planck equation he derived a classical macroscopic equation of motion for the magnetization called Landau-Lifshitz-Bloch

(LLB) which interpolates between the Landau-Lifshitz equation at low temperatures (micromagnetic LLG) and the Bloch equation at high temperatures. In the micromagnetic LLB approach the magnetization dynamics of each macrospin is governed by

$$\frac{d\mathbf{m}_i}{dt} = -\gamma\left[\mathbf{m}_i \times \mathbf{H}^i_{\text{eff}}\right] + \frac{\gamma\alpha_{\parallel}}{m_i^2}\left(\mathbf{m}_i \cdot \mathbf{H}^i_{\text{eff}}\right)\mathbf{m}_i - \frac{\gamma\alpha_{\perp}}{m_i^2}\left[\mathbf{m}_i \times \left[\mathbf{m}_i \times \mathbf{H}^i_{\text{eff}}\right]\right], \tag{2.14}$$

where $\mathbf{m}_i = \mathbf{M}_i/M_e(0)$ with $M_e(0) = M_s(0)$ is the equilibrium saturation magnetization at $T = 0K$. The longitudinal and transverse relaxation parameters are

$$\alpha_{\parallel} = \lambda\frac{2T}{3T_c}, \qquad \alpha_{\perp} = \lambda \cdot \begin{cases} \left[1 - \frac{T}{3T_c}\right] & T \lesssim T_c \\ \frac{2T}{3T_c} & T \gtrsim T_c \end{cases} \tag{2.15}$$

where λ is the coupling to the bath parameter and T_c is the Curie temperature. The effective fields are given by

$$\mathbf{H}^i_{\text{eff}} = \mathbf{H} + \mathbf{H}_{i,\text{EX}} + \mathbf{H}_{i,A} + \begin{cases} \frac{1}{2\tilde{\chi}_{\parallel}}\left(1 - \frac{m_i^2}{m_e^2}\right)\mathbf{m}_i & T \lesssim T_c \\ \frac{J_0}{\mu_{at}}\left(1 - \frac{T}{T_c} - \frac{3m_i^2}{5}\right)\mathbf{m}_i & T \gtrsim T_c \end{cases} \tag{2.16}$$

where $\mathbf{H}$ is the applied magnetic field, $\mathbf{H}_{i,\text{EX}}$ is exchange interaction between macro-spins and it is given by

$$\mathbf{H}_{i,\text{EX}} = \frac{2A_i(T)}{m_i^2 M_s(0)}\nabla^2\mathbf{m}_i = \frac{2A_i(T)}{m_i^2 M_s(0)\triangle^2}\sum_{\langle i,j\rangle}(\mathbf{m}_j - \mathbf{m}_i) \tag{2.17}$$

where $\langle i,j\rangle$ means a sum over neighbours, $\triangle$ is the lateral size of the micromagnetic discretization cell and $A_i(T)$ is the micromagnetic exchange also called stiffness, $\mathbf{H}_{i,A}$ is the anisotropy field given by

$$\mathbf{H}_{i,A} = -\frac{1}{\tilde{\chi}_{\perp}}\left(m_{i,x}\mathbf{e}_x + m_{i,y}\mathbf{e}_y\right) \tag{2.18}$$

where $\widetilde{\chi}_{\perp}$ and $\widetilde{\chi}_{\parallel}$ is transverse and longitudinal susceptibility, respectively. The quantity J_0 is the zero Fourier component of the exchange interaction which is related to the Curie temperature T_c in the MFA through $T_c = J_0/(3k_B)$ and μ_{at} is the atomic magnetic moment. The parameter $m_e = M_e(T)/M_e(0)$ is the normalized equilibrium magnetization. The last term in Eq. (2.16) describes the internal exchange field inside the macrospin.

As we see the LLB equation contains six implicit temperature-dependent parameters: $\lambda(T)$, $M_e(T)$, $A(T)$, $K(T)$, $\widetilde{\chi}_{\parallel}(T)$ and $\widetilde{\chi}_{\perp}(T)$. Typically, the parameter

λ is considered temperature independent, however as we will see in chapter 3 it could also depend on temperature. In the multiscale approach the temperature dependence of $A(T)$ and $K(T)$ is calculated using ASD[111]. The parameter $M_e(T)$ can be obtained experimentally, numerically using ASD or theoretically using the MFA as the solution of the equation $m_e = L(\beta J_0 m_e)$ where $L(x) = \coth(x) - 1/x$ is the Langevin function. The longitudinal susceptibility can be also evaluated from ASD, measured experimentally or calculated using MFA as

$$\widetilde{\chi}_{\parallel}(T) = \begin{cases} \frac{\mu_{at}\beta L'}{1-\beta J_0 L'} & T \lesssim T_c \\ \frac{\mu_{at} T_c}{J_0(T-T_c)} & T \gtrsim T_c \end{cases} \tag{2.19}$$

where L' is the derivative of the Langevin function evaluated at $\beta J_0 m_e$ and $\beta = 1/(k_B T)$. The transverse susceptibility is related to the anisotropy constant K through $\tilde{\chi}_{\perp}(T) = M^2/[2K(T)]$.

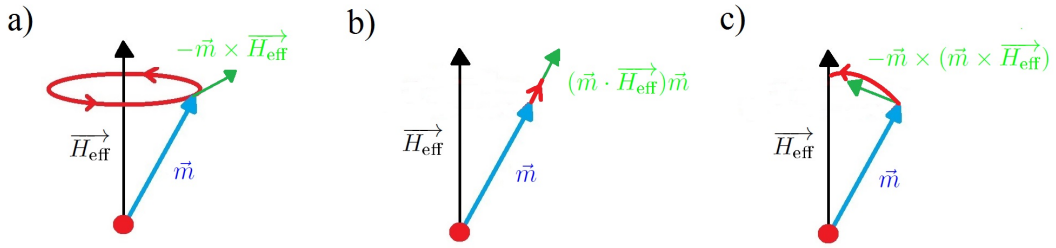

Figure 2.3: Diagram illustrating the meaning of three terms in the LLB equation: a) precession, b) longitudinal dynamic and c) transverse dynamic.

The first term in Eq. (2.14) describes the precession of $\mathbf{m}_i$ around its effective field $\mathbf{H}_{\text{eff}}$ (see Fig.2.3 a)), the second and third terms describe the longitudinal (see Fig.2.3 b)) and transverse (see Fig.2.3 c)) dynamics, respectively. If we compare LLB equation (Eq. (2.14)) with LLG equation (Eq. (2.11)) we notice that LLB eq. contains an extra term which describes the longitudinal relaxation, that is, it drives the dynamics of the magnitude of $\mathbf{m}$ giving a more accurate description of the magnetic behaviour at elevated temperatures. In particular this extra term plays a crucial role in ultrafast magnetization dynamics. Moreover, since the LLB eq. contains the LLG eq. it also describe the damped precession which typically takes place between 0.1 and 1 ns (see Fig. 1.1 a)).

The effective field of the LLB equation given by Eq. (2.16) can be written as

$$\mathbf{H}^i_{\text{eff}} = -\frac{1}{V_i}\frac{\partial \mathcal{F}}{\partial \mathbf{M}_i}. \tag{2.20}$$

where $\mathcal{F}$ is the MFA free energy given by

$$\begin{aligned}\mathcal{F}(\mathbf{M},T) &= \mathcal{F}_0 + \int_V d\mathbf{r}\{-\mathbf{M}\cdot\mathbf{H} + \frac{1}{2\chi_\perp}(M_x^2+M_y^2) + A\left(\nabla\left[\frac{\mathbf{M}}{M}\right]\right)^2 \\ &+ \frac{1}{8M_e^2(T)\chi_\parallel}[M^2 - M_e^2(T)]^2\}, \end{aligned} \tag{2.21}$$

where $\mathcal{F}_0$ is the equilibrium free energy in the absence of anisotropy and magnetic field. In 2001 H. Kachkachi and D. Garanin [74] derived this free energy using a procedure based on the MFA which is described in Appendix D.

Similarly as it was done in the micromagnetic LLG equation, D. Garanin and O. Chubykalo-Fesenko[51] included stochastic thermal fields into the LLB equation. However, Evans *et al.*[42] noticed that this approach doesn't recover the Boltzmann distribution close to T_c at equilibrium. In order to solve this issue they derived an alternative stochastic LLB equation of the form

$$\begin{aligned}\frac{d\mathbf{m}_i}{dt} &= -\gamma\left[\mathbf{m}_i\times\mathbf{H}_{\text{eff}}^i\right] + \frac{\gamma\alpha_\parallel}{m_i^2}\left(\mathbf{m}_i\cdot\mathbf{H}_{\text{eff}}^i\right)\mathbf{m}_i \\ &- \frac{\gamma\alpha_\perp}{m_i^2}\left[\mathbf{m}_i\times\left[\mathbf{m}_i\times\left(\mathbf{H}_{\text{eff}}^i+\boldsymbol{\zeta}_{i,\perp}\right)\right]\right] + \boldsymbol{\zeta}_{i,ad}, \end{aligned} \tag{2.22}$$

where the thermal fields $\boldsymbol{\zeta}_{i,\perp}$ and $\boldsymbol{\zeta}_{i,ad}$ are given by

$$\left\langle\zeta_{i,\perp}^k(0)\zeta_{j,\perp}^l(t)\right\rangle = \frac{2\gamma k_B T\left(\alpha_\perp-\alpha_\parallel\right)}{M_e(0)V_i\alpha_\perp^2}\delta_{ij}\delta_{kl}\delta(t) \tag{2.23}$$

$$\left\langle\zeta_{i,ad}^k(0)\zeta_{j,ad}^l(t)\right\rangle = \frac{2\gamma k_B T\alpha_\parallel}{M_e(0)V_i}\delta_{ij}\delta_{kl}\delta(t) \tag{2.24}$$

where i and j denote macro-spin index, k and l denote the Cartesian components x, y and z.

2.4 Two temperature model

A very successful procedure to model ultrafast magnetization dynamics is to couple the magnetization equation of motion like ASD described in section 2.2[12, 115] or micromagnetic LLB equation[8, 9, 78] described in section 2.3.2 to the so-called two temperature model (2TM). The 2TM model was originally derived by Kaganov *et al.*[75] in 1957, basically it describes the energy transfer between the electron and phonon baths. The system is artificially separated into spin, electron

and phonon degrees of freedom which are considered thermalized, i.e. in quasi-equilibrium. A detailed discussion about the 2TM can be found in Ref.[140]. The 2TM is given by the following two coupled differential equations:

$$\begin{aligned} C_e \frac{dT_e}{dt} &= -G_{e-ph}\left(T_e - T_{ph}\right) + S(t) - C_e \frac{\left(T_e - T_{room}\right)}{\tau_{th}}, \\ C_{ph} \frac{dT_{ph}}{dt} &= G_{e-ph}\left(T_e - T_{ph}\right), \end{aligned} \tag{2.25}$$

where T_e is the electron's temperature, T_{ph} is the phonon's temperature, T_{room} is the room temperature, C_e and C_{ph} are the specific heats of the electrons and lattice, G_{e-ph} is an electron-phonon coupling constant which determines the rate of the energy exchange between the electrons and the lattice, τ_{ph} is the heat diffusion time to the outer space and $S(t)$ is the deposited laser energy. The electronic specific heat C_e is calculated in the free electron approximation $C_e = \gamma_e T_e$ where γ_e is a constant. The heat diffusion time to the outer space τ_{ph} is determined by the slow decay on long term behaviour. Usually, T_{ph} is higher than the Debye temperature, in this case one can assume that the phonon specific heat C_{ph} is a constant. For thin films the deposited laser energy $S(t)$ can be modelled as

$$S(t) = I_0 F e^{-\left(\frac{t}{\tau}\right)^2} \tag{2.26}$$

where F is the fluence, I_0 is a parameter that can be estimated from the experimental reflectivity and τ is the pulse length, typically it has a value of $\tau = 40$ fs.

2.5 Modelling ultrafast magnetization dynamics

The Landau-Lifshitz-Bloch (LLB) equation gives a more accurate description of the high-temperature magnetism than the classical micromagnetism. [35, 96] Due to the appearance of novel high-temperature magnetic applications the use of the LLB-based micromagnetism is progressively becoming more popular. Particularly, in the field of femtosecond optomagnetism, [86] where a sub-ps demagnetization can be induced by the ultrafast heating produced by a femtosecond laser pulse,[115] the LLB equation has recommended itself as an useful approach. This is because it correctly describes the longitudinal magnetization relaxation in the strong internal exchange field, the key property of the magnetization dynamics at the timescale below 1 ps. [6, 9, 144] Although the same characteristics have been proven to be reproduced by atomistic many-body approach, [78] the use of the

LLB micromagnetism for modeling purposes has some advantages: (i) the possibility to perform large scale modeling, for example, thermally-induced domain wall motion in much larger nanostructures [65] and (ii) analytical derivation of, for instance, the domain wall mobility [47] or the demagnetization time scales. [6, 10]

In order to model ultrafast magnetization dynamics we consider that the energy deposited by the femtosecond laser pulse $S(t)$ is absorbed by the electron bath and then this energy is transferred to the phonon bath through the electron-phonon coupling G_{e-ph}. Moreover, we assume that in these short time scales the spin system is only coupled to the electron bath, namely the general coupling to the bath parameter λ which appears in the spin equation of motion (micromagnetic LLB equation or ASD) is refereed to the electron bath and then all temperature-parameters depend on T_e, it means, the electronic temperature extracted from the 2TM is the temperature to which the spin equation of motion is coupled. Fig. 2.4 a) shows a schematic representation of the relation between light, electron, phonon and spin that we consider in our model. As an example, in Fig. 2.4 b) we show the dynamics of the magnetization, electron temperature and phonon temperature obtained by the numerical integration of the non-stochastic LLB equation for one macrospin coupled to the 2TM, the value of the parameters that we used in this example are given by the set I in Table 4.1 for a fluence of 20 mJ/cm^2.

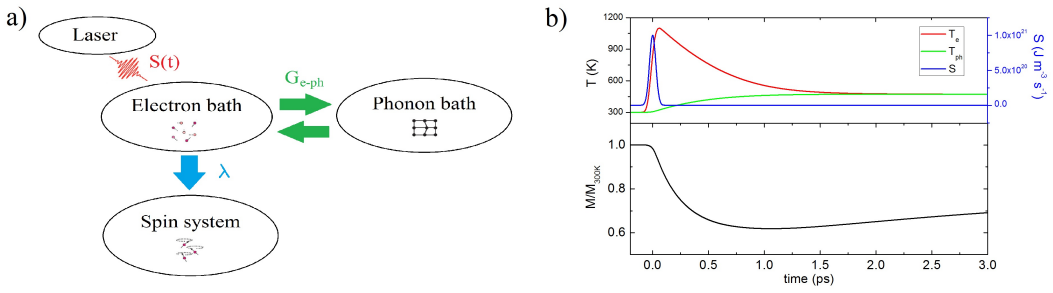

Figure 2.4: a) Schematic representation of the relation between light, electrons, phonons and spins that we consider in our model of the ultrafast magnetization dynamics. b) Dynamics of the magnetization, electron temperature and phonon temperature obtained by the numerical integration of the LLB equation coupled to the 2TM.

2.6 Alternative models

2.6.1 Macroscopic three temperature model

The macroscopic three temperature model (M3TM), [88, 120] has also been successfully used in the description of *femtomagnetism* experiments. The M3TM assumes a collection of two level spin systems with the spin-flip probability of the phonon-mediated Elliot-Yafet (EY) scattering events a_{sf}, and uses a simple self-consistent Weiss mean-field model to evaluate the macroscopic magnetization. The M3TM model reads

$$\frac{dm}{dt} = Rm\frac{T_{ph}}{T_c}\left[1 - m\coth\left(\frac{mT_c}{T_e}\right)\right]. \tag{2.27}$$

where R is a material specific parameter linearly proportional to the spin-flip probability and it reads

$$R = \frac{8a_{sf}G_{e-ph}k_BT_c^2V_{at}}{(\mu_{at}/\mu_B)E_D^2} \tag{2.28}$$

where E_D is the Debye energy and V_{at} is the atomic volume. Eq. (2.27) is coupled to the 2TM. In the resulting system, importantly, the energy separation between levels is determined by a dynamical exchange interaction, similar to the LLB equation, which can be interpreted as a feedback effect to allow the correct account for the high temperature spin fluctuations. [109] This consideration turns out to be a fundamental ingredient for the description of the ultrafast demagnetization in ferromagnets which suggests that the correct account for non-equilibrium thermodynamics is probably more important than the accurate band structure.

2.6.2 Self-consistent Bloch equation

More recently, an alternative model to the M3TM and the LLB models, the so-called self-consistent Bloch (SCB) equation[152] has been suggested. The SCB equation uses a quantum kinetic approach with the instantaneous local equilibrium approximation[39] and the MFA, the resulting equation is given by

$$\frac{d\mathbf{m}}{dt} = -\gamma\mathbf{m}\times\mathbf{H}_{\mathrm{SCB}} - \frac{\mathbf{m}-\mathbf{m}_{eq}(\mathbf{H}_{\mathrm{SCB}})}{\tau_s}, \tag{2.29}$$

where τ_s represents the scattering life time of electron spins, $\mathbf{m}_{eq}$ is the equilibrium magnetization which is determined self-consistently and $\mathbf{H}_{\mathrm{SCB}}$ is the effective field given by

$$\mathbf{H}_{\mathrm{SCB}} = \mathbf{H} + \mathbf{H}_A + \mathbf{H}_d + J_0\mathbf{m}, \tag{2.30}$$

where the meaning of these terms is the same as those introduced in previous sections. If we compare the effective field of the SCB (Eq. (2.30)) and LLB (Eq. (2.16)) equations we observe that the internal exchange field (last term in both expressions) in the SCB equation has a simpler form than in the LLB equation.

3

Quantum Landau-Lifshitz-Bloch equation for ferromagnets

3.1 Introduction

The Landau-Lifshitz-Bloch (LLB) equation gives a more accurate description of the high-temperature magnetism than the classical micromagnetism. [35, 96] Due to the appearance of novel high-temperature magnetic applications the use of the LLB-based micromagnetism is progressively becoming more popular. The LLB formalism has been successfully used to model the heat-assisted magnetic recording, [82, 104] high-temperature spin-torque dynamics, [126] spin-caloritronics [65] and laser-induced magnetization dynamics. [9, 144] Apart from their fundamental interest, these applications are very appealing from technological perspectives that range from energy saving strategies to the increase of the speed of the magnetization switching. Particularly, in the field of femtosecond optomagnetism, [86] where a sub-ps demagnetization can be induced by the ultrafast heating produced by a femtosecond laser pulse,[115] the LLB equation has recommended itself as an useful approach. This is because it correctly describes the longitudinal magnetization relaxation in the strong internal exchange field, the key property of the magnetization dynamics at the timescale below 1 ps. [6, 9, 144] Although the same characteristics have been proven to be reproduced by atomistic many-body approach, [78] the use of the LLB micromagnetism for modeling purposes has some advantages: (i) the possibility to perform large scale modeling, for example, thermally-induced domain wall motion in much larger nanostructures [65] and (ii) analytical derivation of, for instance, the domain wall mobility [47] or the demagnetization time scales. [6, 10]

Up to now, most of works used the classical version of the LLB equation which was derived starting from a Heisenberg spin model and the Landau-Lifshitz equa-

tion for classical atomic spins. [49] This has made the classical LLB approach very popular since a direct comparison between the LLB and the atomistic simulations is therefore possible. [35, 78] However, the classical atomistic simulations mean effectively localized magnetic moments and correspond to the infinite spin number $S \to \infty$. As a consequence, the magnetization versus temperature curve follows a Langevin function rather than the Brillouin function which has been shown to fit better for ferromagnetic metals,[37] such as Ni and Co with $S = 1/2$, Fe with $S = 3/2$ and Gd with $S = 7/2$. In principle, the classical approximation seems hard to justify in the magnetic materials commonly used for ultrafast magnetization dynamics measurements, such as ferromagnetic metals, because of the delocalized nature of the relevant electrons responsible for the magnetic properties. However, recent works which compare laser-induced magnetization dynamics experiments in metals with atomistic spin models[70, 115, 144] as well as with their macroscopic counterpart - the classical LLB model[6, 144]- have proven that both models are very successful in the description and understanding of this phenomenon.

The qLLB equation has been barely investigated for numerical purposes. One of the reasons is the fact that the derivation has been made for the spin-phonon interaction mechanism which historically has been thought as the main contribution to the magnetization damping. This mechanism is important for ps-ns applications at high temperatures such as spincaloritronics. Recent experiment also explore the possibility to excite magnetization dynamics by acoustic pulses in picosecond range [125] (THz excitation) where the phonon mechanism is the predominant one.[83] However, it is believed that for the laser-induced magnetization dynamics the spin-flips occur mainly due to the electron scattering, its relevance may be marginal. Thus, in this chapter we also derive a novel qLLB equation by considering a simple spin-electron interaction as a source for magnetic relaxation.

3.2 Theoretical background for the quantum Landau-Lifshitz-Bloch equation

3.2.1 Basic assumptions for the qLLB equation with spin-phonon interaction

For completeness and for subsequent development, in this subsection we summarize the main aspects and approximations of the derivation of the qLLB equation. The original derivation of the qLLB equation[47] was done assuming a magnetic ion interacting weakly with a thermal phonon bath via direct and the second

order (Raman) spin-phonon processes. The ferromagnetic interactions are taken into account in the mean-field approximation (MFA). The model Hamiltonian is written as:

$$\hat{\mathcal{H}}(t) = \hat{\mathcal{H}}_s(t) + \hat{\mathcal{H}}_{ph} + \hat{V}_{s\text{-}ph}, \tag{3.1}$$

where $\hat{\mathcal{H}}_s$ describes the spin system energy, $\hat{\mathcal{H}}_{ph}$ describes the phonon energy, $\hat{V}_{s\text{-}ph}$ describes the spin-phonon interaction:

$$\begin{aligned} \hat{\mathcal{H}}_s(t) &= -\hat{\boldsymbol{\mu}} \cdot \mathbf{H}^{\mathrm{MFA}}(t) = \gamma \mathbf{H}^{\mathrm{MFA}}(t) \cdot \hat{\mathbf{S}}, \\ \hat{\mathcal{H}}_{ph} &= \sum_q \hbar\omega_q \hat{a}_q^\dagger \hat{a}_q, \\ \hat{V}_{s\text{-}ph} &= -\sum_q V_q(\boldsymbol{\eta} \cdot \hat{\mathbf{S}})(\hat{a}_q^\dagger + \hat{a}_{-q}) - \sum_{p,q} V_{p,q}(\boldsymbol{\eta} \cdot \hat{\mathbf{S}})\hat{a}_p^\dagger \hat{a}_q. \end{aligned} \tag{3.2}$$

In the expressions above $\hat{\boldsymbol{\mu}} = -\gamma\hat{\mathbf{S}}$ is the magnetic moment operator, $\hat{\mathbf{S}}$ is the spin operator, $\gamma = |g|\mu_B/\hbar$ is the gyromagnetic ratio where g is the Landé g-factor, μ_B is the Bohr magneton and $\hbar$ is the reduced Planck constant, $\hat{a}_q^\dagger$ ($\hat{a}_q$) is the creation (annihilation) operator which creates (annihilates) a phonon with frequency ω_q where q stands for the wave vector $\mathbf{k}$ and the phonon polarization.

The vector $\mathbf{H}^{\mathrm{MFA}}$ is an effective field in the MFA given by

$$\mathbf{H}^{\mathrm{MFA}}(t) = \mathbf{H}_E(t) + \mathbf{H}(t) + \mathbf{H}_K = \frac{J_0}{\mu_{\mathrm{at}}}\mathbf{m}(t) + \mathbf{h}(t), \tag{3.3}$$

where $\mathbf{H}_E(t) = (J_0/\mu_{\mathrm{at}})\mathbf{m}(t)$ is the homogeneous part of the exchange field, J_0 is the exchange parameter related in the MFA to the Curie temperature T_c as $J_0 = 3k_BT_cS/(S+1)$, $\mu_{\mathrm{at}} = |g|\mu_B S$ is the atomic magnetic moment, $\mathbf{m}(t) = \langle\hat{\boldsymbol{\mu}}(t)\rangle/\mu_{\mathrm{at}} = -\langle\hat{\mathbf{S}}(t)\rangle/(\hbar S)$ is the reduced magnetization and $\mathbf{h} = \mathbf{H} + \mathbf{H}_K$, where $\mathbf{H}$ is the external magnetic field and $\mathbf{H}_K$ represents the anisotropy field. Note that the original derivation[47] uses the two-site (exchange) anisotropy, since the treatment of the on-site anisotropy with a simple decoupling scheme, used below and suitable for the exchange interactions does not produce a correct temperature dependence for the anisotropy. [16] However, the on-site anisotropy can be later phenomenologically included into the consideration. [49, 78] Additionally, the inhomogeneous exchange field, $\propto (J_0/\mu_{\mathrm{at}})\triangle\mathbf{m}$, may be either taken into account here or lately phenomenologically within the micromagnetic approach. [78]

The first term in the spin-phonon interaction potential $\hat{V}_{s\text{-}ph}$ in Eq. (B.2) takes into account the direct spin-phonon scattering processes which are characterized by the amplitude V_q, and the second term describes the Raman processes with amplitudes $V_{p,q}$. The interaction may be anisotropic via the crystal field, which is taken into account through the parameter $\boldsymbol{\eta}$. The spin-phonon scattering

amplitudes V_q and $V_{p,q}$ can be in principle evaluated on the basis of the *ab-initio* electronic structure theory. Note that the interaction between spin and phonons considered in the Hamiltonian (B.1) is one of the simplest possible forms, which has a linear (in the spin variable) coupling between spin and phonons. Based on the time reversal symmetry argument, it has been discussed[48] that a quadratic spin-phonon coupling may be more physically justified. Nevertheless, it has been demonstrated that Eq. (B.1) is adequate to describe the main qualitative properties of the spin dynamics.

Notice that in the original derivation [47] the definitions of $\hat{\mathcal{H}}_s$ and $\mathbf{m}$ have the opposite sign than here, as consequence in the original derivation the time was reversed in order to obtain the correct final equation of motion. Here we use a more standard definitions of $\hat{\mathcal{H}}_s$ and $\mathbf{m}$ where there is no need to reverse time, therefore here some intermediate equations in the derivation could be different as in Ref. [47] but the same final magnetization equation of motion is obtained.

The derivation of the qLLB equation [47] is based on a standard density matrix approach[25, 50] for a system interacting weakly with a bath. Namely, starting from the Schrödinger equation one can obtain a Liouville equation for the time evolution of the density operator $\hat{\rho} = |\Psi\rangle\langle\Psi|$, where $|\Psi\rangle$ is the wave function of the whole system (spin and phonons). Next, the interactions with the bath are assumed to be small so that they can not cause a significant entanglement between both systems, this allows to factorize the density operator $\hat{\rho}$. Moreover, it is assumed that the bath is in thermal equilibrium (quasi-equilibrium) therefore, the density operator can be factorized by its spin and bath parts as $\hat{\rho}(t) \cong \hat{\rho}_s(t)\hat{\rho}_b^{eq}$, and after averaging over the bath variable one obtains the following equation of motion for the spin density operator $\hat{\rho}_s$[50] (see Appendix A)

$$\begin{aligned}\frac{d}{dt}\hat{\rho}_s(t) &= -\frac{i}{\hbar}\left[\hat{\mathcal{H}}_s(t), \hat{\rho}_s(t)\right] - \hat{U}_0(t)\left(\frac{i}{\hbar} Tr_b\left[\hat{V}_{s\text{-}ph}(t)_I, \hat{\rho}_s(0)_I\hat{\rho}_b^{eq}\right]\right)\hat{U}_0^\dagger(t) \\ &- \hat{U}_0(t)\left(\frac{1}{\hbar^2}\int_0^t dt' Tr_b\left[\hat{V}_{s\text{-}ph}(t)_I, \left[\hat{V}_{s\text{-}ph}(t')_I, \hat{\rho}_s(t')_I\hat{\rho}_b^{eq}\right]\right]\right)\hat{U}_0^\dagger(t) \quad (3.4)\end{aligned}$$

where Tr_b is the trace over the bath variable, $\hat{V}_{s\text{-}ph}(t)_I = \hat{U}_0^\dagger(t)\hat{V}_{s\text{-}ph}\hat{U}_0(t)$, $\hat{U}_0(t) = \hat{U}_{0,s}(t)\hat{U}_{0,b}(t)$ is the time evolution operator in the absence of interaction, $\hat{U}_{0,s}(t)$ and $\hat{U}_{0,b}(t)$ are the time evolution operators in the absence of interaction of the spin system and bath, respectively, $\hat{\rho}_s(t')_I = \hat{U}_{0,s}^\dagger(t')\hat{\rho}_s\hat{U}_{0,s}(t')$, $\hat{\rho}_s(t)$ is written in terms of the Hubbard operators $\hat{X}^{mn} = |m\rangle\langle n|$ (where $|m\rangle$ and $|n\rangle$ are eigenvectors of $\hat{S}^z$, corresponding to the eigenstates $m\,\hbar$ and $n\,\hbar$, respectively), as

$$\hat{\rho}_s(t) = \sum_{m,n}\rho_{s,mn}(t)\hat{X}^{mn}, \quad (3.5)$$

where $\rho_{s,mn}(t) = \langle m|\hat{\rho}_s(t)|n\rangle$. Next, the following approximations are made: (i) the Markov or short memory approximation assuming that the interactions of the spins with the phonon bath are faster than the spin interactions themselves, this approximation means that in Eq. (3.4) the "coarse-grained" derivative is taken over time intervals Δt which are longer than the correlation time of the bath τ_b ($\Delta t \gg \tau_b$) and, (ii) secular approximation, where only the resonant secular terms are retained, which consists in neglecting fast oscillating terms in Eq. (3.4). It forces the time interval to be[25] $\Delta t \gg \hbar/(E_m - E_n)$ where $E_{m(n)}$ is an eigenvalue of $\hat{\mathcal{H}}_s$. For a ferromagnetic material with a strong exchange field H_E we have $E_m - E_n \sim \hbar\gamma H_E$, therefore, for the Curie temperature $T_c \simeq 800$ K we obtain $\Delta t \gg 1/\gamma H_E \sim 10$ fs. Note that a different argument based on the scaling of the perturbation Hamiltonian (singular-coupling limit) can be found in Ref. [26]. We should note that the validity of the above approximations for ultrafast magnetization processes may be questionable and should be checked in future on the basis of comparison with experiments. Note that similar studies for electronic coherence life time in molecular aggregates have found that the influence of the secular approximation in fs timescale is rather weak.[114] At the same time, the elimination of the secular approximation may be necessary for THz excitation of the spin system. On the other hand, if the Markov approximation is removed, it would meant an effective use of the colored noise. Our previous results [7] indicate that the use of the colored noise with correlation time larger than 10 fs considerably slows down the magnetization longitudinal relaxation time leading to time scales not consistent with those observed in experiments.

As a result of these assumptions, one arrives to the equation for the Hubbard operators in the Heisenberg representation[47](see Appendix B)

$$\begin{aligned}\frac{d}{dt}\hat{X}^{mn}(t) &\simeq i\gamma H^{\mathrm{MFA}}(t)\,(m-n)\,\hat{X}^{mn}(t) - \widetilde{W}_1^{ph}\,(m-n)^2\,\hat{X}^{mn}(t)\\ &- \frac{1}{2}\widetilde{W}_2^{ph}\left(l_{m-1}^2 + l_{n-1}^2 + e^{-y_0}(l_m^2 + l_n^2)\right)\hat{X}^{mn}(t)\\ &+ \widetilde{W}_2^{ph}\left(l_m l_n \hat{X}^{m+1,n+1}(t) + e^{-y_0} l_{m-1} l_{n-1}\hat{X}^{m-1,n-1}(t)\right) \qquad (3.6)\end{aligned}$$

where $\widetilde{W}_1^{ph} = \eta_z^2 W_1^{ph}$ and $\widetilde{W}_2^{ph} = \frac{1}{2}W_2^{ph}(\eta_x^2 + \eta_y^2)$, $y_0 = \beta\ \hbar\ \gamma H^{\mathrm{MFA}}$, $l_m = \sqrt{(S-m)(S+1+m)}$, $\beta = 1/k_B T$,

$$W_1^{ph} = \sum_{\mathbf{q},\mathbf{p}} |V_{\mathbf{pq}}|^2 n_p(n_q+1)\pi\delta(\omega_q - \omega_p) \qquad (3.7)$$

$$W_2^{ph} = \sum_{\mathbf{q}} |V_{\mathbf{q}}|^2 (n_q + 1)\pi\delta(\omega_q - \gamma H^{\mathrm{MFA}}) + \sum_{\mathbf{q},\mathbf{p}} |V_{\mathbf{q},\mathbf{p}}|^2 n_p (n_q + 1)\pi\delta(\omega_q - \omega_p - \gamma H^{\mathrm{MFA}}), \tag{3.8}$$

and $n_q = [\exp(\beta\hbar\omega_q) - 1]^{-1}$ is the Bose-Einstein distribution. Using Eq. (3.6) and the relation between the spin operators $\hat{S}^z$, $\hat{S}^{\pm} \equiv \hat{S}^x \pm i\hat{S}^y$ and the Hubbard operators given by

$$\hat{S}^+ = \hbar \sum_{m=-S}^{S-1} l_m \hat{X}^{m+1,m} \ , \ \hat{S}^- = \hbar \sum_{m=-S}^{S-1} l_m \hat{X}^{m,m+1} \ ,$$
$$\hat{S}^z = \hbar \sum_{m=-S}^{S} m\hat{X}^{mm}, \tag{3.9}$$

one obtains a set of coupled equations of motion for the spin component operators which after averaging becomes

$$\frac{d}{dt}\langle \hat{S}^{x(y)} \rangle = \mp\gamma H^{\mathrm{MFA}} \langle \hat{S}^{y(x)} \rangle - (K_1^{ph} + K_2^{ph}) \langle \hat{S}^{x(y)} \rangle + \frac{K_2^{ph}}{\hbar} \tanh\left(\frac{y_0}{2}\right) \langle \hat{S}^{x(y)} \hat{S}^z + \hat{S}^z \hat{S}^{x(y)} \rangle \tag{3.10}$$

$$\frac{d}{dt}\langle \hat{S}^z \rangle = -2 K_2^{ph} \langle \hat{S}^z \rangle - \frac{2}{\hbar} K_2^{ph} \tanh\left(\frac{y_0}{2}\right) \langle (\hat{S}^x)^2 + (\hat{S}^y)^2 \rangle \tag{3.11}$$

where

$$K_1^{ph} = \widetilde{W}_1^{ph}, \tag{3.12}$$
$$K_2^{ph} = \frac{1}{2}\left(1 + e^{-y_0}\right) \widetilde{W}_2^{ph}. \tag{3.13}$$

The decoupling of the Eqs. (3.10) and (3.11) is produced only in three special cases:[47] (i) for $S = 1/2$ where one gets the Bloch equation, also called self-consistent Bloch equation in Ref. [152] (also see below the subsection II.D) (ii) at high temperatures ($k_B T \gg \hbar\gamma H^{\mathrm{MFA}}$) where a different form of the Bloch equation is obtained and (iii) the classical ($S \gg 1$) and low-temperature limits ($k_B T \ll \hbar\gamma H^{\mathrm{MFA}}$) where one obtains the Landau-Lifshitz-Gilbert equation (LLG). For the general case where the decoupling is not possible one can use the method of the modeling distribution functions, [53] assuming a suitable form for the spin density operator as follows

$$\hat{\rho}_s(t) = \mathcal{Z}^{-1} \exp\left[\frac{\mathbf{y}(t) \cdot \hat{\mathbf{S}}}{\hbar}\right] \ , \ \mathcal{Z} = \sum_{m=-S}^{S} \exp\left[ym\right] \tag{3.14}$$

where $\mathbf{y}(t)$ is an auxiliary dimensionless time-dependent function and its equilibrium value is $\mathbf{y}_0 = \beta\gamma\hbar\mathbf{H}^{\mathrm{MFA}} = \beta\mu_{at}\mathbf{H}^{\mathrm{MFA}}/S$.[1] It is possible to show [47] that $\mathbf{y}(t)$ is related to the time-dependent reduced magnetization $\mathbf{m}(t) = -\langle\hat{\mathbf{S}}(t)\rangle/\hbar S$ as

$$\mathbf{m}(t) = B_S(Sy(t))\frac{\mathbf{y}(t)}{y(t)}, \tag{3.15}$$

where $B_S(x) = [(2S+1)/2S]\coth([2S+1]x/2S) - (1/2S)\coth(x/2S)$ is the Brillouin function for the spin value S. The spin operator averages in Eqs. (3.10) and (3.11) are calculated using the density matrix of the spin system given by Eq. (3.14) as $\langle\hat{S}^z\rangle = \mathrm{Tr}(\hat{\rho}_s\hat{S}^z)$ and so on. Finally, after these calculations the Eqs. (3.10) and (3.11) have the following form in terms of the reduced magnetization[47]

$$\begin{aligned}\frac{d\mathbf{m}}{dt} &= -\gamma\mathbf{m}\times\mathbf{h} - K_2^{ph}\frac{\tanh\left(\frac{y_0}{2}\right)}{\tanh\left(\frac{y}{2}\right)}\left(\frac{2(S+1)\tanh\left(\frac{y}{2}\right)}{m} - 1\right)\frac{\mathbf{m}\times(\mathbf{m}\times\mathbf{h})}{mH^{\mathrm{MFA}}} \\ &- 2K_2^{ph}\left(1 - \frac{\tanh\left(\frac{y_0}{2}\right)}{\tanh\left(\frac{y}{2}\right)}\frac{\mathbf{m}\cdot\mathbf{H}^{\mathrm{MFA}}}{mH^{\mathrm{MFA}}}\right)\mathbf{m} \\ &+ (K_2^{ph} - K_1^{ph})\left[\frac{(\mathbf{m}\times\mathbf{h})^2}{(mH^{\mathrm{MFA}})^2}\mathbf{m} + \frac{(\mathbf{m}\cdot\mathbf{H}^{\mathrm{MFA}})\mathbf{m}\times(\mathbf{m}\times\mathbf{h})}{(mH^{\mathrm{MFA}})^2}\right],\end{aligned} \tag{3.16}$$

where y is defined through the relation Eq. (3.15). In Fig.3.1 we show the relation between the vectors $\mathbf{m}$, $\mathbf{H}_E$, $\mathbf{y}$, $\mathbf{h}$, $\mathbf{H}^{\mathrm{MFA}}$ and $\mathbf{y}_0$ at instant t.

3.2.2 Final form of the qLLB equation

Eq. (3.16) is not convenient for numerical modeling or analytical considerations, since at each time step Eq. (3.15) should be solved to find the variable $\mathbf{y}(t)$ from $\mathbf{m}(t)$. To avoid this issue, we have to make further approximations, for instance, one can use that in ferromagnets the exchange field is strong, $H_{\mathrm{E}} \gg h$ in which case h/H_E is a small parameter. Thus, in Eq. (3.16) only the terms linear in this parameter are retained. This assumption is valid both below T_c (where always $H_{\mathrm{E}} \gg h$) and close to T_c where we can use the expansion $H_{\mathrm{E}} \simeq (J_0/\mu_{\mathrm{at}})(m_e + \widetilde{\chi}_{\parallel}h)$, where

$$\widetilde{\chi}_{\parallel}(T) = \left(\frac{\partial m}{\partial h}\right)_{h\to 0} \tag{3.17}$$

[1] Notice that for numerical purposes where μ_{at} is an effective magnetic moment (i.e. it doesn't depends on S) the expression $\mathbf{y}_0 = \beta\mu_{at}\mathbf{H}^{\mathrm{MFA}}/S$ must be used instead of $\mathbf{y}_0 = \beta\gamma\hbar\mathbf{H}^{\mathrm{MFA}}$.

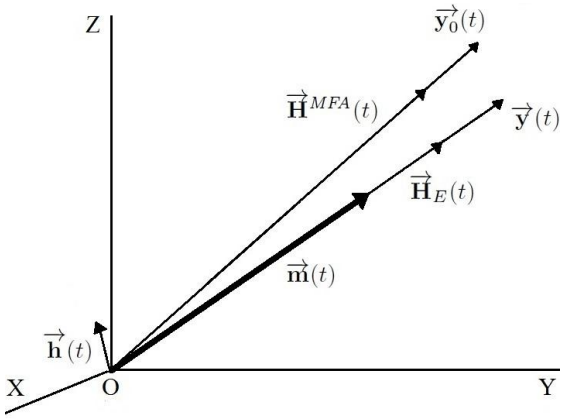

Figure 3.1: Schematic diagram illustrating the relation between the reduced magnetization $\mathbf{m}$ and the vectors $\mathbf{H}_E$, $\mathbf{y}$, $\mathbf{h}$, $\mathbf{H}^{MFA}$ and $\mathbf{y}_0$ at instant t in a non-equilibrium state.

is the reduced linear magnetic susceptibility. Since close to T_c the susceptibility is large, $H_{\rm E} \gg h$ for not too strong external magnetic fields. Further simplification in Eq. (3.16) is obtained using the fact that in stationary dynamic processes y is close to the internal magnetic field direction, ($|y - y_0| \ll y$).[47] With these simplifications Eq. (3.16) is reduced to the qLLB equation in the form

$$\frac{\mathrm{d}\mathbf{m}}{\mathrm{d}t} = -\gamma \mathbf{m} \times \mathbf{H}_{\rm eff} + \gamma\alpha_{\parallel} \frac{\mathbf{m}\cdot\mathbf{H}_{\rm eff}}{m^2}\mathbf{m} - \gamma\alpha_{\perp}\frac{\mathbf{m}\times(\mathbf{m}\times\mathbf{H}_{\rm eff})}{m^2}, \tag{3.18}$$

where $\mathbf{H}_{\rm eff}$ is the effective field given by

$$\mathbf{H}_{\rm eff} = \frac{1}{2\widetilde{\chi}_{\parallel}}\left(1 - \frac{m^2}{m_e^2}\right)\mathbf{m} + \mathbf{h}\ ,\ T < T_c \tag{3.19}$$

where $m_e = B_S(\beta J_0 m_e)$ is the equilibrium magnetization for $h = 0$. The longitudinal susceptibility $\widetilde{\chi}_{\parallel}$ can be evaluated in the MFA at $T < T_c$ as $\widetilde{\chi}_{\parallel} = \mu_{at}\beta B'_S/(1 - \beta B'_S J_0)$ where $B'_S(x) = dB_S/dx$ is evaluated at the equilibrium $B'_S = B'_S(\beta J_0 m_e)$. The parameters $\alpha_{\parallel}$ and $\alpha_{\perp}$ in Eq. (3.18) are the so-called longitudinal and transverse damping parameters, respectively. In the present article we express them in a form which is suitable for the comparison with the classical LLB equation. Below T_c the damping parameters are written

as

$$\alpha_{\parallel} = \lambda \frac{2T}{3T_c} \frac{2q_s}{\sinh(2q_s)} \tag{3.20}$$

$$\alpha_{\perp} = \lambda \left[\frac{\tanh(q_s)}{q_s} - \frac{2T}{3T_c} \left(1 - \frac{K_1^{ph}}{2K_2^{ph}} \right) \right], \tag{3.21}$$

where $q_s = 3T_c m_e/(2(S+1)T)$ and

$$\lambda = K_2^{ph} \frac{(S+1)}{S} \frac{\mu_{at}}{\gamma k_B T}. \tag{3.22}$$

Note that the obtained macroscopic equation has a form similar to the dimensionless Landau-Lifshitz equation, and the damping parameters here are dimensionless as the damping in the LLG equation (corresponding to the Gilbert damping parameter). The relation of the LLB equation to the LLG equation has sense only far from the Curie temperature, as was discussed in Ref. [6].

In Eq. (3.18) all terms are linear in parameter h/H_E. Consequently, in Eqs. (3.20)-(3.22) the field $\mathbf{H}^{\mathrm{MFA}}$ in K_1^{ph} and K_2^{ph} can be evaluated at the equilibrium. Note that for $S \to \infty$ and $K_1^{ph} = K_2^{ph}$, Eqs. (3.20) and (3.21) turns to the damping expressions in the classical LLB equation. [49] This allows us to conclude that λ represents the intrinsic (Gilbert) damping (coupling to the bath) parameter used in the many-spin atomistic approach. Eq. (3.22) therefore relates the microscopic damping and the scattering probabilities through Eqs. (3.7),(3.8),(3.12),(3.13). The temperature dependence of the intrinsic damping is discussed in section III.

Close to T_c, the effective field used in Eq. (3.18) and given by Eq. (3.19) is not very convenient for numerical calculations since $m_e \to 0$ and $\widetilde{\chi}_{\parallel} \to \infty$. To solve this issue we expand the Brillouin function up to the third order in small parameter $x = \beta J_0 m_e$: $B_S(x) \simeq ax/3 - bx^3/45$ and its derivative as $B_S'(x) \simeq a/3 - bx^2/15$ where $a = (S+1)/S$ and $b = ([2S+1]^4 - 1)/(2S)^4$. Thus,

$$m_e^2 \simeq \frac{5A_s}{3}\epsilon \quad , \quad \widetilde{\chi}_{\parallel} = \frac{\mu_{\mathrm{at}} \beta B_S'}{1 - \beta B_S' J_0} \simeq \frac{\mu_{\mathrm{at}}}{J_0} \frac{1}{2\epsilon}, \tag{3.23}$$

where $A_s = 2(S+1)^2/([S+1]^2 + S^2)$ and $\epsilon = (T_c - T)/T_c$ is small close to T_c. Eq. (3.19) can be rewritten as

$$\mathbf{H}_{\mathrm{eff}} = \frac{J_0}{\mu_{\mathrm{at}}} \left(\epsilon - \frac{3m^2}{5A_s} \right) \mathbf{m} + \mathbf{h} \ , \ |\epsilon| \ll 1. \tag{3.24}$$

Above T_c we also re-write the effective field in terms of the longitudinal susceptibility at $T > T_c$, i.e., $\tilde{\chi}_{\parallel} = \mu_{at} T_c/[J_0(T - T_c)]$. This equation is obtained from

Eq. (3.23) and the well-known property[154] of the susceptibility close to T_c, $2\tilde{\chi}_{\parallel,T<T_c}(\epsilon) = \tilde{\chi}_{\parallel,T>T_c}(-\epsilon)$. Thus, above T_c the effective field is written as

$$\mathbf{H}_{\text{eff}} = -\frac{1}{\tilde{\chi}_{\parallel}}\left(1+\frac{3T_c m^2}{5A_s(T-T_c)}\right)\mathbf{m}+\mathbf{h}\ ,\ \frac{T_c}{T-T_c}\gg 1. \tag{3.25}$$

Note that although $\widetilde{\chi}_{\parallel}$ is divergent at T_c as corresponds to the second-order phase transition, the internal fields are the same for any $T_c-\varepsilon$ and $T_c+\varepsilon$ insuring that under the integration of the Eq. (3.18), $\mathbf{m}(t)$ rests continuous through the critical point, as it should be.

On the other hand, in the region just above T_c, $q_s = 0$ and $K_1^{ph} \cong K_2^{ph}$ (see section III), so that the damping parameters become approximately the same and equal to

$$\alpha_{\parallel} = \lambda\frac{2T}{3T_c},\ \ \alpha_{\perp} = \lambda\frac{2T}{3T_c}\left[1+\mathcal{O}(\epsilon)\right],\quad \frac{T_c}{T-T_c}\gg 1 \tag{3.26}$$

where the dependence on the spin value S is included implicitly through λ [see Eq. (3.22)]. For $S\to\infty$ and high temperatures where $K_1^{ph} = K_2^{ph}$ the classical LLB equation above T_c is again recovered.

3.2.3 The qLLB equation for the electron-"impurity" scattering

In this section we derive the qLLB equation for a very simple model for the spin-electron interaction Hamiltonian - the electron-"impurity" scattering model proposed by B. Koopmans *et al.* in Ref. [89] and F. Dalla Longa in Ref. [97] for the laser induced magnetization dynamics. The model assumes an instantaneous thermalization of the optically excited electrons to the Fermi-Dirac distribution. The Hamiltonian considered here consists of a spin system which weakly interacts with a spinless electron bath and it reads

$$\hat{\mathcal{H}}(t) = \hat{\mathcal{H}}_s(t) + \hat{\mathcal{H}}_e + \hat{V}_{s\text{-}e}, \tag{3.27}$$

where $\hat{\mathcal{H}}_s$ is the energy of the spin system, $\hat{\mathcal{H}}_e$ stands for the electron bath energy and $\hat{V}_{s\text{-}e}$ describes the spin-electron interaction energy,

$$\hat{\mathcal{H}}_s(t) = \gamma\mathbf{H}^{\text{MFA}}(t)\cdot\hat{\mathbf{S}}, \tag{3.28}$$

$$\hat{\mathcal{H}}_e = \sum_{\mathbf{k}}(\epsilon_{\mathbf{k}}-\mu)\hat{c}^{\dagger}_{\mathbf{k}}\hat{c}_{\mathbf{k}}, \tag{3.29}$$

$$\hat{V}_{s\text{-}e} = \sum_{\mathbf{k},\mathbf{k'}} V_{\mathbf{k},\mathbf{k'}}(\hat{S}^{+}+\hat{S}^{-})\hat{c}^{\dagger}_{\mathbf{k}}\hat{c}_{\mathbf{k'}}. \tag{3.30}$$

Here $\hat{c}^{\dagger}_{\mathbf{k}}$ ($\hat{c}_{\mathbf{k}}$) is the creation (annihilation) operator which creates (annihilates) an electron with momentum $\mathbf{k}$, $\epsilon_{\mathbf{k}} = \hbar^2 k^2/(2m_{el})$, μ is the chemical potential, m_{el} is the electron mass, $V_{\mathbf{k},\mathbf{k}'}$ describes the scattering amplitude. The vector $\mathbf{H}^{\mathrm{MFA}}$ is given by Eq. (B.3). Note that we have chosen for the spin-electron interaction the minimal model that can capture the main features of the physics involved in the magnetization dynamics. In a slightly more sophisticated approach the electron-phonon scattering may be also included, leading to the two-temperature model. [88] More rigorous approach, the *sp-d* model, allows the description of the ultra-fast magnetization dynamics in magnetic semiconductors[38] and ferromagnetic metals.[57, 101]

Following the same procedure as in the spin-phonon scattering model, we obtain (see Appendix B)

$$\begin{aligned}\frac{d}{dt}\hat{X}^{mn}(t) &\simeq i\gamma H^{\mathrm{MFA}}(t)\,(m-n)\,\hat{X}^{mn}(t)\\ &- \frac{1}{2}\widetilde{W}_2^{el}\left(l_{m-1}^2 + l_{n-1}^2 + e^{-y_0}(l_m^2 + l_n^2)\right)\hat{X}^{mn}(t)\\ &+ \widetilde{W}_2^{el}\left(l_m l_n \hat{X}^{m+1,n+1}(t) + e^{-y_0} l_{m-1} l_{n-1}\hat{X}^{m-1,n-1}(t)\right) \quad (3.31)\end{aligned}$$

where $\widetilde{W}_2^{el} = 2W_2^{el}$ and[1]

$$W_2^{el} = \pi \sum_{\mathbf{k},\mathbf{k}'} |V_{\mathbf{k},\mathbf{k}'}|^2 (1-\widetilde{n}_k)\widetilde{n}_{k'}\delta\left(\gamma H^{\mathrm{MFA}} - \frac{\epsilon_k - \epsilon_{k'}}{\hbar}\right), \quad (3.32)$$

where $\widetilde{n}_k = [\exp(\beta(\epsilon_k - \mu)) + 1]^{-1}$ is the Fermi-Dirac distribution. Comparing Eq. (3.31) and Eq. (3.6) we can see that this mechanism leads to the same formal form for the qLLB equation but with $\eta_y = \eta_z = 0$, $\eta_x = 2$ and W_2^{ph} replaced by W_2^{el}. We notice that since $\eta_z = 0$ we have $K_1^{el} = \widetilde{W}_1^{el} = \eta_z W_1^{el} = 0$, and the damping parameters below T_c are given by

$$\alpha_{\parallel} = \lambda \frac{2T}{3T_c}\frac{2q_s}{\sinh(2q_s)} \quad (3.33)$$

$$\alpha_{\perp} = \lambda\left[\frac{\tanh(q_s)}{q_s} - \frac{2T}{3T_c}\right]. \quad (3.34)$$

Differently to the isotropic spin-phonon scattering qLLB equation, considered above, for the electron-"impurity" scattering qLLB equation in the region just

[1] In our paper Ref. [113] there is an errata in the equation equivalent to Eq. (3.32) and as consequence there are incorrect results in temperature dependence analysis of the relaxation parameters for the electron scattering mechanism. In this thesis we have corrected these erratas.

above T_c the damping parameters are not approximately the same, *i.e.*,

$$\alpha_{\parallel} = \lambda \frac{2T}{3T_c}, \quad \alpha_{\perp} = \lambda \frac{T}{3T_c}\left[1 + \mathcal{O}(\epsilon)\right], \quad \frac{T_c}{T - T_c} \gg 1. \tag{3.35}$$

Note that this is a consequence of the fact that the model (B.48) assumes an anisotropic scattering. In the qLLB model with anisotropic phonon's scattering, defined by $\eta_z = \eta_y = 0$ and $\eta_x = 2$ we obtain the same formal result.

We should point out that the temperature in the qLLB equation for the electron-"impurity" scattering corresponds to the electron bath temperature while for the spin-phonon scattering corresponds to the phonon bath temperature. Therefore, these results validate the coupling of the qLLB equation to the electron bath temperature in the modeling of ultrafast laser induced magnetization dynamics.

3.2.4 The special case with $S = 1/2$.

In the case of $S = 1/2$ we can get more simple forms of the qLLB equation. Indeed, in this case $m(t) = B_{1/2}(y(t)/2) = \tanh(y(t)/2)$ and $m_0(t) = B_{1/2}(y_0(t)/2) = \tanh(y_0(t)/2)$. Moreover, Eq. (3.16) can be further simplified assuming a strong exchange field ($H_E \gg h$) which implies

$$\frac{\mathbf{m} \cdot \mathbf{H}^{MFA}}{m \cdot H^{MFA}} = 1 + O\left(\left[\frac{h}{H_E}\right]^2\right), \tag{3.36}$$

$$(\mathbf{m} \times \mathbf{H}^{MFA})^2 = O\left(\left[\frac{h}{H_E}\right]^2\right), \tag{3.37}$$

and using the vectorial relation $\mathbf{a} \times (\mathbf{b} \times \mathbf{c}) = \mathbf{b}(\mathbf{a} \cdot \mathbf{c}) - \mathbf{c}(\mathbf{a} \cdot \mathbf{b})$, Eq. (3.16) becomes

$$\frac{\mathrm{d}\mathbf{m}}{\mathrm{d}t} = -\gamma \mathbf{m} \times \mathbf{h} - (K_1^{ph} + K_2^{ph})\mathbf{m} + \left[2K_2^{ph} + (K_1^{ph} - K_2^{ph})\frac{m}{m_0}\right]\mathbf{m}_0, \tag{3.38}$$

where $\mathbf{m}_0 = \tanh(y_0/2)\mathbf{H}^{\mathrm{MFA}}/H^{\mathrm{MFA}}$ and K_1^{ph}, K_2^{ph} can be evaluated at equilibrium. In two special cases: (a) when $K_1^{ph} = K_2^{ph}$ or (b) for longitudinal processes only, i.e. for collinear $\mathbf{m}$, $\mathbf{m}_0$ and $\mathbf{H}^{\mathrm{MFA}}$ this equation can be further simplified. In both cases the Eq. (3.38) becomes

$$\frac{\mathrm{d}\mathbf{m}}{\mathrm{d}t} = -\gamma \mathbf{m} \times \mathbf{h} - \frac{\mathbf{m} - \mathbf{m}_0}{\tau_s}, \tag{3.39}$$

where $\tau_s = 1/(2K_2^{ph})$ and the precessional term is zero for the case (b). Eq. (3.39) in Ref. [152] was called the self-consistent Bloch (SCB) equation.

For the case (b) of a pure longitudinal dynamics the Eq. (3.38) becomes

$$\frac{\mathrm{d}m}{\mathrm{d}t} = -\frac{m}{\tau_s}\left[1 - \frac{\tanh\left(\frac{y_0}{2}\right)}{\tanh\left(\frac{y}{2}\right)}\right]. \tag{3.40}$$

Assuming as before that in dynamical processes the deviations between y and y_0 are small i.e. $|y - y_0| \ll y$ we approximate

$$1 - \frac{\tanh\left(\frac{y_0}{2}\right)}{\tanh\left(\frac{y}{2}\right)} = \frac{\tanh\left(\frac{y}{2}\right)}{\tanh\left(\frac{y_0}{2}\right)} - 1 + \mathcal{O}([y - y_0]^2), \tag{3.41}$$

and replacing Eq. (3.41) in Eq. (3.40) one gets

$$\frac{\mathrm{d}m}{\mathrm{d}t} = \frac{m}{\tau_s}\left[1 - m\coth\left(\frac{y_0}{2}\right)\right]. \tag{3.42}$$

We notice that for the case of strong exchange field ($|\mathbf{H}_E| \gg |\mathbf{h}|$) and $S = 1/2$ we can write $y_0/2 \simeq \beta\gamma\ \hbar H_E/2 = mT_c/T$. Eq. (3.42) is the same as used in the M3TM model,[88] in which case τ_s is related to concrete Elliott-Yafet scattering mechanism.

3.3 Temperature dependence of the relaxation parameters

The two main parameters which define the properties of the macroscopic magnetization dynamics can be obtained by linearisation of the LLB equation. Namely, they are the longitudinal relaxation time

$$\tau_\parallel = \frac{\widetilde{\chi}_\parallel}{\gamma\alpha_\parallel}, \tag{3.43}$$

and the transverse relaxation time $\tau_\perp$, i.e. the characteristic time taken by the transverse component of magnetization to relax to the effective field $\mathbf{h}$ including the external field and the anisotropy contributions

$$\tau_\perp = \frac{m_e}{\gamma\, h\alpha_\perp}. \tag{3.44}$$

The corresponding transverse relaxation term of Eq. (3.18) below T_c may be put in the more common form of the macroscopic LLG equation. For this instead of

the normalization of magnetisaion to the total spin polarisation, one should use its normalisation to the saturation magnetization value, i.e. $M_e(T)$. The resulting equation is the same LLB one[6] but with a different damping parameters, called here $\alpha_{\rm LLG}$. This allows to link the transverse magnetization dynamics described by the LLB equation with the macroscopic (Gilbert-like) temperature-dependent damping

$$\tau_{\perp}^{-1} \propto \alpha_{\rm LLG} = \frac{\alpha_{\perp}}{m_e}. \tag{3.45}$$

Note that while both $\alpha_{\parallel}$ and $\alpha_{\perp}$ are continuous through T_C, the parameters $\tau_{\parallel}$ and $\alpha_{\rm LLG}$ diverge at T_c, corresponding to the critical behavior at the phase transition. Next we consider some limiting cases for these characteristic parameters, for relatively low temperatures and temperatures close to T_c.

3.3.1 Longitudinal relaxation time

The longitudinal relaxation time fundamentally depends on the longitudinal susceptibility, $\widetilde{\chi}_{\parallel}$ and the longitudinal damping parameter, $\alpha_{\parallel}$. For the longitudinal susceptibility, using the expansions of the Brillouin function in the corresponding temperature regimes, we obtain

$$\widetilde{\chi}_{\parallel} \cong \frac{\mu_{at}}{k_B T_c} \begin{cases} \frac{T_c}{TS^2} e^{-\frac{3T_c m_e}{T(S+1)}} & T \ll \min(T_c, \frac{T_c}{S}), \\ \frac{T}{9T_c}\left(\frac{S+1}{S}\right) & \frac{T_c}{S} \ll T \ll T_c, \\ \frac{(S+1)}{6S}\frac{T_c}{(T_c-T)} & \frac{T_c}{T_c-T} \gg 1, \\ \frac{(S+1)}{3S}\frac{T_c}{(T-T_c)} & \frac{T_c}{T-T_c} \gg 1. \end{cases} \tag{3.46}$$

Note that the region $T \ll \min(T_c, \frac{T_c}{S})$ does not allow the transition to the classical case ($S \to \infty$). This transition takes place only in the region $T_c/S \ll T \ll T_c$, the latter condition can be satisfied for $S \gg 1$ only. This means that for a given spin $S \gg 1$ the quantum case becomes approximately the classical one only at temperatures $T \gg T_c/S$ (or more exactly $T \gg 3T_c m_e/2S$), this result is obtained from the analysis of the conditions in which the Brillouin function becomes approximately the Langevin one. Using Eqs. (3.46) and the asymptotic behavior of $\alpha_{\parallel}$ in the limiting cases, the longitudinal relaxation time in the limiting cases is given by:

$$\tau_{\parallel} \cong \frac{\mu_{at}}{2\gamma\lambda k_B T_c}\frac{S+1}{S} \begin{cases} \frac{T_c}{TS} & T \ll \min(T_c, \frac{T_c}{S}), \\ \frac{1}{3}\left[1 + \left(\frac{S}{S+1}\right)\frac{T}{T_c}\right] & \frac{T_c}{S} \ll T \ll T_c, \\ \frac{T_c}{2(T_c-T)} & \frac{T_c}{T_c-T} \gg 1, \\ \frac{T_c}{T-T_c} & \frac{T_c}{T-T_c} \gg 1. \end{cases} \tag{3.47}$$

Note that our results are in agreement with the well-known relation, proposed by Koopmans *et al.* [88] that the ultrafast demagnetization time scales with the ratio μ_{at}/T_c. As we pointed out elsewhere, [6] the complete expression involves also the internal coupling to the bath parameter λ, defined by the scattering rate. The two last lines in Eq. (3.47) describe the effect of the critical slowing down near the critical temperature. Furthermore, the relaxation time decreases with the increase of the quantum number S. Note also that the longitudinal relaxation time is twice larger above T_c than below T_c.

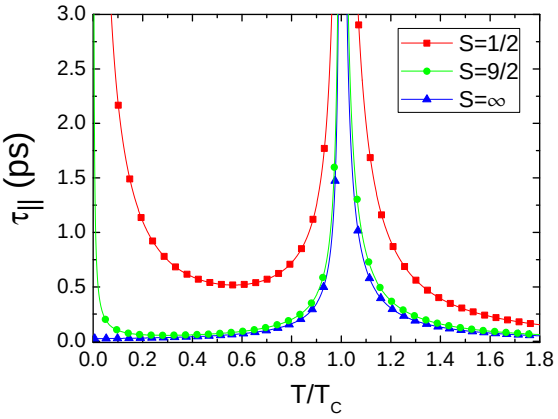

Figure 3.2: Longitudinal relaxation time (Eq. (3.43)) versus temperature using constant $\lambda = 0.02$, $T_c = 650$ K and $\mu_{at} = 0.5\mu_B$ in the three spin cases with $S = 1/2$, $S = 9/2$ and $S = \infty$. The case $S = \infty$ is done by taking the limit $S \to \infty$ in Eq. (3.43), which is equivalent to the classical LLB equation.

Normally in the atomistic simulations one uses a constant in temperature coupling to the bath parameter λ =const. This gives the behaviour for the longitudinal relaxation time that we show in Fig. 3.2 for the two limiting cases $S = 1/2$ and $S = \infty$ and an intermediate case $S = 9/2$. In the whole range of parameters the longitudinal relaxation slows down with the decrease of the spin value S. For a finite spin number S we observe a divergence of the relaxation time at low temperatures which does not happen for $S = \infty$. The intermediate case $S = 9/2$ interpolates between a completely quantum case and a classical case. In this case, all asymptotic behaviors, described by Eqs. (3.47) are observed, the longitudinal relaxation time diverges at low temperatures (as in the quantum case), is almost constant in the intermediate region (as in the classical case) and again diverges approaching to T_c.

The divergence of the longitudinal relaxation time at low temperatures seems to be unphysical although it may be attributed to the freezing of the bath de-

grees of freedom and therefore, impossibility to absorb the energy from the spin system. One should note, however, that taking into account concrete physical mechanisms, the internal damping parameter λ becomes temperature-dependent via Eq. (3.22).

In Fig. 3.3 we present the longitudinal relaxation time as a function of the temperature in constant applied field for the two limiting cases $S = 1/2$ and $S = \infty$. The longitudinal relaxation time was evaluated by direct integration of the qLLB equation with initial conditions $m_0 - m_e = 0.1m_e$. The longitudinal relaxation time is smaller in the classical case than for the quantum one and, as expected, the maximum is displaced for larger values at larger fields. At $T \approx T_C$ the longitudinal relaxation time follows the expression

$$\tau_{||}(H, T = T_C) = \frac{5A_s\mu_{at}}{6\gamma\lambda J_0 m_H^2}, \quad m_H = \left(\frac{5A_s\mu_{at}H}{3J_0}\right)^{1/3} \tag{3.48}$$

where m_H is the field-induced equilibrium magnetization at T_c. Therefore, unlike the statement of Ref. [152], the in-field longitudinal relaxation time, calculated with LLB, does not present any divergence at the Curie temperature.

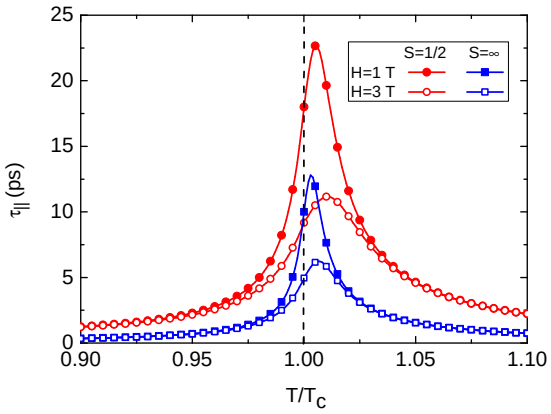

Figure 3.3: The in-field longitudinal relaxation time calculated via direct integration of the qLLB equation with small deviation from the equilibrium. The following parameters are used $T_c = 650$ K, $\mu_{\text{at}} = 0.5\mu_B$, $\lambda = 0.02$ and zero anisotropy constant

3.3.2 Transverse LLG-like damping parameter

For the transverse damping we obtain the following limits

$$\alpha_{LLG} \cong \lambda \begin{cases} \frac{T}{3T_c}\left(2S + \frac{K_1}{K_2}\right) & T \ll \min(T_c, \frac{T_c}{S}), \\ \left[1 - \frac{1}{2S} - \frac{T}{3T_C}\left(1 - \frac{K_1}{K_2}\right)\right] & \frac{T_c}{S} \ll T \ll T_c, \\ \left(1 + \frac{K_1}{K_2}\right)\sqrt{\frac{T_c}{15A_S(T_c - T)}} & \frac{T_c}{T_c - T} \gg 1. \end{cases} \tag{3.49}$$

The temperature dependence of the LLG damping parameter for a constant value of λ and $K_1 = K_2$ is presented in Fig. 3.4 for the two limiting cases $S = 1/2$ and $S = \infty$ and the intermediate case $S = 9/2$. In this case the transverse damping parameter tends to a constant value in the classical case and to a zero value in the quantum case. The transverse relaxation also becomes faster with the increase of the spin number. For simplicity, we have used λ =const and $K_1 = K_2$ in Fig. 3.4 but, as we have seen before, the quantities K_1, K_2 and λ depend on the particular scattering mechanism. Next we study the same limits but taking into account the scattering mechanisms, considered here.

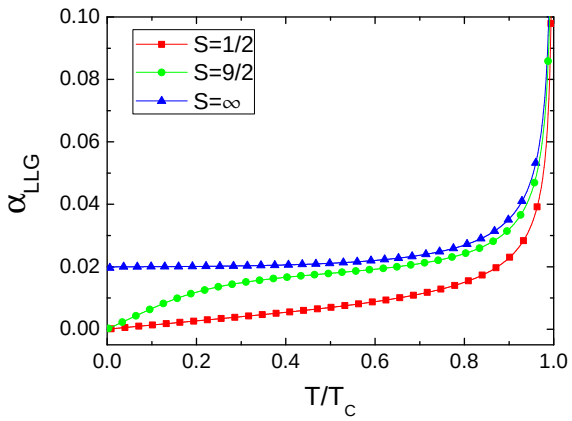

Figure 3.4: LLG damping (Eq. (3.45)) versus temperature using $K_1 = K_2$, constant $\lambda = 0.02$, $T_c = 650$ K and $\mu_{at} = 0.5\mu_B$ for the three spin cases $S = 1/2$, $S = 9/2$ and $S = \infty$. The case $S = \infty$ is done by taking the limit $S \to \infty$ in Eq. (3.45), which is equivalent to the classical case.

3.3.3 Relaxation parameters with temperature-dependent internal scattering mechanisms

3.3.3.1 Scattering via phonons

For the spin-phonon scattering we can evaluate $\widetilde{W}_1^{ph}$ and $\widetilde{W}_2^{ph}$ in Eqs. (3.7), (3.8) using spin-phonon couplings of the type[48, 52]

$$V_{\mathbf{q}} = \frac{\theta_1}{c}\sqrt{\frac{\omega_q}{M}} \quad , \quad V_{\mathbf{qp}} = \theta_2 \frac{\sqrt{\omega_p \omega_q}}{Mc^2} \tag{3.50}$$

where θ_1 and θ_2 are constants, M is the unit cell mass and c is the speed of sound in the material. The evaluation of K_1^{ph} and K_2^{ph} in Eqs. (3.12), (3.13) gives the following result for the isotropic case ($\eta_x = \eta_y = \eta_z = 1$) (see Appendix C)

$$K_1^{ph} \ll K_2^{ph} \simeq \text{const} \quad , \quad k_B T \ll k_B T_D \ll \hbar\gamma H^{\text{MFA}} \tag{3.51}$$

$$K_1^{ph} \simeq K_2^{ph} \propto T^2 \quad , \quad \hbar\gamma H^{\text{MFA}} \ll k_B T_D \ll k_B T \tag{3.52}$$

where T_D is the Debye temperature. Using Eqs. (C.1), (C.2) in Eq. (3.22) we obtain

$$\lambda_{ph} \propto \begin{cases} \frac{1}{T} & k_B T \ll k_B T_D \ll \hbar\gamma H^{\text{MFA}}, \\ T & \hbar\gamma H^{\text{MFA}} \ll k_B T_D \ll k_B T. \end{cases} \tag{3.53}$$

Therefore, if we take into account the temperature dependence of K_1^{ph}, K_2^{ph} and λ_{ph} for the phonon scattering mechanism in Eqs. (3.47) and (3.49) we obtain

$$\tau_{||,ph} \propto \begin{cases} \text{const} & T \ll \min(T_c, \frac{T_c}{S}) \, , \; k_B T \ll k_B T_D \ll \hbar\gamma H^{\text{MFA}} \\ T & \frac{T_c}{S} \ll T \ll T_c \, , \; k_B T \ll k_B T_D \ll \hbar\gamma H^{\text{MFA}} \\ \frac{1}{T|T_c - T|} & \frac{|T_c - T|}{T_c} \ll 1 \, , \; \hbar\gamma H^{\text{MFA}} \ll k_B T_D \ll k_B T, \end{cases} \tag{3.54}$$

and

$$\alpha_{LLG,ph} \propto \begin{cases} \text{const} & T \ll \min(T_c, \frac{T_c}{S}) \, , \; k_B T \ll k_B T_D \ll \hbar\gamma H^{\text{MFA}}, \\ \frac{1}{T} & \frac{T_c}{S} \ll T \ll T_c \, , \; k_B T \ll k_B T_D \ll \hbar\gamma H^{\text{MFA}} \\ \frac{T}{\sqrt{T_c - T}} & \frac{T_c}{T_c - T} \gg 1 \, , \; \hbar\gamma H^{\text{MFA}} \ll k_B T_D \ll k_B T. \end{cases} \tag{3.55}$$

We observe that in the case of a pure phonon mechanism, the longitudinal relaxation time does not diverge at low temperatures. On the other hand, at elevated temperatures the longitudinal magnetization dynamics is slowed down, since close to T_c it is dominated by the divergence of $\widetilde{\chi}_{\parallel}$ [see Eq. (3.46)] rather than by the longitudinal damping parameter, $\alpha_{\parallel} \propto T + \mathcal{O}(\epsilon)$. However, since $\tau_{\perp}^{-1} \propto \alpha_{\text{LLG}}$ we see that at high temperature the transverse magnetization dynamics becomes faster as the temperature gets closer to T_c.

3.3.3.2 Scattering via electrons

For the electron-"impurity" scattering we have found before that $K_1^{el} = 0$, but we should still evaluate K_2^{el}. For this task, we assume that $|V_{\mathbf{k},\mathbf{k}'}|^2 = \mathcal{V} = \text{const}$ and a constant density of states around the Fermi level $D(\epsilon_F)$ (as in Refs. [89] and [97]). With these assumptions, we arrive to (see Appendix C)

$$K_2^{el} = \frac{\pi \mathcal{V} \hbar^2 D(\epsilon_F)^2 \gamma H^{\text{MFA}}}{4} e^{-y_0} \coth\left(\frac{y_0}{2}\right), \tag{3.56}$$

where ϵ_F is the Fermi energy,

$$D(E) = \frac{\Omega}{2\pi^2}\left(\frac{2m_{el}}{\hbar^2}\right)^{\frac{3}{2}}\sqrt{E} \tag{3.57}$$

is the density of states for a free electron gas (taking into account the spin degeneracy) and Ω is the system volume. Therefore, the following limiting cases for K_2^{el} are obtained:

$$K_2^{el} = \frac{\pi \mathcal{V} \hbar^2 D(\epsilon_F)^2 \gamma H^{\text{MFA}}}{4} \begin{cases} e^{-\frac{\hbar\gamma H^{\text{MFA}}}{k_B T}} & k_B T \ll \hbar\gamma H^{\text{MFA}} \\ \frac{2k_B T}{\hbar\gamma H^{\text{MFA}}} & \hbar\gamma H^{\text{MFA}} \ll k_B T \end{cases},$$

and then from Eq. (3.22) we obtain

$$\lambda_{el} \propto \begin{cases} \frac{1}{T} e^{-\frac{\hbar\gamma H^{\text{MFA}}}{k_B T}} & k_B T \ll \hbar\gamma H^{\text{MFA}}, \\ \text{const} & \hbar\gamma H^{\text{MFA}} \ll k_B T. \end{cases} \tag{3.58}$$

And consequently, from Eqs. (3.47) and (3.49) we find

$$\tau_{||,el} \propto \begin{cases} e^{-\frac{\hbar\gamma H^{\text{MFA}}}{k_B T}} & T \ll \min(T_c, \frac{T_c}{S}),\ k_B T \ll \hbar\gamma H^{\text{MFA}} \\ T e^{-\frac{\hbar\gamma H^{\text{MFA}}}{k_B T}} & \frac{T_c}{S} \ll T \ll T_c,\ k_B T \ll \hbar\gamma H^{\text{MFA}} \\ \frac{1}{|T_c - T|} & \frac{|T_c - T|}{T_c} \ll 1,\ \hbar\gamma H^{\text{MFA}} \ll k_B T, \end{cases} \tag{3.59}$$

and

$$\alpha_{LLG,el} \propto \begin{cases} e^{-\frac{\hbar\gamma H^{\text{MFA}}}{k_B T}} & T \ll \min(T_c, \frac{T_c}{S}),\ k_B T \ll \hbar\gamma H^{\text{MFA}}, \\ \frac{1}{T} e^{-\frac{\hbar\gamma H^{\text{MFA}}}{k_B T}} & \frac{T_c}{S} \ll T \ll T_c,\ k_B T \ll \hbar\gamma H^{\text{MFA}} \\ \frac{1}{\sqrt{T_c - T}} & \frac{T_c}{T_c - T} \gg 1,\ \hbar\gamma H^{\text{MFA}} \ll k_B T. \end{cases} \tag{3.60}$$

We observe that $\tau_{||,el}$ and $\alpha_{LLG,el}$ decrease very rapidly for the case $T \ll \min(T_c, T_c/S)$ as $T \to 0$, however for the phonon scattering mechanism they

tend to a constant. Another interesting difference is the temperature dependence of α_{LLG} for the case $T_c/S \ll T \ll T_c$, as $T \to 0$ for the electron scattering $\alpha_{LLG,el}$ decreases while for the phonon scattering $\alpha_{LLG,ph}$ increases. We can conclude that as $T \to 0$ the electron scattering mechanism makes faster the longitudinal relaxation and slower the transverse one ($\tau_\perp \propto 1/\alpha_{LLG}$).

3.4 Numerical comparison between classical and quantum cases

In this section we compare the qLLB equation for $S = 1/2$ and its classical limit ($S \gg 1$). We use the qLLB equation given by Eq. (3.18) for the isotropic phonon scattering mechanism and the high temperature case ($K_1 = K_2$). We note that for a proper comparison between classical and quantum cases, one should take the same magnetic moment μ_{at} and Curie temperature T_c (normally obtained from the experimental measurements) and not vary them with the spin number S. In the opposite case the magnetic moment would increase with S and the Curie temperature decrease and the classical modeling results will not be recovered.

In our simulations we set $\gamma = 1.76 \times 10^{11}$ rad s^{-1} T^{-1}, $T_c = 650$ K, $\mu_{\text{at}} = 0.5\mu_B$ and $\lambda = 0.02$ and zero anisotropy constant. Note that in order to be consistent with the comparison of the SCB with $S = 1/2$ (indistinguishable from the qLLB with $S = 1/2$) and the classical LLB equation, presented in Ref. [153], we choose similar parameters and situations. In Fig. 3.5 we present the dynamics of m_z component for $S = 1/2, \infty$ and for different temperatures where the initial magnetization is set to $\mathbf{m} = (0.05, 0, 0.2)$ and the external applied field is $H_z = -1$T. The initial response is slower for $S = 1/2$ than for $S = \infty$ in agreement with the behavior of the longitudinal relaxation time, presented in Fig. 3.2. Note the variety of different functional responses and that for the two cases below T_c they cannot be represented as a one-exponential relaxation due to the nonlinearity of the LLB equation, prominent for T close to T_c.

In Fig. 3.6 we present the relaxation of m_z at $T = 649$ K, with and without an external field ($H_z = -1$T) where the initial magnetization is set to $\mathbf{m} = (0.05, 0, 0.2)$. We use the qLLB equation for $S = 1/2$ and $S = \infty$ for comparison. Note that again the dynamics is faster for $S = \infty$ than for $S = 1/2$. Since the qLLB and the SCB equations with $S = 1/2$ are the same, we conclude that the classical LLB equation gives a faster relaxation than the SCB equation, contrarily to the results presented in Ref. [153].

Similar to Ref. [153] we define the reversal time as time elapsed between the initial state and the instant of time at which the magnetization begins to reverse

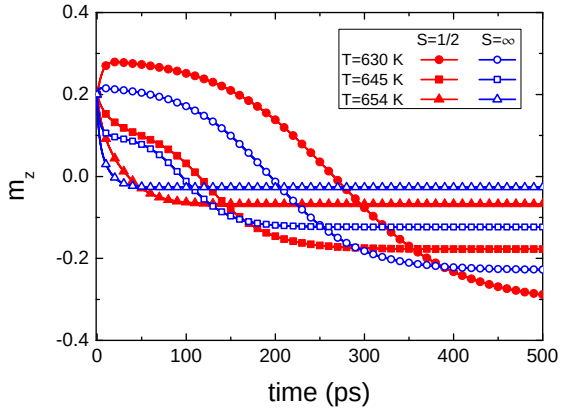

Figure 3.5: The dynamics of m_z component for the longitudinal plus transverse dynamics at 630 K, 645 K and 654 K for $S = 1/2, \infty$ where the initial magnetization is $\mathbf{m} = (0.05, 0, 0.2)$ and the applied field is $H_z = -1$T.

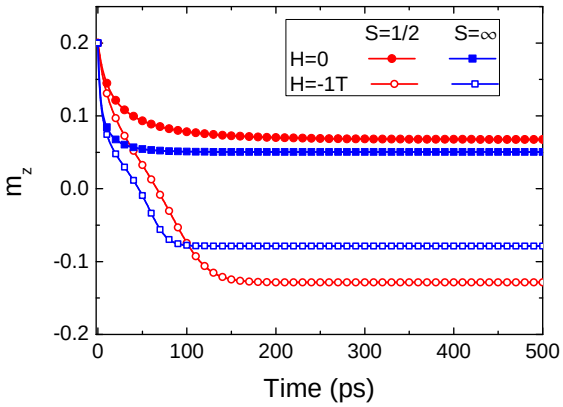

Figure 3.6: The dynamics of m_z component at $T = 649$ K without and with external field $H_z = -1$T for $S = 1/2, \infty$ where the initial magnetization is $\mathbf{m} = (0.05, 0, 0.2)$.

its direction, *i.e.* crosses $m_z = 0$ point. In Fig. 3.7 we present the reversal time versus temperature for $S = 1/2, \infty$ and for two different initial conditions: (i) pure longitudinal dynamics where the initial magnetization is set to $\mathbf{m} = (0, 0, 0.2)$ and (ii) longitudinal plus transverse dynamics where the initial magnetization is set to $\mathbf{m} = (0.05, 0, 0.2)$. We observe that the reversal time (for both the quantum and the classical case) does not present any discontinuity across the Curie temperature and is smaller for $S = \infty$ than for $S = 1/2$, in contradiction to the results

presented in Ref. [153] where the SCB and the classical LLB equation were compared. As was pointed out in several previous publications, [13, 51, 77] slightly below T_c the magnetization reversal becomes linear, *i.e.* occurs by a pure change of the magnetization magnitude. This path becomes not energetically favorable with the decrease of the temperature, the reversal path becomes elliptical and then completely precessional.

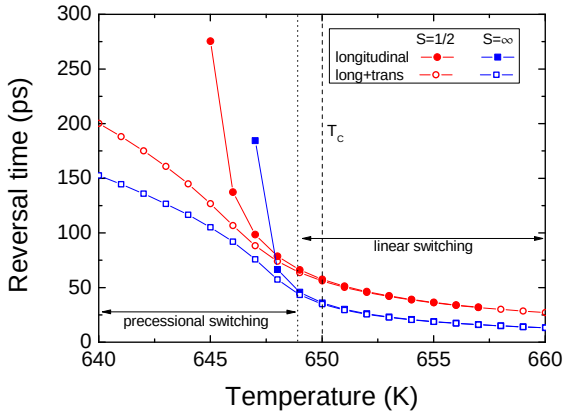

Figure 3.7: Reversal time versus temperature for $S = 1/2, \infty$ and $S = \infty$. In the pure longitudinal dynamics the initial magnetization is set to $\mathbf{m} = (0, 0, 0.2)$ and in the longitudinal plus transverse dynamics the initial magnetization is set to $\mathbf{m} = (0.05, 0, 0.2)$.

3.5 Conclusions

In this chapter we have presented the derivation of the qLLB equation for two simple scattering mechanisms: based on the phonon and the electron-impurity spin-dependent scattering. While the spin-phonon interaction has been historically thought as the main contribution to the damping mechanism (for transverse magnetization dynamics), for the ultrafast laser induced magnetization dynamics the electron mechanism is considered to be the most important contribution. At the same time, the induction of the ultrafast magnetization dynamics via acoustic excitation is becoming increasingly important so that the importance of the phonon-mediated mechanism is still relevant for femtomagnetism. Although in the present work we have only considered the simplest form for the spin-phonon and -electron interaction Hamiltonian, the derivation could be generalized to more complex situations. The form of equation (3.18) is sufficiently general and at

present can be used for modeling of most of the experimental cases, understanding that the parameter λ contains all necessary scattering mechanisms and can be extracted from experimental measurements as it was done before, [6, 9, 88, 139] similar to the Gilbert damping parameter in standard micromagnetic modeling. Importantly, the recently proposed self-consistent Bloch equation [152, 153] and the M3TM model are contained in the qLLB model. [88]

The derivation involves two important approximations: the Markov and the secular. Their validity could be questionable for the ultrafast processes and in the future these approximations should be investigated. At the same time, our comparisons with experiments for Ni[9], Gd[139] and FePt[107] have shown a very good agreement.

The derivation has allowed us to relate the classical internal coupling to the bath parameter λ, used in the atomistic spin model simulations, to the scattering probabilities which could be evaluated on the basis of the *ab-initio* electronic structure calculations, providing the route to a better scheme of the multi-scale modeling of magnetic materials. The temperature dependence of λ will depend on the nature of the concrete scattering mechanism. In the present work we have shown that this parameter is temperature dependent. At the same time, the use of the temperature-independent microscopic damping (coupling to the bath parameter) for laser-induced magnetization dynamics, as it is normally done in the atomistic simulations, is probably reasonable. Our results also include the temperature dependence of macroscopic relaxation parameters: the longitudinal relaxation and the LLG-like transverse damping. We have shown that both transverse and longitudinal relaxation are faster in the classical case than in the quantum one.

The comparison between the classical and the quantum LLB equations has been done in the conditions of the same magnetic moment and the Curie temperature, as corresponds to the spirit of the classical atomistic modeling. Unlike the statement appearing in Ref. [153], the magnetization is continuous when going through T_c, the same happens with the reversal time. In the considered case in this work, the reversal time is smaller in the classical case than in the quantum one, although our investigation shows that this result depends on the system parameters.

The obtained micromagnetic approach can be used for modeling of large structures, such as dots and stripes up to micron-sizes, under the conditions where the use of the LLB equation is necessary.

Conclusiones en español

En este capítulo hemos presentado la derivación de la ecuación de qLLB para dos modelos sencillos basados en la interacción del espín con fonones y con electrones. Mientras que históricamente se ha considerado que la interacción entre espines y fonones es la principal responsable de la relajación magnética transversal, en dinámica magnética ultrarrápida la principal interacción es entre espines y electrones. Al mismo tiempo, la interacción entre espines y fonones también puede ser relevante en la dinámica ultrarrápida cuando ésta es inducida acústicamente. Aunque en este trabajo sólo hemos considerado dos modelos muy sencillos de interacción entre espines con fonones y electrones, estos cálculos se podrían generalizar a modelos más complejos. La forma de la ecuación (3.18) es suficientemente general y puede usarse para modelizar la mayoría de casos experimentales, entendiendo que el parámetro λ contiene todos los mecanismos de interacción necesarios y que pueden ser obtenidos experimentalmente como se ha realizado anteriormente[6, 9, 88, 139], de forma similar a lo que ocurre en la modelización basada en el micromagnetismo estándar con el parámetro de damping de Gilbert. Además, hemos demostrado que la ecuación qLLB contiene las recientemente propuestas ecuaciones de SCB[152, 153] y M3TM[88].

La derivación de la ecuación de qLLB usa dos importantes aproximaciones: la de Markov y la secular. La validez de ambas es cuestionable para procesos de dinámica ultrarrápida, por tanto, en el futuro estas aproximaciones deberían ser investigadas. La comparación entre los resultados obtenidos con la ecuación qLLB y los experimentos en Ni[9], Gd[139] y FePt[107] muestran un gran acuerdo.

Por otro lado, la derivación de la ecuación de qLLB nos ha permitido relacionar el acoplo interno con el baño térmico clásico, que se usa en simulaciones atomísticas, con las probabilidades de interacción que pueden ser evaluadas mediante el cálculo de estructura electrónica, lo que ofrece una mejor ruta para la modelización multiescala de materiales magnéticos. La dependencia con la temperatura de λ dependerá del mecanismo concreto de interacción como hemos visto en este trabajo. Además, hemos demostrado que la relajación transversal y longitudinal es más rápida en el caso clásico que en el cuántico.

El modelo micromagnético basado en la ecuación de qLLB que hemos estudiado puede ser utilizado para describir el comportamiento magnético de estructuras de tamaño del orden de micrometros.

4

Micromagnetic modeling of ultrafast magnetization dynamics in FePt

4.1 Introduction and motivation

The FePt $L1_0$ alloy represents the most important material for novel concepts in magnetic recording due to its high magnetic anisotropy, which ensures long-time thermal stability of nanometer sized bits. Thin films of FePt with perpendicular anisotropy and small grain sizes are the most promising candidates for heat-assisted magnetic recording, which could reach storage densities beyond 1 Tb/inch^2. Patterning continuous FePt into individual bits can in principle extend recording densities to 100 Tb/inch. The ultimate magnetic recording applications will also require faster bit switching and a deeper insight into the processes involved. However, non-deterministic fractioning in ultrafast magnetization reversal can limit the switching speed in recording schemes, and thus has inspired fundamental research for more than a decade. Recently, a new concept of ultrafast all-optical magnetic recording with an unprecedented switching timescale below 1 ps was suggested. This opened new possibilities to reduce the speed limit established by the spin-orbit coupling timescale to that governed by the much stronger exchange interaction.

4.2 Ultrafast magnetization dynamics in FePt using linearly polarized laser pulses

Motivated by the experimental results in FePt of our partners in University of Göttingen (Germany) lead by Prof. M. Münzenberg [106], we have modeled their experimental results in laser induced ultrafast magnetization dynamics using the qLLB equation described in chapter 3 coupled to the 2TM described in section 2.4.

4.2.1 Experimental measurements of ultrafast magnetization dynamics in FePt

In this section we briefly describe the experiment in FePt of our partners in University of Göttingen (Germany) lead by Prof. M. Münzenberg [106]. They studied a 3 nm-thick continuous FePt thin layer, it has a Curie temperature of $T_c = 650$ K, a saturation magnetization at $T = 0$ K of $M_s(0) = 1070$ emu/cm^3 and a perpendicular anisotropy at $T = 0$ K of $K(0) = 2.2 \cdot 10^7$ erg/cm^3.

To heat the sample they used ultrashort linearly polarized laser pulses where the magnetization dynamics was measured using the time-resolved magneto-optical Kerr effect ($\Delta\theta_K/\theta_{K,0}$). The relaxation time τ_M was extracted from the experimental data using the three temperature model (3TM) (Fig. 4.1 b)). Simultaneously, the time-resolved reflectivity ($\Delta R/R$) was determined and it was fitted to an exponential function $R(t) \sim \exp(-t/\tau_E)$ which allows to estimate the relaxation time for the electronic temperature τ_E (Fig. 4.1 a)).

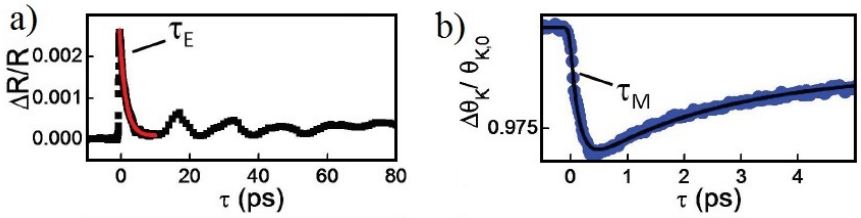

Figure 4.1: a) The reflectivity dynamics from which the exponential decay τ_E is obtained, b) Experimental measurement of ultrafast magnetization dynamics in FePt. Solid line: analytical three temperature model to obtain τ_M.

4.2.2 Micromagnetic modeling

As it was explained in section 2.5 the micromagneic modeling of the ultrafast magnetization dynamics of FePt thin film is based on the qLLB equation coupled

to the 2TM. In particular, we use a multi macro-spin model described by the qLLB equation where the thermal fluctuations are included. This model uses one layer of cubic discretization elements with lateral size $\triangle = 3$ nm, thus, with a volume $V = \triangle^3$ as we show in Fig.4.2.

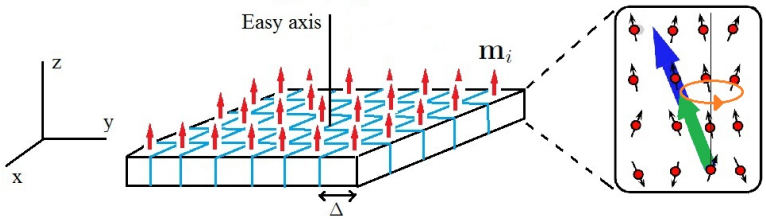

Figure 4.2: Illustration of the multi macro-spin model.

For each cube we write the stochastic LLB equation, describing its average spin polarization $\mathbf{m}_i$, in the following form:

$$\begin{aligned}\frac{d\mathbf{m}_i}{dt} &= -\gamma\left[\mathbf{m}_i \times \mathbf{H}^i_{\text{eff}}\right] + \frac{\gamma\alpha_\parallel}{m_i^2}\left(\mathbf{m}_i \cdot \mathbf{H}^i_{\text{eff}}\right)\mathbf{m}_i \\ &- \frac{\gamma\alpha_\perp}{m_i^2}\left[\mathbf{m}_i \times \left[\mathbf{m}_i \times \left(\mathbf{H}^i_{\text{eff}} + \boldsymbol{\zeta}_{i,\perp}\right)\right]\right] + \boldsymbol{\zeta}_{i,ad},\end{aligned} \tag{4.1}$$

where $m_i = M_i/M_s(0)$ and the effective fields are given by

$$\mathbf{H}^i_{\text{eff}} = \mathbf{H} + \mathbf{H}_{i,d} + \mathbf{H}_{i,\text{EX}} + \mathbf{H}_{i,A} + \begin{cases} \frac{1}{2\tilde{\chi}_\parallel}\left(1 - \frac{m_i^2}{m_e^2}\right)\mathbf{m}_i & T \lesssim T_c \\ -\frac{1}{\tilde{\chi}_\parallel}\left(1 + \frac{3T_c m_i^2}{5a_s(T-T_c)}\right)\mathbf{m}_i & T \gtrsim T_c \end{cases} \tag{4.2}$$

where $a_s = 2(S+1)^2/([S+1]^2 + S^2)$, $\mathbf{H}$ is the applied magnetic field, $\mathbf{H}_{i,d}$ is the demagnetizing field which for a saturated thin film reads (cgs units)

$$\mathbf{H}_{i,d} = -4\pi M_s(0) m_{i,z}\mathbf{e}_z. \tag{4.3}$$

The field $\mathbf{H}_{i,\text{EX}}$ describes the exchange stiffness interaction between macro-spins and it is given by

$$\mathbf{H}_{i,\text{EX}} = \frac{2A_i(T)}{m_i^2 M_s(0)\triangle^2}\sum_{\langle i,j\rangle}(\mathbf{m}_j - \mathbf{m}_i) \tag{4.4}$$

where $\langle i,j\rangle$ means a sum over neighbours and $A_i(T)$ is the exchange stiffness paramater, for FePt it was calculated that $A_i(T) = A_i(m_i) = 2.2\cdot 10^{-6} m_i^{1.76}$ erg/cm [140]. $\mathbf{H}_{i,A}$ is the anisotropy field given by

$$\mathbf{H}_{i,A} = -\frac{1}{\tilde{\chi}_{\perp,i}}\left(m_{i,x}\mathbf{e}_x + m_{i,y}\mathbf{e}_y\right) \tag{4.5}$$

the reduced longitudinal and transverse susceptibilities are

$$\widetilde{\chi}_{\parallel} = \begin{cases} \frac{\mu_{at}\beta B'_S}{1-\beta J_0 B'_S} & T \lesssim T_c \\ \frac{\mu_{at} T_c}{J_0(T-T_c)} & T \gtrsim T_c \end{cases} \tag{4.6}$$

$$\tilde{\chi}_{\perp,i} = \frac{M_s(0) m_i^2}{2K_i(T)} \tag{4.7}$$

where $K_i(T)$ is the anisotropy constant, for FePt it was found that $K_i(T) = K(0)m_i^{2.1}$[111], B'_S is the derivative of the Brillouin function evaluated at $\beta J_0 m_e$, $\beta = 1/(k_B T)$,the relationship between J_0 and T_c is given by $T_c = [(S+1)J_0]/[3k_B S]$. The longitudinal and transverse relaxation parameters are

$$\alpha_{\parallel} = \lambda \frac{2T}{3T_c} \cdot \begin{cases} \frac{2q_s}{\sinh(2q_s)} & T \lesssim T_c \\ 1 & T \gtrsim T_c \end{cases} \tag{4.8}$$

$$\alpha_{\perp} = \lambda \cdot \begin{cases} \left[\frac{\tanh(q_s)}{q_s} - \frac{T}{3T_c} \right] & T \lesssim T_c \\ \frac{2T}{3T_c} & T \gtrsim T_c \end{cases} \tag{4.9}$$

where $q_s = [3T_c m_e]/[2(S+1)T]$ and λ is the microscopic relaxation parameter. In this model we consider that λ is temperature independent and its value is found as a fitting parameter to the experimental magnetization dynamics. The equilibrium magnetization $M_e(T) = M_s(0)m_e$ is obtained using the MFA where m_e is the solution of the equation $m_e = B_S(\beta J_0 m_e)$ where $B_S(x)$ is the Brillouin function. For FePt it was found that the best fit for m_e is obtained with $S = 3/2$ [100]. The values of T_c, $M_s(0)$ and $K(0)$ used in the model are the same as the experimental ones introduced in the previous section. The stochastic fields $\boldsymbol{\zeta}_{i,\perp}$ and $\boldsymbol{\zeta}_{i,ad}$ are given by [42]

$$\left\langle \zeta^k_{i,\perp}(0)\zeta^l_{j,\perp}(t) \right\rangle = \frac{2\gamma k_B T \left(\alpha_{\perp} - \alpha_{\parallel}\right)}{M_s(0)\, \triangle^3\, \alpha_{\perp}^2} \delta_{ij}\delta_{kl}\delta(t) \tag{4.10}$$

$$\left\langle \zeta^k_{i,ad}(0)\zeta^l_{j,ad}(t) \right\rangle = \frac{2\gamma k_B T \alpha_{\parallel}}{M_s(0)\triangle^3} \delta_{ij}\delta_{kl}\delta(t) \tag{4.11}$$

where i and j denote macro-spin index, k and l denote the Cartesian components x, y and z.

Notice that we consider that $\alpha_{\parallel}$ is the same as the one obtained in the isotropic phonon scattering model at elevated temperature where $K_1^{ph} \simeq K_2^{ph}$. However, in the modeling of ultrafast magnetization dynamics in FePt we assume that the magnetic system is coupled to the electron bath, that is, the temperature in the qLLB equation corresponds to the electron's temperature ($T = T_e$) which is obtained from the 2TM described in section 2.4.

4.2.3 Comparison between modeling and experiment

The fitting of the qLLB+2TM to the experimental relaxation times τ_E and τ_M is not unique. We have performed the modeling of the ultrafast magnetization dynamics in FePt using qLLB+2TM equations for two different set of paramaters which are presented in Table 4.1. [1] As we show in Fig. (4.3) both set of paramaters lead to similar values of τ_E and τ_M as in the experiment. However, the electronic temperature and magnetization dynamic obtained using the qLLB+2TM with each set of parameters are different as we show in Fig. 4.4. We see that the set I leads to higher electronic temperatures (Fig. 4.4 a)) than the set II

Parameter set	γ_e (J/m^3K^2)	λ	$\tilde{I}_0$ $(s^{-1}m^{-1})$	G_{e-ph} $(\mathrm{W/m^3K})$	C_{ph} $(\mathrm{Jm^{-3}K^{-1}})$	τ_{ph} (ps)
I	110	0.01	$5 \cdot 10^{18}$	$1.5 \cdot 10^{17}$	$3.7 \cdot 10^{5}$	340
II	1700	0.1	$3 \cdot 10^{19}$	$1.8 \cdot 10^{18}$	$3.3 \cdot 10^{6}$	340

Table 4.1: Overview of parameter set I for the simulation in the case of high electron temperature for FePt and set II for a high value of γ_e (large density of states at the Fermi level) which leads to low electronic temperature.

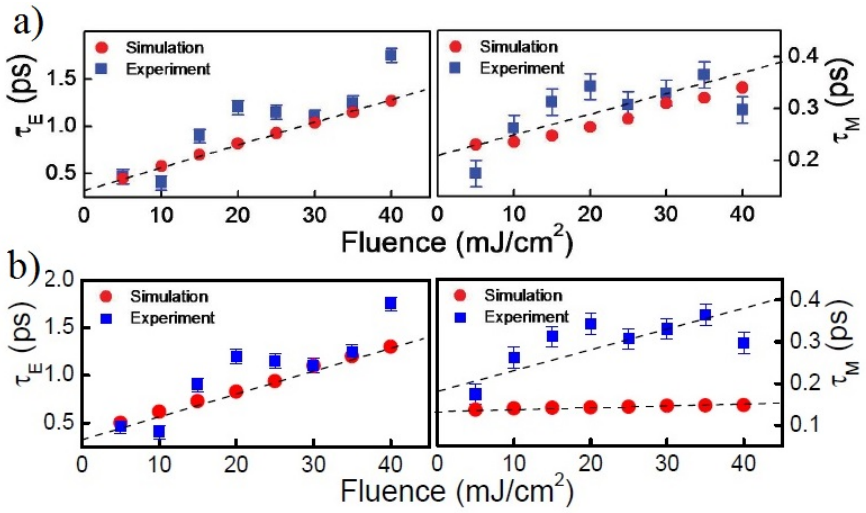

Figure 4.3: Relaxation times τ_E and τ_M as function of the laser fluence obtained experimentally (blue squares) and numerically (red dots) for the parameters a) set I and b) set II given by Table 4.1.

[1] In our paper Ref. [107] there is an errata in the value of the parameter I_0. In this thesis we have corrected this errata.

(Fig. 4.4 b)) mainly due to the small value of γ_e (which implies a small electron's heat capacity C_e), as consequence of these electron temperature dynamics when the fluence is increased a transition from type I (fast remagnetization) to type II (slow remagnetization) magnetization dynamic is obtained (Fig. 4.4 d)) similar to the experiment (Fig. 4.4 c)). The transition from fast to slow remagnetization at high fluences is because the electronic temperature is very close to T_c where the phenomena call critical slowdown takes place (where $\tau_{\parallel} \propto 1/|T - T_c|$, see Eq. (3.47)). On the other hand, the set II leads to lower electronic temperatures (Fig. 4.4 b)) and despite the fact that the demagnetization process during the first picosecond is similar to the experiment the remagnetization is much faster and no transition from type I to type II is observed (Fig. 4.4 e)). One possible explanation of these high electronic temperatures could be that Fe becomes more noble in the FePt $L1_0$ compound [14, 98], which makes the electron's specific heat more similar to Au and Cu with a small γ_e.

Finally, some differences between the magnetization dynamics of the experiment and the model is observed. We see that in the experiment the demagnetization after the first picosecond is smaller for fluences 35 and 40 mJ/cm^2 than for 30 mJ/cm^2 while in the model the demagnetization always increases with the fluence. One possible explanation is that in the experiment the magnetization does not recover in between two laser pulses (e.g. 4 μs pulse repetition) at high fluences, therefore this could lead to a lower normalized demagnetization, however in the simulation the same initial magnetic state is used for all fluences. Moreover, in our micromagnetic simulation we have observed the formation of bubbles (Fig. 4.5 a)) and stripes (Fig. 4.5 b)) during the remagnetization process at high fluences (where system is almost demagnetized after the first ps) which are quite stable.

4.2.4 Magnetization dynamics in high external magnetic fields

In this section we present some numerical results using the qLLB+2TM with the parameter set I in Table 4.1 where high external magnetic field are also used. We consider a system consisting of 50x50x1 macrospins where each one represents the average magnetization of a cubic cell with a volume equal to 3 nm^3. Moreover, periodic boundary conditions in the x and y axis are also included.

In Fig. 4.6 we show the magnetization dynamics with a laser pulse fluence $F = 40$ mJ/cm^3 for different applied fields along the z axis: $H_z = 0, -1, -3, -5$ T. We see that the switching of the magnetization takes place only for the applied fields $H_z = -3, -5$ T. However, we observe that the reversal time t_{rev} (defined

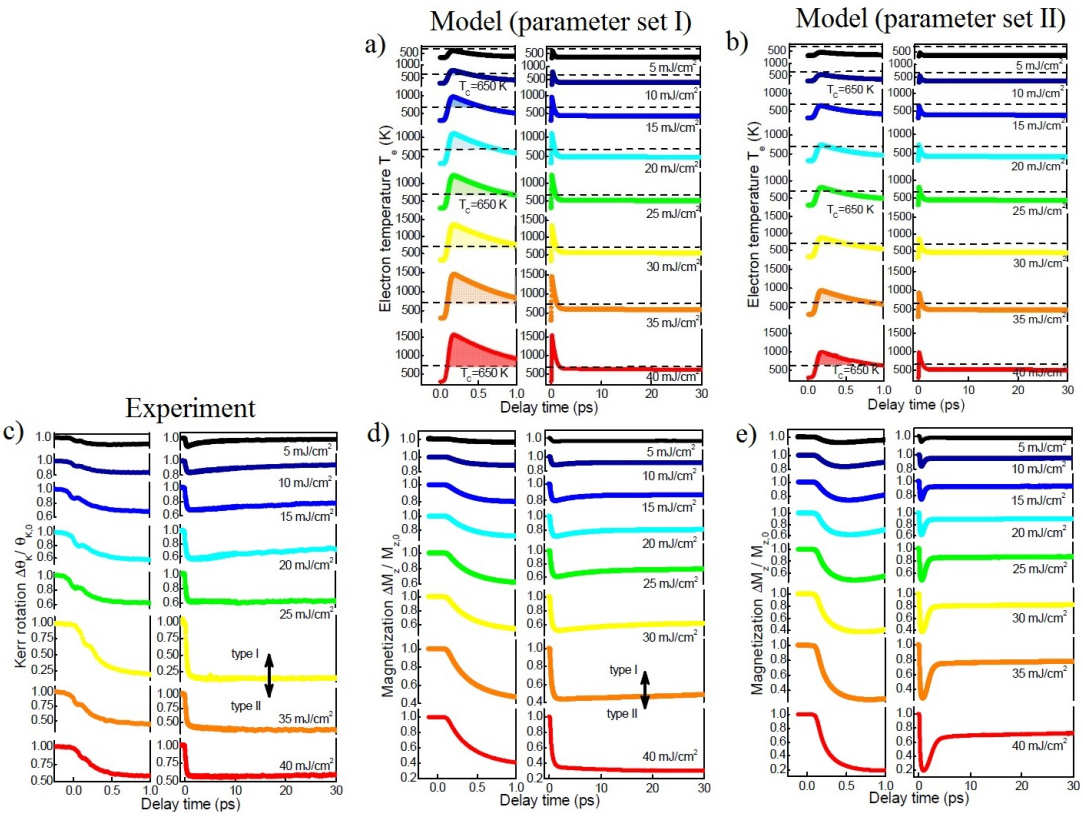

Figure 4.4: a) Electronic temperature dynamics obtained using the 2TM with set I in Table 4.1, b) electronic temperature dynamics obtained using the 2TM with set II in Table 4.1, c) experimental magnetization dynamics measured using the time-resolved magneto-optical Kerr effect ($\Delta\theta_K/\theta_{K,0}$), d) magnetization dynamics obtained using the qLLB+2TM with set I in Table 4.1, e) magnetization dynamics obtained using the qLLB+2TM with set II in Table 4.1.

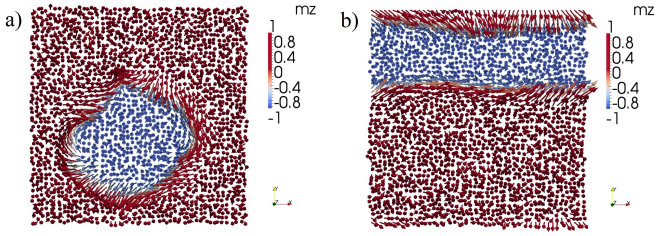

Figure 4.5: a) Bubble b) stripe formed during the remagnetization process at high fluences.

as time elapsed between the initial state and the instant of time at which the z component of the mean magnetization begins to reverse its direction, *i.e.* crosses

$m_z = 0$ point) for each case is very different, in fact, we have that for $H_z = -3$ T the reversal time is $t_{\rm rev} \simeq 0.65$ ns while for $H_z = -5$ T we obtain $t_{\rm rev} \simeq 0.07$ ns.

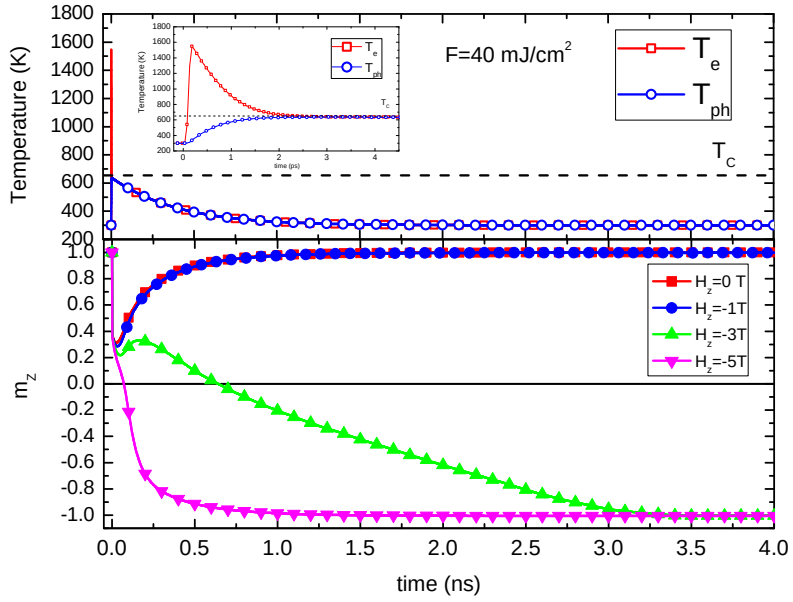

Figure 4.6: (Up) Electron and phonon temperature dynamics with a laser pulse fluence $F = 40$ mJ/cm^3. (Bottom) Normalized average z component of the magnetization (m_z) versus time for different applied fields along the z axis: $H_z = 0, -1, -3, -5$ T.

This is because the external applied field of $H_z = -3$ T can not prevent the recovery of the average z component of the magnetization (m_z) in the up direction between $t \simeq 0.05$ ns and $t \simeq 0.16$ ns where a large magnetic domain pointing in the up direction is formed (see Figs. 4.7 a) and b)). These domains are reversed progressively leading at the final stage to a bubble (see Figs. 4.7 c) and d)) which has a propagation velocity of $v \simeq 250$ m/s and finally it disappears completely at $t \simeq 4$ ns. On the other hand, the external applied field of $H_z = -5$ T is strong enough to avoid the formation of large magnetic domain pointing in the up direction (see Fig. 4.8). We should point out that in all the cases ($H_z = 0, -1, -3, -5$ T) the average transverse magnetization (m_x, m_y) are less than 0.1 during the dynamics showing that there is not a collective precessional motion.

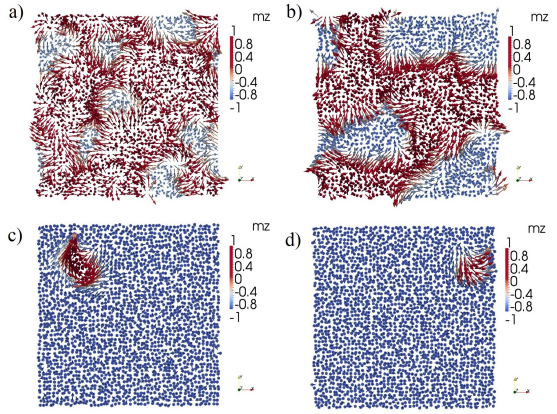

Figure 4.7: Snapshots of system with $F = 40$ mJ/cm^3 and $H_z = -3$ T at times: a) $t = 0.25$ ns, b) $t = 0.5$ ns, c) $t = 3.2$ ns, d) $t = 3.6$ ns.

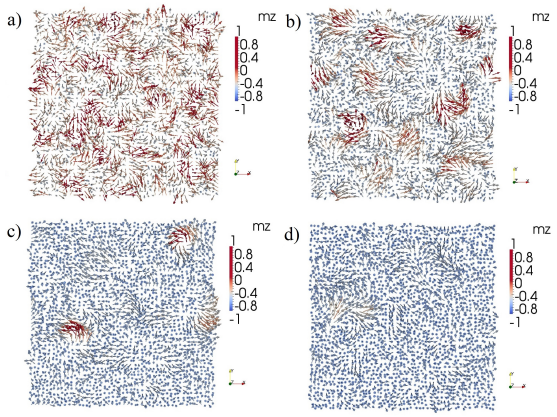

Figure 4.8: Snapshots of system with $F = 40$ mJ/cm^3 and $H_z = -5$ T at times: a) $t = 0.11$ ns, b) $t = 0.15$ ns, c) $t = 0.21$ ns, d) $t = 0.24$ ns.

4.3 All-optical control of the magnetization using circularly polarized laser pulses

Recently, an all-optical control of the magnetization using circularly polarized laser pulses in FePt thin films has been observed[93]. Fig. 4.9 is taken from Ref. [93] and it shows the experimental magneto-optical response in various applied field of a 15-nm FePtAgC granular film sample starting with an initially demagnetized state. We observe that an external applied field of $\sim$ 700 Oe is strong enough to suppress the effects of the helicity of the light.

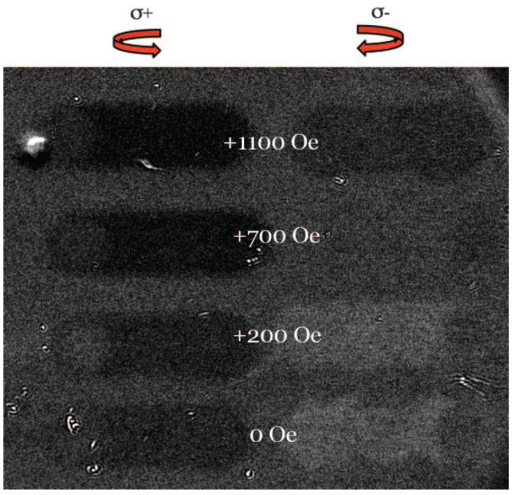

Figure 4.9: Experimental magneto-optical response in various applied field of a 15-nm FePtAgC granular film sample starting with an initially demagnetized state. Figure taken from Ref. [93].

4.3.1 Modeling the inverse Faraday effect

Motivated by these results we have investigated in which conditions we observe a magnetization reversal using our micromagnetic model of FePt. Similar to Ref.[143] we include the effect of the circularly polarized laser pulse (inverse Faraday effect) in our micromagnetic model as a light-induced effective magnetic field of the form

$$\mathbf{H}_{\mathrm{OM}}(t) = \sigma H_{\mathrm{OM}}^{\mathrm{max}} f(t)\mathbf{n}, \tag{4.12}$$

where $\mathbf{n}$ is the unit vector in the direction of the wave vector light, σ gives the degree of circular polarization and is equal to ± 1 and 0 for right-(σ^+), left-handed(σ^-) circularly polarized, and linearly polarized light, respectively. $H_{\mathrm{OM}}^{\mathrm{max}}$ is the maximum value that the light-induced effective field can achieve and we use it as a parameter in our simulations. The function $f(t)$ is given by

$$f(t) = \begin{cases} e^{-\left(\frac{t}{\tau}\right)^2}, & t < 0 \\ e^{-\left(\frac{t}{\tau+2\tau_{\mathrm{decay}}}\right)^2}, & t > 0 \end{cases} \tag{4.13}$$

where τ is the pulse length with a value of $\tau = 40$ fs and τ_{decay} is a parameter.

4.3.2 Results

4.3.2.1 Continuous film

Firstly, we simulate the magnetization dynamics of FePt continuous thin film using same micromagnetic model described in section 4.2.2 where we have added the optical-magnetic field given by Eq. (4.12) to the total effective field given by Eq. (4.2). We consider that the initial magnetization is saturated in the up direction (perpendicular to the thin film) and we use a left-handed circularly polarized laser pulse ($\sigma = -1$) where the direction of the wave vector is perpendicular to the thin film ($\mathbf{n} = \mathbf{e}_z$).

In Figs. 4.10a) we show the dynamics of the optical-magnetic field for different values of the parameter τ_{decay} (upper panel), the dynamics of the electron and phonon temperature (middle panel) and the magnetization dynamics (lower panel) using the values of the parameter of the set I in Table 4.1 for a fluence of $F = 40$ mJ/cm^2 where a magnetization reversed is observed for the cases $\tau_{\text{decay}} = 10, 50$ ps. However, in Figs. 4.10b) we have made the same simulations as in Figs. 4.10a) but assuming a higher electron heat capacity, namely, we set $\gamma_e = 1100$ J/m^{3}K^2, as a consequence the electronic temperature is lower than in the previous case and the same optical-magnetic field can not reverse the magnetization. Therefore, we conclude that high electronic temperatures are needed in order to switch the magnetization using circularly polarized laser pulses.

Now, we would like to investigate if an external magnetic field of the order of 0.1 T can prevent the magnetization switching when a circularly polarized laser pulse is applied to FePt thin film. For this task, we have performed similar simulations as in Fig. 4.10 for different values of the optical-magneto parameters $H_{\text{OM}}^{\max}$ and τ_{decay} using a higher fluence equal to $F = 50$ mJ/cm^2 and without and with an external magnetic field equal to $H_z = 0.1$ T pointing in the same direction of the initial magnetization, that is, opposite to the light-induced effective magnetic field $\mathbf{H}_{OM}$. The results are presented in Fig. 4.11 where switching and no switching regions are separated by a solid line in the case of no external magnetic field and by a dash line in the case with external magnetic field equal to $H_z = 0.1$ T. We observe that the external magnetic field can not prevent the magnetization switching for the cases of high optical-magnetic effects, that is, large $H_{\text{OM}}^{\max}$ and large τ_{decay}.

4.3.2.2 Granular film

In order to simulate the magnetization dynamics of FePt granular thin film we consider the same micromagnetic model than for the continuous thin film but with a lower exchange stiffness $A_i(T) = 2.2 \cdot 10^{-8} m_i^{1.76}$ erg/cm. Therefore now

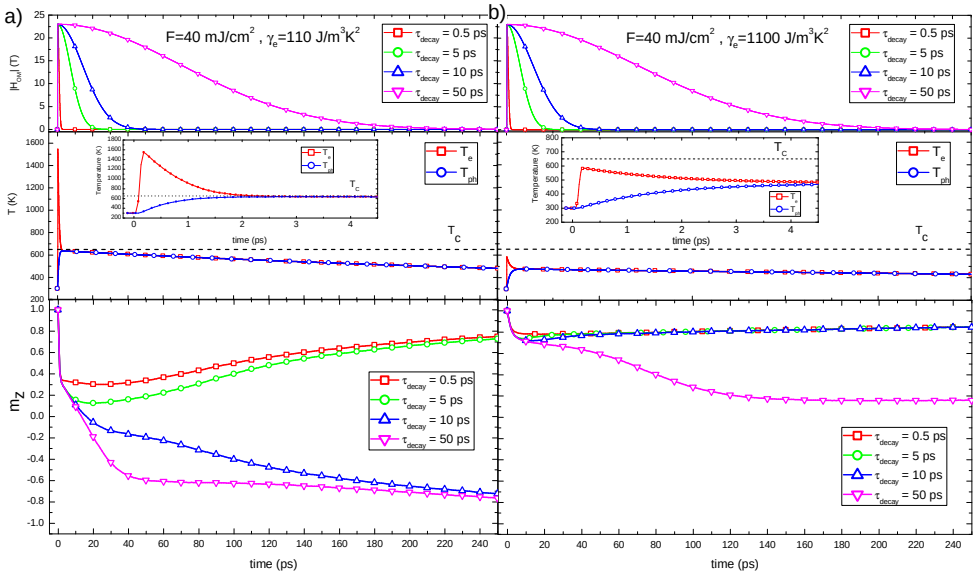

Figure 4.10: a) The dynamics of the optical-magnetic field (upper panel), the dynamics of the electron and phonon temperature (middle panel) and the magnetization dynamics (lower panel) using the values of the parameter of the set I in Table 4.1 for a fluence of $F = 40$ mJ/cm^2. b) The dynamics of the optical-magnetic field (upper panel), the dynamics of the electron and phonon temperature (middle panel) and the magnetization dynamics (lower panel) using the values of the parameter of the set I in Table 4.1 but with $\gamma_e = 1100$ J/m^{3}K^2 and a fluence equal to $F = 40$ mJ/cm^2.

each cubic discretization element represents a FePt grain. Similar as in the experiments described in Ref. [93] we consider a initially demagnetized system, that is, there are almost the same number of grains with the magnetization pointing in the up direction than in the down direction (see Fig. 4.12 a)). Let's assume that when the ultrashort laser pulse heats the sample the electronic temperature follows a spatial Gaussian distribution after the laser heats the sample. As illustration in Fig. 4.12 b) we show a snapshoot of the spatial electronic temperature distribution at the instant when it reaches its maximum value. Lets label 3 regions as: i) Region I where $T_{e,max} \simeq 1800$ K (approximately it corresponds to a spatial homogeneous Te distribution with fluence 50 mJ/cm^2), ii) Region II where $T_{e,max} \simeq 1500$ K (approximately it corresponds to a spatial homogeneous Te distribution with fluence 40 mJ/cm^2) and iii) Region III where $T_{e,max} \simeq 1300$ K (approximately it corresponds to a spatial homogeneous T_e distribution with fluence 30 mJ/cm^2).

Now, we simulate these three regions independently with a spatial homoge-

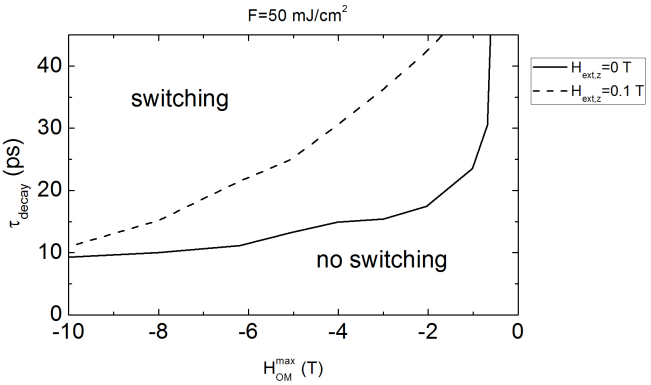

Figure 4.11: Phase diagram showing for which optical-magnetic parameters ($H_{\rm OM}^{\rm max}$ and $\tau_{\rm decay}$) the magnetization switching is achieved. Solid line separates switching and no switching regions for the case of no external magnetic field, and dash line for the case with an external magnetic field equal to $H_z = 0.1$ T opposite to the light-induced effective magnetic field $\mathbf{H}_{OM}$ (dash line).

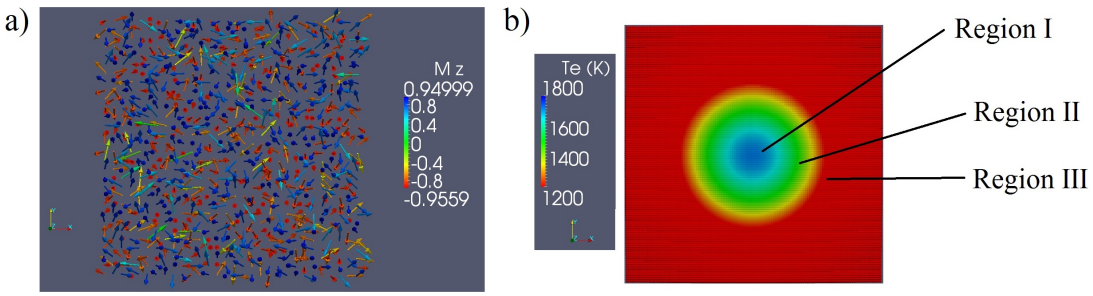

Figure 4.12: a) Initial demagnetized state of FePt granular thin film. b) Snapshoot of the spatial electronic temperature distribution at the instant when it reaches its maximum value.

neous T_e and using the same opto-magnetic field induced by the light polarization ($H_{OM}^{max} = 40$ T, $\tau = 1$ ps), although it could be different in each region like T_e. In Fig. 4.13 a) we show the electronic temperature and opto-magnetic field time evolution in regions I, II and III. In Fig. 4.13 b) we show the magnetization dynamics in these theree regions. We see that for the same field pulse there is an optimum T_e dynamics (region II) where a maximum number of magnetic grains are flipped. Moreover, the final total magnetization at region II is in quantitative agreement with experiments [93], that is, close to 10% of the saturation magnetization.

Since the magnetization is higher in region II than in the other regions then a magnetized ring is formed as it is observed in the experiments[93] at high fluences

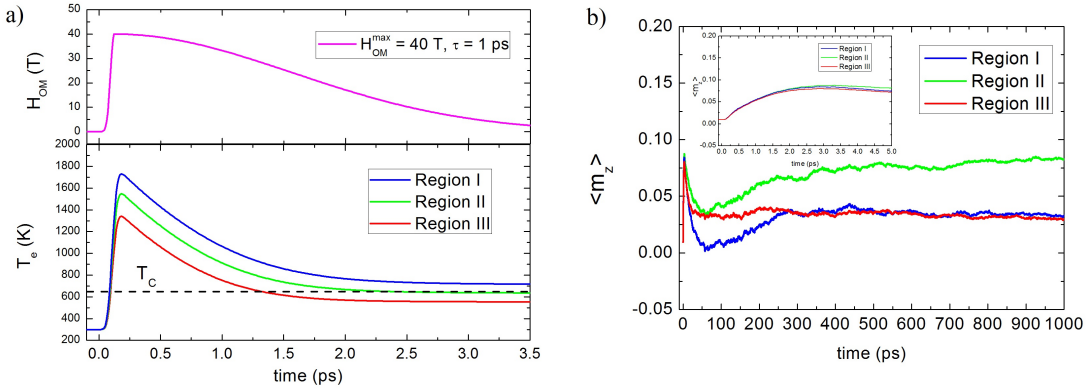

Figure 4.13: a) Electronic temperature and opto-magnetic field time evolution in regions I, II and III. b) Magnetization dynamics in regions I, II and III.

(see Fig. 4.14).

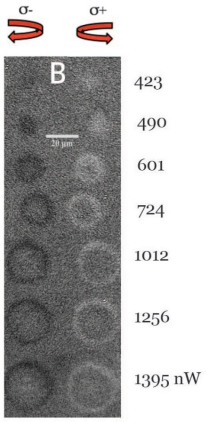

Figure 4.14: Experimental final state of the magnetization in FePtAgC granular film after an ultrashort circularly polarized laser pulse is applied for different laser power. Figure taken from Ref. [93].

4.4 Conclusions

In this chapter we have shown that the micromagnetic model based on the qLLB+2TM can successfully reproduce the ultrafast magnetization dynamics measured in FePt thin films. Additionally, it allows us to conclude that may be Fe becomes more noble in the FePt $L1_0$ compound, which makes the electron's specific heat more similar to Au and Cu with a small γ_e. On the other

hand, our numerical results show that a small electron's specific heat is an important requirement in order to observe magneto-optical effects using circularly polarized laser pulses. Therefore, we think that the low electron's specific heat of the FePt favours to its all-optical control using circularly polarized laser pulses. Finally, our numerical results of granular FePt thin film show that for a given opto-magnetic pulse there is an optimum electronic temperature dynamics where a maximum number of magnetic grains are flipped. As consequence, at high fluence a spatial gaussian-like distribution of the electronic temperature could favour the formation of a magnetized ring in the region where the optimum electronic temperature dynamic takes place as it is observed in the experiments[93].

Conclusiones en español

En este capítulo hemos mostrado que el modelo micromagnético basado en la ecuación de qLLB acoplada con el 2TM puede reproducir satisfactoriamente la magnetización ultrarrápida observada experimentalmente en láminas delgadas de FePt. Además, dicho modelo nos sugiere que el Fe se podría comportar como un material más noble cuando se encuentra es FePt $L1_0$, lo que podría hacer que su capacidad calorífica electrónica sea parecida a Au y Cu, es decir, con un valor pequeño de γ_e. Por otro lado, nuestros resultados numéricos muestran que un valor pequeño de γ_e es un importante requirimiento para poder observar efectos magneto-ópticos lo que favorece el control de la magnetización mediante pulsos polarizados circularmente. Finalmente, nuestras simulaciones en FePt granular muestran que exite una dinámica de temperaturas en la que el efecto magneto-óptico es más intenso, es decir, un mayor número de granos invierten su magnetización. Por tanto, en el caso de pulsos de gran potencia sobre muestras desmagnetizadas, si se asume una distribución espacial de la temperatura tipo gaussiana, entonces en las regiones en donde la dinámica de temperatura es óptima la magnetización sería mayor que en otras regiones dando lugar a un anillo magnetizado como se oberva en los experimentos.

4. MICROMAGNETIC MODELING OF ULTRAFAST MAGNETIZATION DYNAMICS IN FEPT

5

Landau-Lifshitz-Bloch equation for two-component magnets

5.1 Introduction

Ferromagnets are not the only interesting magnetic materials from the point of view of ultrafast magnetization dynamics. Disordered ferrimagnetic alloys like GdFeCo are also very interesting, specially from the technological point of view, since an all optical switching (AOS) has been observed in these materials using an intense ultrashort pulse of circularly polarized light[144] and linearly polarized light[70]. Therefore, the modeling of ultrafast magnetization dynamics in disordered ferrimagnetic alloys is required in order to have a better understanding of this phenomenon. Recently, a modeling for these materials was suggested by Vahaplar *et al.*[144] based on macrospin LLB approach, essentially treating a ferrimagnet as a ferromagnet. The model showed that in order to have the magnetization switching a strong field around 20 T was necessary. This field can, in principle, come in the experiment with circularly polarized light from the inverse Faraday effect. More recently, T. Ostler *et al.* [115] used a multi-spin atomistic approach based on the Heisenberg model showing that the switching occurs without any applied field or even with the field up to 40 T applied in the opposite direction. The predictions for the heat-driven reversal were confirmed in several experiments in magnetic thin films and dots using linearly polarized pulses. Moreover, I. Radu *et al.* [70] used the same atomistic model for the magnetization dynamics to simulate GdFeCo and compared the simulation results to the experimental data measured by the element-specific x-ray magnetic circular dichroism (XMCD). They unexpectedly found that the ultrafast magnetization reversal in this material, where spins are coupled antiferromagnetically, occurs by way of a transient ferromagnetic-like state.

The latter experiments demonstrate the deficiency in application of the macrospin ferromagnetic LLB model to the description of the ultrafast dynamics in a ferrimagnetic material GdFeCo. It is clear that the situation of a ferromagnetic-like state in a ferrimagnetic material cannot be described in terms of a macrospin LLB equation in which a ferrimagnet is essentially treated as a ferromagnet. In a ferromagnetic LLB equation the sublattices cannot have their own dynamics and thus the processes such as the angular momentum transfer between them are essentially ignored. In this situation the only possible reversal mode is the linear relaxation requiring a strong applied magnetic field as was the case of Ref.[144].

On a general basis, atomistic models are convenient to model ferrimagnetic materials but for modeling of larger spatial scales, a macroscopic equation similar to ferromagnetic LLB equation is desirable. This will open a possibility to a correct micromagnetic modeling of ferri- and antiferromagnetic nano and micro structures at ultrafast timescales and and/or high temperatures. Additionally, this can also allow more correct understanding of longitudinal relaxation in two-component (for example, ferrimagnetic) compounds, taking into account the inter-sublattice exchange.

In this chapter we present novel classical and quantum LLB equations for two-component magnets. The classical one is already published[10] and a detailed derivation can be found in Ref.[140], so that in section 5.2 we just present a short introduction to it. However, the quantum case is not published yet, so that in section 5.3 we show a detailed derivation of it.

5.2 Classical LLB equation for two-component magnets

The derivation of the classical LLB for two sublattice magnet has the same starting point as the classical LLB equation [49] for a ferromagnet. Namely, we start with the usual atomistic approach where it is assumed that the spin dynamics is governed by the Langeviin dynamics based on the Landau-Lifshitz-Gilbert equation. From the Fokker-Planck equation derived in Ref.[49] one can obtain an equation for thermal average of the spin polarisation, i.e. the reduced magnetisation $\mathbf{m}_\nu$ (where $\nu = TM, RE$ stands for the transition metal (TM) or rare-earth (RE) sublattice) in a paramagnetic state. For the treatment of ferromagnet, the external field is substituted by the mean field. A detailed discussion about mean-field approximation (MFA) for a disordered ferrimagnet can be found in Ref.[116].

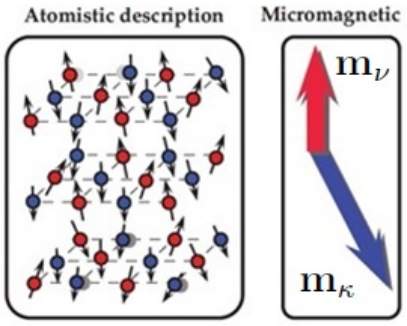

Figure 5.1: Diagram showing a disordered magnetic alloy from the point of view of the atomistic model (left panel) and the micromagnetic LLB model (right panel).

The corresponding set of coupled LLB equations for each sublattice magnetization $\mathbf{m}_\nu$ has the following form, see details in Ref.[10]:

$$\begin{aligned}\frac{d\mathbf{m}_\nu}{dt} &= -\gamma_\nu[\mathbf{m}_\nu \times \mathbf{H}_\nu^{\mathrm{MFA}}] - \Gamma_{\nu,\parallel}\left(1 - \frac{\mathbf{m}_\nu \mathbf{m}_{0,\nu}}{m_\nu^2}\right)\mathbf{m}_\nu \\ &- \Gamma_{\nu,\perp}\frac{[\mathbf{m}_\nu \times [\mathbf{m}_\nu \times \mathbf{m}_{0,\nu}]]}{m_\nu^2},\end{aligned} \tag{5.1}$$

where

$$\mathbf{m}_{0,\nu} = L(\xi_{0,\nu})\frac{\boldsymbol{\xi}_{0,\nu}}{\xi_{0,\nu}}, \quad \boldsymbol{\xi}_{0,\nu} \equiv \beta\mu_\nu \mathbf{H}_\nu^{\mathrm{MFA}}. \tag{5.2}$$

Here $\xi_{0,\nu} \equiv |\boldsymbol{\xi}_{0,\nu}|$, $L(\xi) = \coth(\xi) - 1/\xi$ is the Langevin function,

$$\Gamma_{\nu,\parallel} = \Lambda_{\nu,N}\frac{L(\xi_{0,\nu})}{\xi_{0,\nu}L'(\xi_{0,\nu})}, \quad \Gamma_{\nu,\perp} = \frac{\Lambda_{\nu,N}}{2}\left(\frac{\xi_{0,\nu}}{L(\xi_{0,\nu})} - 1\right) \tag{5.3}$$

describe parallel and perpendicular relaxation, respectively, $\Lambda_{\nu,N} = 2\gamma_\nu\lambda_\nu k_B T/\mu_\nu$ is the characteristic diffusion relaxation rate or, for the thermo-activation escape problem, the Néel attempt frequency. γ_ν is the gyromagnetic ratio, λ_ν is the coupling to the bath parameter, μ_ν is the magnetic moment of sublattice ν, $L'(\xi) = dL/d\xi$, k_B is the Boltzmann constant, T is the bath's temperature and $\beta = 1/k_B T$. The mean fields have the following forms:

$$\mathbf{H}_\nu^{\mathrm{MFA}} = \frac{J_{0,\nu}}{\mu_\nu}\mathbf{m}_\nu + \frac{J_{0,\nu\kappa}}{\mu_\nu}\mathbf{m}_\kappa + \mathbf{h}_\nu \tag{5.4}$$

where $J_{0,\nu} = 3x_\nu k_B T_{c,\nu}$, $J_{0,\nu\kappa} = \pm 3x_\kappa k_B T_{c,\nu\kappa}$ (sign + for ferromagnetic coupling and sign − for antiferromagnetic coupling), x_ν and $x_\kappa = 1 - x_\nu$ are the concentrations of the sublattices ν and κ, respectively. $T_{c,\nu(\kappa)}$ is the Curie temperature

of the pure sublattice $\nu(\kappa)$ and $T_{c,\nu\kappa} = T_{c,\kappa\nu}$ is a temperature which is related to the Curie temperature (T_c) of the system through

$$T_c = \frac{x_\nu T_{c,\nu} + x_\kappa T_{c,\kappa} + \sqrt{(x_\nu T_{c,\nu} - x_\kappa T_{c,\kappa})^2 + 4x_\nu x_\kappa T_{c,\nu\kappa}^2}}{2}. \tag{5.5}$$

The field $\mathbf{h}_\nu = \mathbf{H} + \mathbf{H}_{\mathrm{A},\nu}$ contains the external applied field ($\mathbf{H}$) and the anisotropy field ($\mathbf{H}_{\mathrm{A},\nu}$).

The final LLB form presented below has some approximations and has a worse agreement if large magnetisation changes are involved. However, it is useful for analytic estimations and predictions since the relaxation terms have closed expressions.

Assuming that the longitudinal homogeneous exchange field is large in comparison to the other terms in Eq. (5.4) and after an expansion around the equilibrium up to first order in $\delta m_\nu = m_\nu - m_{e,\nu}$, from Eq. (5.1) one arrives to [10]

$$\begin{aligned} \frac{d\mathbf{m}_\nu}{dt} &= -\gamma_\nu[\mathbf{m}_\nu \times \mathbf{H}_{\mathrm{eff},\nu}] + \gamma_\nu \alpha_\parallel^\nu \frac{\mathbf{m}_\nu \cdot \mathbf{H}_{\mathrm{eff},\nu}}{m_\nu^2}\mathbf{m}_\nu \\ &- \gamma_\nu \alpha_\perp^\nu \frac{[\mathbf{m}_\nu \times [\mathbf{m}_\nu \times \mathbf{H}_{\mathrm{eff},\nu}]]}{m_\nu^2}, \end{aligned} \tag{5.6}$$

where the effective field is given by

$$\begin{aligned} \mathbf{H}_{\mathrm{eff},\nu} &= \mathbf{H} + \mathbf{H}_{\mathrm{A},\nu} + \frac{J_{0,\nu\kappa}}{\mu_\nu}\mathbf{\Pi}_\kappa \\ &- \left[\frac{1}{\Lambda_{\nu\nu}}(m_\nu - m_{e,\nu}) - \frac{1}{\Lambda_{\nu\kappa}}(\tau_\kappa - \tau_{e,\kappa})\right]\frac{\mathbf{m}_\nu}{m_\nu} \end{aligned} \tag{5.7}$$

where $\mathbf{H}_{\mathrm{A},\nu}$ is the anisotropy field, $\mathbf{H}$ is the applied field, $\mathbf{\Pi}_\kappa = -[\mathbf{m}_\nu \times [\mathbf{m}_\nu \times \mathbf{m}_\kappa]]/m_\nu^2$, $\boldsymbol{\tau}_\nu = (\mathbf{m}_\nu \cdot \mathbf{m}_\kappa)/m_\kappa$, $\tau_\nu = |\boldsymbol{\tau}_\nu|$, $\boldsymbol{\tau}_{e,\nu} = (\mathbf{m}_{e,\nu} \cdot \mathbf{m}_{e,\kappa})/m_{e,\kappa}$ and

$$\Lambda_{\nu\nu}^{-1} = \frac{1}{\widetilde{\chi}_{\nu,||}}\left(1 + \frac{J_{0,\nu\kappa}}{\mu_\nu}\widetilde{\chi}_{\kappa,||}\right), \quad \Lambda_{\nu\kappa}^{-1} = \frac{J_{0,\nu\kappa}}{\mu_\nu}, \tag{5.8}$$

The longitudinal susceptibility is given by

$$\widetilde{\chi}_{\nu,||} = \frac{\mu_\kappa \beta L'_\nu J_{0,\nu\kappa}\beta L'_\kappa + \mu_\nu \beta L'_\nu (1 - J_{0,\kappa}\beta L'_\kappa)}{(1 - J_{0,\nu}\beta L'_\nu)(1 - J_{0,\kappa}\beta L'_\kappa) - J_{0,\kappa\nu}\beta L'_\nu J_{0,\nu\kappa}\beta L'_\kappa} \tag{5.9}$$

where $L'_\nu = L'(\xi_{e,\nu}) = dL/d\xi_\nu(\xi_{e,\nu})$, $\xi_{e,\nu} = \beta(J_{0,\nu}m_{e,\nu} + |J_{0,\nu\kappa}|m_{e,\kappa})$ and $\beta = 1/k_B T$. The dampings parameters are

$$\alpha_\parallel^\nu = \frac{2\lambda_\nu}{\beta\tilde{J}_{0,\nu,e}} \quad , \quad \alpha_\perp^\nu = \lambda_\nu\left(1 - \frac{1}{\beta\tilde{J}_{0,\nu,e}}\right) \tag{5.10}$$

where $\tilde{J}_{0,\nu,e} = J_{0,\nu} + |J_{0,\nu\kappa}|(m_{e,\kappa}/m_{e,\nu})$. We notice that the LLB equation given by Eq. (5.6) is only valid at temperatures below the critical temperature T_c.

When temperature goes to T_c ($T \to T_c$) the longitudinal susceptibility goes to infinity ($\widetilde{\chi}_{\nu,||} \to \infty$) and the equilibrium magnetization goes to zero ($m_{e,\nu} \to 0$), as consequence at $T = T_c$ the quantity $\Lambda_{\nu\nu}$ contains an indeterminate form ∞/∞ and the dampings $\alpha_{\parallel}^{\nu}$ and $\alpha_{\perp}^{\nu}$ contain an indeterminate form $0/0$. However, the quantities $\Lambda_{\nu\nu}$, $\alpha_{\parallel}^{\nu}$ and $\alpha_{\perp}^{\nu}$ are continuous function at $T = T_c$, in order to see this fact we can rewrite these quantities in a form suitable for temperatures very close to T_c. To this end we notice that

$$\widetilde{\chi}_{\nu,||}(\epsilon) \simeq \begin{cases} \frac{\mu_\nu(3k_BT_c - J_{0,\kappa}) + \mu_\kappa}{6k_BT_c(6k_BT_c - J_{0,\nu} - J_{0,\kappa})\epsilon}, & T \lesssim T_c \\ \frac{\mu_\nu(3k_BT_c - J_{0,\kappa}) + \mu_\kappa}{3k_BT_c(6k_BT_c - J_{0,\nu} - J_{0,\kappa})(-\epsilon)}, & T \gtrsim T_c \end{cases} \tag{5.11}$$

$$\frac{m_{e,\kappa}}{m_{e,\nu}} \simeq \frac{3k_BT_c - J_{0,\nu}}{|J_{0,\nu\kappa}|} + \mathcal{O}(\epsilon), \quad T \approx T_c \tag{5.12}$$

where $\epsilon = (T_c - T)/T_c$. With the help of Eqs (5.11) and (5.12) we can rewrite Eqs. (5.8) and (5.10) as

$$\Lambda_{\nu\nu}^{-1}(T) \simeq \begin{cases} \frac{6k_B(T_c - T)(6k_BT_c - J_{0,\nu} - J_{0,\kappa})}{\mu_\nu(3k_BT_c - J_{0,\kappa}) + \mu_\kappa J_{0,\nu\kappa}} + \frac{3k_BT_c - J_{0,\nu}}{\mu_\nu}, & T \lesssim T_c \\ \frac{3k_BT_c - J_{0,\nu}}{\mu_\nu}, & T = T_c \\ \frac{3k_B(T - T_c)(6k_BT_c - J_{0,\nu} - J_{0,\kappa})}{\mu_\nu(3k_BT_c - J_{0,\kappa}) + \mu_\kappa J_{0,\nu\kappa}} + \frac{3k_BT_c - J_{0,\nu}}{\mu_\nu}, & T \gtrsim T_c \end{cases} \tag{5.13}$$

$$\alpha_{\parallel}^{\nu} = \alpha_{\perp}^{\nu} \simeq \frac{2\lambda_\nu T}{3T_c} + \mathcal{O}(\epsilon), \quad T \gtrsim T_c. \tag{5.14}$$

We observe that above T_c the longitudinal and transverse dampings are equal to the dampings in the classical LLB equation of a ferromagnet since at these temperatures the system becomes paramgnetic.

As an example in Fig. (5.2) we show the magnetization dynamics obtained from LLB equation given by Eq. (5.1) and LLB equation given Eq. (5.6) for a temperature-step which crosses T_c using parameters similar to GdFeCo with a Gd concentration of 25%. For the quantity $\Lambda_{\nu\nu}$ we used Eq. (5.8) and for $\alpha_{\parallel}^{\nu}$ we used Eq. (5.14).

5.2.1 Comparison between the classical LLB equation and atomistic simulations

Firstly, we would like to point out that atomistic simulations based on a classical Heisenberg Hamiltonian can successfully reproduce the magnetization switching

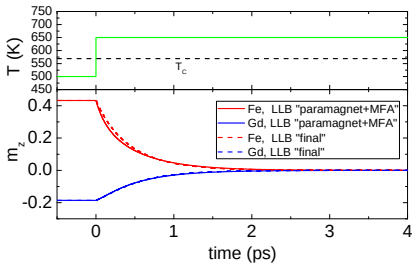

Figure 5.2: Magnetization dynamics obtained from LLB equation given by Eq. (5.1) (solid lines) and LLB equation given Eq. (5.6) (dash lines) for a temperature-step which crosses T_c. For the quantity $\Lambda_{\nu\nu}$ we used Eq. (5.8) and for $\alpha_{\parallel}^{\nu}$ we used Eq. (5.14).

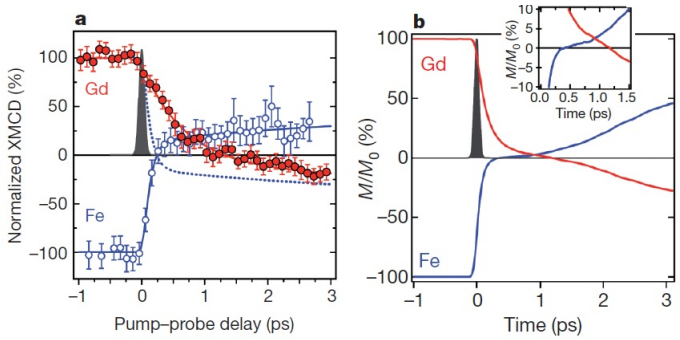

Figure 5.3: a) Element-resolved dynamics of the Fe and Gd magnetic moments measured by time resolved XMCD with femtosecond time resolution. b) Computed time-resolved of the Fe and Gd magnetic moments from atomistic simulations. Figures taken from Ref. [70].

observed experimentally in ferrimagnets like GdFeCo as we show in Figs. 5.3 which are taken from Ref. [70].

Now, let's compare the classical LLB equations derived previously with atomistic simulations based on the stochastic LLG equation. In Figs. 5.4 a) and b) we show the magnetization dynamics obtained from atomistic simulations (square), LLB equation given by Eq. (5.1) and LLB equation given Eq. (5.6) for a low temperature-step and high temperature-step, respectively. We observe that for the case of a high temperature-step the final form of the LLB given by Eq. (5.6) is not a good approximation of the initial LLB equation given by Eq. (5.1) because the assumption of a small deviation from the equilibrium doesn't hold. In Fig. 5.4 c) we show the magnetization dynamics obtained from atomistic simulations, LLB equation given by Eq. (5.1) using an initial state where $\mathbf{m}_{\mathrm{Fe}} \parallel \mathbf{m}_{\mathrm{Gd}} \parallel \mathbf{e}_z$ and LLB equation given Eq. (5.1) using an initial state where $\mathbf{m}_{\mathrm{Fe}}$ and $\mathbf{m}_{\mathrm{Gd}}$ are

not completed parallel to the z-axis for a temperature pulse. As it was pointed out in Ref. [11], we see that in order to switch the magnetization with a temperature pulse using the LLB equation a small deviation from the complete initial anti-parallel state is required.

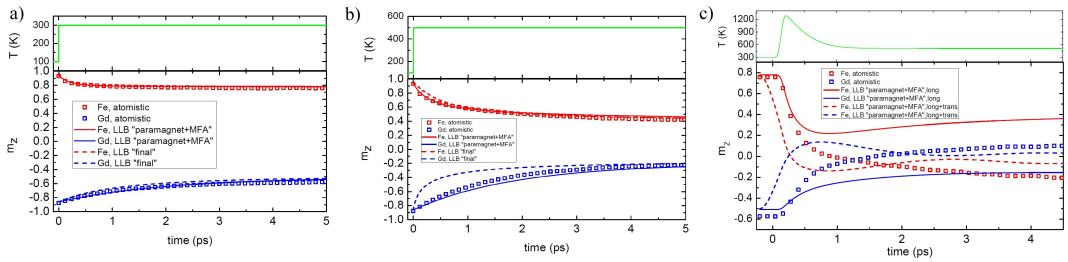

Figure 5.4: Magnetization dynamics obtained from atomistic simulations (squares), LLB equation given by Eq. (5.1) (solid lines) and LLB equation given Eq. (5.6) (dash lines) for: a) a low temperature-step and b) high temperature-step. c) Magnetization dynamics obtained from atomistic simulations (squares), LLB equation given by Eq. (5.1) using an initial state where $\mathbf{m}_{\mathrm{Fe}} \parallel \mathbf{m}_{\mathrm{Gd}} \parallel \mathbf{e}_z$ (solid lines) and LLB equation given Eq. (5.1) using an initial state where $\mathbf{m}_{\mathrm{Fe}}$ and $\mathbf{m}_{\mathrm{Gd}}$ are not completed parallel to the z-axis (dash lines) for a temperature pulse.

5.3 Quantum LLB equation for two-component magnets

For the quantum case we use the same idea as in the classical LLB equation for disordered magnetic alloys described in section 5.2, that is, initially we consider the "paramagnetic" quantum LLB equation (see Eq. (3.8) in Ref. [47]) and then the external magnetic field is replaced by the MFA one in each sublattice. As consequence we have two coupled LLB equations for each sublattice magnetization $\mathbf{m}_\nu$ with the form

$$\begin{aligned}
\frac{d\mathbf{m}_\nu}{dt} &= -\gamma_\nu \mathbf{m}_\nu \times \mathbf{H}_\nu^{\mathrm{MFA}} - 2K_{2,\nu}\left(1 - \frac{\tanh\left(\frac{y_{0,\nu}}{2}\right)}{\tanh\left(\frac{y_\nu}{2}\right)}\frac{\mathbf{m}_\nu \cdot \mathbf{H}_\nu^{\mathrm{MFA}}}{m_\nu H_\nu^{\mathrm{MFA}}}\right)\mathbf{m}_\nu \\
&- K_{2,\nu}\frac{\tanh\left(\frac{y_{0,\nu}}{2}\right)}{\tanh\left(\frac{y_\nu}{2}\right)}\left(\frac{2(S_\nu+1)\tanh\left(\frac{y_\nu}{2}\right)}{m_\nu} - 1\right)\frac{\mathbf{m}_\nu \times (\mathbf{m}_\nu \times \mathbf{H}_\nu^{\mathrm{MFA}})}{m_\nu H_\nu^{\mathrm{MFA}}} \\
&+ (K_{2,\nu} - K_1)\left[\frac{(\mathbf{m}_\nu \times \mathbf{H}_\nu^{\mathrm{MFA}})^2}{(m_\nu H_\nu^{\mathrm{MFA}})^2}\mathbf{m}_\nu + \frac{(\mathbf{m}_\nu \cdot \mathbf{H}_\nu^{\mathrm{MFA}})\mathbf{m}_\nu \times (\mathbf{m}_\nu \times \mathbf{H}_\nu^{\mathrm{MFA}})}{(m_\nu H_\nu^{\mathrm{MFA}})^2}\right]
\end{aligned} \tag{5.15}$$

where $\mathbf{m}_\nu = \langle \hat{\mathbf{S}}_\nu \rangle / \hbar S_\nu$ is the reduced magnetization of the sublattice ν, y_ν is given by the relation $m_\nu = B(S_\nu y_\nu) = B(\mu_\nu y_\nu / \gamma_\nu \hbar)$, $B(x) = [(2S+1)/2S] \coth([2S+1]x/2S) - (1/2S)\coth(x/2S)$ is the Brillouin function for the spin value S, $y_{0,\nu} = \beta \gamma_\nu \hbar H_\nu^{\mathrm{MFA}}$ and

$$K_1 = \sum_{q,p} |V_{p,q}|^2 n_p (n_q + 1) \pi \delta(\omega_q - \omega_p) \tag{5.16}$$

$$\begin{aligned} K_{2,\nu} &= \frac{1}{2}\left(1 + e^{-y_{0,\nu}}\right) \{ \sum_q |V_q|^2 (n_q+1) \pi \delta(\omega_q - \gamma_\nu H_\nu^{\mathrm{MFA}}) \\ &+ \sum_{p,q} |V_{p,q}|^2 n_p (n_q+1) \pi \delta(\omega_q - \omega_p - \gamma_\nu H_\nu^{\mathrm{MFA}}) \}, \end{aligned} \tag{5.17}$$

where $n_q = [\exp(\beta \hbar \omega_q) - 1]^{-1}$ is the Bose-Einstein distribution, w_q is the phonon's frecuency, V_q and $V_{p,q}$ are spin-phonon scattering amplitudes. The mean field $\mathbf{H}_\nu^{\mathrm{MFA}}$ is given by

$$\mathbf{H}_\nu^{\mathrm{MFA}} = \frac{J_{0,\nu}}{\mu_\nu} \mathbf{m}_\nu + \frac{J_{0,\nu\kappa}}{\mu_\nu} \mathbf{m}_\kappa + \mathbf{H} + \mathbf{H}_{\mathrm{A}} \tag{5.18}$$

where $J_{0,\nu} = 3 x_\nu k_B T_{c,\nu} S_\nu / (S_\nu + 1)$, $J_{0,\nu\kappa} = \pm 3 x_\kappa k_B T_{c,\nu\kappa} \sqrt{S_\nu S_\kappa} / \sqrt{(S_\nu + 1)(S_\kappa + 1)}$ (sign $+$ for ferromagnetic coupling and sign $-$ for antiferromagnetic coupling), x_ν and $x_\kappa = 1 - x_\nu$ are the concentrations of the sublattices ν and κ, respectively. $T_{c,\nu(\kappa)}$ is the Curie temperature of the pure sublattice $\nu(\kappa)$ and $T_{c,\nu\kappa} = T_{c,\kappa\nu}$ is a temperature which is related to the Curie temperature (T_c) of the system through

$$T_c = \frac{x_\nu T_{c,\nu} + x_\kappa T_{c,\kappa} + \sqrt{(x_\nu T_{c,\nu} - x_\kappa T_{c,\kappa})^2 + 4 x_\nu x_\kappa T_{c,\nu\kappa}^2}}{2}. \tag{5.19}$$

$\mathbf{H}$ is the external applied field and $\mathbf{H}_{\mathrm{A},\nu}$ is the anisotropy field. The equilibrium solution of Eq. (5.15) is obtained by $\mathbf{m}_\nu \times \mathbf{H}_\nu^{\mathrm{MFA}} = 0$ and $y_\nu = y_{0,\nu} = \beta \gamma_\nu \hbar H_\nu^{\mathrm{MFA}}$, which yields to the Curie-Weiss equations:

$$\mathbf{m}_\nu = B(\beta \mu_\nu H_\nu^{\mathrm{MFA}}) \frac{\mathbf{H}_\nu^{\mathrm{MFA}}}{H_\nu^{\mathrm{MFA}}}; \quad \mathbf{m}_\kappa = B(\beta \mu_\kappa H_\kappa^{\mathrm{MFA}}) \frac{\mathbf{H}_\kappa^{\mathrm{MFA}}}{H_\kappa^{\mathrm{MFA}}}. \tag{5.20}$$

5.3.1 Strong longitudinal exchange field

Now, we write the mean field $\mathbf{H}_\nu^{\mathrm{MFA}}$ in Eq. (5.18) as

$$\mathbf{H}_\nu^{\mathrm{MFA}} = \mathbf{H}_{\mathrm{EX},\nu} + \mathbf{h}_\nu, \tag{5.21}$$

where

$$\mathbf{H}_{\mathrm{EX},\nu} = \frac{J_{0,\nu}}{\mu_\nu}\mathbf{m}_\nu + \frac{J_{0,\nu\kappa}}{\mu_\nu}\mathbf{m}_\kappa, \tag{5.22}$$

$$\mathbf{h}_\nu = \mathbf{H} + \mathbf{H}_{\mathrm{A},\nu}. \tag{5.23}$$

In the same way as it is was done in the classical case[10] we decompose the magnetization vector $\mathbf{m}_\nu$ into two components $\mathbf{m}_\nu = \mathbf{\Pi}_\nu + \boldsymbol{\tau}'_\nu$, where $\mathbf{\Pi}_\nu$ is perpendicular to $\mathbf{m}_\nu$, so that it can be expressed as $\mathbf{\Pi}_\nu = -\left[\mathbf{m}_\kappa \times [\mathbf{m}_\kappa \times \mathbf{m}_\nu]\right]/m_\kappa^2$, and $\boldsymbol{\tau}'_\nu$ is parallel to $\mathbf{m}_\nu$, and it can be expressed as $\boldsymbol{\tau}'_\nu = \mathbf{m}_\kappa(\mathbf{m}_\nu \cdot \mathbf{m}_\kappa)/m_\kappa^2$.

We can shorten the notation by definition of the following new variable $\Theta_{\nu\kappa}$:

$$\Theta_{\nu\kappa} = \frac{\mathbf{m}_\nu \cdot \mathbf{m}_\kappa}{m_\kappa^2} \quad \Longrightarrow \quad \mathbf{m}_\nu = \mathbf{\Pi}_\nu + \Theta_{\nu\kappa}\mathbf{m}_\kappa \tag{5.24}$$

The exchange field $\mathbf{H}_{\mathrm{EX},\nu}$ can be written as a sum of the exchange fields parallel and perpendicular to magnetization $\mathbf{m}_\nu$, that is,

$$\begin{aligned}\mathbf{H}_{\mathrm{EX},\nu} &= \left(\frac{J_{0,\nu}}{\mu_\nu} + \frac{J_{0,\nu\kappa}}{\mu_\nu}\Theta_{\kappa\nu}\right)\mathbf{m}_\nu + \frac{J_{0,\nu\kappa}}{\mu_\nu}\mathbf{\Pi}_\kappa \\ &= \frac{\tilde{J}_{0,\nu}}{\mu_\nu}\mathbf{m}_\nu + \frac{J_{0,\nu\kappa}}{\mu_\nu}\mathbf{\Pi}_\kappa \\ &= \mathbf{H}^{\parallel}_{\mathrm{EX},\nu} + \mathbf{H}^{\perp}_{\mathrm{EX},\nu}\end{aligned} \tag{5.25}$$

where we have defined a new function $\tilde{J}_{0,\nu}(\mathbf{m}_\nu, \mathbf{m}_\kappa) = J_{0,\nu} + J_{0,\nu\kappa}\Theta_{\kappa\nu}(\mathbf{m}_\nu, \mathbf{m}_\kappa)$, $\mathbf{H}^{\parallel}_{\mathrm{EX},\nu} = (\tilde{J}_{0,\nu}/\mu_\nu)\mathbf{m}_\nu$ and $\mathbf{H}^{\perp}_{\mathrm{EX},\nu} = (J_{0,\nu\kappa}/\mu_\nu)\mathbf{\Pi}_\kappa$. In the following we will consider that the transverse contribution is small in comparison to longitudinal one, i.e., $|\mathbf{H}^{\parallel}_{\mathrm{EX},\nu}| \gg |\mathbf{H}^{\perp}_{\mathrm{EX},\nu}|$. This is a good approximation because differently to the ferromagnetic case, where the tranverse fluctuations are defined by the anisotropy and Zeeman fields (of the order of 1 T strength), in the case of ferrimagnets, the fluctuations included in $H^{\perp}_{EX,T}$ are defined by the interlattice exchange field (of the order of 10 T), which is usually very large in comparison to the anisotropy or Zeeman fields. Thus the transverse magnetization fluctuations are small in comparison to the longitudinal component. Therefore, we write the mean field $\mathbf{H}^{\mathrm{MFA}}_\nu$ as

$$\mathbf{H}^{\mathrm{MFA}}_\nu = \mathbf{H}^{\parallel}_{\mathrm{EX},\nu} + \mathbf{h}'_\nu \tag{5.26}$$

where $\mathbf{h}'_\nu = \mathbf{h}_\nu + \mathbf{H}^{\perp}_{EX,\nu}$ and $|\mathbf{H}^{\parallel}_{\mathrm{EX},\nu}| \gg |\mathbf{h}'_\nu|$ and we are going to retain only terms linear in $\mathbf{h}'_\nu$ in Eq. (5.15). First, we have

$$\frac{\mathbf{m}_\nu \cdot \mathbf{H}^{\mathrm{MFA}}_\nu}{m_\nu H^{\mathrm{MFA}}_\nu} = 1 + \mathcal{O}(h'^2_\nu) \tag{5.27}$$

similarly,

$$(\mathbf{m}_\nu \times \mathbf{H}_\nu^{\mathrm{MFA}}) \cdot (\mathbf{m}_\nu \times \mathbf{H}_\nu^{\mathrm{MFA}}) = \mathcal{O}(h_\nu'^2) \tag{5.28}$$

Further, in stationary dynamic processes deviations from equilibrium $y_\nu - y_{0,\nu}$ are small ($|y_\nu - y_{0,\nu}| \ll y_\nu$), hence

$$1 - \frac{\tanh\left(\frac{y_{0,\nu}}{2}\right)}{\tanh\left(\frac{y_\nu}{2}\right)} = \frac{y_\nu - y_{0,\nu}}{\sinh(y_\nu)} + \mathcal{O}([y_{0,\nu} - y_\nu]^2) \tag{5.29}$$

where the quantity $y_\nu - y_{0,\nu}$ can be written as

$$\begin{aligned} y_\nu - y_{0,\nu} &= y_\nu - g_\nu \mu_B \beta |\mathbf{H}_{EX,\nu}^{\parallel} + \mathbf{h}_\nu'| \\ &= y_\nu - \beta\gamma_\nu\hbar\frac{\tilde{J}_{0,\nu}}{\mu_\nu} m_\nu - \frac{\beta\gamma_\nu\hbar\mathbf{m}_\nu \cdot \mathbf{h}_\nu'}{m_\nu} + \mathcal{O}(h_\nu'^2) \end{aligned} \tag{5.30}$$

Now we calculate $y_\nu = y_\nu(m_\nu)$ using a Taylor expansion around $y_\nu(m_{\nu,e}) = \beta\gamma_\nu\hbar H_{\mathrm{EX},\nu,e}$, $H_{\mathrm{EX},\nu,e} = (J_{0,\nu}/\mu_\nu)m_{\nu,e} + (|J_{0,\nu\kappa}|/\mu_\nu)m_{\kappa,e}$ where $m_{\nu,e} = |\mathbf{m}_{\nu,e}|$ is the equilibrium magnetization in the absence of anisotropy and external field (that is, the solution of Eqs. (5.20) with $h_\nu = 0$) up to first order in $\delta m_\nu = m_\nu - m_{\nu,e}$, that is,

$$\begin{aligned} y_\nu &= y_\nu(m_\nu) = y_\nu(m_{\nu,e}) + \left(\frac{\partial y_\nu}{\partial m_\nu}\right)_{m_{\nu,e}} \delta m_\nu + \mathcal{O}(\delta m_\nu^2) \\ &= \beta\gamma_\nu\hbar\left[\frac{J_{0,\nu}}{\mu_\nu} m_{\nu,e} + \frac{J_{0,\nu\kappa}}{\mu_\nu}\tau_{\kappa,e}\right] + \frac{1}{S_\nu B_\nu'}\delta m_\nu \end{aligned} \tag{5.31}$$

where $\tau_{\kappa,e} = (\mathbf{m}_{\nu,e} \cdot \mathbf{m}_{\kappa,e})/m_{\nu,e}$ and $B_\nu' = B'(S_\nu\beta\gamma_\nu\hbar H_{\mathrm{EX},\nu,e})$. Replacing Eq. (5.31) in Eq. (5.30) we obtain

$$\begin{aligned} y_\nu - y_{0,\nu} &= \beta\gamma_\nu\hbar\left(\frac{1 - \beta J_{0,\nu} B_\nu'}{\mu_\nu \beta B_\nu'}\right)\delta m_\nu - \beta\gamma_\nu\hbar\frac{J_{0,\nu\kappa}}{\mu_\nu}\delta\tau_\kappa \\ &- \frac{\beta\gamma_\nu\hbar\mathbf{m}_\nu \cdot \mathbf{h}_\nu'}{m_\nu} + \mathcal{O}(h_\nu'^2) \end{aligned} \tag{5.32}$$

where $\delta\tau_\kappa = \tau_\kappa - \tau_{\nu,e}$, $\tau_\kappa = (\mathbf{m}_\nu \cdot \mathbf{m}_\kappa)/m_\kappa$. Moreover, we can write Eq. (5.32) in terms of the longitudinal susceptibility $\widetilde{\chi}_{\nu,\parallel}$ using (see Ref. [10])[1]

$$\frac{1 - \beta J_{0,\nu} B_\nu'}{\mu_\nu \beta B_\nu'} = \frac{1}{\widetilde{\chi}_{\nu,\parallel}}\left(1 + \frac{J_{0,\nu\kappa}}{\mu_\nu}\widetilde{\chi}_{\kappa,\parallel}\right) \tag{5.33}$$

[1] In this thesis we use a different definition of the longitudinal susceptibility than in Ref.[10]. In this thesis for the case of antiferremagnetic coupling we define $\widetilde{\chi}_{\nu,||} = [\partial m_\nu/\partial H_z]_{H_z=0}$ and $\widetilde{\chi}_{\kappa,||} = -[\partial m_\kappa/\partial H_z]_{H_z=0}$.

where the longitudinal susceptibility is given by

$$\widetilde{\chi}_{\nu,\parallel} = \frac{\mu_\kappa \beta B'_\nu J_{0,\nu\kappa} \beta B'_\kappa + \mu_\nu \beta B'_\nu \left(1 - J_{0,\kappa} \beta B'_\kappa\right)}{\left(1 - J_{0,\nu} \beta B'_\nu\right)\left(1 - J_{0,\kappa} \beta B'_\kappa\right) - J_{0,\kappa\nu} \beta B'_\nu J_{0,\nu\kappa} \beta B'_\kappa}. \tag{5.34}$$

Therefore, substituting Eq. (5.33) into Eq. (5.32) we obtain

$$\begin{aligned} y_\nu - y_{0,\nu} &= \beta \gamma_\nu \hbar \\ &\cdot \left[\frac{1}{\widetilde{\chi}_{\nu,\parallel}}\left(1 + \frac{J_{0,\nu\kappa}}{\mu_\nu}\widetilde{\chi}_{\kappa,\parallel}\right)\delta m_\nu - \frac{J_{0,\nu\kappa}}{\mu_\nu}\delta\tau_\kappa - \frac{\mathbf{m}_\nu \cdot \mathbf{h}'_\nu}{m_\nu}\right] \end{aligned} \tag{5.35}$$

and replacing Eq. (5.35) in Eq. (5.29) we have

$$1 - \frac{\tanh\left(\frac{y_{0,\nu}}{2}\right)}{\tanh\left(\frac{y_\nu}{2}\right)} = -\frac{\beta\gamma_\nu \hbar m_{\nu,e}}{\sinh(y_\nu(m_{\nu,e}))m_\nu^2}\mathbf{m}_\nu \cdot \mathbf{H}_{\text{eff},\nu} \tag{5.36}$$

where $y_\nu(m_{\nu,e}) = \beta\gamma_\nu\hbar H_{\text{EX},\nu,e}$ and

$$\mathbf{H}_{\text{eff},\nu} = \left[-\frac{1}{\widetilde{\chi}_{\nu,\parallel}}\left(1 + \frac{J_{0,\nu\kappa}}{\mu_\nu}\widetilde{\chi}_{\kappa,\parallel}\right)\delta m_\nu + \frac{J_{0,\nu\kappa}}{\mu_\nu}\delta\tau_\kappa\right]\frac{\mathbf{m}_\nu}{m_{\nu,e}} + \mathbf{h}'_\nu \tag{5.37}$$

is the effective field. Now, we are ready to simplify Eq. (5.15). Using Eqs. (5.27), (5.28) and (5.36) we can write the second term in the r.h.s. of Eq. (5.15) as

$$-2K_{2,\nu}\left(1 - \frac{\tanh\left(\frac{y_{0,\nu}}{2}\right)}{\tanh\left(\frac{y_\nu}{2}\right)}\frac{\mathbf{m}_\nu \cdot \mathbf{H}_\nu^{\text{MFA}}}{m_\nu H_\nu^{\text{MFA}}}\right)\mathbf{m}_\nu = \gamma_\nu\left[\frac{2K_{2,\nu}\beta\hbar m_{\nu,e}}{\sinh(y_\nu(m_{\nu,e}))}\right]\frac{(\mathbf{m}_\nu \cdot \mathbf{H}_{\text{eff},\nu})}{m_\nu^2}\mathbf{m}_\nu, \tag{5.38}$$

similarly, the third term in the r.h.s. of Eq. (5.15) becomes

$$\begin{aligned} &- K_{2,\nu}\frac{\tanh\left(\frac{y_{0,\nu}}{2}\right)}{\tanh\left(\frac{y_\nu}{2}\right)}\left(\frac{2(S_\nu+1)\tanh\left(\frac{y_\nu}{2}\right)}{m_\nu} - 1\right)\frac{\mathbf{m}_\nu \times (\mathbf{m}_\nu \times \mathbf{H}_\nu^{\text{MFA}})}{m_\nu H_\nu^{\text{MFA}}} \\ &= -K_{2,\nu}m_{\nu,e}\left(\frac{2(S_\nu+1)\tanh\left(\frac{y_\nu(m_{\nu,e})}{2}\right)}{m_{\nu,e}} - 1\right)\frac{\mathbf{m}_\nu \times (\mathbf{m}_\nu \times \mathbf{H}_{\text{eff},\nu})}{m_\nu^2 H_{\text{EX},\nu,e}} \end{aligned} \tag{5.39}$$

and the forth term in the r.h.s. of Eq. (5.15) reads

$$\begin{aligned} &(K_{2,\nu} - K_1)\left[\frac{(\mathbf{m}_\nu \times \mathbf{H}_\nu^{\text{MFA}})^2}{(m_\nu H_\nu^{\text{MFA}})^2}\mathbf{m}_\nu + \frac{(\mathbf{m}_\nu \cdot \mathbf{H}_\nu^{\text{MFA}})\mathbf{m}_\nu \times (\mathbf{m}_\nu \times \mathbf{H}_\nu^{\text{MFA}})}{(m_\nu H_\nu^{\text{MFA}})^2}\right] \\ &= m_{\nu,e}(K_{2,\nu} - K_1)\left[\frac{\mathbf{m}_\nu \times (\mathbf{m}_\nu \times \mathbf{H}_{\text{eff},\nu})}{m_\nu^2 H_{\text{EX},\nu,e}}\right]. \end{aligned} \tag{5.40}$$

Hence, replacing Eqs. (5.38), (5.39) and (5.40) in Eq.(5.15) we obtain

$$\begin{aligned}\frac{d\mathbf{m}_\nu}{dt} &= -\gamma_\nu \mathbf{m}_\nu \times \mathbf{H}_{\text{eff},\nu} + \gamma_\nu \frac{\alpha_\nu^{\parallel}}{m_\nu^2}(\mathbf{H}_{\text{eff},\nu}\cdot\mathbf{m}_\nu)\mathbf{m}_\nu \\ &- \gamma_\nu \frac{\alpha_\nu^{\perp}}{m_\nu^2}\mathbf{m}_\nu \times (\mathbf{m}_\nu \times \mathbf{H}_{\text{eff},\nu}) \end{aligned} \tag{5.41}$$

where

$$\alpha_\nu^{\parallel} = \frac{2\lambda_\nu}{\beta\tilde{J}_{0,\nu,e}}\left(\frac{S_\nu}{S_\nu+1}\right)\frac{2q_\nu}{\sinh(2q_\nu)} \tag{5.42}$$

$$\alpha_\nu^{\perp} = \lambda_\nu\left[\frac{\tanh(q_\nu)}{q_\nu} - \frac{2S_\nu}{(S_\nu+1)\beta\tilde{J}_{0,\nu,e}}\left(1-\frac{K_1}{2K_{2,\nu}}\right)\right] \tag{5.43}$$

where $\tilde{J}_{0,\nu,e} = J_{0,\nu} + J_{0,\nu\kappa}(\mathbf{m}_{e,\nu}\cdot\mathbf{m}_{e,\kappa})/m_{e,\nu}^2 = J_{0,\nu} + |J_{0,\nu\kappa}|(m_{e,\kappa}/m_{e,\nu})$, $q_\nu = (\beta\tilde{J}_{0,\nu,e}m_{e,\nu})/(2S_\nu)$ and $\lambda_\nu = [\beta\mu_\nu K_{2,\nu}(S_\nu+1)]/[\gamma_\nu S_\nu]$ and the effective field is given by Eq. (5.37), that is,

$$\begin{aligned}\mathbf{H}_{\text{eff},\nu} &= \left[-\frac{1}{\Lambda_{\nu\nu}}(m_\nu - m_{\nu,e}) + \frac{1}{\Lambda_{\nu\kappa}}(\tau_\kappa - \tau_{\kappa,e})\right]\frac{\mathbf{m}_\nu}{m_\nu} \\ &+ \frac{J_{0,\nu\kappa}}{\mu_\nu}\mathbf{\Pi}_\kappa + \mathbf{H} + \mathbf{H}_{A,\nu} \end{aligned} \tag{5.44}$$

where

$$\Lambda_{\nu\nu}^{-1} = \frac{1}{\widetilde{\chi}_{\nu,\parallel}}\left(1 + \frac{J_{0,\nu\kappa}}{\mu_\nu}\widetilde{\chi}_{\kappa,\parallel}\right), \tag{5.45}$$

$$\Lambda_{\nu\kappa}^{-1} = \frac{J_{0,\nu\kappa}}{\mu_\nu}. \tag{5.46}$$

In Fig. 5.5 we show a comparison between Eq. (5.15) and Eq. (5.41) for a temperature step. As we see Eq. (5.41) is a good approximation of Eq. (5.15) for small deviations from the equilibrium state. As we will see in the next chapter the advantage of (5.41) is that from it one can obtain an analytical expression of the longitudinal relaxation time as function of the system's parameters. However, Eq. (5.41) should not be used in dynamical processes with high deviations from the equilibrium state, for such situations Eq. (5.15) should be used instead.

5.4 Limiting cases of the qLLB equation

In Fig. 5.6 we show a diagram which describes the limiting cases of the qLLB equation for disordered magnetic alloys given by Eq. (5.41). Namely, taking the

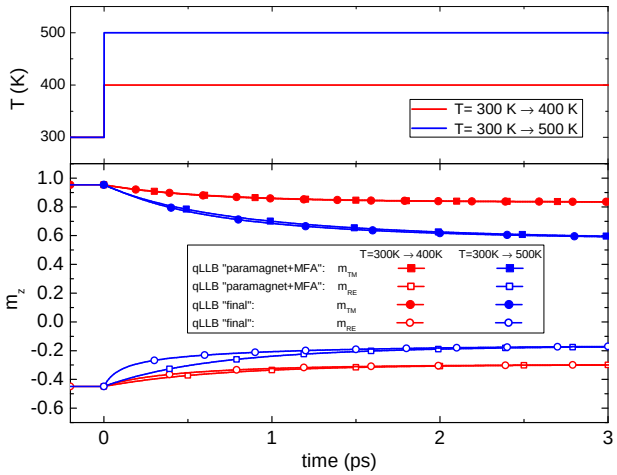

Figure 5.5: Comparison between Eq. (5.15) called "paramagnet+MFA" and Eq. (5.41) called "final" for two temperature steps.

limits $S_\nu \to \infty$ and $S_\kappa \to \infty$ in Eq. (5.41) one arrives to the classical LLB equation for disordered magnetic alloys, that is, Eq. (5.6). If the limit $x_\kappa \to 0$ (i.e., the impurities are removed) is taken in Eq. (5.6) then one arrives to the classical LLB equation of a ferromagnet described in Ref. [49]. On the other hand, if the limit $x_\kappa \to 0$ is taken in Eq. (5.41) then one arrives to the qLLB equation for a ferromagnet given in Eq. (3.18). Finally, if the limit $S \to \infty$ is done in Eq. (3.18) one obtains the classical LLB equation of a ferromagnet described in Ref. [49].

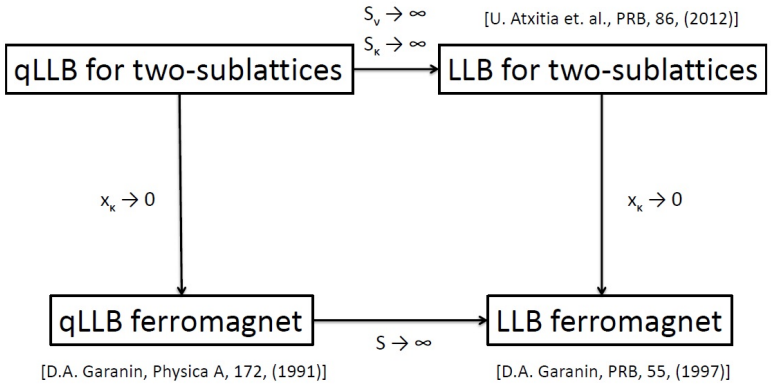

Figure 5.6: Diagram showing the limiting cases of the qLLB equation for a two-sublattice magnet.

5.5 Comparison between quantum and classical LLB equation for two-component magnets

In this section we compare the qLLB equation for disordered magnetic alloys with its classical counterpart. We choose the values of the exchange parameters similar to GdFeCo which corresponds to $T_{c,TM} = 722$ K, $T_{c,RE} = 290$ K and $T_{c,TM-RE} = 251$ K. For FeCo sublattice we use the spin number equal to 1/2 and for Gd equal to 7/2.

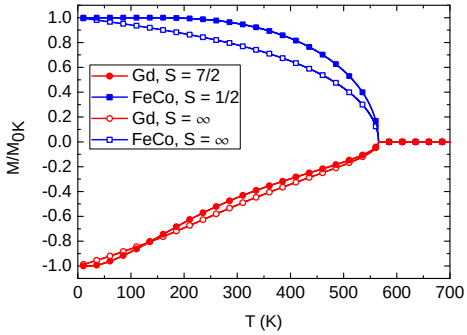

Figure 5.7: Comparison of the equilibrium magnetization between the quantum and classical case.

In Fig. 5.7 we show the equilibrium magnetization versus temperature for the classical and quantum case for a Gd concentration of $x_{Gd} = 0.25$, we get $T_c = 565$ K. We also use $\gamma_{TM} = \gamma_{RE} = 1.76 \times 10^7$ rad s^{-1} Oe^{-1} and $\lambda_{TM} = \lambda_{RE} = 0.1$.

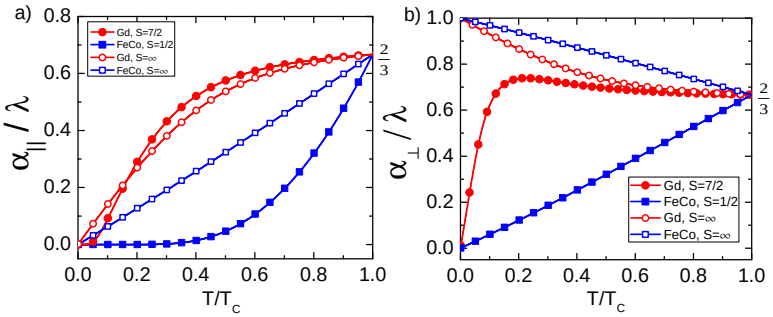

Figure 5.8: a) Longitudinal damping versus temperature, b) Transverse damping versus temperature.

In Figs. 5.8 we present the longitudinal and transverse dampings versus temperature for quantum and classical case. We see that since Gd spin is quite high

($S_{Gd} = 7/2$) its dampings is very similar to the classical case, however for FeCo the quantum case is smaller than in the classical limit for both dampings. In Fig. 5.9 we show a comparison of the normalized magnetization dynamics between the quantum and classical case for a temperature step. We observe that in the quantum case for FeCo we have a slower longitudinal relaxation than in the classical one.

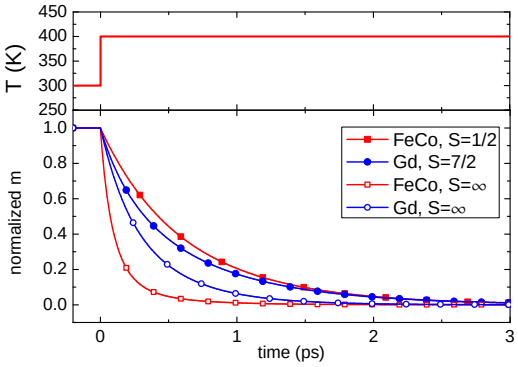

Figure 5.9: Comparison of the normalized magnetization dynamics between the quantum and classical case for a temperature step.

5.6 Conclusions

In this chapter we have presented novel quantum and classical LLB equations for two-component magnets, which can be applied to ferrimagnetic materials like GdFeCo where an ultrafast switching has been reported [70, 136] but also to ferromagnetic alloys like Permalloy. The new equations constitute an important step forward in description of the dynamics of ferrimagnets which is traditionally based on two-coupled macroscopic LLG equations. For example, the FMR and exchange modes have recently attracted attention due to possibility to optically excite them [105, 135]. Their temperature dependence can be now correctly understood in terms of our approach [128]. Furthermore, recent ultrafast dynamics experiments using XMCD showed different sublattice dynamics on ultrafast timescale in a two-sublattice magnets such as GdFeCo [70] or FeNi [118], which can be modeled using this new approach. These equations can serve in the future as a basis for multiscale modeling in two-component systems at high temperatures and/or ultrafast timescales, in the same way as the LLB equation for ferromagnets [78]. This also opens a possibility for micromagnetic modeling of ultrafast dynamics in large structures, such as sub-micron and micron-size ferrimagnetic

dots, whose dimensions do not allow modeling by atomistic approach. Similarly, it will be useful for static micromagnetic modeling at high temperatures, such as thermally-driven domain wall motion in nanostructures.

Conclusiones en español

En este capítulo hemos presentado unas nuevas ecuaciones de LLB clásica y cuántica para materiales magnéticos compuestos de dos subredes, las cuales pueden ser utilizadas para describir la dinámica ultrarrápida en materiales ferrimagnéticos como GdFeCo sino tambien para aleaciones ferromagnéticas como Permalloy. Estas ecuaciones constituyen un paso importante en la descripción de la dinámica de materiales ferrimagnéticos los cuales tradicionalmente han sido descritos usando dos ecuaciones macroscópicas de LLG acopladas. Estas ecuaciones pueden servir como base para la modelización multiescala en sistema de dos componentes a altas temperaturas y/o escalas de tiempo ultrarrápida, de forma similar que la ecuación de LLB en materiales ferromagnéticos[78]. Además, estas ecuaciones abren la posibilidad de una modelización micromagnética de la dinámica ultrarrápida en sistemas de gran tamaño que no pueden ser modelizados mediante simulaciones atomísticas.

6

Relaxation rates and switching time of disordered ferrimagnets

6.1 Introduction

The possibility to switch magnetization at the ultra-fast timescale with laser pulses has been fascinating the scientific community for already more than 15 years. Up to now the ultra-fast heat-mediated switching has been observed in the antiferromagnetically coupled materials such as disordered ferrimagnetis GdFeCo[70], TbCo[4], TbFe[61], TbFeCo [32], DyCo [102], HoFeCo [102], synthetic ferrimagnets [43, 102, 131]. The switching mechanism involves the angular momentum transfer from the ferromagnetic precessional mode to the aniferromagnetic one [12]. These materials consist of sublattices with different demagnetisation speed: fast transition metal material and slow rare earth material. Under the influence of the laser pulse the fast material arrives at almost zero magnetisation. At this moment the magnetisation of the slow material has a non-zero value and provides an exchange field acting on the fast material. The switching is fast due to the fact that it occurs in a string exchange field. Therefore, one could expect that the most efficient switching would correspond to the situation where the difference in the speed in two two materials is the highest.

The main features of the ultra-fast dynamics in these materials are very well described by the atomistic simulations based on the Heisenberg model with Langevin dynamics. However, the LLB equation for disordered magnetic alloys that we have presented in the previous chapter is a suitable tool to understand the difference in demagnetisation speeds of two-component coupled materials.

6.2 Linearised LLB equation

In order to analyse the demagnetisation speeds of two-component coupled materials we linearise the qLLB equation given by Eq. (5.41). Namely, we assume that the magnetization of each sublattice is parallel (ferromagnetic coupling) or antiparallel (antiferromagnetic coupling) to each other ($\tau_\kappa = (\mathbf{m}_\nu \cdot \mathbf{m}_\kappa)/m_\nu = \pm m_\kappa$, $\tau_{\kappa,e} = \pm m_{\kappa,e}$ where sign + is for ferromagnetic coupling and sign − is for antiferromagnetic coupling), and we neglect the anisotropy and external magnetic fields. Thus Eq. (5.41) for the magnetisation of the sublattice $\nu = \text{TM,RE}$ becomes

$$\frac{dm_\nu}{dt} = -\gamma_\nu \alpha_\parallel^\nu \left[\frac{1}{\Lambda_{\nu\nu}} (m_\nu - m_{e,\nu}) - \frac{1}{\Lambda_{\nu\kappa}} (m_\kappa - m_{e,\kappa}) \right], \tag{6.1}$$

where $m_\nu = |\mathbf{m}_\nu|$ and all the quantities have the same meaning as in the previous chapter, except $\Lambda_{\nu\kappa}^{-1} = |J_{0,\nu\kappa}|/\mu_\nu$. Then, taking into account that $dm_{e,\nu}/dt = 0$ we arrive to the linearised qLLB equation of the form

$$\frac{d}{dt} \begin{pmatrix} \delta m_{\text{TM}} \\ \delta m_{\text{RE}} \end{pmatrix} = \mathcal{A}_\parallel \begin{pmatrix} \delta m_{\text{TM}} \\ \delta m_{\text{RE}} \end{pmatrix}, \tag{6.2}$$

where $\delta m_{\text{TM(RE)}} = m_{\text{TM(RE)}} - m_{e,\text{TM(RE)}}$ and the matrix $\mathcal{A}_\parallel$ reads

$$\mathcal{A}_\parallel = \begin{pmatrix} -\gamma_{\text{TM}} \alpha_\parallel^{\text{TM}}/\Lambda_{\text{TT}} & \gamma_{\text{TM}} \alpha_\parallel^{\text{TM}}/\Lambda_{\text{TR}} \\ \gamma_{\text{RE}} \alpha_\parallel^{\text{RE}}/\Lambda_{\text{RT}} & -\gamma_{\text{RE}} \alpha_\parallel^{\text{RE}}/\Lambda_{\text{RR}} \end{pmatrix} = \begin{pmatrix} -\Gamma_{\text{TT}} & \Gamma_{\text{TR}} \\ \Gamma_{\text{RT}} & -\Gamma_{\text{RR}} \end{pmatrix}. \tag{6.3}$$

It is important to note that the matrix elements in equation (6.3) are temperature dependent. The general solution of the characteristic equation, $|\mathcal{A}_\parallel - \Gamma^\pm \mathcal{I}| = 0$, gives two different eigenvalues

$$\Gamma^\pm = \frac{-(\Gamma_{\text{TT}} + \Gamma_{\text{RR}}) \pm \sqrt{(\Gamma_{\text{TT}} - \Gamma_{\text{RR}})^2 + 4\Gamma_{\text{RT}}\Gamma_{\text{TR}}}}{2} \tag{6.4}$$

corresponding to the eigenvectors $\mathbf{v}_\pm = (\Gamma_{\text{TR}}, -(\Gamma_{\text{TT}} + \Gamma^\pm))$. In ferromagnets, relaxation can usually be described well by only one relaxation rate, at least in the linear regime. By contrast, in two sublattice ferrimagnets, a combination of the two characteristic relaxation rates $\Gamma^\pm$ describes the magnetization relaxation of each sublattice with a weighting determined by the eigenvectors. This means that one cannot describe the relaxation of a two-component system with as single exponential decay function except in some limits.

6.3 Application to GdFeCo

To be more specific, we consider a model of $Gd_x(FeCo)_{q=1-x}$ alloy. The numerical value of the MFA exchange parameters ($J_{\text{FeCo-FeCo}}$, $J_{\text{Gd-Gd}}$ and $J_{\text{FeCo-Gd}}$) are obtained from a renormalization[116] of the atomistic exchange parameters given in Ref. [12], that is, $J^{\text{atom}}_{\text{FeCo-FeCo}} = 6.92 \cdot 10^{-21}$ J, $J^{\text{atom}}_{\text{Gd-Gd}} = 2.78 \cdot 10^{-21}$ J and $J^{\text{atom}}_{\text{FeCo-Gd}} = -2.41 \cdot 10^{-21}$ J, in order to get the same Curie temperatures. However, one we should note that the alloy has a shared Curie temperature. The magnetic moments used are $\mu_{FeCo} = 1.92\mu_B$ and $\mu_{Gd} = 7.63\mu_B$ where μ_B is the Bohr magneton. Furthermore, the generic character of the ferrimagnet is simulated by varying the antiferromagnetic coupling strength, $J^{\text{atom}}_{\text{FeCo-Gd}}$. Note that the two-sublattices have a shared Curie temperature except for a very small inter-sublattice coupling.

In Fig. 6.1 we present the matrix elements of $\mathcal{A}_{\parallel}$ and $\Gamma^{\pm}$ as function of the temperature using a rare-earth concentration of $x = 0.25$ for the quantum case with $S_{FeCo} = 1/2$ and $S_{Gd} = 7/2$ (Fig. 6.1 a)) and classical limit $S_{FeCo} = \infty$ and $S_{Gd} = \infty$ (Fig. 6.1 b)). Let's define the temperature where $\Gamma_{TT} = \Gamma_{RR}$ as the "coupling temperature" T_{co}. We see that in the quantum case there are two couplings temperatures $T_{co,1}$ and $T_{co,2}$, these temperatures allows as to identify three temperature regions: i) at $T < T_{co,1}$ we have $\Gamma_{TT} \simeq |\Gamma^{+}|$ and $\Gamma_{RR} \simeq |\Gamma^{-}|$, ii) at $T_{co,1} < T < T_{co,2}$ we have $\Gamma_{TT} \simeq |\Gamma^{-}|$ and $\Gamma_{RR} \simeq |\Gamma^{+}|$, iii) at $T_{co,2} < T$ we have $\Gamma_{TT} \simeq |\Gamma^{+}|$ and $\Gamma_{RR} \simeq |\Gamma^{-}|$. However, in the classical limit there is just one coupling temperature, thus we can identify two temperature regions: i) at $T < T_{co}$ we have $\Gamma_{TT} \simeq |\Gamma^{-}|$ and $\Gamma_{RR} \simeq |\Gamma^{+}|$, ii) at $T_{co} < T$ we have $\Gamma_{TT} \simeq |\Gamma^{+}|$ and $\Gamma_{RR} \simeq |\Gamma^{-}|$.

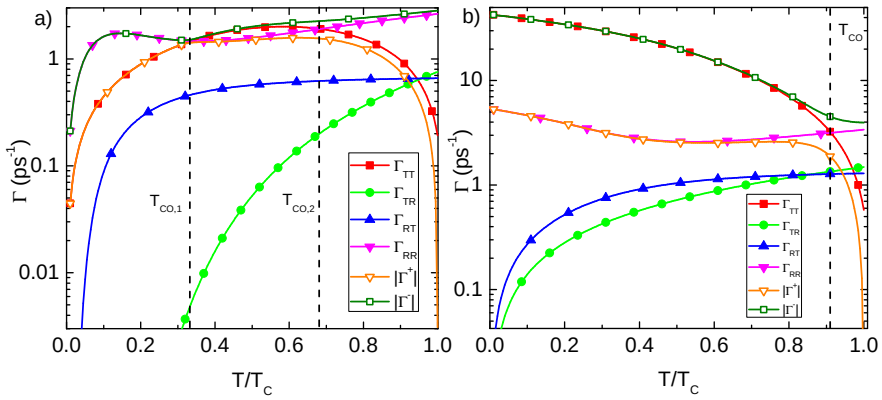

Figure 6.1: The matrix elements of $\mathcal{A}_{\parallel}$ and $\Gamma^{\pm}$ as function of the temperature using a rare-earth concentration of $x = 0.25$ for a) quantum case with $S_{FeCo} = 1/2$ and $S_{Gd} = 7/2$, b) classical limit $S_{FeCo} = \infty$ and $S_{Gd} = \infty$.

6.3.1 Longitudinal relaxation rates

In the classical limit at low temperatures ($T < T_{co}$) we also have that $\Gamma_{TT(RR)} \gg \Gamma_{TR(RT)}$, therefore the longitudinal relaxation time of each sublattice in this temperature region can be written as $\tau_{TM} \simeq 1/\Gamma_{TT}$ and $\tau_{RE} \simeq 1/\Gamma_{RR}$. Thus each subsystem could be characterized by the corresponding longitudinal time $\tau_{TM,RE}$, although we should stress that the rates Γ_{RR}, Γ_{TT} depend on parameters of both subsystems. Taking into account that the exchange field is large, one can estimate the longitudinal relaxation time of each sublattice in this region as

$$\tau_\nu \approx \frac{1}{2\gamma_\nu \lambda_\nu m_{\nu,e} H^{ex}_{\nu,e}}, \tag{6.5}$$

where

$$H^{ex}_{\nu,e} = \frac{J_{0,\nu}}{\mu_\nu} m_{e,\nu} + \frac{|J_{0,\nu\kappa}|}{\mu_\nu} m_{e,\kappa}. \tag{6.6}$$

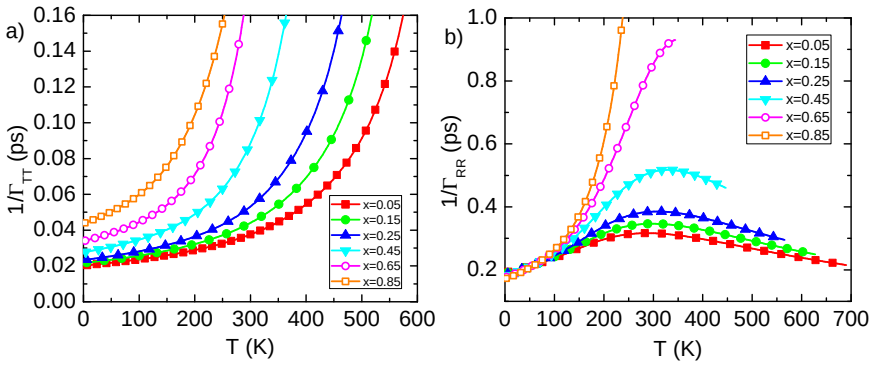

Figure 6.2: a) $1/\Gamma_{TT} \simeq \tau_{TM}$ as function of the temperature for different rare-earth concentrations, b)$1/\Gamma_{RR} \simeq \tau_{RE}$ as function of the temperature for different rare-earth concentrations.

Furthermore, the temperature dependence of $\tau^{\parallel}_{TM,RE}$ (obtained from the evaluation of $1/\Gamma_{TT,RR}$ given by Eq. (6.3)) varying the inter-sublattice strength is presented in Fig. 6.3 for $x = 0.25$, and in Fig. 6.2 - varying the RE concentration and fixing the inter-sublattice exchange. For large temperatures the TM material experience critical slowing down. The behavior of the RE material is more complicated. Namely, only for large coupling and intermediate RE concentration the critical slowing down at common Curie temperature occurs. In all other cases the slowing down occurs at temperatures corresponding to the individual Curie temperature of the RE material. The functional dependence of relaxation times can be understood taken into account that it is inversely proportional to

the exchange field through Eq. (6.5) which in turn is proportional to the inter-sublattice exchange field. As the coupling strength increases, the MFA exchange field increases and, thus, both RE and TM become slower. At the same time, the dependence of the exchange field on the RE concentration via Eq. (6.6) is more complicated. It follows from Eqs. (6.5) and (6.6) that for $J_{0,\mathrm{TM}}m_{\mathrm{T}} > J_{0,\mathrm{TR}}m_{\mathrm{R}}$ the exchange field acting on the TM decreases with the rare earth concentration and the TM material becomes slower in agreement with Fig. 6.2 (a). The same happens for the RE elements if $J_{0,\mathrm{TR}}m_{\mathrm{T}} > J_{0,\mathrm{RE}}m_{\mathrm{R}}$, in agreement with Fig. 6.2 (b). At the same time it is clear that for larger inter-sublattice exchange coupling the above inequality for the TM metal can be violated, while for the RE it always holds. Thus, we can have situation in which TM fastens with concentration while the RE still slows down. The transition between the two behaviors is depicted in Fig. 6.4, where we present only concentration values typical for the experiment and corresponding to the window where the magnetisation switching takes place. The decrease of the TM relaxation time with concentration for large inter-sublattice exchange strength indicates that one can expect a non-trivial behavior as a function of concentration.

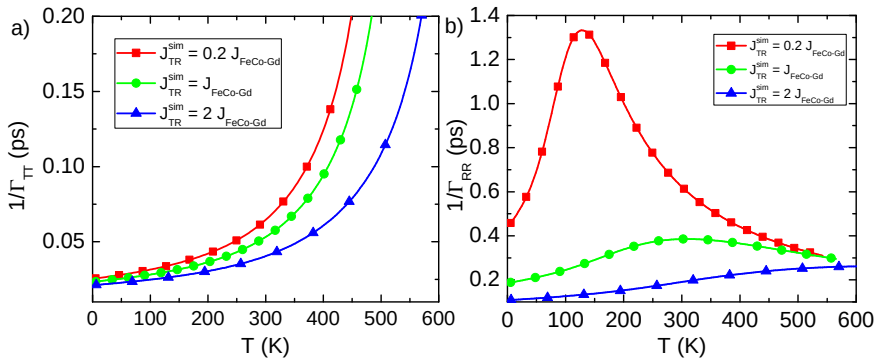

Figure 6.3: a) $1/\Gamma_{TT} \simeq \tau_{TM}$ as function of the temperature for different inter-sublattice interaction strength (J_{TR}^{sim}) with $x = 0.25$, b)$1/\Gamma_{RR} \simeq \tau_{RE}$ as function of the temperature for different inter-sublattice interaction strength (J_{TR}^{sim}) with $x = 0.25$.

At high temperatures the estimation of the relaxation rates based on only one eigenvalue is not valid. However, to comply with the widely used procedure, we fit the numerically integrated relaxation time at high temperatures to one exponential function for each sub-lattice. The integration of the original LLB equation (5.6) is performed with initial conditions taken as a small deviations of each sublattice from its equilibrium, i.e., $m_\nu(0) = m_{e,\nu} + \delta m_{e,\nu}$. The results are presented in Fig. 6.5 for three temperatures above the coupling temperature

in comparison with the analytically estimated relaxation time. One observes that, firstly, the linear one-exponential approximation is valid for small coupling strength. Secondly, at high temperatures the RE accelerates as a function of temperature while the TM slows down. This phenomena is also present in the behavior of the matrix elements and the combined rates in Fig. 6.1 and can be explained by the fact that while the TM has a critical behavior at the common Curie temperature, the RE material presents a strong critical behavior in the temperature, close to its own Curie temperature but its relaxation rates are almost constant at high temperatures.

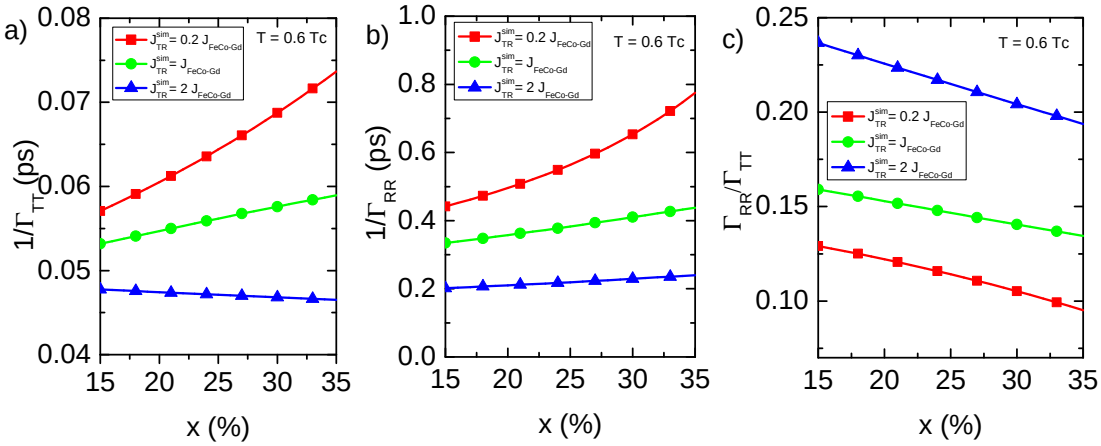

Figure 6.4: a) $1/\Gamma_{TT}$, b) $1/\Gamma_{RR}$ and c) Γ_{RR}/Γ_{TT} versus the rare-earth concentration for different strength couplings between both sublattices (J^{sim}_{TR}) at $T = 0.6T_c$.

To analyse the consequences of the above conclusions on the switching of a ferrimagnet, we can adopt a usually made simplification by considering a step function for the electronic temperature (see, for example. Refs.[5, 12]). We also note from previous atomistic simulations that the switching occurs well after the laser pulse is gone. Thus although the electronic temperature may go above the Curie temperature, the relaxation time of a sublattice during the ultra-fast laser-induced switching may be approximately characterized by its relaxation at the final (quasi-equilibrium) electron temperature which is below T_C. The switching in GdFeCo will be effective if τ_{TM} is small and τ_{RE} is large, since in this case we could expect a large field acting on the TM material. This reasoning indicates that if the quasi-equilibrium temperature stays close to T_C, the switching is ineffective, since in this case the TM relaxation time is as large as that of the RE. The switching diagram as a function of the temperatures can be found in Refs.[5, 12, 144] and indicates that the switching is suppressed for high temperatures. Here we are interested to understand the phenomena as a function of the RE

concentration. The results presented in Fig. 6.5 indicate that the most effective conditions for the switching and usual inter-sublattice strength should correspond to systems with larger Gd concentrations. Indeed, then TM becomes faster and the field acting on it in the moment when it reaches almost zero magnetisation -larger. Fig. 6.5 also indicates that the situation may change for more coupled alloys.

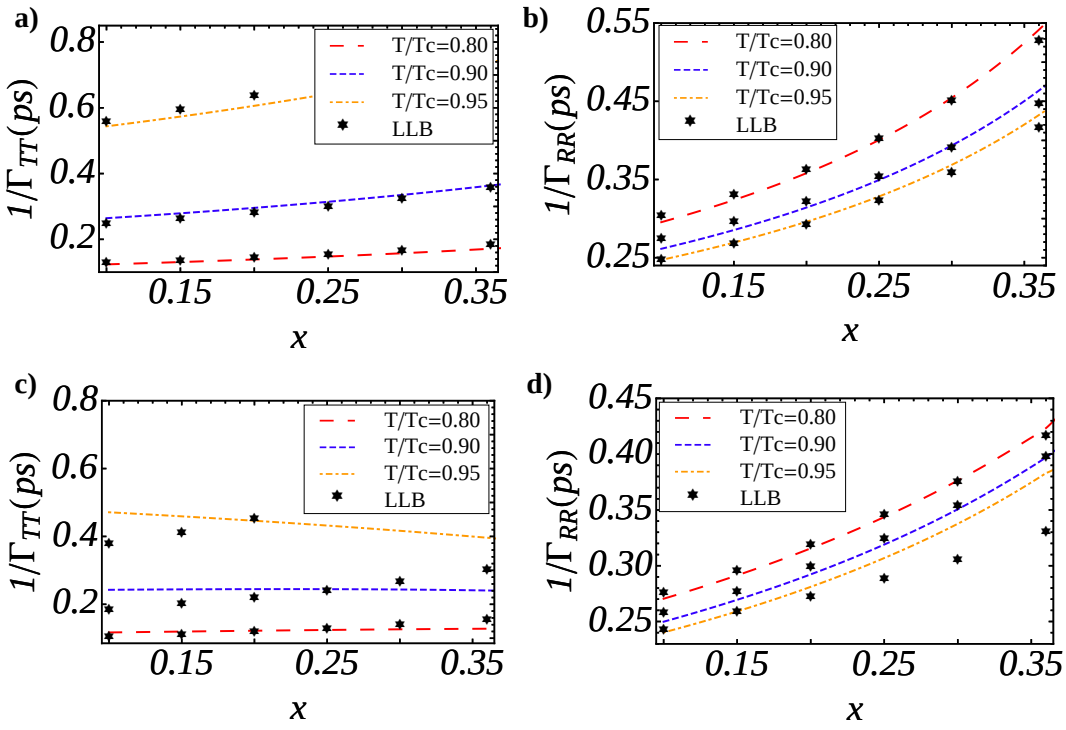

Figure 6.5: $1/\Gamma_{TT}$ and $1/\Gamma_{RR}$ as a function of the rare-earth concentration for different reduced temperatures. The lines indicate the relaxation times obtained via the evaluation of the eigenvalues Eq.(6.3) while the points indicate the direct numerical integration of the LLB Equation and fit to the one-exponential function. The Figs. 6.5 a), b) corresponding to the strength coupling values $J_{FeCo-Gd} = 0.2J^{MFA}_{FeCo-Gd}$, and Figs. 6.5 c), d) for $J_{FeCo-Gd} = J^{MFA}_{FeCo-Gd}$.

To check the predictions, we perform atomistic modeling of a disordered TM-RE ferrimagnet under the influence of ultra-fast laser pulse. The model is described in details in Refs. [5, 12]. The dynamics is modelled by the Langevin dynamics based on Landau-Lifshitz-Gilbert equation of motion for localized atomic magnetic moments, see e.g. Ref. [12]. The input electron temperature is dynamically varied using the two-temperature model with the parameters from Ref.[12]. In Fig. 6.6 we present the reversal time $t_{\mathrm{rev},TM(RE)}$ of each sublattice (defined

as time elapsed between the initial state and the instant of time at which the average magnetization starts to reverse its direction, *i.e.* crosses $m_{z,TM(RE)} = 0$ point) versus the rare-earth concentration for two values of the inter-sublattice strength couplings. In agreement with the predictions of the relaxation rates, the switching is faster for a strongly coupled system and the RE switching time increases as a function of the its concentration. The behavior of the TM is more complicated. In fact, its dependence on concentration is not very pronounced. In the situation corresponding to the usual FeCoGd coupling strength, the TM switching time decreases with the RE concentration. Our findings are in agreement with the fact that the switching window is larger for FeCoGd material with larger Gd concentration, see Ref.[5]. They are also in agreement with recently published experimental results [56] where the XMCD measurements in GdFeCo have shown that the material is not homogeneous and the reversal starts in Gd-rich regions. In agreement with the results presented in Fig.6.6, those regions, indeed would correspond to the minimum TM reversal time and the maximum field coming from the RE. For larger coupling strength, however, the reversal time as a function of Gd concentration has a maximum and then decreases. This indicates that in this case the reversal could start in regions with smaller Gd concentration.

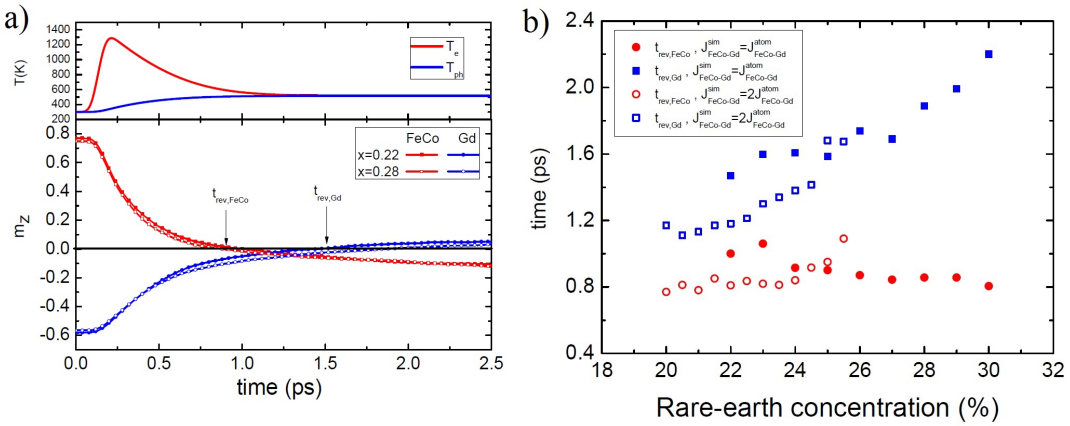

Figure 6.6: a) Magnetization dynamics obtained by atomistic simulations for $x = 0.22$ and $x = 0.28$, b) the reversal time $t_{\mathrm{rev},FeCo(Gd)}$ versus the rare-earth concentration for different strength couplings between both sublattices.

6.4 Conclusions

In this chapter we have analysed the temperature and concentration dependence of the relaxation rates of the "fast" and "slow" components of ferrimagnetic alloys within the framework of the Landau-Lifshitz-Bloch model for ferrimagnets. Our results indicate that the "fast" (TM) material experience critical slowing down at the common Curie temperature, while the "slow" RE material does not do this. Both materials typically slow down as a function of the RE concentration although this dependence can be reverted for the TM for large inter-sublattice coupling strengths. This has a remarkable consequence on the switching time. We show that for the values of the coupling strength corresponding to typical parameters of the GdFeCo sublattice the reversal should start in Gd rich region. The situation may be opposite for compounds with stronger inter-sublattice couplings.

Conclusiones en español

En este capítulo hemos analizado la dependencia con la temperatura y la concentración de los tiempos de relajación de los componentes "rápido" y "lento" en la aleación ferrimagnética de GdFeCo usando la ecuación de LLB para materiales formados por dos componentes. Nuestros resultados muestran la dinámica longitudinal del material "rápido" (TM) se hace extraordinariamente más lenta cerca de la temperatura de Curie común, mientras que para el material "lento" (RE) no ocurre este hecho. De forma general, a medida que aumenta la concentración de RE la dinámica longitudinal de ambos compuestos se hacen más lentos aunque esta tendencia puede invertirse en el TM para altos valores del acoplo de canje entre ambos compuestos. Este hecho tiene consecuencias importantes en el tiempo de inversión magnética. Para valores de canje similares a GdFeCo obtenemos que la inversión ultrarrápida debería iniciarse en la regiones con mayor concentración de Gd. Sin embargo, para valores de canje entre los compuestos mayores podría ocurrir lo opuesto.

6. RELAXATION RATES AND SWITCHING TIME OF DISORDERED FERRIMAGNETS

7

Free energy of a two sublattice magnet

7.1 Introduction

In magnetism from the free energy (Helmholtz free energy) one can extract interesting properties of a magnetic system like equilibrium magnetization, effective field, susceptibility, heat capacity,... In 1963 Brown[27] developed a zero-temperature magnetic free energy where the magnetization is considered as a fixed length vector. This approach can also be also applied at low temperatures (far below the Curie temperature T_c) taking into account the temperature dependence of parameters like the magnetization saturation, anisotropy,.... On the other hand, close to T_c the magnetic free energy can be written as a Landau expansion[95] where the magnetization can change in length and direction. In 2001 H. Kachkachi and D. Garanin[74] derived a generalized free energy within the MFA for a weakly anisotropic ferromagnet which is valid in the whole range of temperature (see Eq. (2.21)).

From the point of view high temperature dynamics (like ultrafast magnetism) the free energy is also very interesting since the effective field of the classical LLB equation for ferromagnets can be recovered from it[49]. For the case of two-component magnets Mentink *et al.*[108] presented a general theoretical framework for ultrafast spin dynamics where the effective fields were extracted from a free energy derived by Baryakhtar[15].

In this chapter we investigate the free energy for two sublattice magnets. In principle, there are several approaches of calculating the free energy within the MFA. However, Agra *et al.*[3] showed that the route called "alternative MFA formulation" (which was followed by H. Kachkachi *et al.*[74] to derive a generalized free energy for ferromagnets) can lead to non-physical free energy landscapes for

two sublattice systems. In appendix D we present the calculation of the free energy of a classical Heisenberg two sublattice magnet using the "alternative MFA formulation" and we show that for some exchange parameter values the expected equilibrium states are saddle points instead of minimums. Alternatively, the route called "variational MFA procedure" leads to physical energy landscapes for the all range of exchange parameters, therefore in this chapter we present a detailed derivation of the free energy for two sublattice magnets using this approach.

7.2 Heisenberg Hamiltonian of a two sublattice magnet

In ultrafast magnetism the main interaction in the exchange one. Therefore, for simplicity we consider a two-sublattice magnet described by the following Heisenberg Hamiltonian

$$\mathcal{H} = -\frac{1}{2}\sum_{i,j\in A;i\neq j} J_{ij}\mathbf{s}_i\cdot\mathbf{s}_j - \frac{1}{2}\sum_{i,j\in B;i\neq j} J_{ij}\mathbf{s}_i\cdot\mathbf{s}_j - \sum_{i\in A,j\in B} J_{ij}\mathbf{s}_i\cdot\mathbf{s}_j \quad (7.1)$$

where i, j are lattices sites, J_{ij} is the Heisenberg exchange interaction parameter and $\mathbf{s}_i = \boldsymbol{\mu}_i/\mu_i$ is the unit length classical spin vector with $\mu_i = \mu_{A(B)}$ is the magnetic moment of the atom A(B). Notice that in the last term Eq. (7.1) there isn't a factor 1/2 since in these summations no double counting takes place.

7.3 Calculation of the free energy using the variational procedure

Firstly, we introduce briefly the variational free energy technique[3]. The exact free energy of the system described by the Hamiltonian (7.1) is given by

$$\mathcal{F} = -\frac{1}{\beta}\ln\mathcal{Z} = -\frac{1}{\beta}\ln\left[\int e^{-\beta\mathcal{H}}\mathbf{ds}_1...\mathbf{ds}_n\right] \quad (7.2)$$

where $\mathcal{Z}$ is the partition function, $\beta = 1/(k_BT)$ with k_B being the Boltzmann constant and n is total number of spins. Now, the Hamiltonian is written as

$$\mathcal{H} = \mathcal{H}_0 + (\mathcal{H} - \mathcal{H}_0) \quad (7.3)$$

where $\mathcal{H}_0$ is a trial Hamiltonian, then after some rearrangement the free energy becomes

$$\mathcal{F} = \mathcal{F}_0 - \frac{1}{\beta}\ln\langle e^{-\beta(\mathcal{H}-\mathcal{H}_0)}\rangle_0 \quad (7.4)$$

where $\mathcal{F}_0$ is the free energy corresponding to the trial Hamiltonian, that is,

$$\mathcal{F}_0 = -\frac{1}{\beta}\ln \mathcal{Z}_0, \quad \mathcal{Z}_0 = \int e^{-\beta\mathcal{H}_0}\mathbf{ds}_1...\mathbf{ds}_n \tag{7.5}$$

and the symbol $\langle ...\rangle_0$ stands for

$$\langle A\rangle_0 \;=\; \frac{1}{\mathcal{Z}_0}\int e^{-\beta\mathcal{H}_0}A\mathbf{ds}_1...\mathbf{ds}_n, \tag{7.6}$$

where A is an arbitrary function. It can be proven [132] that Eq. (7.4) leads to the Bogoliubov inequality:

$$\mathcal{F} \le \mathcal{F}_v = \mathcal{F}_0 + \langle \mathcal{H} - \mathcal{H}_0\rangle_0 = \mathcal{F}_0 + \langle \mathcal{H}\rangle_0 - \langle \mathcal{H}_0\rangle_0. \tag{7.7}$$

We notice that the smaller is $\mathcal{F}_v$ the better approximation is to the exact free energy $\mathcal{F}$. Therefore, the idea is to calculate $\mathcal{F}_v$ using a suitable trial Hamiltonian $\mathcal{H}_0$ which depends on some parameters, then the minimization of $\mathcal{F}_v$ over these parameters will give the values of them at which $\mathcal{F}_v$ is minimum, that is, the best approximation to the exact free energy $\mathcal{F}$.

7.3.1 General free energy

Now we are ready to calculate the free energy of a two sublattice magnet. For this task, we use the analogous form of the trial Hamiltonian $\mathcal{H}_0$ for the two-sublattice Heisenberg ferro- (ferri- or antiferro-) magnet as suggested in Ref. [3] for the Ising antiferromagnet, that is,

$$\mathcal{H}_0 \;=\; -\mu_A\mathbf{H}_A^{\mathrm{MFA}}\sum_{i\in A}\mathbf{s}_i - \mu_B\mathbf{H}_B^{\mathrm{MFA}}\sum_{i\in B}\mathbf{s}_i \tag{7.8}$$

where

$$\mathbf{H}_{A(B)}^{\mathrm{MFA}} \;=\; \frac{J_{0,A(B)}}{\mu_{A(B)}}\mathbf{m}_{A(B)} + \frac{J_{0,AB(BA)}}{\mu_{A(B)}}\mathbf{m}_{B(A)} \tag{7.9}$$

where $J_{0,A} = x_A z J_{AA}$, $J_{0,B} = x_B z J_{BB}$, $J_{0,AB} = x_B z J_{AB}$, $J_{0,BA} = x_A z J_{AB}$, z is the number of nearest neighbours in the ordered lattice, $x_{A(B)}$ is the concentration of atoms of type A(B) and $\mathbf{m}_{A(B)}$ are parameters which later will have the meaning of the sublattice magnetisation. The partition function corresponding to the trial Hamiltonian Eq. (7.8) is given by

$$\begin{aligned}\mathcal{Z}_0 \;&=\; \int e^{-\beta\mathcal{H}_0(\mathbf{s}_1,...,\mathbf{s}_n)}\mathbf{ds}_1\mathbf{ds}_2...\mathbf{ds}_n \\ &=\; (4\pi)^n\left[\frac{\sinh\left(\beta\mu_A H_A^{\mathrm{MFA}}\right)}{\beta\mu_A H_A^{\mathrm{MFA}}}\right]^{nx_A}\left[\frac{\sinh\left(\beta\mu_B H_B^{\mathrm{MFA}}\right)}{\beta\mu_B H_B^{\mathrm{MFA}}}\right]^{nx_B}.\end{aligned} \tag{7.10}$$

and the free energy corresponding to this partition function is

$$\mathcal{F}_0 = -\frac{1}{\beta}\ln \mathcal{Z}_0 = -\frac{n}{\beta}\ln(4\pi) - \frac{nx_A}{\beta}\Lambda(\xi_A) - \frac{nx_B}{\beta}\Lambda(\xi_B) \tag{7.11}$$

where $\Lambda(x) = \ln[\sinh(x)/x]$ and $\xi_{A(B)} = |\boldsymbol{\xi}_{A(B)}|$ with $\boldsymbol{\xi}_{A(B)} = \beta\mu_{A(B)}\mathbf{H}^{\rm MFA}_{A(B)}$. On the other hand, if we average in Eqs. (7.1) and (7.8) then we have

$$\begin{aligned}\langle\mathcal{H}\rangle_0 &= -\frac{1}{2}\sum_{i,j\in A, i\neq j} J_{ij}\langle \mathbf{s}_i\cdot\mathbf{s}_j\rangle_0 - \frac{1}{2}\sum_{i,j\in B, i\neq j} J_{ij}\langle \mathbf{s}_i\cdot\mathbf{s}_j\rangle_0 \\ &- \sum_{i\in A, j\in B} J_{ij}\langle \mathbf{s}_i\cdot\mathbf{s}_j\rangle_0, \end{aligned}\tag{7.12}$$

$$\langle\mathcal{H}_0\rangle_0 = -\mu_A\mathbf{H}^{\rm MFA}_A\sum_{i\in A}\langle\mathbf{s}_i\rangle_0 - \mu_B\mathbf{H}^{\rm MFA}_B\sum_{i\in B}\langle\mathbf{s}_i\rangle_0. \tag{7.13}$$

Moreover, with the help of Eq. (7.6) one finds that $\langle\mathbf{s}_i\cdot\mathbf{s}_j\rangle_0 = \langle\mathbf{s}_i\rangle_0\cdot\langle\mathbf{s}_j\rangle_0$ and

$$\langle\mathbf{s}_{i\in A}\rangle_0 = L(\xi_A)\frac{\boldsymbol{\xi}_A}{\xi_A} \quad ; \quad \langle\mathbf{s}_{i\in B}\rangle_0 = L(\xi_B)\frac{\boldsymbol{\xi}_B}{\xi_B} \tag{7.14}$$

where $L(x) = \coth(x) - 1/x$ is the Langevin function. Hence, if we replace Eq. (7.14) in Eqs. (7.12) and (7.13) and we take into account only first neighbours interaction then we arrive to

$$\begin{aligned}\langle\mathcal{H}\rangle_0 &= -\frac{nx_A}{2}J_{0,A}L(\xi_A)^2 - \frac{nx_B}{2}J_{0,B}L(\xi_B)^2 \\ &- nx_AJ_{0,AB}L(\xi_A)L(\xi_B)\frac{\boldsymbol{\xi}_A\cdot\boldsymbol{\xi}_B}{\xi_A\xi_B}\end{aligned}\tag{7.15}$$

$$\langle\mathcal{H}_0\rangle_0 = \frac{nx_A}{\beta}\xi_AL(\xi_A) + \frac{nx_B}{\beta}\xi_BL(\xi_B). \tag{7.16}$$

Finally, if we replace Eqs. (7.11), (7.15) and (7.16) in Eq. (7.7) we find

$$\begin{aligned}\mathcal{F}\leq\mathcal{F}_v(\mathbf{m}_A,\mathbf{m}_B) &= -\frac{n}{\beta}\ln(4\pi) - \frac{nx_A}{\beta}\Lambda(\xi_A) - \frac{nx_B}{\beta}\Lambda(\xi_B) \\ &- \frac{nx_A}{2}J_{0,A}L(\xi_A)^2 - \frac{nx_B}{2}J_{0,B}L(\xi_B)^2 \\ &- nx_AJ_{0,AB}L(\xi_A)L(\xi_B)\frac{\boldsymbol{\xi}_A\cdot\boldsymbol{\xi}_B}{\xi_A\xi_B} \\ &+ \frac{nx_A}{\beta}\xi_AL(\xi_A) + \frac{nx_B}{\beta}\xi_BL(\xi_B).\end{aligned}\tag{7.17}$$

The minimization of $\mathcal{F}_v$ over the parameters $\mathbf{m}_A$ and $\mathbf{m}_B$, that is,

$$\frac{\partial\mathcal{F}_v}{\partial\mathbf{m}_A} = 0 \quad ; \quad \frac{\partial\mathcal{F}_v}{\partial\mathbf{m}_B} = 0 \tag{7.18}$$

leads to the Curie-Weiss equations

$$\mathbf{m}_{A,e} = L(\xi_{A,e})\frac{\boldsymbol{\xi}_{A,e}}{\xi_{A,e}} \quad ; \quad \mathbf{m}_{B,e} = L(\xi_{B,e})\frac{\boldsymbol{\xi}_{B,e}}{\xi_{B,e}}. \tag{7.19}$$

where $\boldsymbol{\xi}_{A(B),e} = \beta[J_{0,A(B)}\mathbf{m}_{A(B),e} + J_{0,AB(BA)}\mathbf{m}_{B(A),e}]$. The state $(\mathbf{m}_A, \mathbf{m}_B) = (\mathbf{m}_{A,e}, \mathbf{m}_{B,e})$ represents the equilibrium state where $\mathcal{F}_v$ has its minimum value, and since $\mathcal{F} \leq \mathcal{F}_v$ (see Eq. (7.7)) then $\mathcal{F}_v$ evaluated at the state $(\mathbf{m}_{A,e}, \mathbf{m}_{B,e})$ gives the best approximation to the exact free energy $\mathcal{F}$. For the pure longitudinal case, that is, $\mathbf{m}_A \parallel \mathbf{m}_B \parallel \mathbf{e}_z$, we obtain the following free energy per spin from Eq. (7.17)

$$\begin{aligned} \frac{1}{n}\mathcal{F}_v(m_{A,z}, m_{B,z}) &= -\frac{1}{\beta}\ln(4\pi) - \frac{x_A}{\beta}\Lambda(\xi_{A,z}) - \frac{x_B}{\beta}\Lambda(\xi_{B,z}) \\ - &\frac{x_A}{2}J_{0,A}L(\xi_{A,z})^2 - \frac{x_B}{2}J_{0,B}L(\xi_{B,z})^2 \\ - &x_A J_{0,AB}L(\xi_{A,z})L(\xi_{B,z}) + \frac{x_A}{\beta}\xi_{A,z}L(\xi_{A,z}) + \frac{x_B}{\beta}\xi_{B,z}L(\xi_{B,z}), \end{aligned} \tag{7.20}$$

where $\xi_{A(B),z} = \beta[J_{0,A(B)}m_{A(B),z} + J_{0,AB(BA)}m_{B(A),z}]$. Or equivalently,

$$\frac{\mathcal{F}_v}{n} = E - TS, \tag{7.21}$$

where E is the internal energy per spin given by

$$\begin{aligned} E = \frac{1}{n}\langle\mathcal{H}\rangle_0 &= -\frac{x_A}{2}J_{0,A}L(\xi_{A,z})^2 - \frac{x_B}{2}J_{0,B}L(\xi_{B,z})^2 \\ &- x_A J_{0,AB}L(\xi_{A,z})L(\xi_{B,z}), \end{aligned} \tag{7.22}$$

and S is the entropy per spin given by

$$S = k_B \ln\tilde{\Omega}, \tag{7.23}$$

$$\widetilde{\Omega} = 4\pi\left[\frac{\sinh(\xi_{A,z})e^{\xi_{A,z}L(\xi_{A,z})}}{\xi_{A,z}}\right]^{x_A}\left[\frac{\sinh(\xi_{B,z})e^{\xi_{B,z}L(\xi_{B,z})}}{\xi_{B,z}}\right]^{x_B}. \tag{7.24}$$

7.3.2 Second derivative test of the free energy obtained from the variational procedure

In this section we perform the second derivative test to the general free energy given by Eq. (7.20). The second derivative test discriminant of Eq. (7.20) is

$$\begin{aligned} D(m_{A,z}, m_{B,z}) &\equiv \left(\frac{\partial^2 \mathcal{F}_v}{\partial m_{A,z}^2}\right)\left(\frac{\partial^2 \mathcal{F}_v}{\partial m_{B,z}^2}\right) - \left[\frac{\partial^2 \mathcal{F}_v}{\partial m_{A,z}\partial m_{B,z}}\right]^2 \\ &= n^2 x_A x_B \beta \frac{a_A a_B}{J_{0,A} J_{0,B}} (J_{0,A} J_{0,B} - J_{0,AB} J_{0,BA})^2 \\ &\cdot \left[1 - a_A - a_B + \left(1 - \frac{J_{0,AB}^2}{J_{0,A} J_{0,B}}\right) a_A a_B\right], \end{aligned} \tag{7.25}$$

where $a_\nu = \beta J_{0,\nu} L'(\xi_{\nu,z})$ and

$$\frac{\partial^2 \mathcal{F}_v}{\partial m_{A,z}^2}(m_{A,z}, m_{B,z}) = n x_A J_{0,A} \left[a_A(1 - a_A) + a_B \frac{J_{0,AB} J_{0,BA}}{J_{0,A} J_{0,B}}(1 - 2a_A - a_B)\right]. \tag{7.26}$$

If $(m_{0,A,z}, m_{0,B,z})$ is a local extremum of $\mathcal{F}_v$ then we have the following cases:

- $D(m_{0,A,z}, m_{0,B,z}) > 0$ and $\frac{\partial^2 \mathcal{F}_v}{\partial m_{A,z}^2}|_{(m_{0,A,z}, m_{0,B,z})} > 0$ then $(m_{0,A,z}, m_{0,B,z})$ is a local minimum.
- $D(m_{0,A,z}, m_{0,B,z}) > 0$ and $\frac{\partial^2 \mathcal{F}_v}{\partial m_{A,z}^2}|_{(m_{0,A,z}, m_{0,B,z})} < 0$ then $(m_{0,A,z}, m_{0,B,z})$ is a local maximum.
- $D(m_{0,A,z}, m_{0,B,z}) < 0$ then $(m_{0,A,z}, m_{0,B,z})$ is a saddle point.
- $D(m_{0,A,z}, m_{0,B,z}) = 0$ higher order test must be used.

The analysis shows that there is a critical temperature T_c given by

$$T_c = \frac{J_{0,\nu} + J_{0,\kappa} + \sqrt{(J_{0,\nu} + J_{0,\kappa})^2 + 4(J_{0\nu\kappa} J_{0,\kappa\nu} - J_{0,\nu} J_{0,\kappa})}}{6 k_B}, \tag{7.27}$$

where if $T < T_c$ there are three extremal points, namely: two minimums $(m_{e,A,z,1}, m_{e,B,z,1})$ and $(m_{e,A,z,2}, m_{e,B,z,2})$ which are the solutions of the Curie-Weiss equations (see Eq. (7.19)) and one saddle point $(0, 0)$. If $T > T_c$ then there is just one extremal point which is a minimum $(0, 0)$. At $T = T_c$ there is one extremal point which is $(0, 0)$ however since $D(0, 0) = 0$ higher order test must be used in order to know its type.

7.3.3 Landau free energy

Close to the critical temperature we have $|\xi_{z,\nu}| \ll 1$, so that

$$\Lambda(\xi_{\nu,z}) \simeq \frac{\xi_{\nu,z}^2}{6} - \frac{\xi_{\nu,z}^4}{180} \quad , \quad L(\xi_{\nu,z}) \simeq \frac{\xi_{\nu,z}}{3} - \frac{\xi_{\nu,z}^3}{45}. \tag{7.28}$$

If we replace these approximations in Eq. (7.20) and we keep the terms up to fourth order in the sublattice magnetization $m_{\nu,z}$ then we obtain

$$\begin{aligned} \frac{1}{n}\mathcal{F}_v(m_{A,z}, m_{B,z}) &= -\frac{1}{\beta}\ln(4\pi) + D_{A^2} m_{A,z}^2 + D_{B^2} m_{B,z}^2 \\ + \; & D_{AB} m_{A,z} m_{B,z} + D_{A^4} m_{A,z}^4 + D_{B^4} m_{B,z}^4 + D_{A^3B} m_{A,z}^3 m_{B,z} \\ + \; & D_{B^3A} m_{A,z} m_{B,z}^3 + D_{A^2B^2} m_{A,z}^2 m_{B,z}^2, \end{aligned} \tag{7.29}$$

where

$$D_{\nu^2} = \frac{\beta}{18} x_\nu \left[w_\nu J_{0,\nu}^2 + w_\kappa J_{0,\kappa\nu} J_{0,\nu\kappa} - 2\beta J_{0,\kappa\nu} J_{0,\nu\kappa} J_{0,\nu} \right], \tag{7.30}$$

$$D_{\nu\kappa} = \frac{\beta}{9} x_\nu J_{0,\nu\kappa} \left[w_\nu J_{0,\nu} + w_\kappa J_{0,\kappa} - \beta(J_{0,\nu} J_{0,\kappa} + J_{0,\nu\kappa} J_{0,\kappa\nu}) \right], \tag{7.31}$$

$$D_{\nu^4} = \frac{\beta^3}{540} x_\nu \left[u_\nu J_{0,\nu}^4 + u_\kappa J_{0,\nu\kappa} J_{0,\kappa\nu}^3 + 4\beta J_{0,\nu} J_{0,\nu\kappa} J_{0,\kappa\nu} (J_{0,\kappa\nu}^2 + J_{0,\nu}^2) \right], \tag{7.32}$$

$$\begin{aligned} D_{\nu^3\kappa} &= \frac{\beta^3}{135} x_\nu J_{0,\nu\kappa} [u_\nu J_{0,\nu}^3 + u_\kappa J_{0,\kappa} J_{0,\kappa\nu}^2 \\ &+ \beta(J_{0,\kappa\nu}^3 J_{0,\nu\kappa} + 3 J_{0,\nu} J_{0,\kappa} J_{0,\kappa\nu}^2 + 3 J_{0,\nu}^2 J_{0,\nu\kappa} J_{0,\kappa\nu} + J_{0,\nu}^3 J_{0,\kappa})], \end{aligned} \tag{7.33}$$

$$\begin{aligned} D_{\nu^2\kappa^2} &= \frac{\beta^3}{90} J_{0,\nu\kappa} J_{0,\kappa\nu} [u_\nu x_\kappa J_{0,\nu}^2 + u_\kappa x_\nu J_{0,\kappa}^2 \\ &+ 2\beta(J_{0,\nu} J_{0,\kappa} + J_{0,\nu\kappa} J_{0,\kappa\nu})(x_\kappa J_{0,\nu} + x_\nu J_{0,\kappa})], \end{aligned} \tag{7.34}$$

where $w_\nu = 3 - \beta J_{0,\nu}$ and $u_\nu = 4\beta J_{0,\nu} - 9$. In Fig. 7.1 we present a comparison between Eq. (7.20) and Eq. (7.29) as a function of $m_{A,z}$ using the constraint $m_{B,z} = m_{B,e,z}$ at $T = 0.95 T_c$. In Fig. 7.2 we show the coefficients D given by Eqs. (7.30)-(7.34) as function of the temperature using the parameters of GdFeCo given in table 7.1 (with A=FeCo and B=Gd) for a) $x_B = 0.25$ and b) $x_B = 0.5$.

7.3.4 Expansion around the equilibrium

Below the critical temperature there are two equilibrium states $(m_{A,e,z,1}, m_{B,e,z,1})$ and $(m_{A,e,z,2}, m_{B,e,z,2})$ which are the solutions of the Curie-Weiss equations (Eq. (7.19)). Let's expand the free energy given by Eq. (7.20) around one of these

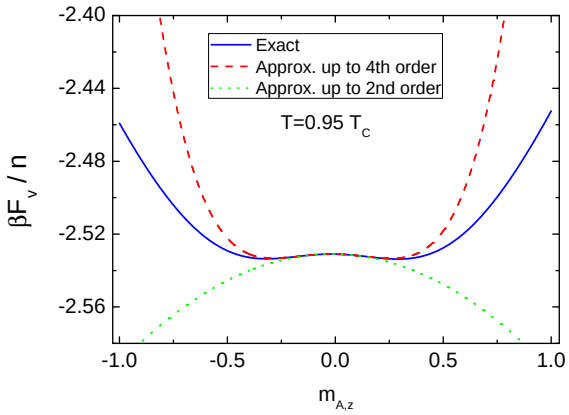

Figure 7.1: Comparison between Eq. (7.20) (blue solid line), Eq. (7.29) (red dash line) and Eq. (7.29) up to second order (green dash line) as a function of $m_{A,z}$ using the constraint $m_{B,z} = m_{B,e,z}$ at $T = 0.95T_c$.

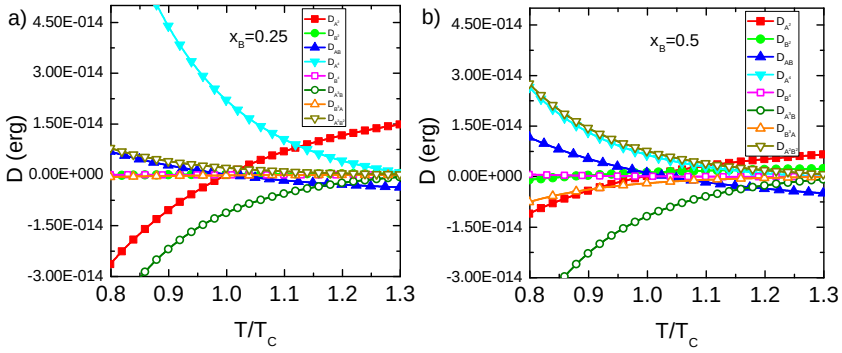

Figure 7.2: Coefficients D given by Eqs. (7.30)-(7.34) as function of the temperature using the parameters of GdFeCo given in table 7.1 (with A=FeCo and B=Gd) for a) $x_B = 0.25$ and b) $x_B = 0.5$.

two minimums $(m_{A,e,z}, m_{B,e,z})$ up to second order in $\delta m_{\nu,z} = m_{\nu,z} - m_{\nu,e,z}$ where $\nu = A, B$. To this end we use the following Taylor expansions in Eq. (7.20)

$$\Lambda(\xi_{\nu,z}) = \Lambda(\xi_{\nu,e,z}) + L_\nu \delta\xi_{\nu,z} + \frac{1}{2} L'_\nu \delta\xi^2_{\nu,z} \tag{7.35}$$

$$L(\xi_{\nu,z}) = m_{\nu,e,z} + L'_\nu \delta\xi_{\nu,z} + \frac{1}{2} L''_\nu \delta\xi^2_{\nu,z} \tag{7.36}$$

where $\delta\xi_{\nu,z} = \beta[J_{0,\nu}\delta m_{\nu,z} + J_{0,\nu\kappa}\delta m_{\kappa,z}]$, $m_{\nu,e,z} = L_\nu = L(\xi_{\nu,e,z})$, $L'_\nu(x) = dL/dx$ and $L''_\nu(x) = d^2L/dx^2$ evaluated at $\xi_{\nu,e,z} = \beta[J_{0,\nu}m_{\nu,e,z} + J_{0,\nu\kappa}m_{\kappa,e,z}]$. This leads

to

$$\begin{aligned}\frac{1}{n}\mathcal{F}_v(m_{A,z},m_{B,z}) &= \frac{1}{n}\mathcal{F}_{v,eq}+\Omega_{AA}\delta m_{A,z}^2+\Omega_{BB}\delta m_{B,z}^2\\ &+ \Omega_{AB}\delta m_{A,z}\delta m_{B,z}\end{aligned} \tag{7.37}$$

where $\mathcal{F}_{v,eq}$ is the free energy given by Eq. (7.20) evaluated at the equilibrium state $(m_{A,e,z},m_{B,e,z})$, that is,

$$\begin{aligned}\frac{1}{n}\mathcal{F}_{v,eq} &= \frac{1}{n}\mathcal{F}_v(m_{A,e,z},m_{B,e,z})\\ &= -\frac{1}{\beta}\ln(4\pi)-\frac{x_A}{\beta}\Lambda(\xi_{A,e,z})-\frac{x_B}{\beta}\Lambda(\xi_{B,e,z})\\ &+ \frac{x_A}{2}J_{0,A}m_{A,e,z}^2+\frac{x_B}{2}J_{0,B}m_{B,e,z}^2+x_AJ_{0,AB}m_{A,e,z}m_{e,B,z}\end{aligned} \tag{7.38}$$

and

$$\Omega_{AA} = \beta x_A[J_{0,A}^2\Gamma_{AA}+J_{0,AB}J_{0,BA}\Gamma_{BB}-J_{0,A}J_{0,AB}J_{0,BA}\beta L'_AL'_B] \tag{7.39}$$

$$\Omega_{BB} = \beta x_B[J_{0,B}^2\Gamma_{BB}+J_{0,AB}J_{0,BA}\Gamma_{AA}-J_{0,B}J_{0,AB}J_{0,BA}\beta L'_AL'_B] \tag{7.40}$$

$$\begin{aligned}\Omega_{AB} &= \beta J_{0,AB}J_{0,BA}[2(J_{0,A}\Gamma_{AA}+J_{0,B}\Gamma_{BB})\\ &- (J_{0,A}J_{0,B}+J_{0,AB}J_{0,BA})\beta L'_AL'_B]\end{aligned} \tag{7.41}$$

where

$$\Gamma_{\nu\nu} = \frac{1}{2}L'_\nu(1-\beta J_{0,\nu}L'_\nu). \tag{7.42}$$

As we have mentioned Eq. (7.37) is an expansion around one of the two equilibrium states, it means that it is a good approximation of Eq. (7.20) only close to that state, therefore Eq. (7.37) should not be used to evaluate the free energy landscape, for this task Eq. (7.20) should be used instead. In Fig. 7.3 we show a comparison between Eq. (7.20) and Eq. (7.37) as a function of $m_{A,z}$ using the constraint $m_{B,z}=m_{B,e,z}$. Above the critical temperature we have $m_{\nu,e}=0$ and $L'_\nu=1/3$ so that $\delta m_{\nu,z}=m_{\nu,z}$, $\Omega_{\nu\nu}=D_{\nu^2}$ and $\Omega_{\nu\kappa}=D_{\nu\kappa}$, it means that Eq. (7.37) becomes the Landau free energy given by Eq. (7.29) up to second order.

7.4 Pure ferromagnetic case

In this section we perform the pure ferromagnetic limit for the general free energy (Eq. (7.20)), the landau free energy (Eq. (7.29)) and the free energy after the expansion around the equilibrium (Eq. (7.37)).

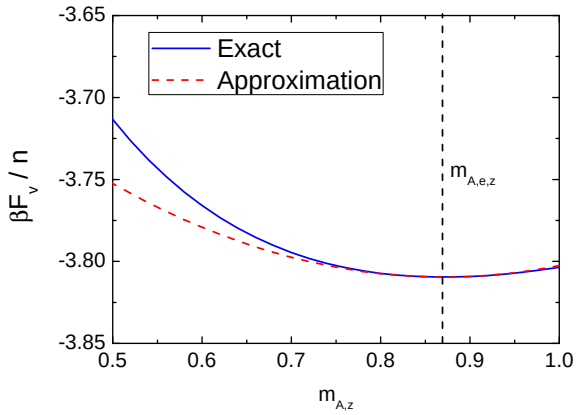

Figure 7.3: Comparison between Eq. (7.20) (blue solid line) and Eq. (7.37) (red dash line) as a function of $m_{A,z}$ using the constraint $m_{B,z} = m_{B,e,z}$.

7.4.1 General free energy

There are two different ways to make the pure ferromagnetic limit and they should be equivalent. One way is to think that since it is a pure material all atoms are of the same type, therefore the starting point is

$$\mathcal{H} = -\frac{1}{2} \sum_{i,j \in A; i \neq j} J_{ij} \mathbf{s}_i \cdot \mathbf{s}_j, \tag{7.43}$$

where $J_{ij} > 0$. Therefore, we have $J_{0,A} = J_0 > 0$, $x_A = 1$ and $x_B = 0$, so that the free energy depends only on one free parameter $m_{A,z}$. Hence, the free energy given by Eq. (7.20) becomes

$$\frac{1}{n}\mathcal{F}_v(m_{A,z}) = -\frac{1}{\beta}\ln(4\pi) - \frac{1}{\beta}\Lambda(\xi_{A,z}) - \frac{1}{2}J_{0,A}L(\xi_{A,z})^2 + \frac{1}{\beta}\xi_{A,z}L(\xi_{A,z}) \tag{7.44}$$

where $\xi_{A,z} = \beta J_{0,A} m_{A,z}$.

Another way is to consider at first stage a material with the same amount of two different atoms A and B ($\mu_A \neq \mu_B$, $x_A = x_B = 1/2$) which interact only between them ferromagnetically ($J_{ij} > 0$), hence the starting Hamiltonian is of the form

$$\mathcal{H} = -\sum_{i \in A, j \in B} J_{ij} \mathbf{s}_i \cdot \mathbf{s}_j, \tag{7.45}$$

which leads to Eq. (7.20) with the following parameters $J_{0,AB} > 0$, $J_{0,A} = J_{0,B} =$

0 and $x_A = x_B = 1/2$, that is,

$$\begin{aligned} \frac{1}{n}\mathcal{F}_v(m_{A,z}, m_{B,z}) &= -\frac{1}{\beta}\ln(4\pi) - \frac{1}{2\beta}\Lambda(\xi_{A,z}) - \frac{1}{2\beta}\Lambda(\xi_{B,z}) \\ - \quad \frac{1}{4}J_{0,AB}L(\xi_{A,z})L(\xi_{B,z}) &+ \frac{1}{2\beta}\xi_{A,z}L(\xi_{A,z}) + \frac{1}{2\beta}\xi_{B,z}L(\xi_{B,z}), \end{aligned} \tag{7.46}$$

where $\xi_{A(B),z} = \beta J_{0,AB} m_{B(A),z}/2$. Notice that if now we assume that the atoms of type A are equal to B, that is, $\mu_A = \mu_B$ we can not recover Eq. (7.44) from Eq. (7.46) in a natural way. In order to recover Eq. (7.44) from Eq. (7.46) one has to do two things: i) replace $J_{0,AB}/2$ by $J_{0,AB}$ in Eq. (7.46) which comes from the double counting in the initial Hamiltonian Eq. (7.45), ii) use the constraint $m_{A,z} = m_{B,z}$ because the atoms of type A are equal to type B and they point in the same direction. Doing so Eq. (7.46) becomes Eq. (7.44) and then both ways lead to the same free energy for a pure ferromagnet.

7.4.2 Landau free energy

In the pure ferromagnetic limit, we have $x_A = 1$, $x_B = 0$ and $J_{0,A} = 3k_B T_c$, therefore Eqs. (7.30-7.34) become

$$D_{A^2} = -\frac{J_{0,A}}{2}\epsilon + \mathcal{O}(\epsilon^2) \quad , \quad D_{A^4} = \frac{3J_{0,A}}{20} + \mathcal{O}(\epsilon), \tag{7.47}$$

$$D_{B^2} = D_{AB} = D_{A^3B} = D_{B^3A} = D_{B^4} = D_{A^2B^2} = 0, \tag{7.48}$$

where $\epsilon = (T_c - T)/T_c$, so that Eq. (7.29) reads

$$\frac{\mathcal{F}_v}{n}(m_{A,z}) = -\frac{1}{\beta}\ln(4\pi) - \frac{J_{0,A}\epsilon}{2}m_{A,z}^2 + \frac{3J_{0,A}}{20}m_{A,z}^4, \tag{7.49}$$

which is the Landau free energy for a ferromagnet given in Ref. [74].

7.4.3 Expansion around the equilibrium

If we apply the pure ferromagnetic limit $x_A = 1$ and $x_B = 0$ in Eq. (7.37) then we obtain

$$\frac{1}{n}\mathcal{F}_v(m_{A,z}) = \frac{1}{n}\mathcal{F}_{v,eq} + \frac{\beta}{2}J_{0,A}^2 L'_A\left[1 - \beta J_{0,A}L'_A\right]\delta m_{A,z}^2 \tag{7.50}$$

where $L'_A = L'(\xi_{e,A,z})$, $\xi_{e,A,z} = \beta J_{0,A} m_{A,e,z}$ and

$$\frac{1}{n}\mathcal{F}_{v,eq} = -\frac{1}{\beta}\ln(4\pi) - \frac{1}{\beta}\Lambda(\xi_{A,e,z}) + \frac{1}{2}J_{0,A}m_{A,e,z}^2. \tag{7.51}$$

In the MFA the longitudinal susceptibility is $\widetilde{\chi}_{\parallel,A} = (\beta\mu_A L'_A)/(1-\beta J_{0,A} L'_A)$, hence

$$L'_A = \frac{\widetilde{\chi}_{\parallel,A}}{\beta(J_{0,A}\widetilde{\chi}_{\parallel,A} + \mu_A)}, \tag{7.52}$$

if we replace Eq. (7.52) in Eq. (7.50) we find

$$\frac{1}{n}\mathcal{F}_v(m_{A,z}) = \frac{1}{n}\mathcal{F}_{v,eq} + \frac{\mu_A}{2\widetilde{\chi}_{\parallel,A}}\left[1 - \frac{1}{1+\frac{J_{0,A}\widetilde{\chi}_{\parallel,A}}{\mu_A}}\right]^2 \delta m^2_{A,z}. \tag{7.53}$$

Close to the Curie temperature T_c we have $J_{0,A}\widetilde{\chi}_{\parallel,A}/\mu_A \gg 1$, then we can write Eq. (7.53) as

$$\frac{1}{n}\mathcal{F}_v(m_{A,z}) = \frac{1}{n}\mathcal{F}_{v,eq} + \frac{\mu_A}{2\widetilde{\chi}_{\parallel,A}}\delta m^2_{A,z} + \mathcal{O}\left(\frac{1}{1+\frac{J_{0,A}\widetilde{\chi}_{\parallel,A}}{\mu_A}}\right), \tag{7.54}$$

which is same free energy obtained through the "alternative MFA formulation" in Ref. [74]. On the other hand, at low temperatures $|\xi_{e,A,z}| \gg 1$, so that

$$L'_A = L'(\xi_{e,A,z}) \simeq \frac{1}{\xi^2_{e,A,z}} + \mathcal{O}(e^{-2\xi_{e,A,z}}), \tag{7.55}$$

therefore, Eq. (7.50) becomes

$$\frac{1}{n}\mathcal{F}_v(m_{A,z}) = \frac{1}{n}\mathcal{F}_{v,eq} + \frac{\delta m^2_{A,z}}{2\beta m^2_{e,A,z}} + \mathcal{O}\left(\frac{\delta m^2_{A,z}}{\beta^2 J_{0,A}}\right). \tag{7.56}$$

In the limit $T \to 0$ we have $\mathcal{F}_v(m_{A,z}) = \mathcal{F}_{v,eq}$ which implies that the free energy of a non-equilibrium state ($m_{A,z} \neq m_{A,e,z}$) is the same than a equilibrium state ($m_{A,z} = m_{A,e,z}$), which clearly is a non-physical result. However, at low temperatures the free energy obtained through the "alternative MFA formulation", $\mathcal{F}_a$, in Ref. [74] reads

$$\frac{1}{n}\mathcal{F}_a(m_{A,z}) = \frac{1}{n}\mathcal{F}_{v,eq} + \frac{J_{0,A}}{2}\delta m^2_{A,z} + \mathcal{O}\left(\frac{\delta m^2_{A,z}}{\beta}\right), \tag{7.57}$$

which in the limit $T \to 0$ gives a more reasonable result than Eq. (7.56). These facts are also observed in the two sublattice case as we show in Figs. D.1 a) and b).

7.5 Numerical results

In this section we present numerical results of the free energy derived through the variational procedure, $\mathcal{F}_v$ (Eq. (7.20)), for GdFeCo and Permalloy ($Fe_{20}Ni_{80}$).

7.5.1 GdFeCo

We consider a model of GdFeCo where one species is attributed to Gd and the other is an effective moment of FeCo. In Table 7.1 we show the value of the exchange parameter for GdFeCo (similar to Ref. [12]) that we have used in our simulations. Notice that the magnetic moment values are not required since we are only considering the exchange interaction.

	zJ(Joule)
FeCo-FeCo	2.99×10^{-20}
Gd-Gd	1.19×10^{-20}
Gd-FeCo	-1.04×10^{-20}

Table 7.1: Table with parameters of GdFeCo.

In Fig. 7.4 we show the equilibrium magnetization of GdFeCo for different rare earth concentration $x_{Gd} = 0.1, 0.25, 0.5$ and 0.75 obtained as a numerical solution of the Curie-Weiss equation (Eq. (7.19)).

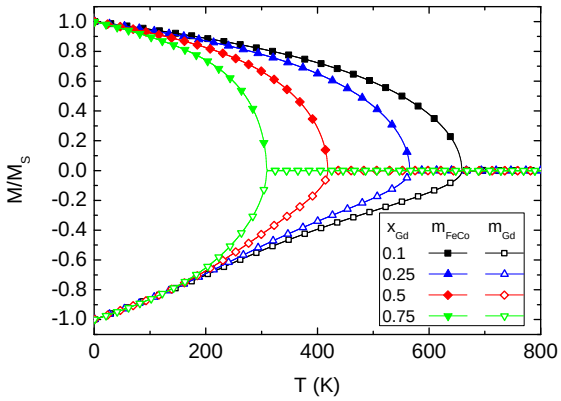

Figure 7.4: Equilibrium magnetization of GdFeCo for different rare earth concentration $x_{Gd} = 0.1, 0.25, 0.5$ and 0.75.

In Fig. 7.5 we present the reduced free energy $\beta\mathcal{F}_v/n$ (Eq. (7.20)) as function of $m_{\nu,z}$ at $T = 500$ K for different rare-earth concentration: a) $x_{Gd} = 0.15$, b) $x_{Gd} = 0.25$, c) $x_{Gd} = 0.5$ and d) $x_{Gd} = 0.75$. The curve illustrates that the free energy of a two-sublattice system has two minima at $T < T_c$ and undergo a transition to a paramagnetic state with one minima at $m_{\nu,e,z} = 0$ for a paramagnetic state for $T > T_c$.

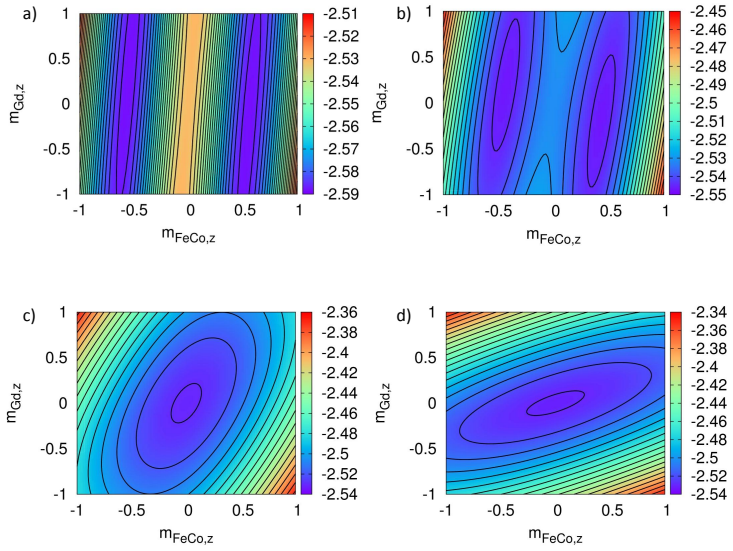

Figure 7.5: The reduced free energy $\beta\mathcal{F}_v/n$ (Eq. (7.20)) as function of $m_{\nu,z}$ at $T = 500$ K for different rare-earth concentration: a) $x_{Gd} = 0.15$, b) $x_{Gd} = 0.25$, c) $x_{Gd} = 0.5$ and d) $x_{Gd} = 0.75$.

In Fig. 7.6 we present the energy barrier $(\beta/n)|\Delta\mathcal{F}_v| = (\beta/n)|\mathcal{F}_v(m_{FeCo,e,z}, m_{Gd,e,z}) - \mathcal{F}_v(0,0)|$ as function of the temperature for two rare-earth-concentration $x_{Gd} = 0.15$ and $x_{Gd} = 0.75$. Note that the temperature is normalized to T_c which is different for different concentrations, in fact, at the same temperature the barrier is much larger for $x_{Gd} = 0.15$ than for $x_{Gd} = 0.75$. The curves illustrate that the energy barriers for longitudinal motion becomes small close to the Curie temperature.

7.5.2 Permalloy

In order to evaluate the free energy for Permalloy ($Fe_{20}Ni_{80}$) we use the exchange parameters given by Table 7.2 (similar to Ref. [64]).

In Fig. 7.7 we show the equilibrium magnetization of $Fe_{20}Ni_{80}$ using the parameters given in Table 7.2. In Fig. 7.8 we present the reduced free energy $\beta\mathcal{F}_v/n$ (Eq. (7.20)) as function of $m_{\nu,z}$ using the parameters given in Table 7.2

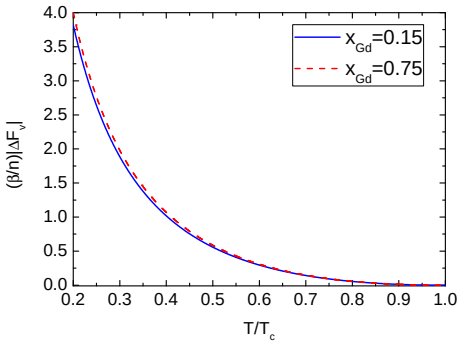

Figure 7.6: Energy barrier $(\beta/n)|\Delta\mathcal{F}_v| = (\beta/n)|\mathcal{F}_v(m_{FeCo,e,z}, m_{Gd,e,z}) - \mathcal{F}_v(0,0)|$ as function of the temperature for two rare-earth-concentration $x_{Gd} = 0.15$ and $x_{Gd} = 0.75$.

	zJ(Joule)
Fe-Fe	3.22×10^{-20}
Ni-Ni	6.19×10^{-21}
Fe-Ni	2.62×10^{-20}

Table 7.2: Table with parameters of Permalloy.

at $T = 100$, 200, 300 and 400 K. We observe that at $T = 100$, 200 and 300 K the free energy has two minima ($T < T_c$) and undergo a transition to a paramagnetic state with one minima at $m_{\nu,e,z} = 0$ for $T = 400$ K ($T > T_c$).

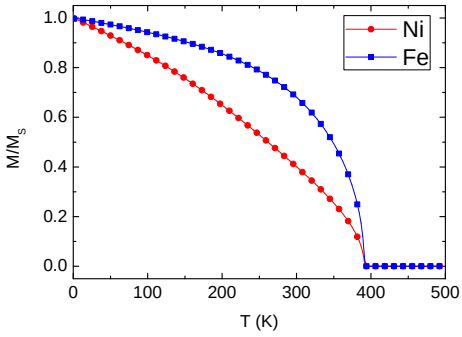

Figure 7.7: Equilibrium magnetization of $Fe_{20}Ni_{80}$.

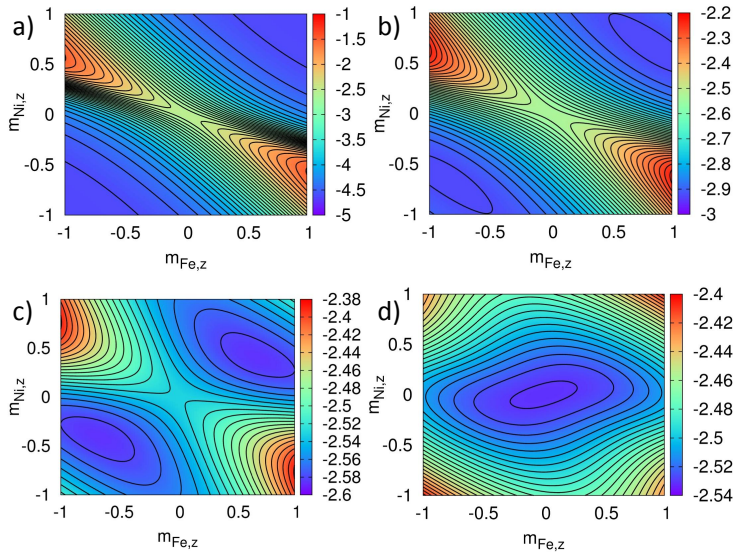

Figure 7.8: The reduced free energy $\beta\mathcal{F}_v/n$ (Eq. (7.20)) as function of $m_{\nu,z}$ using the parameters given in Table 7.2 at: a) $T = 100$ K, b) $T = 200$ K, c) $T = 300$ K and d) $T = 400$ K.

7.6 Conclusions

In this chapter we have presented the calculation of the free energy for two-component magnets (taking into account only the exchange interaction) using two different approaches based on the MFA: i) the variational MFA procedure and ii) the alternative MFA formulation (which was presented in Appendix D). Both routes give the same equilibrium free energy and as consequence the same magnetic equilibrium thermodynamic properties of the system. They also give the same energy barriers. However, as it is pointed out in Ref. [3] they give different free energy landscapes, in particular we found that for two sublattice magnets with $J_{0,A}J_{0,B} < J_{0,AB}J_{0,BA}$ (like in Permalloy) the alternative MFA formulation can lead to non-physical free energy landscapes where the expected equilibrium states corresponds to saddle points instead of minimums. However, at low temperatures (specially in the limit $T \to 0$) the alternative MFA formulation leads to more reasonable free energy landscape than the the variational MFA procedure.

Conclusiones en español

En este capítulo hemos presentado el cálculo de la energía libre para materiales magnéticos formados por dos componentes usando dos métodos diferentes basa-

dos en la aproximación de campo medio: i) el procedimiento variacional y ii) un método alternativo descrito en el Apéndice D. Ambos procedimientos dan lugar a la misma energía libre de equilibrio, y por tanto, dan lugar a las mismas propiedades termodinámicas de equilibrio. Ambos procedimeintos también dan las mismas barreras de energía. Sin embargo, como se indica en la referncia [3] cada procedimiento da lugar a mapas de energía diferentes, en particular hemos encontrado que para sistemas de dos compuestos con $J_{0,A}J_{0,B} < J_{0,AB}J_{0,BA}$ (como ocurre en Permalloy) el método alternativo puede dar lugar a mapas de energía sin sentido físico donde los estados de equilibrio esperados corresponden a puntos de silla en vez de mínimos. Por otro lado, a bajas temperaturas (especialmente en el límite $T \to 0$) el método alternativo da lugar a mapas de energía más razonables que el método variacional.

Appendix A

Density matrix formalism

A.1 Density matrix and density operator

The general wave function or state $|\Psi\rangle$ of an isolated quantum system can be written as a linear combination of the basis states $|\Psi_m\rangle$ as

$$|\Psi\rangle = \sum_m c_m |\Psi_m\rangle. \tag{A.1}$$

The expectation value of an observable $\hat{A}$ is given by

$$\langle \hat{A} \rangle \equiv \langle \Psi | \hat{A} | \Psi \rangle = \sum_{m,n} c_m c_n^* \langle \Psi_n | \hat{A} | \Psi_m \rangle = \sum_{m,n} c_m c_n^* A_{nm}, \tag{A.2}$$

where $A_{nm} = \langle \Psi_n | \hat{A} | \Psi_m \rangle$, then the density matrix ρ is defined as

$$\rho_{mn} = c_m c_n^*, \tag{A.3}$$

so that Eq. (A.2) becomes

$$\langle \hat{A} \rangle = \sum_{m,n} \rho_{mn} A_{nm}. \tag{A.4}$$

Alternatively, it is also useful to write $\langle \hat{A} \rangle$ in terms of the density operator defined as

$$\hat{\rho} = |\Psi\rangle\langle\Psi| = \sum_{m,n} \rho_{mn} |\psi_m\rangle\langle\psi_n|, \tag{A.5}$$

in this case the expectation value of an observable $\hat{A}$ reads

$$\langle \hat{A} \rangle = Tr\{\hat{A}\hat{\rho}\} = Tr\{\hat{\rho}\hat{A}\}, \tag{A.6}$$

where Tr stands for the trace, that is, the summation of the diagonal elements of a matrix.

A.2 Small system interacting weakly with a bath in thermal equilibrium

A.2.1 Density operator

For systems interacting with their environment one can use the basis states that are direct products of those of the small system $|\psi_m\rangle$ and those of the environment $|\phi_w\rangle$

$$|\Psi_{mw}\rangle = |\psi_m\rangle \otimes |\phi_w\rangle \equiv |\psi_m \phi_w\rangle, \tag{A.7}$$

therefore, the quantum mechanical states of the whole system (considered as isolated) can be written in the form

$$|\Psi\rangle = \sum_{mw} C_{mw} |\Psi_{mw}\rangle, \tag{A.8}$$

and the expression for the expectation value of an observable $\hat{A}$ of the small system becomes

$$\langle \hat{A} \rangle \equiv \langle \Psi | \hat{A} | \Psi \rangle = \sum_{mw,nw'} C_{mw} C^*_{nw'} \langle \Psi_{nw'} | \hat{A} | \Psi_{mw} \rangle, \tag{A.9}$$

so that the density matrix is

$$\rho_{mw,nw'} = C_{mw} C^*_{nw'}, \tag{A.10}$$

if the interaction between the system and the environment is weak then there is a very small entanglement between them, thus the coefficient C_{mw} nearly factorizes into $C_{nw} \cong c_m d_w$ and the wave function of the whole system reads

$$|\Psi\rangle \cong |\psi\rangle \otimes |\phi\rangle = \sum_m c_m |\psi_m\rangle \sum_w d_w |\phi_w\rangle, \tag{A.11}$$

where $|\psi\rangle = \sum_m c_m |\psi_m\rangle$ and $|\phi\rangle = \sum_w d_w |\phi_w\rangle$, moreover the total density matrix Eq. (A.10) becomes

$$\rho_{mw,nw'} \cong \rho^s_{m,n} \rho^b_{w,w'} = c_m c^*_n d_w d^*_{w'}. \tag{A.12}$$

where $\rho^s_{m,n} = c_m c^*_n$ and $\rho^b_{w,w'} = d_w d^*_{w'}$. Consequently, the total density operator also approximately factorizes

$$\hat{\rho} \cong \hat{\rho}_s \hat{\rho}_b. \tag{A.13}$$

where $\hat{\rho}_s = |\psi\rangle\langle\psi|$ and $\hat{\rho}_b = |\phi\rangle\langle\phi|$. Finally, if the bath is assumed to be in thermal equilibrium then its density operator is given by

$$\hat{\rho}_b^{eq} = \frac{1}{Z_b} \exp\left(-\frac{\hat{\mathcal{H}}_b}{k_B T}\right), \tag{A.14}$$

where $\hat{\mathcal{H}}_b$ is the bath Hamiltonian, k_B is the Boltzmann constant, T is the bath's temperature and Z_b is the partition function given by $Z_b = \sum_m e^{-E_m/(k_B T)}$ with E_m is an eigenvalue of the operator $\hat{\mathcal{H}}_b$. Therefore, the density operator of a small system interacting weakly with bath in thermal equilibrium reads

$$\hat{\rho} \cong \hat{\rho}_s \hat{\rho}_b^{eq}. \tag{A.15}$$

Calculating the expectation value of an observable $\hat{A}$ of the small system can be done in two steps: i) first calculating the trace over the variables of the bath and ii) then calculating the trace over the basis states of the small system. The first step yields the reduced density operator for the small system

$$\hat{\rho}_s = Tr_b\{\hat{\rho}\}, \tag{A.16}$$

where Tr_b is the partial trace over the bath variables.

A.2.2 Temporal evolution of the density operator

Let's write the Hamiltonian of a small system interacting with a bath as

$$\hat{\mathcal{H}}(t) = \hat{\mathcal{H}}_0(t) + \hat{V}, \quad \hat{\mathcal{H}}_0(t) = \hat{\mathcal{H}}_s(t) + \hat{\mathcal{H}}_b, \tag{A.17}$$

where $\hat{\mathcal{H}}_s$ and $\hat{\mathcal{H}}_b$ are the Hamiltonians of the small system and the bath, respectively, and $\hat{V}$ describes the interaction between them. Here we consider that the total Hamiltonian is time dependent through the Hamiltonian of the small system as it is done in the derivation of the qLLB equation. If the state or wave function of the whole system is $|\Psi(t)\rangle$ at instant t then the time derivative of the density operator is

$$\frac{\partial\hat{\rho}(t)}{\partial t} = \frac{\partial}{\partial t}(|\Psi(t)\rangle\langle\Psi(t)|) = \left(\frac{\partial}{\partial t}|\Psi(t)\rangle\right)\langle\Psi(t)| + |\Psi(t)\rangle\left(\frac{\partial}{\partial t}\langle\Psi(t)|\right) \tag{A.18}$$

and with the help of the Schrödinger equation and its conjugate one obtains the quantum Liouville equation

$$\frac{\partial\hat{\rho}(t)}{\partial t} = -\frac{i}{\hbar}\left[\hat{\mathcal{H}}(t), \hat{\rho}(t)\right] \equiv -\frac{i}{\hbar}(\hat{\mathcal{H}}(t)\hat{\rho}(t) - \hat{\rho}(t)\hat{\mathcal{H}}(t)). \tag{A.19}$$

It is convenient to write the Liouville equation in terms of the density operator in the interaction picture

$$\hat{\rho}(t)_I = \hat{U}_0^\dagger(t)\hat{\rho}(t)\hat{U}_0(t), \tag{A.20}$$

where $\hat{U}_0(t)$ is the time evolution operator in the absence of interaction. From the Schrödinger equation in the absence of interaction one obtains

$$i\hbar\frac{\partial}{\partial t}\hat{U}_0(t) = \hat{\mathcal{H}}_0(t)\hat{U}_0(t), \quad \hat{U}_0^\dagger(t) = \hat{U}_0^{-1}(t). \tag{A.21}$$

In case $\hat{\mathcal{H}}_0$ is time independent the solution of Eq. (A.21) is $\hat{U}_0(t) = e^{-i\hat{\mathcal{H}}_0 t/\hbar}$. Since the Hamiltonian of the bath $\hat{\mathcal{H}}_b$ is time independent we can write

$$\hat{U}_0(t) = \hat{U}_{0,s}(t)\hat{U}_{0,b}(t), \quad \hat{U}_{0,b}(t) = e^{-i\hat{\mathcal{H}}_b t/\hbar}, \tag{A.22}$$

where $\hat{U}_{0,s}(t)$ and $\hat{U}_{0,b}(t)$ are the time evolution operators in the absence of interaction of the small system and the bath, respectively. Calculating the time derivative in Eq. (A.20) and with the help of Eqs. (A.19) and (A.21) one arrives to

$$\frac{\partial\hat{\rho}(t)_I}{\partial t} = -\frac{i}{\hbar}\left[\hat{V}(t)_I, \hat{\rho}(t)_I\right], \tag{A.23}$$

where $\hat{V}(t)_I = \hat{U}_0^\dagger(t)\hat{V}\hat{U}_0(t)$. Now, integrating over time in Eq. (A.23) we have

$$\hat{\rho}(t)_I = \hat{\rho}(0)_I - \frac{i}{\hbar}\int_0^t dt' \left[\hat{V}(t')_I, \hat{\rho}(t')_I\right], \tag{A.24}$$

and inserting it back into Eq. (A.23) one obtains the integro-differential equation

$$\frac{d}{dt}\hat{\rho}(t)_I = -\frac{i}{\hbar}\left[\hat{V}(t)_I, \hat{\rho}(0)_I\right] - \frac{1}{\hbar^2}\int_0^t dt' \left[\hat{V}(t)_I \left[\hat{V}(t')_I, \hat{\rho}(t')_I\right]\right] \tag{A.25}$$

which is still an exact relation. If we assume that the interaction between the small system and the bath is weak then entanglement between them is small, thus the density operator of the whole system factorizes, see Eq. (A.12). If we additionally assume that the bath is at thermal equilibrium (quasiequilibrium) then from Eqs. (A.14) and (A.15) we have

$$\hat{\rho}(t)_I \cong \hat{\rho}_s(t)_I\hat{\rho}_b^{eq} = \hat{\rho}_s(t)_I\frac{1}{Z_b}\exp\left(-\frac{\hat{\mathcal{H}}_b}{k_BT}\right). \tag{A.26}$$

Using Eq. (A.26) one can transform Eq. (A.25) into the density operator equation for the small system by making a trace over the bath variables according to Eq. (A.16)

$$\frac{d}{dt}\hat{\rho}_s(t)_I = -\frac{i}{\hbar}Tr_b\left[\hat{V}(t)_I, \hat{\rho}_s(0)_I\hat{\rho}_b^{eq}\right] - \frac{1}{\hbar^2}\int_0^t dt' Tr_b\left[\hat{V}(t)_I\left[\hat{V}(t')_I, \hat{\rho}_s(t')_I\hat{\rho}_b^{eq}\right]\right]. \tag{A.27}$$

Now, we want to obtain the time evolution equation for the reduced density operator $\hat{\rho}_s(t)$, for this task we use that

$$\hat{\rho}_s(t) = \hat{U}_0(t)\hat{\rho}_s(t)_I\hat{U}_0^\dagger(t) \tag{A.28}$$

so that the time derivative of Eq. (A.28) is

$$\frac{d}{dt}\hat{\rho}_s(t) = -\frac{i}{\hbar}\left[\hat{\mathcal{H}}_s(t), \hat{\rho}_s(t)\right] + \hat{U}_0(t)\left(\frac{d}{dt}\hat{\rho}_s(t)_I\right)\hat{U}_0^\dagger(t) \tag{A.29}$$

and if we substitute Eq. (A.27) in Eq. (A.29) we obtain

$$\begin{aligned}\frac{d}{dt}\hat{\rho}_s(t) &= -\frac{i}{\hbar}\left[\hat{\mathcal{H}}_s(t), \hat{\rho}_s(t)\right] - \hat{U}_0(t)\left(\frac{i}{\hbar}Tr_b\left[\hat{V}(t)_I, \hat{\rho}_s(0)_I\hat{\rho}_b^{eq}\right]\right)\hat{U}_0^\dagger(t) \\ &- \hat{U}_0(t)\left(\frac{1}{\hbar^2}\int_0^t dt' Tr_b\left[\hat{V}(t)_I, \left[\hat{V}(t')_I, \hat{\rho}_s(t')_I\hat{\rho}_b^{eq}\right]\right]\right)\hat{U}_0^\dagger(t).\end{aligned} \tag{A.30}$$

The interaction operator $\hat{V}$ in the models used to derive the qLLB has the general form

$$\hat{V} = \hat{Q}\sum_j \hat{F}_j, \tag{A.31}$$

where $\hat{F}_j$ are bath operators and the $\hat{Q}$ is an operator acting only on the variables of the dynamic system. Therefore, in the following we will consider $\hat{V}$ to be given by Eq. (A.31), so that in the interaction picture it reads

$$\hat{V}(t)_I = \hat{U}_0^\dagger(t)\hat{V}\hat{U}_0(t) = \hat{Q}(t)_I\sum_j \hat{F}(t)_{Ij}, \tag{A.32}$$

where

$$\hat{Q}(t)_I = \hat{U}_{0,s}^\dagger(t)\hat{Q}\hat{U}_{0,s}(t), \quad \hat{F}(t)_{Ij} = \hat{U}_{0,b}^\dagger(t)\hat{F}_j\hat{U}_{0,b}(t). \tag{A.33}$$

where $\hat{U}_{0,b}(t) = e^{-i\hat{\mathcal{H}}_b t/\hbar}$ (see A.22). Inserting the Eq. (A.32) into Eq. (A.30), taking into account that the operators $\hat{F}_j$ and $\hat{Q}_j$ commute and using the cyclic

property of the trace ($Tr\{\hat{A}\hat{B}\hat{C}\} = Tr\{\hat{C}\hat{A}\hat{B}\} = Tr\{\hat{B}\hat{C}\hat{A}\}$) gives

$$\begin{aligned}
&\frac{d}{dt}\hat{\rho}_s(t) = -\frac{i}{\hbar}\left[\hat{\mathcal{H}}_s(t), \hat{\rho}_s(t)\right] \\
- \;& \hat{U}_0(t)\frac{i}{\hbar}\sum_i \left\{\hat{Q}(t)_I\hat{\rho}_s(0)_I Tr_b\left(\hat{F}(t)_{Ii}\hat{\rho}_b^{eq}\right) - \hat{\rho}_s(0)_I\hat{Q}(t)_I Tr_b\left(\hat{\rho}_b^{eq}\hat{F}(t)_{Ii}\right)\right\}\hat{U}_0^\dagger(t) \\
- \;& \hat{U}_0(t)\frac{1}{\hbar^2}\sum_{ij}\int_0^t dt'\{\left[\hat{Q}(t)_I, \hat{Q}(t')_I\hat{\rho}_s(t')_I\right] Tr_b\left(\hat{F}(t)_{Ii}\hat{F}(t')_{Ij}\hat{\rho}_b^{eq}\right)\}\hat{U}_0^\dagger(t) \\
- \;& \hat{U}_0(t)\frac{1}{\hbar^2}\sum_{ij}\int_0^t dt'\{\left[\hat{\rho}_s(t')_I\hat{Q}(t')_I, \hat{Q}(t)_I\right] Tr_b\left(\hat{F}(t')_{Ij}\hat{F}(t)_{Ii}\hat{\rho}_b^{eq}\right)\}\hat{U}_0^\dagger(t). \quad \text{(A.34)}
\end{aligned}$$

In Eq. (A.34) the quantity $Tr_b\left(\hat{F}(t)_{Ii}\hat{\rho}_b^{eq}\right)$ can be written as

$$\begin{aligned}
Tr_b\left(\hat{F}(t)_{Ii}\hat{\rho}_b^{eq}\right) &= Tr_b\left(\hat{\rho}_b^{eq}\hat{F}(t)_{Ii}\right) = \sum_N \langle N|\hat{F}(t)_{Ii}\hat{\rho}_b^{eq}|N\rangle \\
&= \sum_{NM}\langle N|\hat{F}(t)_{Ii}|M\rangle\langle M|\hat{\rho}_b^{eq}|N\rangle, \quad \text{(A.35)}
\end{aligned}$$

where the trace has been conveniently expressed in terms of eigenstates $|N\rangle$ of $\hat{\mathcal{H}}_b$, so that the equilibrium density matrix $\hat{\rho}_b^{eq}$ is diagonal in this representation, it means, $\langle M|\hat{\rho}_b^{eq}|N\rangle = 0$ if $M \neq N$. On the other hand, the diagonal elements of the operators $\hat{F}_i$ that are used in the derivation of the qLLB are equal to 0, it means, $\langle N|\hat{F}(t)_{Ii}|M\rangle = 0$ if $M = N$, therefore from Eq. (A.35) we have

$$Tr_b\left(\hat{F}(t)_{Ii}\hat{\rho}_b^{eq}\right) = Tr_b\left(\hat{\rho}_b^{eq}\hat{F}(t)_{Ii}\right) = 0, \quad \text{(A.36)}$$

if we substitute Eq. (A.36) in Eq. (A.34) we obtain

$$\begin{aligned}
\frac{d}{dt}\hat{\rho}_s(t) &= -\frac{i}{\hbar}\left[\hat{\mathcal{H}}_s(t), \hat{\rho}_s(t)\right] \\
&- \hat{U}_0(t)\frac{1}{\hbar^2}\sum_{ij}\int_0^t dt'\{\left[\hat{Q}(t)_I, \hat{Q}(t')_I\hat{\rho}_s(t')_I\right] Tr_b\left(\hat{F}(t)_{Ii}\hat{F}(t')_{Ij}\hat{\rho}_b^{eq}\right)\}\hat{U}_0^\dagger(t) \\
&- \hat{U}_0(t)\frac{1}{\hbar^2}\sum_{ij}\int_0^t dt'\{\left[\hat{\rho}_s(t')_I\hat{Q}(t')_I, \hat{Q}(t)_I\right] Tr_b\left(\hat{F}(t')_{Ij}\hat{F}(t)_{Ii}\hat{\rho}_b^{eq}\right)\}\hat{U}_0^\dagger(t) \quad \text{(A.37)}
\end{aligned}$$

The quantities

$$Tr_b\left(\hat{F}(t)_{Ii}\hat{F}(t')_{Ij}\hat{\rho}_b^{eq}\right) = \langle\hat{F}(t)_{Ii}\hat{F}(t')_{Ij}\rangle \quad \text{(A.38)}$$

$$Tr_b\left(\hat{F}(t')_{Ij}\hat{F}(t)_{Ii}\hat{\rho}_b^{eq}\right) = \langle\hat{F}(t')_{Ij}\hat{F}(t)_{Ii}\rangle \quad \text{(A.39)}$$

are *time correlation functions*. They describe the correlation which exists on average between interactions occurring at times t and t'. Since the reservoir is assumed to be large and such that it quickly dissipates the effects of the interaction it is expected that $\langle \hat{F}(t)_{Ii} \hat{F}(t')_{Ij} \rangle$ will be non zero for some time interval $t - t' \leq \tau_r$, where τ_r is typical of the reservoir and is called the *correlation time* of the reservoir. Interactions at time t and t' become progressively less correlated for $t - t' > \tau_r$ and become uncorrelated for $t - t' \gg \tau_r$ in which case

$$\langle \hat{F}(t')_{Ij} \hat{F}(t)_{Ii} \rangle \approx \langle \hat{F}(t)_{Ii} \hat{F}(t')_{Ij} \rangle \approx 0 \qquad (t - t' \gg \tau_r) \tag{A.40}$$

therefore, the integral in Eq. (A.27) is effectively only non zero for a time interval $t - t' \leq \tau_r$, that is, between times $t' \approx t - \tau_r$ and $t' = t$. It follows that the values of $\hat{\rho}_s(t')_I$ at times t' outside this interval have little or nor influence on $\frac{d}{dt}\hat{\rho}_s(t)_I$ at time t. If τ_r is much smaller than the characteristic time τ_s, required for $\hat{\rho}_s(t)_I$ to change appreciably on a macroscopic scale,

$$\tau_r \ll \tau_s \tag{A.41}$$

then $\hat{\rho}_s(t')_I$ can be replaced by $\hat{\rho}_s(t)_I$ in the integrand of Eq. (A.37), this replacement is called the Markoff approximation. **Substitution of $\hat{\rho}_s(t')_I$ for $\hat{\rho}_s(t)_I$ in Eq. (A.37) implies that it is not possible to describe the details of the system motion for time intervals comparable to τ_r.** Furthermore, since the time intervals are much larger than τ_r then the time derivative of $\hat{\rho}_s(t)$ becomes

$$\frac{d}{dt}\hat{\rho}_s(t) \to \frac{\triangle \hat{\rho}_s(t)}{\triangle t} = \frac{\hat{\rho}_s(t + \triangle t) - \hat{\rho}_s(t)}{\triangle t} \qquad where \quad \triangle t \gg \tau_r. \tag{A.42}$$

On the other hand, if we use the following commutation relation

$$[AB, C] = A\,[B, C] + [A, C]\,B \tag{A.43}$$

then Eq. (A.37) can be written as

$$\begin{aligned}
\frac{d}{dt}\hat{\rho}_s(t) &= -\frac{i}{\hbar}\left[\hat{\mathcal{H}}_s(t),\hat{\rho}_s(t)\right] \\
&- \hat{U}_0(t)\frac{1}{\hbar^2}\sum_{ij}\int_0^t dt'\{\hat{Q}(t')_I\left[\hat{Q}(t)_I,\hat{\rho}_s(t)_I\right]Tr_b\left(\hat{F}(t)_{Ii}\hat{F}(t')_{Ij}\hat{\rho}_b^{eq}\right)\}\hat{U}_0^\dagger(t) \\
&- \hat{U}_0(t)\frac{1}{\hbar^2}\sum_{ij}\int_0^t dt'\{\left[\hat{\rho}_s(t)_I,\hat{Q}(t)_I\right]\hat{Q}(t')_I Tr_b\left(\hat{F}(t')_{Ij}\hat{F}(t)_{Ii}\hat{\rho}_b^{eq}\right)\}\hat{U}_0^\dagger(t) \\
&- \hat{U}_0(t)\frac{1}{\hbar^2}\sum_{ij}\int_0^t dt'\{\left[\hat{Q}(t')_I,\hat{Q}(t)_I\right]\hat{\rho}_s(t)_I Tr_b\left(\hat{F}(t)_{Ii}\hat{F}(t')_{Ij}\hat{\rho}_b^{eq}\right)\}\hat{U}_0^\dagger(t) \\
&- \hat{U}_0(t)\frac{1}{\hbar^2}\sum_{ij}\int_0^t dt'\{\hat{\rho}_s(t)_I\left[\hat{Q}(t')_I,\hat{Q}(t)_I\right]Tr_b\left(\hat{F}(t')_{Ij}\hat{F}(t)_{Ii}\hat{\rho}_b^{eq}\right)\}\hat{U}_0^\dagger(t).
\end{aligned} \tag{A.44}$$

The last two integrals have very little influence on $\frac{d}{dt}\hat{\rho}_s(t)$ at time t in the Markoff approximation, this is due to the fact that in the last two integrals when $t' = t$ the integrand in both terms are equal to zero (since $[\hat{Q}_I(t),\hat{Q}_I(t)] = 0$), and when $t' \neq t$ then $t \geq t' + dt' = t' + \triangle t' \gg t' + \tau_r$ so $t - t' \gg \tau_r$ which implies Eq. (A.40), therefore when $t' \neq t$ the integrand is approximately zero in both terms. Bearing this in mind, we neglect the last two integrals in r.h.s. of Eq. (A.44) , so that Eq. (A.44) becomes

$$\begin{aligned}
\frac{d}{dt}\hat{\rho}_s(t) &= -\frac{i}{\hbar}\left[\hat{\mathcal{H}}_s(t),\hat{\rho}_s(t)\right] \\
&- \hat{U}_0(t)\frac{1}{\hbar^2}\sum_{ij}\int_0^t dt'\{\hat{Q}(t')_I\left[\hat{Q}(t)_I,\hat{\rho}_s(t)_I\right]Tr_b\left(\hat{F}(t)_{Ii}\hat{F}(t')_{Ij}\hat{\rho}_b^{eq}\right)\}\hat{U}_0^\dagger(t) \\
&+ \hat{U}_0(t)\frac{1}{\hbar^2}\sum_{ij}\int_0^t dt'\{\left[\hat{Q}(t)_I,\hat{\rho}_s(t)_I\right]\hat{Q}(t')_I Tr_b\left(\hat{F}(t')_{Ij}\hat{F}(t)_{Ii}\hat{\rho}_b^{eq}\right)\}\hat{U}_0^\dagger(t).
\end{aligned} \tag{A.45}$$

Now we introduce the variable $t'' = t - t'$ and $dt'' = -dt'$ in Eq. (A.45) the integral $\int_0^t dt' \cdots$ is transformed into the integral $\int_0^t dt'' \cdots$ and if we want to describe the system motion for time intervals much larger than τ_r (so we have $t \gg \tau_r$) then the upper integration limit can be extended to infinity $\int_0^\infty dt'' \cdots$,

thus Eq. (A.45) can be written as

$$\begin{aligned}
&\frac{d}{dt}\hat{\rho}_s(t) = -\frac{i}{\hbar}\left[\hat{\mathcal{H}}_s(t), \hat{\rho}_s(t)\right] \\
- \;& \hat{U}_0(t)\frac{1}{\hbar^2}\sum_{ij}\int_0^\infty dt''\{\hat{Q}(t-t'')_I\left[\hat{Q}(t)_I, \hat{\rho}_s(t)_I\right] Tr_b\left(\hat{F}(t)_{Ii}\hat{F}(t-t'')_{Ij}\hat{\rho}_b^{eq}\right)\}\hat{U}_0^\dagger(t) \\
+ \;& \hat{U}_0(t)\frac{1}{\hbar^2}\sum_{ij}\int_0^\infty dt''\{\left[\hat{Q}(t)_I, \hat{\rho}_s(t)_I\right]\hat{Q}(t-t'')_I Tr_b\left(\hat{F}(t-t'')_{Ij}\hat{F}(t)_{Ii}\hat{\rho}_b^{eq}\right)\}\hat{U}_0^\dagger(t),
\end{aligned} \tag{A.46}$$

and now returning to the variable $t' = t - t''$ we finally get

$$\begin{aligned}
&\frac{d}{dt}\hat{\rho}_s(t) = -\frac{i}{\hbar}\left[\hat{\mathcal{H}}_s(t), \hat{\rho}_s(t)\right] \\
- \;& \hat{U}_0(t)\frac{1}{\hbar^2}\sum_{ij}\int_{-\infty}^t dt'\{\hat{Q}(t')_I\left[\hat{Q}(t)_I, \hat{\rho}_s(t)_I\right] Tr_b\left(\hat{F}(t)_{Ii}\hat{F}(t')_{Ij}\hat{\rho}_b^{eq}\right)\}\hat{U}_0^\dagger(t) \\
+ \;& \hat{U}_0(t)\frac{1}{\hbar^2}\sum_{ij}\int_{-\infty}^t dt'\{\left[,\hat{Q}(t)_I, \hat{\rho}_s(t)_I\right]\hat{Q}(t')_I Tr_b\left(\hat{F}(t')_{Ij}\hat{F}(t)_{Ii}\hat{\rho}_b^{eq}\right)\}\hat{U}_0^\dagger(t).
\end{aligned} \tag{A.47}$$

Finally, if we multiply by $\hat{U}_0(t)$ on the right and by $\hat{U}_0^\dagger(t)$ on the left in Eqs. (A.47) and (A.29) then we obtain

$$\begin{aligned}
&\hat{U}_0^\dagger(t)\left(\frac{d}{dt}\hat{\rho}_s(t)\right)\hat{U}_0(t) = -\frac{i}{\hbar}\left[\hat{\mathcal{H}}_s(t), \hat{\rho}_s(t)_I\right] \\
- \;& \frac{1}{\hbar^2}\sum_{ij}\int_{-\infty}^t dt'\hat{Q}(t')_I\left[\hat{Q}(t)_I, \hat{\rho}_s(t)_I\right] Tr_b\left(\hat{F}(t)_{Ii}\hat{F}(t')_{Ij}\hat{\rho}_b^{eq}\right) \\
+ \;& \frac{1}{\hbar^2}\sum_{ij}\int_{-\infty}^t dt'\left[\hat{Q}(t)_I, \hat{\rho}_s(t)_I\right]\hat{Q}(t')_I Tr_b\left(\hat{F}(t')_{Ij}\hat{F}(t)_{Ii}\hat{\rho}_b^{eq}\right),
\end{aligned} \tag{A.48}$$

and

$$\hat{U}_0^\dagger(t)\left(\frac{d}{dt}\hat{\rho}_s(t)\right)\hat{U}_0(t) \;=\; -\frac{i}{\hbar}\left[\hat{\mathcal{H}}_s(t), \hat{\rho}_s(t)_I\right] + \frac{d}{dt}\hat{\rho}_s(t)_I, \tag{A.49}$$

therefore, combining Eqs. (A.48) and (A.49) we find

$$\begin{aligned}
\frac{d}{dt}\hat{\rho}_s(t)_I = \; & - \frac{1}{\hbar^2}\sum_{ij}\int_{-\infty}^t dt'\hat{Q}(t')_I\left[\hat{Q}(t)_I, \hat{\rho}_s(t)_I\right] Tr_b\left(\hat{F}(t)_{Ii}\hat{F}(t')_{Ij}\hat{\rho}_b^{eq}\right) \\
& + \frac{1}{\hbar^2}\sum_{ij}\int_{-\infty}^t dt'\left[\hat{Q}(t)_I, \hat{\rho}_s(t)_I\right]\hat{Q}(t')_I Tr_b\left(\hat{F}(t')_{Ij}\hat{F}(t)_{Ii}\hat{\rho}_b^{eq}\right).
\end{aligned} \tag{A.50}$$

Appendix B

Equation of motion of the Hubbard operator

B.1 Scattering via phonons

The original derivation of the qLLB equation[47] was done assuming a magnetic ion interacting weakly with a thermal phonon bath via direct and the second order (Raman) spin-phonon processes. The ferromagnetic interactions are taken into account in the mean-field approximation (MFA). The model Hamiltonian is written as:

$$\hat{\mathcal{H}}(t) = \hat{\mathcal{H}}_s(t) + \hat{\mathcal{H}}_{ph} + \hat{V}_{s\text{-}ph}, \tag{B.1}$$

where $\hat{\mathcal{H}}_s$ describes the spin system energy, $\hat{\mathcal{H}}_{ph}$ describes the phonon energy, $\hat{V}_{s\text{-}ph}$ describes the spin-phonon interaction:

$$\begin{aligned} \hat{\mathcal{H}}_s(t) &= -\hat{\boldsymbol{\mu}} \cdot \mathbf{H}^{\mathrm{MFA}}(t) = \gamma \mathbf{H}^{\mathrm{MFA}}(t) \cdot \hat{\mathbf{S}}, \\ \hat{\mathcal{H}}_{ph} &= \sum_q \hbar\omega_q \hat{a}_q^\dagger \hat{a}_q, \\ \hat{V}_{s\text{-}ph} &= -\sum_q V_q(\boldsymbol{\eta}\cdot\hat{\mathbf{S}})(\hat{a}_q^\dagger + \hat{a}_{-q}) - \sum_{p,q} V_{p,q}(\boldsymbol{\eta}\cdot\hat{\mathbf{S}})\hat{a}_p^\dagger \hat{a}_q. \end{aligned} \tag{B.2}$$

In the expressions above $\hat{\boldsymbol{\mu}} = -\gamma\hat{\mathbf{S}}$ is the magnetic moment operator, $\hat{\mathbf{S}}$ is the spin operator, $\gamma = |g|\mu_B/\hbar$ is the gyromagnetic ratio where g is the Landé g-factor, μ_B is the Bohr magneton and $\hbar$ is the reduced Planck constant, $\hat{a}_q^\dagger$ ($\hat{a}_q$) is the creation (annihilation) operator which creates (annihilates) a phonon with frequency ω_q where q stands for the wave vector $\mathbf{k}$ and the phonon polarization.

The vector $\mathbf{H}^{\mathrm{MFA}}$ is an effective field in the MFA given by

$$\mathbf{H}^{\mathrm{MFA}}(t) = \mathbf{H}_E(t) + \mathbf{H}(t) + \mathbf{H}_K = \frac{J_0}{\mu_{\mathrm{at}}}\mathbf{m}(t) + \mathbf{h}(t), \tag{B.3}$$

where $\mathbf{H}_E(t) = (J_0/\mu_{\rm at})\mathbf{m}(t)$ is the homogeneous part of the exchange field, J_0 is the exchange parameter related in the MFA to the Curie temperature T_c as $J_0 = 3k_BT_cS/(S+1)$, $\mu_{\rm at} = |g|\mu_B S$ is the atomic magnetic moment, $\mathbf{m}(t) = \langle\hat{\boldsymbol{\mu}}(t)\rangle/\mu_{\rm at} = -\langle\hat{\mathbf{S}}(t)\rangle/(\hbar S)$ is the reduced magnetization and $\mathbf{h} = \mathbf{H}+\mathbf{H}_K$, where $\mathbf{H}$ is the external magnetic field and $\mathbf{H}_K$ represents the anisotropy field. The first term in the spin-phonon interaction potential $\hat{V}_{s\text{-}ph}$ in Eq. (B.2) takes into account the direct transformation processes which are characterized by the amplitude V_q, and the second term describes the Raman processes with amplitudes $V_{p,q}$. The interaction may be anisotropic via the crystal field, which is taken into account through the parameter $\boldsymbol{\eta}$.

Notice that in the original derivation [47] the definitions of $\hat{\mathcal{H}}_s$ and $\mathbf{m}$ have the opposite sign than here, as consequence in the original derivation the time was reversed in order to obtain the correct final equation of motion. Here we use a more standard definitions of $\hat{\mathcal{H}}_s$ and $\mathbf{m}$ where there is no need to reverse time, therefore here some intermediate equations in the derivation could be different as in Ref. [47] but the same final magnetization equation of motion is obtained.

Now, we are ready to use the spin-phonon scattering model in Eq. (A.50). Comparing Eqs. (A.17), (A.31) and (B.2) we see that $\hat{\mathcal{H}}_b = \hat{\mathcal{H}}_{ph}$ and

$$\begin{aligned}
\hat{V} &= \hat{V}_{s\text{-}ph} = \hat{Q}(\hat{F}_d + \hat{F}_R),\\
\hat{Q} &= \boldsymbol{\eta}\cdot\hat{\mathbf{S}},\\
\hat{F}_d &= -\sum_q V_q(\hat{a}_q^\dagger + \hat{a}_{-q}),\\
\hat{F}_R &= -\sum_{p,q} V_{p,q}\hat{a}_p^\dagger\hat{a}_q.
\end{aligned} \tag{B.4}$$

Moreover, it is convenient to write the spin density operator $\hat{\rho}_s(t)$ in terms of the Hubbard operators $\hat{X}^{mn} = |m\rangle\langle n|$ (where $|m\rangle$ and $|n\rangle$ are eigenvectors of $\hat{S}^z$, corresponding to the eigenstates $m\,\hbar$ and $n\,\hbar$, respectively) as

$$\hat{\rho}_s(t) = \sum_{m,n}\rho^s_{mn}(t)\hat{X}^{mn}, \tag{B.5}$$

where $\rho^s_{mn}(t) = \langle m|\hat{\rho}_s(t)|n\rangle$. Thus, if we replace Eqs. (B.4) and (B.5) in Eq. (A.50) we obtain

$$\sum_{m,n}\frac{d}{dt}(\rho^s_{mn}(t)\hat{X}^{mn}(t)) = \sum_{m,n}\rho^s_{mn}(t)\hat{R}^{mn}(t), \tag{B.6}$$

where

$$\begin{aligned}\hat{R}^{mn}(t) &= -\frac{1}{\hbar^2}\int_{-\infty}^{t} dt' \boldsymbol{\eta}\cdot\hat{\mathbf{S}}(t')\left[\boldsymbol{\eta}\cdot\hat{\mathbf{S}}(t),\hat{X}^{mn}(t)\right]\sum_{ij} Tr_b\left(\hat{F}(t)_{Ii}\hat{F}(t')_{Ij}\hat{\rho}_b^{eq}\right)\\ &+ \frac{1}{\hbar^2}\int_{-\infty}^{t} dt' \left[\boldsymbol{\eta}\cdot\hat{\mathbf{S}}(t),\hat{X}^{mn}(t)\right]\boldsymbol{\eta}\cdot\hat{\mathbf{S}}(t')\sum_{ij} Tr_b\left(\hat{F}(t')_{Ij}\hat{F}(t)_{Ii}\hat{\rho}_b^{eq}\right),\end{aligned} \tag{B.7}$$

where $\hat{X}^{mn}(t)=\hat{U}_{0,s}^{\dagger}(t)\hat{X}^{mn}\hat{U}_{0,s}(t)$ and $\hat{\mathbf{S}}(t)=\hat{U}_{0,s}^{\dagger}(t)\hat{\mathbf{S}}\hat{U}_{0,s}(t)$. Let's work out the l.h.s of Eq. (B.6) as

$$\begin{aligned}&\sum_{m,n}\frac{d}{dt}(\rho_{mn}^{s}(t)\hat{X}^{mn}(t)) = \sum_{m,n}\rho_{mn}^{s}(t)\frac{d}{dt}\hat{X}^{mn}(t)+\sum_{m,n}\hat{X}^{mn}(t)\frac{d}{dt}\rho_{mn}^{s}(t)\\ =\ &\sum_{m,n}\rho_{mn}^{s}(t)\frac{d}{dt}\hat{X}^{mn}(t)-\frac{i}{\hbar}\sum_{m,n}\hat{X}^{mn}(t)\langle m|[(\gamma\mathbf{H}^{\mathrm{MFA}}(t)+\boldsymbol{\eta})\cdot\hat{\mathbf{S}},\hat{\rho}_s(t)]|n\rangle\end{aligned} \tag{B.8}$$

where the Liouville equation (see Eq. (A.19)) for the spin system has been used in the last step. Since the interaction between the spin system and the bath is weak we can assume that $\gamma|\mathbf{H}^{\mathrm{MFA}}|\gg|\boldsymbol{\eta}|$, thus we make the approximation $\gamma\mathbf{H}^{\mathrm{MFA}}+\boldsymbol{\eta}\simeq\gamma\mathbf{H}^{\mathrm{MFA}}$ in Eq. (B.8), hence

$$\begin{aligned}&\sum_{m,n}\frac{d}{dt}(\rho_{mn}^{s}(t)\hat{X}^{mn}(t))\\ \simeq\ &\sum_{m,n}\rho_{mn}^{s}(t)\left\{\frac{d}{dt}\hat{X}^{mn}(t)-\frac{i}{\hbar}\sum_{m',n'}\hat{X}^{m'n'}(t)\langle m'|[\hat{\mathcal{H}}_s(t),\hat{X}^{mn}]|n'\rangle\right\}.\end{aligned} \tag{B.9}$$

Replacing Eq. (B.9) in Eq. (B.6) leads to an equation of the form $\sum_{m,n}\rho_{mn}^{s}(t)A_{mn}=0$, which implies $A_{mn}=0$ for any m,n indices, that is,

$$\frac{d}{dt}\hat{X}^{mn}(t)=\frac{i}{\hbar}\sum_{m',n'}\hat{X}^{m'n'}(t)\langle m'|[\hat{\mathcal{H}}_s(t),\hat{X}^{mn}]|n'\rangle+\hat{R}^{mn}(t), \tag{B.10}$$

where the first term in the r.h.s. is the conservative term and $\hat{R}^{mn}(t)$ describes the relaxation of the spin system.

B.1.1 Conservative term

In order to avoid tedious calculations let's consider that MFA field is parallel to the z-axis at instant t, that is, $\mathbf{H}^{\mathrm{MFA}}=H^{\mathrm{MFA}}\mathbf{e}_z$, the final results may be easily

generalized. Now, using the relation between $\hat{S}_z$ and $\hat{X}^{mn}$ given by

$$\hat{S}_z = \hbar \sum_{m=-S}^{S} m\hat{X}^{mm}, \tag{B.11}$$

and the property $\hat{X}^{mn}\hat{X}^{lr} = \hat{X}^{mr}\delta_{nl}$ the conservative term in Eq. (B.10) becomes

$$\frac{i}{\hbar}\sum_{m',n'} \hat{X}^{m'n'}(t)\langle m'|[\hat{\mathcal{H}}_s(t), \hat{X}^{mn}]|n'\rangle = i\gamma H^{\mathrm{MFA}}(t)(m-n)\hat{X}^{mn}(t). \tag{B.12}$$

B.1.2 Relaxation term

Now we work out the relaxation term $\hat{R}^{mn}(t)$ given by Eq. (B.7). Firstly, we focus on the quantity

$$\begin{aligned}\sum_{i,j} Tr_b\left(\hat{F}(t)_{Ii}\hat{F}(t')_{Ij}\hat{\rho}_b^{eq}\right) &= Tr_b\left(\hat{F}_d(t)\hat{F}_d(t')\hat{\rho}_b^{eq}\right) + Tr_b\left(\hat{F}_d(t)\hat{F}_R(t')\hat{\rho}_b^{eq}\right) \\ &+ Tr_b\left(\hat{F}_R(t)\hat{F}_d(t')\hat{\rho}_b^{eq}\right) + Tr_b\left(\hat{F}_R(t)\hat{F}_R(t')\hat{\rho}_b^{eq}\right)\end{aligned} \tag{B.13}$$

where $\hat{F}_d(t) = e^{i\hat{\mathcal{H}}_b t/\hbar}\hat{F}_d e^{-i\hat{\mathcal{H}}_b t/\hbar}$. The first term in the r.h.s. of Eq. (B.13) reads

$$\begin{aligned}Tr_b\left(\hat{F}_d(t)\hat{F}_d(t')\hat{\rho}_b^{eq}\right) &= Tr_b\left(\hat{F}_d\hat{F}_d(t'-t)\hat{\rho}_b^{eq}\right) = \sum_n \langle n|\hat{F}_d\hat{F}_d(t'-t)\hat{\rho}_b^{eq}|n\rangle \\ = \sum_n \langle n|\sum_q V_q(\hat{a}_q^\dagger + \hat{a}_{-q})e^{\frac{i}{\hbar}\hat{\mathcal{H}}_b(t'-t)}&\sum_p V_p(\hat{a}_p^\dagger + \hat{a}_{-p})e^{-\frac{i}{\hbar}\hat{\mathcal{H}}_b(t'-t)}\frac{1}{Z_b}e^{-\beta\hat{\mathcal{H}}_b}|n\rangle\end{aligned} \tag{B.14}$$

where $|n\rangle$ are eigenvectors of $\hat{\mathcal{H}}_b$. It is convenient to write $|n\rangle$ in the occupation number representation[69], that is,

$$|n\rangle = |\nu_{\mathbf{k}_1\lambda_1}, ..., \nu_{\mathbf{k}_\alpha\lambda_\beta}, ...\rangle \tag{B.15}$$

where $\nu_{\mathbf{k}_\alpha\lambda_\beta}$ is the number of phonons in the mode $\mathbf{k}_\alpha\lambda_\beta$ (where $\mathbf{k}$ is the momentum vector and λ is the polarization), therefore the trace becomes

$$Tr_b(...) = \sum_n \langle n|...|n\rangle \quad \Longrightarrow \quad Tr_b(...) = \sum_{\mathbf{k}\lambda}\sum_{\nu_{\mathbf{k}\lambda}} \langle n|...|n\rangle. \tag{B.16}$$

When the operators $\hat{a}_q = \hat{a}_{\mathbf{k}_\alpha\lambda_\beta}$, $\hat{a}_q^\dagger = \hat{a}^\dagger_{\mathbf{k}_\alpha\lambda_\beta}$ and $\hat{\mathcal{H}}_b$ act over the eigenstates $|n\rangle$ lead to

$$\begin{aligned}
\hat{a}^\dagger_{\mathbf{k}_\alpha\lambda_\beta}|n\rangle &= \hat{a}^\dagger_{\mathbf{k}_\alpha\lambda_\beta}|...,\nu_{\mathbf{k}_\alpha\lambda_\beta},...\rangle = \sqrt{\nu_{\mathbf{k}_\alpha\lambda_\beta}+1}|...,\nu_{\mathbf{k}_\alpha\lambda_\beta}+1,...\rangle,\\
\hat{a}_{\mathbf{k}_\alpha\lambda_\beta}|n\rangle &= \hat{a}_{\mathbf{k}_\alpha\lambda_\beta}|...,\nu_{\mathbf{k}_\alpha\lambda_\beta}-1,...\rangle = \sqrt{\nu_{\mathbf{k}_\alpha\lambda_\beta}}|...,\nu_{\mathbf{k}_\alpha\lambda_\beta}-1,...\rangle,\\
\hat{\mathcal{H}}_b|n\rangle &= \sum_{\mathbf{k}\lambda}\hbar w_{\mathbf{k}\lambda}\hat{a}^\dagger_{\mathbf{k}\lambda}\hat{a}_{\mathbf{k}\lambda}|n\rangle = (E_{\mathbf{k}_1\lambda_1}+...+E_{\mathbf{k}_\alpha\lambda_\beta}+...)|n\rangle = E_n|n\rangle,
\end{aligned}$$

where $E_{\mathbf{k}_\alpha\lambda_\beta} = \hbar w_{\mathbf{k}_\alpha\lambda_\beta}\nu_{\mathbf{k}_\alpha\lambda_\beta}$. Furthermore, the operators $\hat{a}_p$ and $\hat{a}_p^\dagger$ follows the commutator rules:

$$\begin{aligned}
\left[\hat{a}_p,\hat{a}_q^\dagger\right] &= \hat{a}_p\hat{a}_q^\dagger - \hat{a}_q^\dagger\hat{a}_p = \delta_{p,q},\\
\left[\hat{a}_p,\hat{a}_q\right] &= \hat{a}_p\hat{a}_q - \hat{a}_q\hat{a}_p = 0,\\
\left[\hat{a}_p^\dagger,\hat{a}_q^\dagger\right] &= \hat{a}_p^\dagger\hat{a}_q^\dagger - \hat{a}_q^\dagger\hat{a}_p^\dagger = 0.
\end{aligned}$$

The last fact that we should take into account is that the set of eigenstates $\{|n\rangle\}$ is an orthonormal basis, then we have $\langle m|n\rangle = \delta_{mn}$. Now, we are ready to calculate in detail Eq. (B.14) as

$$\begin{aligned}
& Tr_b\left(\hat{F}_d(t)\hat{F}_d(t')\hat{\rho}_b^{eq}\right) = Tr_b\left(\hat{F}_d\hat{F}_d(t'-t)\hat{\rho}_b^{eq}\right)\\
=\ & \frac{1}{Z_b}\sum_{n,p,q}V_pV_q\langle n|(\hat{a}_q^\dagger+\hat{a}_{-q})e^{\frac{i}{\hbar}\hat{\mathcal{H}}_b(t'-t)}(\hat{a}_p^\dagger+\hat{a}_{-p})e^{-\frac{i}{\hbar}\hat{\mathcal{H}}_b(t'-t)}e^{-\beta\hat{\mathcal{H}}_b}|n\rangle\\
=\ & \frac{1}{Z_b}\sum_{n,p,q}V_pV_q\langle n|(\hat{a}_q^\dagger+\hat{a}_{-q})e^{\frac{i}{\hbar}\hat{\mathcal{H}}_b(t'-t)}(\hat{a}_p^\dagger+\hat{a}_{-p})|n\rangle e^{-\frac{i}{\hbar}E_n(t'-t)}e^{-\beta E_n}\\
=\ & \frac{1}{Z_b}\sum_{n,p,q}V_pV_q\langle n|(\hat{a}_q^\dagger+\hat{a}_{-q})e^{\frac{i}{\hbar}\hat{\mathcal{H}}_b(t'-t)}\\
\cdot\ & (\sqrt{\nu_p+1}|...,\nu_p+1,...\rangle+\sqrt{\nu_{-p}}|...,\nu_{-p}-1,...\rangle)e^{-\frac{i}{\hbar}E_n(t'-t)}e^{-\beta E_n}\\
=\ & \frac{1}{Z_b}\sum_{n,p,q}V_pV_q\langle n|(\hat{a}_q^\dagger+\hat{a}_{-q})e^{\frac{i}{\hbar}}\\
\cdot\ & \left(\sqrt{\nu_p+1}e^{iw_p(t'-t)}|...,\nu_p+1,...\rangle+\sqrt{\nu_{-p}}e^{-iw_p(t'-t)}|...,\nu_{-p}-1,...\rangle\right)e^{-\beta E_n}\\
=\ & \frac{1}{Z_b}\sum_{n,p}V_p^2[(\nu_p+1)e^{iw_p(t'-t)}+\nu_{-p}e^{-iw_{-p}(t'-t)}]e^{-\beta E_n} \qquad \text{(B.17)}
\end{aligned}$$

and taking into account that

$$\sum_n\frac{\nu_p}{Z_b}e^{-\beta E_n} \equiv \langle\nu_p\rangle = n_p = \frac{1}{e^{\beta w_p}-1}, \qquad \text{(B.18)}$$

$$\frac{1}{Z_b}\sum_n e^{-\beta E_n} = \frac{Z_b}{Z_b} = 1, \qquad \text{(B.19)}$$

where n_p is the Bose-Einstein distribution, then Eq.(B.17) becomes

$$Tr_b\left(\hat{F}_d(t)\hat{F}_d(t')\hat{\rho}_b^{eq}\right) = \sum_p V_p^2\left\{(n_p+1)\,e^{iw_p(t'-t)} + n_p e^{-iw_p(t'-t)}\right\}. \quad \text{(B.20)}$$

Performing similar calculations one arrives to

$$Tr_b\left(\hat{F}_R(t)\hat{F}_R(t')\hat{\rho}_b^{eq}\right) = \sum_{q,p} V_{q,p}^2 n_q(n_p+1)e^{i(w_p-w_q)(t'-t)}, \quad \text{(B.21)}$$

$$Tr_b\left(\hat{F}_d(t)\hat{F}_R(t')\hat{\rho}_b^{eq}\right) = Tr_b\left(\hat{F}_R(t)\hat{F}_d(t')\hat{\rho}_b^{eq}\right) = 0, \quad \text{(B.22)}$$

hence if we replace Eqs. (B.20-B.22) in Eq. (B.13) then we obtain

$$\sum_{i,j} Tr_b\left(\hat{F}(t)_{Ii}\hat{F}(t')_{Ij}\hat{\rho}_b^{eq}\right) = f(t'-t) \quad \text{(B.23)}$$

where

$$f(\tau) = \sum_p V_p^2\left\{(n_p+1)\,e^{iw_p\tau} + n_p e^{-iw_p\tau}\right\} + \sum_{q,p} V_{q,p}^2 n_p(n_q+1)e^{-i(w_p-w_q)\tau}. \quad \text{(B.24)}$$

From Eq. (B.23) we also have

$$\sum_{i,j} Tr_b\left(\hat{F}(t')_{Ii}\hat{F}(t)_{Ij}\hat{\rho}_b^{eq}\right) = f(t-t'), \quad \text{(B.25)}$$

therefore replacing Eqs. (B.23) and (B.25) in Eq. (B.7) leads to

$$\begin{aligned}\hat{R}^{mn}(t) &= -\frac{1}{\hbar^2}\int_{-\infty}^{t} dt' \boldsymbol{\eta}\cdot\hat{\mathbf{S}}(t')\left[\boldsymbol{\eta}\cdot\hat{\mathbf{S}}(t), \hat{X}^{mn}(t)\right] f(t'-t) \\ &+ \frac{1}{\hbar^2}\int_{-\infty}^{t} dt' \left[\boldsymbol{\eta}\cdot\hat{\mathbf{S}}(t), \hat{X}^{mn}(t)\right]\boldsymbol{\eta}\cdot\hat{\mathbf{S}}(t') f(t-t'). \quad \text{(B.26)}\end{aligned}$$

Next step is to evaluate the integral

$$\int_{-\infty}^{t} dt' \boldsymbol{\eta}\cdot\hat{\mathbf{S}}(t') f(t-t'), \quad \text{(B.27)}$$

where the retarded $\hat{\mathbf{S}}(t')$ is assumed to precess around a static field $H^{\mathrm{MFA}}(t)$. This assumption is based on the fact that the kernel of the integral given by (B.27) is localized in $|t-t'| \lesssim \tau_r$ due to the function $f(t-t')$, thus in this time range the

change of $\hat{\mathcal{H}}_s(t')$ is negligible and it can be considered time independent in the evaluation of the integral ($\hat{\mathcal{H}}_s(t') \simeq \hat{\mathcal{H}}_s(t)$), that is,

$$\begin{aligned}\hat{\mathbf{S}}(t') = \hat{U}_{0,s}^{\dagger}(t')\hat{\mathbf{S}}\hat{U}_{0,s}(t') &\simeq e^{\frac{i}{\hbar}\hat{\mathcal{H}}_s(t)t'}\hat{\mathbf{S}}e^{-\frac{i}{\hbar}\hat{\mathcal{H}}_s(t)t'} \\ &= e^{\frac{i}{\hbar}\gamma H^{\mathrm{MFA}}(t)\hat{S}_z t'}\hat{\mathbf{S}}e^{-\frac{i}{\hbar}\gamma H^{\mathrm{MFA}}(t)\hat{S}_z t'}, \end{aligned} \tag{B.28}$$

which leads to

$$\hat{S}_z(t') = \hat{S}_z(t), \qquad \hat{S}^{\pm}(t') = e^{\mp i\gamma H^{\mathrm{MFA}}(t)(t'-t)}\hat{S}^{\pm}(t) \tag{B.29}$$

$$\boldsymbol{\eta}\cdot\hat{\mathbf{S}}(t') = \eta_z\hat{S}_z(t) + \frac{\eta^+}{2}e^{i\gamma H^{\mathrm{MFA}}(t)(t'-t)}\hat{S}^-(t) + \frac{\eta^-}{2}e^{-i\gamma H^{\mathrm{MFA}}(t)(t'-t)}\hat{S}^+(t), \tag{B.30}$$

where $\eta^{\pm} = \eta_x \pm i\eta_y$ and $\hat{S}^{\pm} = \hat{S}_x \pm i\hat{S}_y$. If we replace Eq.(B.30) in Eq.(B.27) and introducing the variable $\tau = t - t'$ we get

$$\begin{aligned}&\int_{-\infty}^{t} dt' \boldsymbol{\eta}\cdot\hat{\mathbf{S}}(t')f(t-t') = \int_0^{\infty} d\tau \boldsymbol{\eta}\cdot\hat{\mathbf{S}}(t-\tau)f(\tau) \\ &= \eta_z\hat{S}_z(t)\int_0^{\infty} d\tau f(\tau) + \frac{\eta^+}{2}\hat{S}^-(t)\int_0^{\infty} d\tau e^{-i\gamma H^{\mathrm{MFA}}(t)\tau}f(\tau) \\ &+ \frac{\eta^-}{2}\hat{S}^+(t)\int_0^{\infty} d\tau e^{i\gamma H^{\mathrm{MFA}}(t)\tau}f(\tau), \end{aligned} \tag{B.31}$$

and using Eq. (B.24) and the identity $\int_0^{\infty} dx e^{iwx} = \pi\delta(w)$ we can write the first integral in the r.h.s. of Eq.(B.31) as

$$\eta_z\hat{S}_z(t)\int_0^{\infty} d\tau f(\tau) = \eta_z\hat{S}_z(t)W_1^{ph} \tag{B.32}$$

where

$$W_1^{ph} = \sum_{q,p} V_{q,p}^2 n_q(n_p+1)\pi\delta(w_q - w_p). \tag{B.33}$$

Similarly, the second integral in the r.h.s. of Eq.(B.31) becomes

$$\frac{\eta^+}{2}\hat{S}^-(t)\int_0^{\infty} d\tau e^{-i\gamma H^{\mathrm{MFA}}(t)\tau}f(\tau) = \frac{\eta^+}{2}\hat{S}^-(t)W_2^{ph} \tag{B.34}$$

where

$$W_2^{ph} = \sum_q V_q^2(n_q+1)\pi\delta\left(w_q - \gamma H^{\mathrm{MFA}}\right) + \sum_{q,p} V_{q,p}^2 n_q(n_p+1)\pi\delta\left(w_p - w_q - \gamma H^{\mathrm{MFA}}\right), \tag{B.35}$$

where $H^{\mathrm{MFA}} = H^{\mathrm{MFA}}(t)$. Finally, the third integral in the r.h.s. of Eq. (B.31) reads

$$\frac{\eta^-}{2}\hat{S}^+(t)\int_0^\infty d\tau e^{i\gamma H^{\mathrm{MFA}}(t)\tau}f(\tau) = \frac{\eta^-}{2}\hat{S}^+(t)e^{-y_0(t)}W_2^{ph} \tag{B.36}$$

where $y_0(t) = \beta\hbar\gamma H^{\mathrm{MFA}}(t)$. Thus replacing Eqs. (B.32), (B.34) and (B.36) in Eq.(B.31) we obtain

$$\int_{-\infty}^{t} dt' \boldsymbol{\eta}\cdot\hat{\mathbf{S}}(t')f(t-t') = \eta_z\hat{S}_z(t)W_1^{ph} + \frac{\eta^+}{2}\hat{S}^-(t)W_2^{ph} + \frac{\eta^-}{2}\hat{S}^+(t)e^{-y_0(t)}W_2^{ph} \tag{B.37}$$

Following the same procedure one arrives to

$$\int_{-\infty}^{t} dt' \boldsymbol{\eta}\cdot\hat{\mathbf{S}}(t')f(t'-t) = \eta_z\hat{S}_z(t)W_1^{ph} + \frac{\eta^+}{2}\hat{S}^-(t)e^{-y_0}W_2^{ph} + \frac{\eta^-}{2}\hat{S}^+(t)W_2^{ph} \tag{B.38}$$

therefore, if we substitute Eqs.(B.37) and (B.38) in Eq. (B.26) we obtain

$$\begin{aligned}
\hat{R}^{mn}(t) &= -\frac{\eta_z}{\hbar^2}W_1^{ph}\left[\hat{S}_z(t)\left[\boldsymbol{\eta}\cdot\hat{\mathbf{S}}(t),\hat{X}^{mn}(t)\right]\right] \\
&- \frac{1}{2\hbar^2}W_2^{ph}\{\eta^+e^{-y_0}\hat{S}^-(t)+\eta^-\hat{S}^+(t)\}\left[\boldsymbol{\eta}\cdot\hat{\mathbf{S}}(t),\hat{X}^{mn}(t)\right] \\
&+ \frac{1}{2\hbar^2}W_2^{ph}\left[\boldsymbol{\eta}\cdot\hat{\mathbf{S}}(t),\hat{X}^{mn}(t)\right]\{\eta^+\hat{S}^-(t)+\eta^-e^{-y_0}\hat{S}^+(t)\}
\end{aligned} \tag{B.39}$$

B.1.3 Final form of the Hubbard operator equation of motion

Inserting the conservative term Eq. (B.12) and the relaxation term Eq. (B.39) in Eq. (B.10), we find

$$\begin{aligned}
\frac{d}{dt}\hat{X}^{mn}(t) &= i\gamma H^{\mathrm{MFA}}(t)(m-n)\hat{X}^{mn}(t) - \frac{\eta_z}{\hbar^2}W_1^{ph}\left[\hat{S}_z(t)\left[\boldsymbol{\eta}\cdot\hat{\mathbf{S}}(t),\hat{X}^{mn}(t)\right]\right] \\
&- \frac{1}{2\hbar^2}W_2^{ph}\{\eta^+e^{-y_0}\hat{S}^-(t)+\eta^-\hat{S}^+(t)\}\left[\boldsymbol{\eta}\cdot\hat{\mathbf{S}}(t),\hat{X}^{mn}(t)\right] \\
&+ \frac{1}{2\hbar^2}W_2^{ph}\left[\boldsymbol{\eta}\cdot\hat{\mathbf{S}}(t),\hat{X}^{mn}(t)\right]\{\eta^+\hat{S}^-(t)+\eta^-e^{-y_0}\hat{S}^+(t)\}.
\end{aligned} \tag{B.40}$$

This equation is quite complicated, fortunately it can be greatly simplified with the help of the secular approximation[25]. If the "coarse-grained" time step ($dt = \Delta t$) satisfies

$$\Delta t \gg \frac{1}{\gamma H^{\mathrm{MFA}}(t)}, \tag{B.41}$$

then the high frequency terms which contain $\hat{X}^{m'n'}(t)$ with $m'-n'-m+n \neq 0$ in the r.h.s. of Eq. (B.40) can be neglected since they average out in the time integration. For example, using the relation between the spin and Hubbard operators given by Eq. (3.9) and the property $X^{mn}X^{lr} = X^{mr}\delta_{nl}$ we can write the second term in the r.h.s. of Eq. (B.40) as

$$\begin{aligned}
&\frac{\eta_z}{\hbar^2}W_1^{ph}\left[\hat{S}_z(t)\left[\boldsymbol{\eta}\cdot\hat{\mathbf{S}}(t),\hat{X}^{mn}(t)\right]\right] = \eta_z^2 W_1^{ph}\,(m-n)^2\,\hat{X}^{mn}(t)\\
+\;&\frac{1}{2}\eta_z\eta^+ W_1^{ph}\left((m-1-n)l_{m-1}X^{m-1,n}(t)+(n+1-m)l_n\hat{X}^{m,n+1}(t)\right)\\
+\;&\frac{1}{2}\eta_z\eta^- W_1^{ph}\left((m+1-n)l_{m-1}X^{m+1,n}(t)+(n-1-m)l_{n-1}\hat{X}^{m,n-1}(t)\right).
\end{aligned} \tag{B.42}$$

In the secular approximation we can neglect the terms which contain $\hat{X}^{m-1,n}(t) = \hat{X}^{m',n'}(t)$, $\hat{X}^{m,n+1}(t)$, $\hat{X}^{m+1,n}(t)$ and $\hat{X}^{m,n-1}(t)$ in Eq. (B.42) since $m'-n'-m+n \neq 0$, thus

$$\frac{\eta_z}{\hbar^2}W_1^{ph}\left[\hat{S}_z(t)\left[\boldsymbol{\eta}\cdot\hat{\mathbf{S}}(t),\hat{X}^{mn}(t)\right]\right] \simeq \eta_z^2 W_1^{ph}\,(m-n)^2\,\hat{X}^{mn}(t). \tag{B.43}$$

Similarly, in the secular approximation the third and fourth term in the r.h.s. of Eq. (B.40) become

$$\begin{aligned}
&\frac{1}{2\hbar^2}W_2^{ph}\{\eta^+e^{-y_0}\hat{S}^-(t)+\eta^-\hat{S}^+(t)\}\left[\boldsymbol{\eta}\cdot\hat{\mathbf{S}}(t),\hat{X}^{mn}(t)\right]\\
\simeq\;&\frac{1}{4}W_2^{ph}\eta^-\eta^+\left(l_{m-1}^2+e^{-y_0}l_m^2\right)\hat{X}^{mn}(t)\\
-\;&\frac{1}{4}W_2^{ph}\eta^-\eta^+\left(l_m l_n\hat{X}^{m+1,n+1}(t)+e^{-y_0}l_{m-1}l_{n-1}\hat{X}^{m-1,n-1}(t)\right),
\end{aligned} \tag{B.44}$$

and

$$\begin{aligned}
&\frac{1}{2\hbar^2}W_2^{ph}\left[\boldsymbol{\eta}\cdot\hat{\mathbf{S}}(t),\hat{X}^{mn}(t)\right]\{\eta^+\hat{S}^-(t)+\eta^-e^{-y_0}\hat{S}^+(t)\}\\
\simeq\;&\frac{1}{4}W_2^{ph}\eta^-\eta^+\left(l_m l_n\hat{X}^{m+1,n+1}(t)+e^{-y_0}l_{m-1}l_{n-1}\hat{X}^{m-1,n-1}(t)\right)\\
-\;&\frac{1}{4}W_2^{ph}\eta^-\eta^+\left(l_{n-1}^2+e^{-y_0}l_n^2\right)\hat{X}^{mn}(t).
\end{aligned} \tag{B.45}$$

Finally, Eqs. (B.43), (B.44) and (B.45) are substituted in Eq.(B.40) which leads to

$$\begin{aligned}
\frac{d}{dt}\hat{X}^{mn}(t) \;\simeq\;& i\gamma H^{\mathrm{MFA}}(t)\,(m-n)\,\hat{X}^{mn}(t) - \widetilde{W}_1^{ph}\,(m-n)^2\,\hat{X}^{mn}(t)\\
-\;&\frac{1}{2}\widetilde{W}_2^{ph}\left(l_{m-1}^2+l_{n-1}^2+e^{-y_0}(l_m^2+l_n^2)\right)\hat{X}^{mn}(t)\\
+\;&\widetilde{W}_2^{ph}\left(l_m l_n\hat{X}^{m+1,n+1}(t)+e^{-y_0}l_{m-1}l_{n-1}\hat{X}^{m-1,n-1}(t)\right)
\end{aligned} \tag{B.46}$$

where $\widetilde{W}_1^{ph} = \eta_z^2 W_1^{ph}$ and $\widetilde{W}_2^{ph} = \frac{1}{2} W_2^{ph}(\eta_x^2 + \eta_y^2)$.

B.2 Scattering via electrons

In this section we derive the qLLB equation for a simple model for the spin-electron interaction Hamiltonian - the electron-"impurity" scattering model proposed by B. Koopmans *et al.* in Ref. [89] for the laser induced magnetization dynamics. The model assumes an instantaneous thermalization of the optically excited electrons to the Fermi-Dirac distribution. The Hamiltonian considered here consists of a spin system which weakly interacts with a spinless electron bath and it reads

$$\hat{\mathcal{H}}(t) = \hat{\mathcal{H}}_s(t) + \hat{\mathcal{H}}_e + \hat{V}_{s\text{-}e}, \tag{B.47}$$

where $\hat{\mathcal{H}}_s$ is the energy of the spin system, $\hat{\mathcal{H}}_e$ stands for the electron bath energy and $\hat{V}_{s\text{-}e}$ describes the spin-electron interaction energy,

$$\begin{aligned} \hat{\mathcal{H}}_s(t) &= \gamma \mathbf{H}^{\mathrm{MFA}}(t) \cdot \hat{\mathbf{S}}, \\ \hat{\mathcal{H}}_e &= \sum_{\mathbf{k}} (\epsilon_{\mathbf{k}} - \mu) \hat{c}_{\mathbf{k}}^{\dagger} \hat{c}_{\mathbf{k}}, \\ \hat{V}_{s\text{-}e} &= \sum_{\mathbf{k},\mathbf{k'}} V_{\mathbf{k},\mathbf{k'}} (\hat{S}^{+} + \hat{S}^{-}) \hat{c}_{\mathbf{k}}^{\dagger} \hat{c}_{\mathbf{k'}}. \end{aligned} \tag{B.48}$$

Here $\hat{c}_{\mathbf{k}}^{\dagger}$ ($\hat{c}_{\mathbf{k}}$) is the creation (annihilation) operator which creates (annihilates) an electron with momentum $\mathbf{k}$, $\epsilon_{\mathbf{k}} = \hbar^2 k^2/(2m_{el})$, μ is the chemical potential, m_{el} is the electron mass, $V_{\mathbf{k},\mathbf{k'}}$ describes the scattering amplitude. The vector $\mathbf{H}^{\mathrm{MFA}}$ is given by Eq. (B.3).

Now, we use the electron-"impurity" scattering in Eq. (A.50). Comparing Eqs. (A.17), (A.31) and (B.48) we see that $\hat{\mathcal{H}}_b = \hat{\mathcal{H}}_e$ and

$$\begin{aligned} \hat{V} &= \hat{V}_{s\text{-}e} = \hat{Q}\hat{F}, \\ \hat{Q} &= \hat{S}^{+} + \hat{S}^{-}, \\ \hat{F} &= \sum_{\mathbf{k},\mathbf{k'}} V_{\mathbf{k},\mathbf{k'}} \hat{c}_{\mathbf{k}}^{\dagger} \hat{c}_{\mathbf{k'}}. \end{aligned} \tag{B.49}$$

Firstly, we notice that the operator $\hat{Q}$ can be written as

$$\hat{Q} = \hat{S}^{+} + \hat{S}^{-} = 2\hat{S}_x = \boldsymbol{\eta} \cdot \hat{\mathbf{S}}, \quad \eta_y = \eta_z = 0, \quad \eta_x = 2, \tag{B.50}$$

therefore, we see the operator $\hat{Q}$ used in the electron-"impurity" scattering model is a particular case ($\eta_y = \eta_z = 0, \eta_x = 2$) of the operator $\hat{Q}$ used in the spin-phonon scattering model. Now, if we replace Eqs. (B.49) and (B.5) in Eq.

(A.50) and we follow the same procedure as in the spin-phonon scattering model we arrive to

$$\frac{d}{dt}\hat{X}^{mn}(t) = \frac{i}{\hbar}\sum_{m',n'}\hat{X}^{m'n'}(t)\langle m'|[\hat{\mathcal{H}}_s(t), \hat{X}^{mn}]|n'\rangle + \hat{R}^{mn}(t), \quad \text{(B.51)}$$

where

$$\begin{aligned}
&\hat{R}^{mn}(t) = \\
-\ &\frac{1}{\hbar^2}\int_{-\infty}^{t} dt'(\hat{S}^{+}(t') + \hat{S}^{-}(t'))\left[\hat{S}^{+}(t) + \hat{S}^{-}(t), \hat{X}^{mn}(t)\right] Tr_b\left(\hat{F}(t)\hat{F}(t')\hat{\rho}_b^{eq}\right) \\
+\ &\frac{1}{\hbar^2}\int_{-\infty}^{t} dt'\left[\hat{S}^{+}(t) + \hat{S}^{-}(t), \hat{X}^{mn}(t)\right](\hat{S}^{+}(t') + \hat{S}^{-}(t'))Tr_b\left(\hat{F}(t')\hat{F}(t)\hat{\rho}_b^{eq}\right).
\end{aligned} \quad \text{(B.52)}$$

We see that the conservative term is the same as in the spin-phonon scattering model given by Eq. (B.12).

B.2.1 Relaxation term

Let's work out the relaxation term $\hat{R}^{mn}(t)$ given by Eq. (B.52). Firstly, let's calculate the quantity

$$\begin{aligned}
&Tr_b\left(\hat{F}(t)\hat{F}(t')\hat{\rho}_b^{eq}\right) = Tr_b\left(\hat{F}\hat{F}(t'-t)\hat{\rho}_b^{eq}\right) \\
=\ &\sum_{\nu}\langle\nu|\sum_{\mathbf{k},\mathbf{k}'} V_{\mathbf{k},\mathbf{k}'}\hat{c}^{\dagger}_{\mathbf{k}}\hat{c}_{\mathbf{k}'}e^{\frac{i}{\hbar}\hat{\mathcal{H}}_e(t'-t)}\sum_{\mathbf{k}'',\mathbf{k}'''} V_{\mathbf{k}'',\mathbf{k}'''}\hat{c}^{\dagger}_{\mathbf{k}''}\hat{c}_{\mathbf{k}'''}e^{-\frac{i}{\hbar}\hat{\mathcal{H}}_e(t'-t)}\frac{1}{Z_e}e^{-\beta\hat{\mathcal{H}}_e}|\nu\rangle,
\end{aligned} \quad \text{(B.53)}$$

where $|\nu\rangle$ are eigenvectors of $\hat{\mathcal{H}}_e$. It is convenient to write $|\nu\rangle$ in the occupation number representation[69], that is,

$$|\nu\rangle = |\nu_{\mathbf{k}_1}, ..., \nu_{\mathbf{k}_\alpha}, ...\rangle, \quad \text{(B.54)}$$

where $\nu_{\mathbf{k}_\alpha}$ is the number of electrons with momentum $\mathbf{k}_\alpha$ ($\nu_{\mathbf{k}_\alpha}$ must be equal to 0 or 1 due to the Pauli exclusion principle), therefore the trace becomes

$$Tr_b(...) = \sum_{\nu}\langle\nu|...|\nu\rangle \quad \Longrightarrow \quad Tr_b(...) = \sum_{\mathbf{k}}\sum_{\nu_{\mathbf{k}}=0}^{1}\langle\nu|...|\nu\rangle. \quad \text{(B.55)}$$

B. EQUATION OF MOTION OF THE HUBBARD OPERATOR

When the operators $\hat{c}_{\mathbf{k}_\alpha}$, $\hat{c}^\dagger_{\mathbf{k}_\alpha}$ and $\hat{\mathcal{H}}_e$ act over the eigenstates $|\nu\rangle$ we have

$$\hat{c}^\dagger_{\mathbf{k}_\alpha}|\nu\rangle = \hat{c}^\dagger_{\mathbf{k}_\alpha}|...,\nu_{\mathbf{k}_\alpha},...\rangle = \xi_{\mathbf{k}_\alpha}\sqrt{\nu_{\mathbf{k}_\alpha}+1}|...,\nu_{\mathbf{k}_\alpha}+1,...\rangle,$$

$$\begin{aligned}\hat{c}_{\mathbf{k}_\alpha}|\nu\rangle &= \hat{c}_{\mathbf{k}_\alpha}|...,\nu_{\mathbf{k}_\alpha}-1,...\rangle = \xi_{\mathbf{k}_\alpha}\sqrt{\nu_{\mathbf{k}_\alpha}}|...,\nu_{\mathbf{k}_\alpha}-1,...\rangle,\\ \hat{\mathcal{H}}_e|\nu\rangle &= \sum_{\mathbf{k}}(\epsilon_{\mathbf{k}}-\mu)\hat{c}^\dagger_{\mathbf{k}}\hat{c}_{\mathbf{k}}|\nu\rangle = \epsilon_\nu|\nu\rangle,\end{aligned}$$

where $\epsilon_\nu = \nu_{\mathbf{k}_1}(\epsilon_{\mathbf{k}_1}-\mu)+...+\nu_{\mathbf{k}_\alpha}(\epsilon_{\mathbf{k}_\alpha}-\mu)+...$ and $\xi_{\mathbf{k}_\alpha} = \pm 1$ according to

whether $\sum_{\beta<\alpha}\nu_{\mathbf{k}_\beta}$ is an even or a odd integer. Furthermore, the operators $\hat{c}_{\mathbf{k}}$ and $\hat{c}^\dagger_{\mathbf{k}}$ follows the commutator rules:

$$\{\hat{c}_{\mathbf{k}},\hat{c}^\dagger_{\mathbf{k}'}\} \equiv \hat{c}_{\mathbf{k}}\hat{c}^\dagger_{\mathbf{k}'}+\hat{c}^\dagger_{\mathbf{k}'}\hat{c}_{\mathbf{k}} = \delta_{\mathbf{k},\mathbf{k}'},$$

$$\{\hat{c}_{\mathbf{k}},\hat{c}_{\mathbf{k}'}\} \equiv \hat{c}_{\mathbf{k}}\hat{c}_{\mathbf{k}'}+\hat{c}_{\mathbf{k}'}\hat{c}_{\mathbf{k}} = 0,$$

$$\{\hat{c}^\dagger_{\mathbf{k}},\hat{c}^\dagger_{\mathbf{k}'}\} \equiv \hat{c}^\dagger_{\mathbf{k}}\hat{c}^\dagger_{\mathbf{k}'}+\hat{c}^\dagger_{\mathbf{k}'}\hat{c}^\dagger_{\mathbf{k}} = 0.$$

Finally, we notice that the set of eigenstates $\{|\nu\rangle\}$ is an orthonormal basis, then we have $\langle\nu|\nu'\rangle = \delta_{\nu\nu'}$. Now, we are ready to calculate in detail Eq. (B.53) as

$$
\begin{aligned}
& Tr_b\left(\hat{F}(t)\hat{F}(t')\hat{\rho}_b^{eq}\right) = Tr_b\left(\hat{F}\hat{F}(t'-t)\hat{\rho}_b^{eq}\right) \\
= & \sum_{\nu}\sum_{\mathbf{k},\mathbf{k}'}\sum_{\mathbf{k}'',\mathbf{k}'''} V_{\mathbf{k},\mathbf{k}'}V_{\mathbf{k}'',\mathbf{k}'''}\langle\nu|\hat{c}_{\mathbf{k}}^{\dagger}\hat{c}_{\mathbf{k}'}e^{\frac{i}{\hbar}\hat{\mathcal{H}}_e(t'-t)}\hat{c}_{\mathbf{k}''}^{\dagger}\hat{c}_{\mathbf{k}'''}|\nu\rangle e^{-\frac{i}{\hbar}\epsilon_\nu(t'-t)}\frac{1}{Z_e}e^{-\beta\epsilon_\nu} \\
= & \sum_{\nu}\sum_{\mathbf{k},\mathbf{k}'}\sum_{\mathbf{k}'',\mathbf{k}'''} V_{\mathbf{k},\mathbf{k}'}V_{\mathbf{k}'',\mathbf{k}'''}\langle\nu|\hat{c}_{\mathbf{k}}^{\dagger}\hat{c}_{\mathbf{k}'}e^{\frac{i}{\hbar}\hat{\mathcal{H}}_e(t'-t)}|...,\nu_{\mathbf{k}''}+1,...,\nu_{\mathbf{k}'''}-1,...\rangle \\
\cdot & \ \xi_{\mathbf{k}''}\xi_{\mathbf{k}'''}\sqrt{\nu_{\mathbf{k}''}+1}\sqrt{\nu_{\mathbf{k}'''}}e^{-\frac{i}{\hbar}\epsilon_\nu(t'-t)}\frac{1}{Z_e}e^{-\beta\epsilon_\nu} \\
= & \sum_{\nu}\sum_{\mathbf{k},\mathbf{k}'}\sum_{\mathbf{k}'',\mathbf{k}'''} V_{\mathbf{k},\mathbf{k}'}V_{\mathbf{k}'',\mathbf{k}'''}\langle\nu|\hat{c}_{\mathbf{k}}^{\dagger}\hat{c}_{\mathbf{k}'}|...,\nu_{\mathbf{k}''}+1,...,\nu_{\mathbf{k}'''}-1,...\rangle \\
\cdot & \ \xi_{\mathbf{k}''}\xi_{\mathbf{k}'''}\sqrt{\nu_{\mathbf{k}''}+1}\sqrt{\nu_{\mathbf{k}'''}}e^{\frac{i}{\hbar}(\epsilon_{\mathbf{k}''}-\epsilon_{\mathbf{k}'''})(t'-t)}\frac{1}{Z_e}e^{-\beta\epsilon_\nu} \\
= & \sum_{\nu}\sum_{\mathbf{k},\mathbf{k}'}\sum_{\mathbf{k}'',\mathbf{k}'''} V_{\mathbf{k},\mathbf{k}'}V_{\mathbf{k}'',\mathbf{k}'''}\langle\nu|\hat{c}_{\mathbf{k}}^{\dagger}\hat{c}_{\mathbf{k}'}\hat{c}_{\mathbf{k}''}^{\dagger}\hat{c}_{\mathbf{k}'''}|\nu\rangle e^{\frac{i}{\hbar}(\epsilon_{\mathbf{k}''}-\epsilon_{\mathbf{k}'''})(t'-t)}\frac{1}{Z_e}e^{-\beta\epsilon_\nu} \\
= & \sum_{\nu}\sum_{\mathbf{k},\mathbf{k}'}\sum_{\mathbf{k}'',\mathbf{k}'''} V_{\mathbf{k},\mathbf{k}'}V_{\mathbf{k}'',\mathbf{k}'''}\langle\nu|\hat{c}_{\mathbf{k}}^{\dagger}\hat{c}_{\mathbf{k}'}\hat{c}_{\mathbf{k}''}^{\dagger}\hat{c}_{\mathbf{k}'''}|\nu\rangle\delta_{\mathbf{k}\mathbf{k}'''}\delta_{\mathbf{k}'\mathbf{k}''}e^{\frac{i}{\hbar}(\epsilon_{\mathbf{k}''}-\epsilon_{\mathbf{k}'''})(t'-t)}\frac{1}{Z_e}e^{-\beta\epsilon_\nu} \\
= & \sum_{\nu}\sum_{\mathbf{k},\mathbf{k}'}|V_{\mathbf{k},\mathbf{k}'}|^2\langle\nu|\hat{c}_{\mathbf{k}}^{\dagger}\hat{c}_{\mathbf{k}'}\hat{c}_{\mathbf{k}'}^{\dagger}\hat{c}_{\mathbf{k}}|\nu\rangle e^{\frac{i}{\hbar}(\epsilon_{\mathbf{k}'}-\epsilon_{\mathbf{k}})(t'-t)}\frac{1}{Z_e}e^{-\beta\epsilon_\nu} \\
= & \sum_{\nu}\sum_{\mathbf{k},\mathbf{k}'}|V_{\mathbf{k},\mathbf{k}'}|^2\langle\nu|(1-\hat{c}_{\mathbf{k}'}^{\dagger}\hat{c}_{\mathbf{k}'})\hat{c}_{\mathbf{k}}^{\dagger}\hat{c}_{\mathbf{k}}|\nu\rangle e^{\frac{i}{\hbar}(\epsilon_{\mathbf{k}'}-\epsilon_{\mathbf{k}})(t'-t)}\frac{1}{Z_e}e^{-\beta\epsilon_\nu} \\
= & \sum_{\nu}\sum_{\mathbf{k},\mathbf{k}'}|V_{\mathbf{k},\mathbf{k}'}|^2(1-\nu_{\mathbf{k}'})\nu_{\mathbf{k}}e^{\frac{i}{\hbar}(\epsilon_{\mathbf{k}'}-\epsilon_{\mathbf{k}})(t'-t)}\frac{1}{Z_e}e^{-\beta\epsilon_\nu}
\end{aligned}
\tag{B.56}
$$

where we have used the replacement $\langle\nu|\hat{c}_{\mathbf{k}}^{\dagger}\hat{c}_{\mathbf{k}'}\hat{c}_{\mathbf{k}''}^{\dagger}\hat{c}_{\mathbf{k}'''}|\nu\rangle = \langle\nu|\hat{c}_{\mathbf{k}}^{\dagger}\hat{c}_{\mathbf{k}'}\hat{c}_{\mathbf{k}''}^{\dagger}\hat{c}_{\mathbf{k}'''}|\nu\rangle\delta_{\mathbf{k}\mathbf{k}'''}\delta_{\mathbf{k}'\mathbf{k}''}$ which follows from the orthogonality of the states and the fact that $\mathbf{k} \neq \mathbf{k}'$ and $\mathbf{k}'' \neq \mathbf{k}'''$ in the interaction operator $\hat{F}$. Finally, using

$$
\begin{aligned}
\sum_{\nu}\frac{\nu_{\mathbf{k}}}{Z_e}e^{-\beta\epsilon_\nu} &\equiv \langle\nu_{\mathbf{k}}\rangle = \tilde{n}_k = \frac{1}{e^{\beta(\epsilon_k-\mu)}+1}, \\
\sum_{\nu}\frac{\nu_{\mathbf{k}}\nu_{\mathbf{k}'}}{Z_e}e^{-\beta\epsilon_\nu} &\equiv \langle\nu_{\mathbf{k}}\nu_{\mathbf{k}'}\rangle = \langle\nu_{\mathbf{k}}\rangle\langle\nu_{\mathbf{k}'}\rangle = \tilde{n}_k\tilde{n}_{k'},
\end{aligned}
$$

where $\tilde{n}_k$ is the Fermi-Dirac distribution, we arrive to

$$Tr_b\left(\hat{F}(t)\hat{F}(t')\hat{\rho}_b^{eq}\right) = \sum_{\mathbf{k},\mathbf{k'}} |V_{\mathbf{k},\mathbf{k'}}|^2(1-\tilde{n}_{k'})\tilde{n}_k e^{\frac{i}{\hbar}(\epsilon_{k'}-\epsilon_k)(t'-t)} \equiv g(t'-t). \tag{B.57}$$

Similarly, we also have

$$Tr_b\left(\hat{F}(t')\hat{F}(t)\hat{\rho}_b^{eq}\right) = g(t-t'). \tag{B.58}$$

Replacing Eqs. (B.57) and (B.58) in Eq. (B.52) we have

$$\begin{aligned}\hat{R}^{mn}(t) = & - \frac{1}{\hbar^2}\int_{-\infty}^{t} dt'(\hat{S}^+(t')+\hat{S}^-(t'))\left[\hat{S}^+(t)+\hat{S}^-(t),\hat{X}^{mn}(t)\right]g(t'-t) \\ & + \frac{1}{\hbar^2}\int_{-\infty}^{t} dt'\left[\hat{S}^+(t)+\hat{S}^-(t),\hat{X}^{mn}(t)\right](\hat{S}^+(t')+\hat{S}^-(t'))g(t-t'),\end{aligned} \tag{B.59}$$

where now we should evaluate the integral

$$\int_{-\infty}^{t} dt'(\hat{S}^+(t')+\hat{S}^-(t'))g(t-t'). \tag{B.60}$$

Following the same steps as in the spin-phonon scattering model, we use Eq. (B.29) and we introduce the variable $\tau = t - t'$, hence

$$\begin{aligned}\int_{-\infty}^{t} dt'(\hat{S}^+(t')+\hat{S}^-(t'))g(t-t') &= \hat{S}^+(t)\int_0^{\infty} d\tau e^{i\gamma H^{\mathrm{MFA}}(t)\tau}g(\tau) \\ &+ \hat{S}^-(t)\int_0^{\infty} d\tau e^{-i\gamma H^{\mathrm{MFA}}(t)\tau}g(\tau).\end{aligned} \tag{B.61}$$

Using the identity $\int_0^{\infty} dx e^{iwx} = \pi\delta(w)$ the first integral in the r.h.s. of Eq. (B.61) reads

$$\begin{aligned}&\int_0^{\infty} d\tau e^{i\gamma H^{\mathrm{MFA}}(t)\tau}g(\tau) = e^{-y_0}e^{y_0}\pi\sum_{\mathbf{k},\mathbf{k'}}|V_{\mathbf{k},\mathbf{k'}}|^2(1-\tilde{n}_{k'})\tilde{n}_k\delta\left(\gamma H^{\mathrm{MFA}} - \frac{\epsilon_k-\epsilon_{k'}}{\hbar}\right) \\ &= e^{-y_0}\pi\sum_{\mathbf{k},\mathbf{k'}}|V_{\mathbf{k},\mathbf{k'}}|^2(1-\tilde{n}_{k'})\tilde{n}_k e^{\beta(\epsilon_k-\epsilon_{k'})}\delta\left(\gamma H^{\mathrm{MFA}} - \frac{\epsilon_k-\epsilon_{k'}}{\hbar}\right) \\ &= e^{-y_0}\pi\sum_{\mathbf{k},\mathbf{k'}}|V_{\mathbf{k},\mathbf{k'}}|^2(1-\tilde{n}_{k})\tilde{n}_{k'}\delta\left(\gamma H^{\mathrm{MFA}} - \frac{\epsilon_k-\epsilon_{k'}}{\hbar}\right) \\ &= e^{-y_0}W_2^{el},\end{aligned} \tag{B.62}$$

where $y_0 = \beta\hbar\gamma H^{\rm MFA}$ and

$$W_2^{el} = \pi \sum_{\mathbf{k},\mathbf{k'}} |V_{\mathbf{k},\mathbf{k'}}|^2 (1-\tilde{n}_k)\tilde{n}_{k'} \delta\left(\gamma H^{\rm MFA} - \frac{\epsilon_k - \epsilon_{k'}}{\hbar}\right). \tag{B.63}$$

On the other hand, the second integral in the r.h.s. of Eq. (B.61) reads

$$\int_0^\infty d\tau e^{-i\gamma H^{\rm MFA}(t)\tau} g(\tau) = W_2^{el}, \tag{B.64}$$

Replacing Eqs. (B.62) and (B.64) in Eq. (B.61) leads to

$$\int_{-\infty}^{t} dt' (\hat{S}^+(t') + \hat{S}^-(t')) g(t-t') \;=\; W_2^{el}(e^{-y_0}\hat{S}^+(t) + \hat{S}^-(t)). \tag{B.65}$$

Similarly, one finds

$$\int_{-\infty}^{t} dt' (\hat{S}^+(t') + \hat{S}^-(t')) g(t'-t) \;=\; W_2^{el}(\hat{S}^+(t) + e^{-y_0}\hat{S}^-(t)). \tag{B.66}$$

Finally, if Eqs. (B.65) and (B.66) are used in Eq. (B.59) then we obtain that the relaxation term becomes

$$\begin{aligned} \hat{R}^{mn}(t) = &- \frac{1}{\hbar^2} W_2^{el}(\hat{S}^+(t) + e^{-y_0}\hat{S}^-(t)) \left[\hat{S}^+(t) + \hat{S}^-(t), \hat{X}^{mn}(t)\right] \\ &+ \frac{1}{\hbar^2} \left[\hat{S}^+(t) + \hat{S}^-(t), \hat{X}^{mn}(t)\right] W_2^{el}(e^{-y_0}\hat{S}^+(t) + \hat{S}^-(t)). \end{aligned} \tag{B.67}$$

B.2.2 Final form of the Hubbard operator equation of motion

Inserting the conservative term Eq. (B.12) and the relaxation term Eq. (B.67) in Eq. (B.51) leads to

$$\begin{aligned} \frac{d}{dt}\hat{X}^{mn}(t) &= i\gamma H^{\rm MFA}(t)(m-n)\hat{X}^{mn}(t) \\ &- \frac{1}{\hbar^2} W_2^{el}(\hat{S}^+(t) + e^{-y_0(t)}\hat{S}^-(t)) \left[\hat{S}^+(t) + \hat{S}^-(t), \hat{X}^{mn}(t)\right] \\ &+ \frac{1}{\hbar^2} W_2^{el} \left[\hat{S}^+(t) + \hat{S}^-(t), \hat{X}^{mn}(t)\right] (e^{-y_0(t)}\hat{S}^+(t) + \hat{S}^-(t)). \end{aligned} \tag{B.68}$$

If we compare Eq. (B.68) with Eq. (B.40) we see that Eq. (B.68) can be obtained from Eq. (B.40) just setting $\eta_y = \eta_z = 0$, $\eta_x = 2$ ($\eta^\pm = 2$) and replacing W_2^{ph} by W_2^{el}. Therefore, we can follow the same steps as in the spin-phonon scattering

model and at the end we can make these replacements. Thus, if we only keep the secular terms in Eq. (B.68) then we finally arrive to

$$\begin{aligned}\frac{d}{dt}\hat{X}^{mn}(t) &\simeq i\gamma H^{\mathrm{MFA}}(t)\,(m-n)\,\hat{X}^{mn}(t)\\ &- \frac{1}{2}\widetilde{W}_2^{el}\left(l_{m-1}^2+l_{n-1}^2+e^{-y_0}(l_m^2+l_n^2)\right)\hat{X}^{mn}(t)\\ &+ \widetilde{W}_2^{el}\left(l_m l_n \hat{X}^{m+1,n+1}(t)+e^{-y_0}l_{m-1}l_{n-1}\hat{X}^{m-1,n-1}(t)\right), \quad \text{(B.69)}\end{aligned}$$

where

$$\widetilde{W}_2^{el} = 2W_2^{el} = 2\pi\sum_{\mathbf{k},\mathbf{k}'}|V_{\mathbf{k},\mathbf{k}'}|^2(1-\tilde{n}_k)\tilde{n}_{k'}\delta\left(\gamma H^{\mathrm{MFA}}-\frac{\epsilon_k-\epsilon_{k'}}{\hbar}\right). \quad \text{(B.70)}$$

Appendix C

Evaluation of relaxation parameters

C.1 Scattering via phonons

In this section we evaluate the relaxation parameters K_1^{ph} and K_2^{ph} for the isotropic case ($\eta_x = \eta_y = \eta_z = 1$), which are given by

$$K_1^{ph} = W_1^{ph}, \tag{C.1}$$

$$K_2^{ph} = \frac{1}{2}\left(1 + e^{-y_0}\right) W_2^{ph}, \tag{C.2}$$

where

$$W_1^{ph} = \sum_{\mathbf{p},\mathbf{q}} |V_{\mathbf{pq}}|^2 n_p(n_q + 1)\pi\delta(\omega_q - \omega_p), \tag{C.3}$$

$$\begin{aligned} W_2^{ph} &= \sum_{\mathbf{q}} |V_{\mathbf{q}}|^2 (n_q + 1)\pi\delta(\omega_q - \gamma H^{\mathrm{MFA}}) \\ &+ \sum_{\mathbf{q},\mathbf{p}} |V_{\mathbf{pq}}|^2 n_p(n_q + 1)\pi\delta(\omega_q - \omega_p - \gamma H^{\mathrm{MFA}}), \end{aligned} \tag{C.4}$$

where $n_q = [\exp(\beta\hbar\omega_q) - 1]^{-1}$ is the Bose-Einstein distribution. Let's first calculate the quantity K_1^{ph}. For this task we assume that the spin-phonon couplings are of the type[48, 52]

$$V_{\mathbf{q}} = \theta_1\sqrt{\frac{\omega_q}{\Omega}} \quad , \quad V_{\mathbf{pq}} = \theta_2\frac{\sqrt{\omega_p\omega_q}}{\Omega} \tag{C.5}$$

where θ_1 and θ_2 are constants, $\Omega = Mc^2$, M is the unit cell mass, c is the speed of sound in the material and $w_q = cq$. Moreover, the summations over $\mathbf{p}$ and $\mathbf{q}$ in Eq. (C.3) can be replaced by an integral taking the limit $v_0 \to \infty$ where v_0 is the unit cell volume, that is,

$$\sum_{\mathbf{q}} \longrightarrow \frac{v_0}{(2\pi)^3} \int d\mathbf{q}. \tag{C.6}$$

Hence,

$$\begin{aligned} K_1^{ph} &= W_1^{ph} = \frac{\pi\theta_2^2 v_0^2}{(2\pi)^6\Omega^2} \int d\mathbf{q} w_q \int d\mathbf{p} w_p n_p(n_q+1)\delta(\omega_q - \omega_p) \\ &= \frac{\pi\theta_2^2 v_0^2 (4\pi)^2}{(2\pi)^6\Omega^2} \int dq\, q^2 w_q \int dp\, p^2 w_p n_p(n_q+1)\delta(\omega_q - \omega_p) \\ &= \frac{\theta_2^2 v_0^2}{4\pi^3\Omega^2 c^6} \int_0^{w_{max}} dw_q w_q^3 \int_0^{w_{max}} dw_p w_p^3 n_p(n_q+1)\delta(\omega_q - \omega_p) \\ &= \frac{\theta_2^2 v_0^2}{4\pi^3 M^2 c^{10}} \int_0^{w_{max}} dw_q w_q^6 n_q(n_q+1), \end{aligned} \tag{C.7}$$

where $w_{max} = k_B T_D/\hbar$ with T_D is the Debye temperature. Similarly, the quantity W_2^{ph} is calculated as

$$\begin{aligned} W_2^{ph} &= \frac{\theta_1^2 v_0}{2\pi\Omega c^3} \int_0^{w_{max}} dw_q w_q^3 (n_q+1)\delta(\omega_q - \gamma H^{\mathrm{MFA}}) \\ &+ \frac{\theta_2^2 v_0^2}{4\pi^3\Omega^2 c^6} \int_0^{w_{max}} dw_q w_q^3 \int_0^{w_{max}} dw_p w_p^3 n_p(n_q+1)\delta(\omega_q - \omega_p - \gamma H^{\mathrm{MFA}}) \\ &= \frac{\theta_1^2 v_0 (\gamma H^{\mathrm{MFA}})^3}{2\pi M c^5} \left[\frac{e^{y_0}}{e^{y_0}-1}\right] \\ &+ \frac{\theta_2^2 v_0^2}{4\pi^3 M^2 c^{10}} \int_0^{w_{max}} dw_q w_q^3 (w_q - \gamma H^{\mathrm{MFA}})^3 \left(\frac{n_q+1}{e^{\beta\hbar w_q} e^{-y_0} - 1}\right). \end{aligned} \tag{C.8}$$

Therefore, the replacement of Eq. (C.8) in Eq. (C.2) leads to

$$\begin{aligned} K_2^{ph} &= \frac{\theta_1^2 v_0 (\gamma H^{\mathrm{MFA}})^3}{4\pi M c^5} \coth\left(\frac{y_0}{2}\right) \\ &+ \frac{\theta_2^2 v_0^2\,(1+e^{y_0})}{8\pi^3 M^2 c^{10}} \int_0^{w_{max}} dw_q w_q^3 (w_q - \gamma H^{\mathrm{MFA}})^3 \left(\frac{n_q+1}{e^{\beta\hbar w_q} - e^{y_0}}\right). \end{aligned} \tag{C.9}$$

C.1.1 Temperature limits

C.1.1.1 Case $k_B T_D \ll k_B T \ll \hbar\gamma H^{\mathbf{MFA}}$

At low temperatures ($\hbar\gamma H^{\mathrm{MFA}} \gg k_B T, y_0 \gg 1$) we have $e^{y_0} \gg 1$ and $\coth(y_0/2) \simeq 1$, thus

$$\begin{aligned} K_2^{ph} &\simeq \frac{\theta_1^2 v_0 (\gamma H^{\mathrm{MFA}})^3}{4\pi M c^5} \\ &+ \frac{\theta_2^2 v_0^2 e^{y_0}}{8\pi^3 M^2 c^{10}} \int_0^{w_{max}} dw_q w_q^3 (w_q - \gamma H^{\mathrm{MFA}})^3 \left(\frac{n_q + 1}{e^{\beta\hbar w_q} - e^{y_0}} \right). \end{aligned} \quad \text{(C.10)}$$

Additionally, if $\hbar\gamma H^{\mathrm{MFA}} \gg k_B T_D = \hbar w_{max}$ then $e^{\beta\hbar w_q} \ll e^{y_0}$, hence

$$K_2^{ph} \simeq \frac{\theta_1^2 v_0 (\gamma H^{\mathrm{MFA}})^3}{4\pi M c^5} + \frac{\theta_2^2 v_0^2 (\gamma H^{\mathrm{MFA}})^3}{8\pi^3 M^2 c^{10}} \int_0^{w_{max}} dw_q w_q^3 \, (n_q + 1). \quad \text{(C.11)}$$

Moreover, if $T_D \ll T$ ($\hbar w_q \leq \hbar w_{max} \ll k_B T$) then $n_q + 1 \simeq k_B T/(\hbar w_q)$, thus

$$K_2^{ph} \simeq A + BT, \quad \text{(C.12)}$$

where $A = [\theta_1^2 v_0 (\gamma H^{\mathrm{MFA}})^3]/[4\pi M c^5]$ and $B = [\theta_2^2 v_0^2 (\gamma H^{\mathrm{MFA}})^3 k_B^4 T_D^3]/[24\pi^3 M^2 c^{10} \hbar^4]$. Similarly, from Eq. (C.7) we have

$$K_1^{ph} \simeq \frac{\theta_2^2 v_0^2}{4\pi^3 M^2 c^{10}} \int_0^{w_{max}} dw_q w_q^6 \left(\frac{k_B T}{\hbar w_q} \right)^2 = CT^2, \quad \text{(C.13)}$$

where $C = [\theta_2^2 v_0^2 k_B^7 T_D^5]/[20\pi^3 M^2 c^{10} \hbar^7]$.

C.1.1.2 Case $k_B T \ll k_B T_D \ll \hbar\gamma H^{\mathbf{MFA}}$

If we assume that $k_B T_D \ll \hbar\gamma H^{\mathrm{MFA}}$ and $k_B T \ll \hbar\gamma H^{\mathrm{MFA}}$ then we obtain Eq. (C.11). Now if we also consider that $k_B T \ll k_B T_D$ then $k_B T \ll \hbar w_{cut} \ll \hbar w_{max}$ and $n_q + 1 \simeq 1$ for $w_{cut} \leq w_q$, therefore we can write

$$\int_0^{w_{max}} dw_q w_q^3 \, (n_q + 1) \simeq \int_0^{w_{cut}} dw_q w_q^3 \, (n_q + 1) + \int_{w_{cut}}^{w_{max}} dw_q w_q^3. \quad \text{(C.14)}$$

As $T \to 0$ we have that $w_{cut} \to 0$ and since $\lim_{w_q \to 0} w_q^3 \, (n_q + 1) = 0$ then at very low temperatures the first integral in the r.h.s. of Eq. (C.14) is much smaller than the other integral, therefore we can approximate

$$\int_0^{w_{max}} dw_q w_q^3 \, (n_q + 1) \simeq \int_0^{w_{max}} dw_q w_q^3 = \frac{k_B^4 T_D^4}{4\hbar^4}. \quad \text{(C.15)}$$

Thus for this case Eq. (C.11) becomes

$$K_2^{ph} \simeq \frac{\theta_1^2 v_0 (\gamma H^{\rm MFA})^3}{4\pi M c^5} + \frac{\theta_2^2 v_0^2 (\gamma H^{\rm MFA})^3 k_B^4 T_D^4}{32\pi^3 M^2 c^{10} \hbar^4} = cte. \tag{C.16}$$

On the other hand, if in Eq. (C.7) we introduce the variable $u = (\hbar w_q)/(k_B T)$ then we have

$$\begin{aligned} K_1^{ph} &= \frac{\theta_2^2 v_0^2 k_B^7 T^7}{4\pi^3 M^2 c^{10} \hbar^7} \int_0^{\frac{T_D}{T}} du u^6 \frac{e^u}{(e^u-1)^2} \\ &\simeq \frac{\theta_2^2 v_0^2 k_B^7 T^7}{4\pi^3 M^2 c^{10} \hbar^7} \int_0^{\infty} du u^6 \frac{e^u}{(e^u-1)^2} = \left(\frac{4\pi^3 \theta_2^2 v_0^2 k_B^7}{21 M^2 c^{10} \hbar^7} \right) T^7, \end{aligned} \tag{C.17}$$

Therefore, we see that as $T \to 0$ we have $K_1^{ph} \ll K_2^{ph}$.

C.1.1.3 Case $\hbar\gamma H^{\rm MFA} \ll k_B T_D \ll k_B T$

At high temperatures where $\hbar\gamma H^{\rm MFA} \ll k_B T_D \ll k_B T$ we have $e^{y_0} \simeq 1$, $\coth(y_0/2) \simeq 0$ and $\gamma H^{\rm MFA} \ll w_{cut} \ll w_{max}$, so that from Eq. (C.9) we find

$$K_2^{ph} \simeq K_1^{ph} = \frac{\theta_2^2 v_0^2}{4\pi^3 M^2 c^{10}} \int_0^{w_{max}} dw_q w_q^6 n_q (n_q + 1). \tag{C.18}$$

Moreover, we also have $n_q(n_q+1) \simeq (k_B^2 T^2)/(\hbar^2 w_q^2)$, thus

$$K_2^{ph} \simeq K_1^{ph} \simeq \left(\frac{\theta_2^2 v_0^2 k_B^7 T_D^5}{4\pi^3 M^2 c^{10} \hbar^7} \right) T^2. \tag{C.19}$$

C.2 Scattering via electrons

In this section we evaluate the relaxation parameter K_2^{el}. We have found that K_2^{el} is described by an analogue equation to Eq. (3.13), that is,

$$K_2^{el} = \frac{1}{2} \left(1 + e^{-y_0} \right) \widetilde{W}_2^{el}, \tag{C.20}$$

where $y_0 = \beta\hbar\gamma H^{\rm MFA}$ and

$$\widetilde{W}_2^{el} = 2W_2^{el} = 2\pi \sum_{\mathbf{k},\mathbf{k}'} |V_{\mathbf{k},\mathbf{k}'}|^2 (1 - \tilde{n}_k) \tilde{n}_{k'} \delta \left(\gamma H^{\rm MFA} - \frac{\epsilon_k - \epsilon_{k'}}{\hbar} \right). \tag{C.21}$$

Firstly, let's work out in detail the quantity $\widetilde{W}_2^{el}$. To this end we assume that $|V_{\mathbf{k},\mathbf{k}'}|^2 = \mathcal{V} = \text{const}$ (as in Refs. [89] and [97]). Moreover, the summations over

$\mathbf{k}$ and $\mathbf{k}'$ in Eq. (C.21) can be replaced by an integral taking the limit $\Omega \to \infty$ where Ω is the volume of the system, that is,

$$\sum_{\mathbf{k}} \longrightarrow \frac{\Omega}{(2\pi)^3} \int d\mathbf{k}. \tag{C.22}$$

Hence,

$$\begin{aligned} \widetilde{W}_2^{el} &= \frac{2\pi \mathcal{V} \Omega^2 \hbar}{(2\pi)^6} \int d\mathbf{k} \int d\mathbf{k'} (1-\tilde{n}_k)\tilde{n}_{k'} \delta\left(\hbar\gamma H^{\mathrm{MFA}} - \epsilon_k + \epsilon_{k'}\right) \\ &= \frac{\mathcal{V}\Omega^2\hbar}{2\pi^3} \int_0^\infty dk\, k^2 \int_0^\infty dk'\, k'^2 (1-\tilde{n}_k)\tilde{n}_{k'} \delta\left(\hbar\gamma H^{\mathrm{MFA}} - \epsilon_k + \epsilon_{k'}\right) \end{aligned} \tag{C.23}$$

where the property $\delta(x-(a/c)) = |c|\delta(cx-a)$ with $c \neq 0$ has used. Now, using $dk\, k^2 = d\epsilon_k D(\epsilon_k)\pi^2/\Omega$ where

$$D(\epsilon) = \frac{\Omega}{2\pi^2} \left(\frac{2m_{el}}{\hbar^2}\right)^{\frac{3}{2}} \sqrt{\epsilon}, \tag{C.24}$$

is the density of states for a free electron gas (taking into account the degeneracy of the spin), m_{el} is the mass of the electron, then we obtain

$$\begin{aligned} \widetilde{W}_2^{el} &= \frac{\mathcal{V}\hbar\pi}{2} \int_0^\infty d\epsilon_{k'}\, D(\epsilon_{k'}) \tilde{n}_{k'} \int_0^\infty d\epsilon_k\, D(\epsilon_k)(1-\tilde{n}_k) \delta\left(\hbar\gamma H^{\mathrm{MFA}} - \epsilon_k + \epsilon_{k'}\right) \\ &= \frac{\mathcal{V}\hbar\pi}{2} \int_0^\infty d\epsilon_{k'}\, D(\epsilon_{k'}) D(\epsilon_{k'} + \hbar\gamma H^{\mathrm{MFA}}) \left[\frac{1}{e^{\beta(\epsilon_{k'}-\mu)}+1}\right] \left[1 - \frac{1}{e^{\beta(\epsilon_{k'}-\mu)} e^{y_0}+1}\right]. \end{aligned} \tag{C.25}$$

Now, we introduce the variable $\epsilon = \epsilon_{k'} - \mu$ and we assume a constant density of states around the Fermi level $D(\epsilon_F)$ (as in Refs. [89] and [97]), thus

$$\begin{aligned} \widetilde{W}_2^{el} &= \frac{\mathcal{V}\hbar\pi}{2} \int_{-\mu}^\infty d\epsilon\, D(\epsilon+\mu) D(\epsilon+\mu+\hbar\gamma H^{\mathrm{MFA}}) \left[\frac{1}{e^{\beta\epsilon}+1}\right] \left[1 - \frac{1}{e^{\beta\epsilon} e^{y_0}+1}\right] \\ &\simeq \frac{\mathcal{V}\hbar\pi D(\epsilon_F)^2}{2} \int_{-\infty}^\infty d\epsilon \left[\frac{1}{e^{\beta\epsilon}+1}\right] \left[1 - \frac{1}{e^{\beta\epsilon} e^{y_0}+1}\right]. \end{aligned} \tag{C.26}$$

Finally, taking into account that

$$\int_{-\infty}^\infty dx \left[\frac{1}{e^{\beta x}+1}\right] \left[1 - \frac{1}{e^{\beta x} b + 1}\right] = \frac{\ln(b)}{\beta(b-1)}, \tag{C.27}$$

we find

$$\widetilde{W}_2^{el} = \frac{\mathcal{V}\hbar\pi D(\epsilon_F)^2}{2} \left[\frac{\hbar\gamma H^{\mathrm{MFA}}}{e^{y_0}-1}\right]. \tag{C.28}$$

Therefore, if we replace Eq.(C.28) in Eq.(C.20), we obtain

$$K_2^{el} = Ae^{-y_0} \coth\left(\frac{y_0}{2}\right), \tag{C.29}$$

where $A = \mathcal{V}\hbar^2\pi D(\epsilon_F)^2\gamma H^{\mathrm{MFA}}/4$.

C.2.1 Temperature limits

At low temperatures ($y_0 \gg 1$) we have $e^{-y_0}\coth(y_0/2) \simeq e^{-y_0}$, thus

$$K_2^{el} \simeq Ae^{-y_0}. \tag{C.30}$$

On the other hand, at high temperatures ($y_0 \ll 1$) we have $e^{-y_0}\coth\left(\frac{y_0}{2}\right) \simeq 2/y_0$, hence

$$K_2^{el} \simeq \frac{2A}{y_0} = \frac{\pi}{2}\hbar\mathcal{V}D(\epsilon_F)^2 k_B T. \tag{C.31}$$

Appendix D

Free energy for two sublattice magnets within the alternative mean-field formulation

D.1 Free energy derivation

In this appendix we present the calculation of the free energy for two-sublattice magnets using an alternative mean-field formulation [3, 74]. The system is described by following Heisenberg Hamiltonian

$$\mathcal{H} = -\frac{1}{2}\sum_{i,j\in A;i\neq j} J_{ij}\mathbf{s}_i\cdot\mathbf{s}_j - \frac{1}{2}\sum_{i,j\in B;i\neq j} J_{ij}\mathbf{s}_i\cdot\mathbf{s}_j - \sum_{i\in A,j\in B} J_{ij}\mathbf{s}_i\cdot\mathbf{s}_j \quad \text{(D.1)}$$

where i, j are lattices sites, J_{ij} is the Heisenberg exchange interaction parameter and $\mathbf{s}_i = \boldsymbol{\mu}_i/\mu_i$ is the unit length classical spin vector with $\mu_i = \mu_{A(B)}$ is the magnetic moment of the atom A(B). For simplicity, we consider an homogeneous state, that is, the average magnetization of each sublattice, $\mathbf{m}_A \equiv \langle \mathbf{s}_{i\in A}\rangle$ and $\mathbf{m}_B \equiv \langle \mathbf{s}_{i\in B}\rangle$, is the same everywhere. Now, let's write the spin product $\mathbf{s}_i\cdot\mathbf{s}_j$ as

$$\begin{aligned}\mathbf{s}_i\cdot\mathbf{s}_j &= [\mathbf{s}_i-\mathbf{m}_i+\mathbf{m}_i]\cdot[\mathbf{s}_j-\mathbf{m}_j+\mathbf{m}_j]\\ &= -\mathbf{m}_i\cdot\mathbf{m}_j+\mathbf{m}_i\cdot\mathbf{s}_j+\mathbf{m}_j\cdot\mathbf{s}_i+[\mathbf{s}_i-\mathbf{m}_i]\cdot[\mathbf{s}_j-\mathbf{m}_j]\\ &\simeq -\mathbf{m}_i\cdot\mathbf{m}_j+\mathbf{m}_i\cdot\mathbf{s}_j+\mathbf{m}_j\cdot\mathbf{s}_i \quad \text{(D.2)}\end{aligned}$$

where $\mathbf{m}_i = \mathbf{m}_{A(B)}$ if $\mathbf{s}_{i\in A(B)}$. In the alternative mean-field formulation the quantity $[\mathbf{s}_i-\mathbf{m}_i]\cdot[\mathbf{s}_j-\mathbf{m}_j]$ (which is quadratic in the difference between the spin value and its average) is neglected. Hence, if we replace (D.2) in (7.1) and we

consider only nearest neighbours interactions we obtain the following the MFA Hamiltonian

$$\mathcal{H}^{a}_{\rm MFA} = \mathcal{H}_{00} - \mu_A \mathbf{H}^{\rm MFA}_A \sum_{i\in A} \mathbf{s}_i - \mu_B \mathbf{H}^{\rm MFA}_B \sum_{i\in B} \mathbf{s}_i \quad (D.3)$$

where $\mathbf{H}^{\rm MFA}_{A(B)}$ is given by Eq. (7.9) and

$$\mathcal{H}_{00} = \frac{nx_A}{2}\mathbf{m}_A\left[J_{0,A}\mathbf{m}_A + J_{0,AB}\mathbf{m}_B\right] + \frac{nx_B}{2}\mathbf{m}_B\left[J_{0,B}\mathbf{m}_B + J_{0,AB}\mathbf{m}_A\right] \quad (D.4)$$

The partition function corresponding to the MFA Hamiltonian $\mathcal{H}^{a}_{\rm MFA}$ given by Eq. (D.3) is

$$\begin{aligned} \mathcal{Z}_a &= \int e^{-\beta\mathcal{H}^{a}_{\rm MFA}} \mathbf{ds}_1 ... \mathbf{ds}_n \\ &= e^{-\beta\mathcal{H}_{00}} (4\pi)^n \left[\frac{\sinh\left(\beta\mu_A H^{\rm MFA}_A\right)}{\beta\mu_A H^{\rm MFA}_A}\right]^{nx_A} \left[\frac{\sinh\left(\beta\mu_B H^{\rm MFA}_B\right)}{\beta\mu_B H^{\rm MFA}_B}\right]^{nx_B} . \end{aligned} \quad (D.5)$$

Therefore, the free energy in the alternative mean-field formulation is

$$\mathcal{F}_a = -\frac{1}{\beta}\ln\mathcal{Z}_a = \mathcal{H}_{00} - \frac{n}{\beta}\ln(4\pi) - \frac{nx_A}{\beta}\Lambda(\xi_A) - \frac{nx_B}{\beta}\Lambda(\xi_B), \quad (D.6)$$

where $\xi_{A(B)} \equiv \beta\mu_{A(B)}H^{\rm MFA}_{A(B)}$ and $\Lambda(x) = \ln\left[\sinh(x)/x\right]$. The minimum condition

$$\frac{\partial\mathcal{F}_a}{\partial\mathbf{m}_A} = 0 \quad ; \quad \frac{\partial\mathcal{F}_a}{\partial\mathbf{m}_B} = 0 \quad (D.7)$$

leads to the Curie-Weiss equations given by Eq. (7.19). For the pure longitudinal case, that is, $\mathbf{m}_A \parallel \mathbf{m}_B \parallel \mathbf{H} \parallel \mathbf{e}_z$, we obtain the following free energy from Eq. (D.6)

$$\begin{aligned} \frac{1}{n}\mathcal{F}_a(m_{A,z}, m_{B,z}) &= -\frac{1}{\beta}\ln(4\pi) - \frac{x_A}{\beta}\Lambda(\xi_{A,z}) - \frac{x_B}{\beta}\Lambda(\xi_{B,z}) \\ &+ \frac{x_A}{2}J_{0,A}m^2_{A,z} + \frac{x_B}{2}J_{0,B}m^2_{B,z} + x_A J_{0,AB}m_{A,z}m_{B,z}. \end{aligned} \quad (D.8)$$

We notice that this free energy $\mathcal{F}_a$ evaluated at the equilibrium state $(m_{A,e,z}, m_{B,e,z})$ is equal to the equilibrium free energy obtained with the variational procedure $\mathcal{F}_v$ (see Eq. (7.38)). Since the equilibrium thermodynamic properties (like entropy, specific heat, ...) are extracted from the equilibrium free energy, then both routes (the variational procedure and the alternative mean-field formulation) give the same magnetic equilibrium thermodynamic properties of the system. In Figs. D.1 we show a comparison between the free energy obtained with the variational procedure Eq. (7.20) and with the alterantive mean-field formulation Eq. (D.8) using the parameters of GdFeCo given in table 7.1 with $x_{Gd} = 0.25$ and the constraint $m_{Gd,z} = m_{Gd,e,z}$ at $T = 0.2T_c$ (Fig. D.1 a)) and $T = 0.9T_c$ (Fig. D.1 b)).

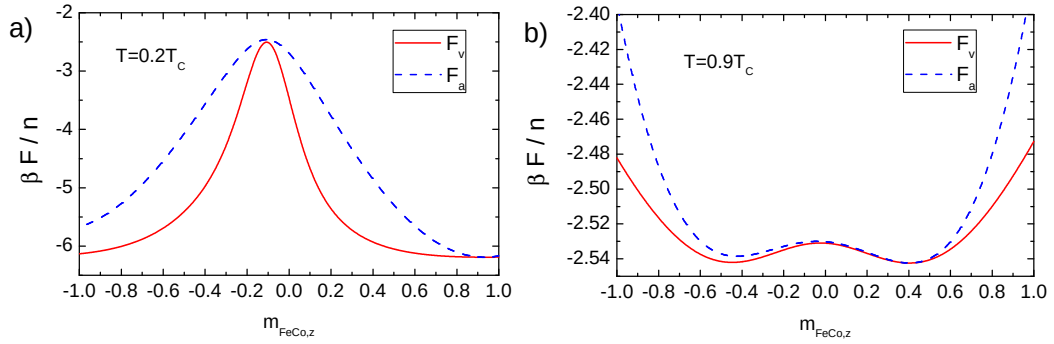

Figure D.1: Comparison between the free energy obtained with the variational procedure $\mathcal{F}_v$ (Eq. (7.20)) and with the alterantive mean-field formulation $\mathcal{F}_a$ (Eq. (D.8)) using the parameters of GdFeCo given in table 7.1 with $x_{Gd} = 0.25$ and the constraint $m_{Gd,z} = m_{Gd,e,z}$ at: a) $T = 0.2T_c$,b) $T = 0.9T_c$.

D.2 Second derivative test

However, the free energy obtained with the alternative mean-field formulation can lead to non-physical free energy landscapes for $m_{A,z}$ and $m_{B,z}$ considered as freely varying variables.[3] In order to see this fact we are going to make the second derivative test to Eq. (D.8). The second derivative test discriminant of Eq. (D.8) is

$$\begin{aligned} D(m_{A,z}, m_{B,z}) &\equiv \left(\frac{\partial^2 \mathcal{F}_a}{\partial m_{A,z}^2}\right)\left(\frac{\partial^2 \mathcal{F}_a}{\partial m_{B,z}^2}\right) - \left[\frac{\partial^2 \mathcal{F}_a}{\partial m_{A,z}\partial m_{B,z}}\right]^2 \\ &= n^2 x_A x_B \beta (J_{0,A}J_{0,B} - J_{0,AB}J_{0,BA}) \\ &\cdot \left[1 - a_A - a_B + \left(1 - \frac{J_{0,AB}J_{0,BA}}{J_{0,A}J_{0,B}}\right) a_A a_B\right] \end{aligned} \tag{D.9}$$

where $a_\nu = \beta J_{0,\nu} L'(\xi_\nu)$ and

$$\frac{\partial^2 \mathcal{F}_a}{\partial m_{\nu,z}^2}(m_{A,z}, m_{B,z}) = n x_\nu J_{0,\nu}\left[1 - a_\nu - \frac{J_{0,\nu\kappa}J_{0,\kappa\nu}}{J_{0,\nu}J_{0,\kappa}} a_\kappa\right]. \tag{D.10}$$

The detail analysis of the extremum's classification (see section 7.3.2) is quite tedious since D and $\partial^2 \mathcal{F}_a / \partial m_{A,z}^2$ depend on five parameters: $J_{0,A}$, $J_{0,B}$, $J_{0,AB}$, x_A and T. Therefore, in order to illustrate that the alternative mean-field formulation can lead to non-physical free energy landscapes we are going to show just one example. Let's consider two exchange parameter sets I and II given by Table D.1 with $x_A = 0.2$ and $T = 200$ K.

D. FREE ENERGY FOR TWO SUBLATTICE MAGNETS WITHIN THE ALTERNATIVE MEAN-FIELD FORMULATION

	Set I	Set II
zJ_{AA} (J)	3.22×10^{-20}	3.22×10^{-20}
zJ_{BB} (J)	6.19×10^{-21}	6.19×10^{-21}
zJ_{AB} (J)	1.24×10^{-20}	2.62×10^{-20}

Table D.1: Table with the exchange parameters of set I and II.

We notice that in the set I we have $J_{0,A}J_{0,B} > J_{0,AB}J_{0,BA}$ and in the set II we have $J_{0,A}J_{0,B} < J_{0,AB}J_{0,BA}$. Moreover, the values in set II are the same as in Permalloy (see Table 7.2). It can be checked numerically that at one of the solution of the Curie-Weiss equation $(m_{A,e,z}, m_{B,e,z})$ using both set of parameter's value we have

$$\frac{\partial^2 \mathcal{F}_a}{\partial m_{A,z}^2}(m_{A,e,z}, m_{B,e,z}) > 0 \tag{D.11}$$

$$1 - a_{A,e} - a_{B,e} + \left(1 - \frac{J_{0,AB}J_{0,BA}}{J_{0,A}J_{0,B}}\right) a_{A,e}a_{B,e} > 0 \tag{D.12}$$

where $a_{\nu,e} = \beta J_{0,\nu} L'(\xi_{\nu,e})$. Therefore, from Eq. (D.9) we see that $D > 0$ if $J_{0,A}J_{0,B} > J_{0,AB}J_{0,BA}$ (like in the parameter set I) so that $(m_{A,e,z}, m_{B,e,z})$ is a local minimum, however for $J_{0,A}J_{0,B} < J_{0,AB}J_{0,BA}$ (like in the parameter set II) we have $D < 0$ so that $(m_{A,e,z}, m_{B,e,z})$ is a saddle point which has not physical sense. Therefore, the alternative mean-field formulation can lead to non-physical free energy landscape in the case of two sublattice magnets with $J_{0,A}J_{0,B} < J_{0,AB}J_{0,BA}$ (like in Permalloy). In Fig. D.2 we present the reduced free energy $\beta\mathcal{F}_a/n$ (Eq. (D.8)) for: a) the parameter set I ($J_{0,A}J_{0,B} > J_{0,AB}J_{0,BA}$) where the two solutions of the Curie-Weiss equation are minimums, and b) parameter set II ($J_{0,A}J_{0,B} < J_{0,AB}J_{0,BA}$) where the two solutions of the Curie-Weiss equation are saddle points.

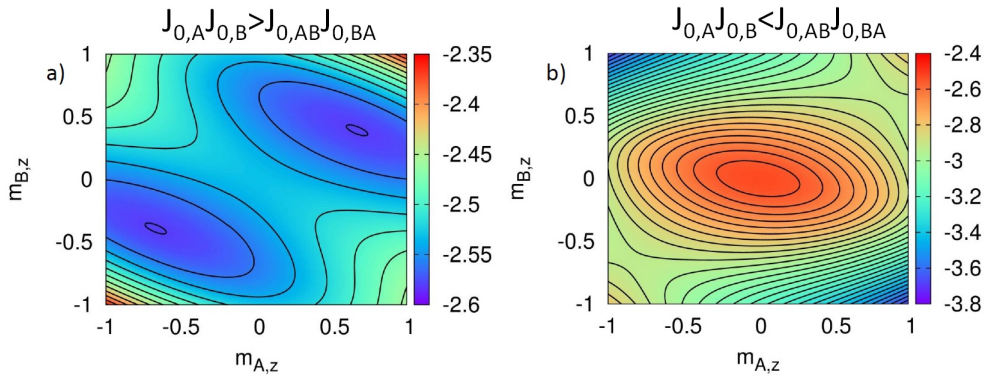

Figure D.2: The reduced free energy $\beta\mathcal{F}_a/n$ (Eq. (D.8)) using $x_A = 0.2$, $T = 200$ K and the exchange parameters given by Table D.1: a) set I ($J_{0,A}J_{0,B} > J_{0,AB}J_{0,BA}$) and b) set II ($J_{0,A}J_{0,B} < J_{0,AB}J_{0,BA}$).

D. FREE ENERGY FOR TWO SUBLATTICE MAGNETS WITHIN THE ALTERNATIVE MEAN-FIELD FORMULATION

References

[1] H. Adachi, K. Uchida, E. Saitoh, and S. Maekawa. *Reports on Progress in Physics*, **76**:036501, 2013. 16, 17

[2] M. Aeschlimann, M. Bauer, S. Pawlik, W. Weber, R. Burgermeister, D. Oberli, and H. C. Siegmann. **Ultrafast spin-dependent electron dynamics in fcc Co**. *Phys. Rev. Lett.*, **79**:5158, 1997. 2

[3] R. Agra, F. van Wijland, and E. Trizac. *European Journal of Physics*, **27**:407, 2006. 99, 100, 101, 114, 115, 149, 151

[4] S. Alebrand, M. Gottwald, M. Hehn, D. Steil, M. Cinchetti, D. Lacour, E. E. Fullerton, M. Aeschlimann, and S. Mangin. *Appl. Phys. Lett.*, **101**:162408, 2012. 7, 89

[5] U. Atxitia, J. Barker, R. W. Chantrell, and O. Chubykalo-Fesenko. *Phys. Rev. B*, **89**:224421, 2014. 94, 95, 96

[6] U. Atxitia and O. Chubykalo-Fesenko. **Ultrafast magnetization dynamics rates within the Landau-Lifshitz-Bloch model**. *Phys. Rev. B*, **84**:144414, Oct 2011. 14, 29, 30, 33, 34, 41, 46, 47, 55, 56

[7] U. Atxitia, O. Chubykalo-Fesenko, R. W. Chantrell, U. Nowak, and A. Rebei. **Ultrafast Spin Dynamics: The Effect of Colored Noise**. *Phys. Rev. Lett.*, **102**:057203, 2009. 37

[8] U. Atxitia, O. Chubykalo-Fesenko, N. Kazantseva, D. Hinzke, U. Nowak, and R. W. Chantrell. **LLB-Micromagnetic modelling of laser-induced magnetisation dynamics**. *Appl. Phys. Lett.* , **91**:232507, 2007. 14, 28

[9] U. Atxitia, O. Chubykalo-Fesenko, J. Walowski, A. Mann, and M. Münzenberg. **Evidence for thermal mechanisms in laser-induced femtosecond spin dynamics**. *Phys. Rev. B*, **81**(17):174401, May 2010. 1, 14, 28, 29, 33, 55, 56

[10] U. Atxitia, P. Nieves, and O. Chubykalo-Fesenko. *Phys. Rev. B*, **86**, 2012. 30, 33, 74, 75, 76, 81, 82

REFERENCES

[11] U. Atxitia, T. Ostler, J. Barker, R. F. L. Evans, R. W. Chantrell, and O. Chubykalo-Fesenko. *Phys. Rev. B*, **87**:224417, 2013. 10, 79

[12] J. Barker, U. Atxitia, T. A. Ostler, O. Hovorka, O. Chubykalo-Fesenko, and R. W. Chantrell. *Scientific Reports*, **3**:3262, 2013. 7, 10, 13, 28, 89, 91, 94, 95, 111

[13] J. Barker, R. F. L. Evans, R. W. Chantrell, D. Hinzke, and U. Nowak. *Appl. Phys. Lett.*, **97**:192504, 2010. 54

[14] C. Barreteau and Spanjaard. *J. Phys. Cond. Mat.*, **24**:406004, 2012. 62

[15] V. G. Baryakhtar. **Crystal symmetry and structure of relaxation terms in the dynamic equations of motion for antiferromagnetics**. *Zhurnal Eksperimentalnoi i Teoreticheskoi Fiziki*, **94**:196, 1988. 99

[16] R. Bastardis, U. Atxitia, O. Chubykalo-Fesenko, and H. Kachkachi. *Phys. Rev. B*, **86**:094415, 2012. 35

[17] M. Battiato, G. Barbalinardo, and P. M. Oppeneer. *Phys. Rev. B*, **89**:014413, 2014. 9

[18] M. Battiato, K. Carva, and P. M. Oppeneer. **Superdiffusive Spin Transport as a Mechanism of Ultrafast Demagnetization**. *Phys. Rev. Lett.*, **105**(2):027203, Jul 2010. 10, 11

[19] G. E. W. Bauer, E. Saitoh, and B. J. van Wees. *Nature Materials*, **11**:391, 2012. 16

[20] E. Beaurepaire, M. Maret, V. Halté, J.-C. Merle, A. Daunois, and J.-Y. Bigot. **Spin dynamics in $CoPt_3$ alloy films: A magnetic phase transition in the femtosecond time scale**. *Phys. Rev. B*, **58**:12134, 1998. 3

[21] E. Beaurepaire, J.-C. Merle, A. Daunois, and J. Y. Bigot. **Ultrafast spins dynamics in ferromagnetic nickel**. *Phys. Rev. Lett.*, **76**:4250, 1996. 1, 2, 3, 4, 13

[22] N. Bergeard, V.Lopez-Flores, V. Halte, M. Hehn, C. Stamm, N. Pontius, E. Beaurepaire, and C. Boeglin. *Nat. Comm.*, **5**:3466, 2014. 5

[23] P. Biagioni, J. S. Huang, L. Duo, M. Finazzi, and B. Hecht. *Phys. Rev. Lett.*, **102**:256801, 2009. 16

[24] J.-Y. Bigot, V. Mircea, and E. Beaurepaire. **Coherent ultrafast magnetism induced by femtosecond laser pulses**. *Nat. Phys.*, **5**:515–520, 2009. 13

[25] K. Blum. *Density Matrix Theory and applications*. Plenum Press, New York, 1981. 36, 37, 134

[26] H. P. Breuer and F. Petruccione. *The theory of Quantum Open Systems*. Oxford University Press, New York, 2002. 37

[27] W. F. Brown. *Micromagnetics*. Wiley, New York, 1963. 18, 99

[28] W. F. Brown. **Thermal Fluctuations of a single-domain particle**. *Phys. Rev.*, **130**:1677, 1963. 19, 25

[29] E. Carpene, E. Mancini, C. Dallera, M. Brenna, E. Puppin, and S. De Silvestri. **Dynamics of electron-magnon interaction and ultrafast demagnetization in thin iron films**. *Phys. Rev. B*, **78**:174422, 2008. 1, 2, 12

[30] K. Carva, M. Battiato, and P. M. Oppeneer. ***Ab Initio* Investigation of the Elliott-Yafet Electron-Phonon Mechanism in Laser-Induced Ultrafast Demagnetization**. *Phys. Rev. Lett.*, **107**:207201, Nov 2011. 12

[31] R. W. Chantrell, M. Wongsam, T. Schrefl, and J. Fidler. **Micromagnetics I: Basic principles**. In K. H. J. Buschow, R. W. Cahn, M. C. Flemings, B. Ilschner, E. J. Kramer, and S. Mahajan, editors, *Encyclopedia of Materials: Science and Technology*. Elsevier, Amsterdam, 2001. 18

[32] T. Y. Cheng, J. Wu, M. Willcox, T. Liu, J. W. Cai, R. W. Chantrell, and Y. B. Xu. **Temperature Dependence of All-Optical Ultrafast Magnetization Switching in TbFeCo**. *Magnetics, IEEE Transactions on*, **48**(11):3387–3389, 11 2012. 7, 89

[33] O. Chubykalo, J. D. Hannay, M. A. Wongsam, R. W. Chantrell, and J. M. González. **Langevin dynamic simulation of spin waves in a micromagnetic model**. *Phys. Rev. B*, **65**:184428, 2002. 25

[34] O. Chubykalo, R. Smirnov-Rueda, M. A. Wongsam, R. W. Chantrell, U. Nowak, and J. M. González. **Brownian dynamics approach to interacting magnetic moments**. *J. Magn. Magn. Mat.*, **266**:28, 2003. 19

[35] O. Chubykalo-Fesenko, U. Nowak, R. W. Chantrell, and D. Garanin. **Dynamic approach for micromagnetics close to the Curie temperature**. *Phys. Rev. B*, **74**:094436, 2006. 19, 25, 29, 33, 34

[36] J.M. Coey. *Magnetism and magnetic materials*. Cambridge University Press, New York, 2009. 23, 24

[37] B. D. Cullity. *Introduction to Magnetic Materials*. Addison-Wesley, Reading, MA, 1972. 34

[38] Łukasz Cywiński and L. J. Sham. **Ultrafast demagnetization in the $sp-d$ model: A theoretical study**. *Phys. Rev. B*, **76**(4):045205, Jul 2007. 12, 43

[39] R. W. Davies and F. A. Blum. *Phys. Rev. B*, **3**:3321, 1971. 31

[40] A. Eschenlohr, M. Battiato, P. Maldonado, N. Pontius, T. Kachel, K. Holldack, R. Mitzner, A. Fhlisch, P. M. Oppeneer, and C. Stamm. *Nature*, **12**:3546, 2013. 6, 11

[41] R. F. L. Evans, W. J. Fan, P. Chureemart, T. A. Ostler, M. O. A. Ellis, and R. W. Chantrell. *Journal Physics Condensed Matter*, **26**:103202, 2014. 22

[42] R. F. L. Evans, D. Hinzke, U. Atxitia, U. Nowak, R. W. Chantrell, and O. Chubykalo-Fesenko. **Stochastic form of the Landau-Lifshitz-Bloch equation**. *Phys. Rev. B*, **85**:014433, Jan 2012. 28, 60

[43] Richard FL Evans, Thomas A. Ostler, Roy W. Chantrell, Ilie Radu, and Theo Rasing. **Ultrafast thermally induced magnetic switching in synthetic ferrimagnets**. *Applied Physics Letters*, **104**(8):082410, 2014. 7, 89

[44] F. García Sánchez. *Modeling of field and thermal magnetization reversal in nanostructured magnetic materials*. PhD thesis, Instituto de Ciencia de Materiales de Madrid (ICMM) - Universidad Autónoma de Madrid, 2007. 14

[45] J. Fidler and T. Schrefl. **Micromagnetic modelling — the current state of the art**. *J. Phys. D: Appl. Phys.*, **33**:R135, 2000. 18

[46] M. Djordjevic G. X. Miao A. Gupta A. V. Ramos K. Gehrke Moshnyaga K. Samwer J. Schmalhorst A. Thomas A. Hütten G. Reiss J. S. Moodera G. M. Müller, J. Walowski and M. Münzenberg. **Spin polarization in half-metals probed by femtosecond spin excitation**. *Nature Mat.*, **8**:56, 2009. 2

[47] D. A. Garanin. **Generalized Equation of Motion for a Ferromagnet**. *Physica A*, **172**:470, 1991. 30, 33, 34, 35, 36, 37, 38, 39, 40, 79, 127, 128

[48] D. A. Garanin. *Phys. Rev. E*, **55**:2569, 1997. 36, 50, 143

[49] D. A. Garanin. **Fokker - Planck and Landau - Lifshitz - Bloch equation for classical ferromagnets**. *Phys. Rev. B*, **55**:3050, 1997. 19, 25, 34, 35, 41, 74, 85, 99

[50] D. A. Garanin. *Adv. Chem. Phys.*, **147**:213, 2012. 36

[51] D. A. Garanin and O. Chubykalo-Fesenko. **Thermal fluctuations and longitudinal relaxation of single-domain magnetic particles at elevated temperatures**. *Phys. Rev. B*, **70**:212409, 2004. 28, 54

[52] D. A. Garanin and E. M. Chudnovsky. *Phys. Rev. B*, **56**:11102, 1997. 50, 143

[53] D. A. Garanin, V. V. Ishtchenko, and L. V. Panina. *Teor. Mat. Fiz.*, **82**, 1990. 38

[54] J. L. García-Palacios and F. J. Lázaro. **Langevin-dynamics study of the dynamical properties of small magnetic particles**. *Phys. Rev. B*, **58**:14937, 1998. 25

[55] T. Gilbert. **A phenomenological Theory of Damping in Ferromagnetic Materials**. *IEEE Trans. Magn.*, **40**:6, 2004. 19

[56] C. E. Graves, A. H. Reid, T. Wang, B. Wu, S. de Jong, K. Vahaplar, I. Radu, D. P. Bernstein, M. Messerschmidt, L. Mller, R. Coffee, M. Bionta, S. W. Epp, R. Hartmann, N. Kimmel, G. Hauser, A. Hartmann, P. Holl, H. Gorke, J. H. Mentink, A. Tsukamoto, A. Fognini, J. J. Turner, W. F. Schlotter, D. Rolles, H. Soltau, L. Strder, Y. Acremann, A. V. Kimel, A. Kirilyuk, Th. Rasing, J. Sthr, A. O. Scherz, and H. A. Dürr. *Nature*, **12**:3597, 2013. 5, 96

[57] V. N. Gridnev. *Phys. Rev. B*, **88**:014405, 2013. 43

[58] G. Grinstein and R. H. Koch. **Coarse Graining in Micromagnetics**. *Phys. Rev. Lett.*, **90**:207201, May 2003. 19, 25

[59] J. Güdde, U. Conrad, V. Jähnke, J. Hohlfeld, and E. Matthias. **Magnetization dynamics of Ni and Co films on Cu(001) and of bulk nickel surfaces**. *Phys. Rev. B*, **59**:R6608–R6611, Mar 1999. 2

[60] L. Le Guyader, I. Radu, A. Echenlohr, S. El Moussaoui, M. Buzzi, I. Razdolski, R. Medapalli, M. Savoini, C. Stamm, R. Mitzner, K. Hooldack, T. Kachel, a. Tsukamoto, A. itoh, A. Kirilyuk, Th. Raising, F. nolting, and A.V. Kimel. *Ultrafast magnetism I:Influence of the magnetization compensation point on the all-optical magnetization switching.* Springer, Switzerland, 2015. 7

[61] A. Hassdenteufel, B. Hebler, C. Schubert, A. Liebig, M. Teich, M. Aeschlimann M. Helm, M. Albrecht, and Rudolf Bratschitsch. *Adv. Mater.*, **25**:3122, 2013. 7, 89

[62] R. Hertel. **Theory of the inverse Faraday effect in metals**. *Journal of Magnetism and Magnetic Materials*, **202**:L1–L4, 2005. 8

[63] R. Hertel, S. Gliga, M. Fähnle, and C. M. Schneider. **Ultrafast Nanomagnetic Toggle Switching of Vortex Cores**. *Phys. Rev. Lett.*, **98**:117201, Mar 2007. 9

[64] D. Hinzke, U. Atxitia, K. Carva, P. Nieves, O. Fesenko-Chubykalo, P. Oppeneer, and U. Nowak. **Multiscale modeling of ferromagnetic alloys**. unpublished. 112

[65] D. Hinzke and U. Nowak. **Domain Wall Motion by the Magnonic Spin Seebeck Effect**. *Phys. Rev. Lett.*, **107**:027205, Jul 2011. 17, 30, 33

[66] J. Hohlfeld, Th. Gerrits, M. Bilderbeek, Th. Rasing, H. Awano, and T. Ohta. **Fast magnetization reversal of GdFeCo induced by femtosecond laser pulses**. *Phys. Rev. Lett.*, **65**:012413, 2001. 4

[67] J. Hohlfeld, E. Matthias, R. Knorren, and K. H. Bennemann. **Nonequilibrium magnetization dynamics of nickel**. *Phys. Rev. Lett.*, **78**:4861, 1997. 2, 3

[68] Y. Horovitz, S. Eliezer, A. Ludmirsky, Z. Henis, E. Moshe, R. Shpitalnik, and B. Arad. *Appl. Phys. Lett.*, **78**:9, 1997. 8

[69] K. Huang. *Statistical Mechanics*. John Wiley and Sons, New York, 1987. 130, 137

[70] Radu I., Vahaplar K., Stamm C., Kachel T., Pontius N., Durr H. A., Ostler T. A., Barker J., Evans R. F. L., Chantrell R. W., Tsukamoto A., Itoh A., Kirilyuk A., Rasing Th., and Kimel A. V. **Transient ferromagnetic-like state mediating ultrafast reversal of antiferromagnetically coupled spins**. *Nature*, **472**:205, 2011. 3, 4, 8, 9, 34, 73, 78, 87, 89

[71] C. M. Jaworski, R. C. Myers, E. Johnston-Halperin, and J. P. Heremans. *Nature*, **487**:11221, 2012. 16

[72] C. M. Jaworski, J. Yang, S. Mack, D. D. Awschalom, J. P. Heremans, and R. C. Myers. *Nature Materials*, **9**:2860, 2010. 16

[73] G. Ju, A. Vertikov, A.V. Nurmikko, C. Canady, G. Xiao, R. Farrow, and A Cebollada. *Phys. Rev. B*, **57**:R700–R703, 1998. 3, 8

[74] H. Kachkachi and D.A. Garanin. **Magnetic free energy at elevated temperatures and hysteresis of magnetic particles**. *Physica A*, **291**:485–500, 2001. 28, 99, 109, 110, 149

[75] M. I. Kaganov, I. M. Lifshitz, and L. V. Tanatarov. **Relaxation between electrons and the crystalline lattice**. *Sov. Phys. JETP*, **4**:173, 1957. 28

[76] T. Kawahara. *J. Appl. Phys.*, **109**:07D325, 2011. 17

[77] N. Kazantseva, D. Hinzke, R.W. Chantrell, and U. Nowak. **Linear and elliptical magnetization reversal close to the Curie temperature**. *Europhys. Lett.*, **86**:27006, 2009. 54

[78] N. Kazantseva, D. Hinzke, U. Nowak, R. W. Chantrell, U. Atxitia, and O. Chubykalo-Fesenko. **Towards multiscale modelling of magnetic materials: Simulations of FePt**. *Phys. Rev. B*, **77**:184428, 2008. 14, 28, 29, 33, 34, 35, 87, 88

[79] N. Kazantseva, D. Hinzke, U. Nowak, R. W. Chantrell, and O. Chubykalo-Fesenko. **Atomistic models of ultrafast reversal**. *Phys. Stat. Sol.*, **244**:4389, 2007. 13, 25

[80] N. Kazantseva, U. Nowak, R. W. Chantrell, J. Hohlfeld, and A. Rebei. **Slow recovery of the magnetisation after a sub-picosecond heat-pulse**. *Europhys. Lett.*, **81**:27004, 2008. 13

[81] A. R. Khorsand, M. Savoini, A. Kirilyuk, A.V. Kimel, A. Tsukamoto, A. Itoh, and Th. Rasing. *Phys. Rev. Lett.*, **108**:127205, 2012. 5, 7, 9

[82] U. Kilic, G. Finocchio, T. Hauet, S. H. Florez, G. Aktas, and O. Ozatay. *Appl. Phys. Lett.*, **101**, 2012. 33

[83] J. W. Kim, M. Vomir, and J.-Y. Bigot. *Phys. Rev. Lett.*, **109**:166601, 2012. 34

[84] A. V. Kimel, A. Kirilyuk, P. A. Usachev, R. V. Pisarev, A. M. Balbashov, and Th. Rasing. **Ultrafast non-thermal control of magnetization by instantaneous photomagnetic pulses**. *Nature*, **435**:655, 2005. 8

[85] A. V. Kimel, R. V. Pisarev, J. Hohlfeld, and Th. Rasing. **Ultrafast Quenching of the Antiferromagnetic Order in $FeBO_3$: Direct Optical Probing of the Phonon-Magnon Coupling**. *Phys. Rev. Lett.*, **89**:287401, Dec 2002. 2

[86] Andrei Kirilyuk, Alexey V. Kimel, and Theo Rasing. **Ultrafast optical manipulation of magnetic order**. *Rev. Mod. Phys.*, **82**:2731–2784, Sep 2010. 29, 33

[87] B. Koopmans, J. E. M. Haverkort, , W. J. M. de Jonge, and G. Karczewski. *Journal of Applied Physics*, **85**:9, 1999. 3

[88] B. Koopmans, G. Malinowski, F. Dalla Longa, D. Steiauf, M. Fhnle, T. Roth, M. Cinchetti, and M. Aeschlimann. **Explaining the paradoxical diversity of ultrafast laser-induced demagnetization**. *Nat. Mat.*, **9**:259265, 2010. 2, 11, 14, 31, 43, 45, 47, 55, 56

[89] B. Koopmans, J. J. M. Ruigrok, F. Dalla Longa, and W. J. M. de Jonge. **Unifying ultrafast magnetization dynamics**. *Phys. Rev. Lett.*, **95**:267207, 2005. 2, 42, 51, 136, 146, 147

[90] B. Koopmans, M. van Kampen, J. T. Kohlhepp, and W. J. M. de Jonge. **Ultrafast Magneto-Optics in Nickel: Magnetism or Optics?** *Phys. Rev. Lett.*, **85**:844, 2000. 3

[91] Michael Krauss, Tobias Roth, Sabine Alebrand, Daniel Steil, Mirko Cinchetti, Martin Aeschlimann, and Hans Christian Schneider. **Ultrafast demagnetization of ferromagnetic transition metals: The role of the Coulomb interaction**. *Phys. Rev. B*, **80**(18):180407, Nov 2009. 12

[92] V. V. Kruglyak, R. J. Hicken, M. Ali, B. J. Hickey, A. T. G. Pym, and B. K. Tanner. *Appl. Phys. B*, **71**:233104, 2005. 8

[93] C-H. Lambert, S. Mangin, B. S. D. Ch. S. Varaprasad, Y. K. Takahashi, M. Hehn, M. Cinchetti, G. Malinowski, K. Hono, Y. Fainman, M. Aeschlimann, and E. E. Fullerton. *Science*, **345**:1337, 2014. 7, 8, 65, 66, 68, 69, 70, 71

[94] D. L. Landau and E. Lifshitz. **On the theory of the dispersion of magnetic permeability in ferromagnetic bodies**. *Phys. Z. Sowjetunion*, **8**:153, 1935. 19

[95] L.D. Landau and E.M. Lifshitz. *Electrodynamics of continuous media*. Pergamon Press, New York, 1984. 99

[96] K. M. Lebecki, D. Hinzke, U. Nowak, and O. Chubykalo-Fesenko. *Phys. Rev. B*, **86**, 2012. 29, 33

[97] F. Dalla Longa. *Laser-induced magnetization dynamics*. PhD thesis, Eindhoven University of Technology, 2008. 42, 51, 146, 147

[98] Z. Lu, R. V. Chepulskii, and W. H. Butler. *Phys. Rev. B*, **81**:094437, 2010. 62

[99] A. Lyberatos and R. W. Chantrell. **Thermal Fluctuations in a pair of magnetostatistically coupled particles**. *J. Appl. Phys.*, **73**:6501, 1993. 25

[100] A. Lyberatos and K. Y. Guslienko. **Thermal stability of the magnetization following thermomagnetic writing in perpendicular media**. *J. Appl. Phys.*, **94**:1119, 2003. 60

[101] A. Manchon, L. Xu Q. Li, and S. Zhang. *Phys. Rev. B*, **85**:064408, 2012. 43

[102] S. Mangin, M. Gottwald, C-H. Lambert, D. Steil, V. Uhlí, L. Pang, M. Hehn, S. Alebrand, M. Cinchetti, G. Malinowski, Y. Fainman, M. Aeschlimann, and E. E. Fullerton. **Engineered materials for all-optical helicity-dependent magnetic switching**. *Nat Mater*, **13**(3):286–292, 2014. 7, 89

[103] B. Marchon, T. Pitchford, Y. Hsia, and S. Gangopadhyay. *Advances in Tribology*, **2013**:521086, 2013. 14

[104] T. W. McDaniel. *Journal of Applied Physics*, **112**:013914, 2012. 15, 33

[105] A. Mekonnen, M. Cormier, A. V. Kimel, A. Kirilyuk, A. Hrabec, L. Ranno, and Th. Raising. *Phys. Rev. B*, **107**:117202, 2011. 87

[106] J. Mendil. *Ultrafast demagnetization dynamics in ferromagnetic thin films with perpendicular anisotropy*. Master's thesis, Georg-August-Universität, Göttingen, 2012. 58

[107] J. Mendil, P. Nieves, O. Chubykalo-Fesenko, J. Walowski, T. Santos, S. Pisana, and M. Münzenberg. *Sci. Rep.*, **4**:3980, 2014. 3, 14, 55, 56, 61

[108] J. H. Mentink, J. Hellsvik, D. V. Afanasiev, B. A. Ivanov, A. Kirilyuk, A. V. Kimel, O. Eriksson, M. I. Katsnelson, and Th. Rasing. **Ultrafast Spin Dynamics in Multisublattice Magnets**. *Phys. Rev. Lett.*, **108**:057202, Jan 2012. 10, 99

[109] B. Y. Mueller, A. Baral, S. Vollmar, M. Cinchetti, M. Aeschlimann, H. C. Schneider, and B. Rethfeld. *Phys. Rev. Lett.*, **111**:167204, 2013. 12, 31

[110] M. Münzenberg. *Nature Materials*, **9**:184, 2010. 3, 12

[111] N. Kazantseva. *Dynamic response of the magnetisation to picosecond heat pulses*. PhD thesis, University of York, 2008. 25, 27, 60

[112] Y. Nakatani, Y. Uesaka, N. Hayashi, and H. Fukushima. **Computer simulation of thermal fluctuation of fine particle magnetization based on Langevin equation**. *J. Magn. Magn. Mat.*, **168**:347, 1997. 25

[113] P. Nieves, D. Serantes, U. Atxitia, and O. Chubykalo-Fesenko. *Phys. Rev. B*, **90**:104428, 2014. 14, 43

[114] J. Olšina and T. Mančal. *J. Mol. Model*, **16**:1765, 2010. 37

[115] T.A. Ostler, J. Barker, R.F.L. Evans, R.W. Chantrell, U. Atxitia, O. Chubykalo-Fesenko, S. El Moussaoui, L. Le Guyader, E. Mengotti, L.J. Heyderman, F. Nolting, A. Tsukamoto, A. Itoh,

D. Afanasiev, B.A. Ivanov, A.M. Kalashnikova, K. Vahaplar, J. Mentink, A. Kirilyuk, Th. Rasing, and A.V. Kimel. **Ultrafast heating as a sufficient stimulus for magnetization reversal in a ferrimagnet**. *Nature Communications*, **3**:666, 2012. 5, 7, 9, 13, 28, 29, 33, 34, 73

[116] Thomas A. Ostler, Richard F. L. Evans, Roy W. Chantrell, Unai Atxitia, Oksana Chubykalo-Fesenko, Ilie Radu, Radu Abrudan, Florin Radu, Arata Tsukamoto, A. Itoh, Andrei Kirilyuk, Theo Rasing, and Alexey Kimel. **Crystallographically amorphous ferrimagnetic alloys: Comparing a localized atomistic spin model with experiments**. *Phys. Rev. B*, **84**:024407, Jul 2011. 74, 91

[117] I. L. Prejbeanu, M. Kerekes, R. C. Sousa, H. Sibuet, O. Redon, B. Dieny, and J. P. Nozières. *J. Phys: Condens. Matter*, **19**:165218, 2007. 17, 18

[118] I. Radu, C. Stamm, A. Eschenlohr, K. Vahaplar, T. Kachel, N. Pontius, R. Mitzner, K. Holldack, A. Fhlish, F. Radu, R. F. L. Evans, T. A. Ostler, J. Mentink, A. Tsukamoto R. W. Chantrell, A. Itoh, A. Kirilyuk, A.V. Kimel, and Th. Rasing. **Ultrafast Distinct Spin Dynamics in Multi-component Magnetic Alloys and Heterostructures**. submitted. 87

[119] H. Regensburger, R. Vollmer, and J. Kirschner. **Time-resolved magnetization-induced second-harmonic generation from the** Ni(110) **surface**. *Phys. Rev. B*, **61**:14716, 2000. 2

[120] T. Roth, A.J. Schellekens, S. Alebrand, O. Schmitt, D. Steil, B. Koopmans, M. Cinchetti, and M. Aeschlimann. *Physical Review X*, **2**:021006, 2012. 3, 31

[121] D. Rudolf, C. La-O-Vorakiat, M. Battiato, R. Adam, J. M. Shaw, E. Turgut, P. Maldonado, S. Mathias, P. Grychtol, T. J. Silva H. T. Nembach, M. Aeschlimann, H. C. Kapteyn, M. Murnane, C. Schneider, and P. Oppeneer. *Nat. Comm.*, **3**:1037, 2012. 6, 11

[122] E. Saitoh, M. Ueda, H. Miyajima, and G. Tatara. *Appl. Phys. Lett.*, **88**:182509, 2006. 16

[123] M. Savoini, P. Biagioni, G. Lakhwani, S. C. J. Meskers, L. Duo, and M. Finazzi. *Opt. Lett.*, **34**:3571, 2009. 16

[124] A. J. Schellekens and B. Koopmans. *Phys. Rev. Lett.*, **110**:217204, 2013. 12

[125] A. V. Scherbakov, A. S. Salasyuk, A. V. Akimov, X. Liu, M. Bombeck, D. R. Yakovlev C. Brüggemann, V. F. Sapega, J. K. Furdyna, and M. Bayer. *Phys. Rev. Lett.*, **105**, 2010. 34

[126] C. Schieback, D. Hinzke, M. Kläui, U. Nowak, and P. Nielaba. **Temperature dependence of the current-induced domain wall motion from a modified Landau-Lifshitz-Bloch equation**. *Phys. Rev. B*, **80**:214403, Dec 2009. 33

[127] F. Schlickeiser, U. Ritzmann, D. Hinzke, and U. Nowak. *Phys. Rev. Lett.*, **113**:097201, 2014. 17

[128] Frank Schlickeiser. *Computer Simulation of the Dynamics of Ferrimagnets.* Master's thesis, University of Konstanz, 2011. 87

[129] A. Scholl, L. Baumgarten, R. Jacquemin, and W. Eberhardt. **Ultrafast spin dynamics of ferromagnetic thin films observed by fs spin-resolved two-photon photoemisson**. *Phys. Rev. Lett.*, **79**:5146, 1997. 2, 3

[130] W. Scholz, T. Schrefl, and J. Fidler. **Micromagnetic simulation of thermally activated switching in fine particles**. *J. Magn. Magn. Mat.*, **233**:296, 2001. 25

[131] C. Schubert, A. Hassdenteufel, P. Matthes, J. Schmidt, M. Helm, R. Bratschitsch, and M. Albrecht. **All-optical helicity dependent magnetic switching in an artificial zero moment magnet**. *Applied Physics Letters*, **104**(8):082406, 2014. 7, 89

[132] R. Skomski and J.M. Coey. *Permanent Magnetism.* Institute of Physics Publishing, Bristol and Philadelphia, 1999. 101

[133] C. Stamm, T. Kachel, N. Pontius, R. Mitzner, T. Quast, K. Holldack, S. Khan, C. Lupulescu, E. F. Aziz, M. Wietstruk, H. A. Drr, and W. Eberhardt. **Femtosecond modification of electron localization and transfer of angular momentum in nickel**. *Nature Mater.*, **6**:740, 2007. 2

[134] C. D. Stanciu, F. Hansteen, A. V. Kimel, A. Kirilyuk, A. Tsukamoto, A. Itoh, and Th. Rasing. **All-Optical Magnetic Recording with Circularly Polarized Light**. *Phys. Rev. Lett.*, **99**:047601, 2007. 2, 4, 7, 8, 9, 16

[135] C. D. Stanciu, A. V. Kimel, F. Hansteen, A. Tsukamoto, A. Itoh, A. Kirilyuk, and Th. Rasing. **Ultrafast spin dynamics across compensation points in ferrimagnetic GdFeCo: The role of angular momentum compensation**. *Phys. Rev. B*, **73**:220402(R), 2006. 87

[136] C. D. Stanciu, A. Tsukamoto, A. V. Kimel, F. Hansteen, A. Kirilyuk, A. Itoh, and Th. Rasing. **Subpicosecond Magnetization Reversal across Ferrimagnetic Compensation Points**. *Phys. Rev. Lett.*, **99**:217204, 2007. 87

[137] D. Steiauf and M. Fähnle. **Elliott-Yafet mechanism and the discussion of femtosecond magnetization dynamics**. *Phys. Rev. B*, **79**(14):140401, Apr 2009. 11

[138] J. Stöhr and H.C. Siegmann. *Magnetism*. Springer-Verlag, Berlin, 2006. 2

[139] M. Sultan, U. Atxitia, O. Chubykalo-Fesenko, A. Melnikov, and U. Bovensiepen. *Phys. Rev. B*, **85**:184407, 2012. 14, 55, 56

[140] school = Instituto de Ciencia de Materiales de Madrid (ICMM) - Universidad Autónoma de Madrid year = 2012 U. Atxitia Macizo, title = Modeling of ultrafast laser-induced magnetization dynamics within the Landau-Lifshitz-Bloch approach. PhD thesis. 29, 59, 74

[141] K. Uchida, S. Takahashi, K. Harii, J. Ieda, W. Koshibae, K. Ando, S. Maekawa, and E. Saitoh. *Nature*, **455**:778, 2008. 1, 16

[142] K. Uchida, J. Xiao, H. Adachi, J. Ohe, S. Takahashi, J. Ieda, T. Ota, Y. Kajiwara, H. Umezawa, H. Kawai, G. E. W. Bauer, S. Maekawa, and E. Saitoh. *Nature Materials*, **9**:2856, 2010. 16

[143] K. Vahaplar, A. M. Kalashnikova, A.V. Kimel, S. Gerlach, D. Hinzke, U. Nowak, R. Chantrell, A. Tsukamoto, A. Itoh, A. Kirilyuk, and Th. Rasing. *Phys. Rev. B*, **85**:104402, 2012. 5, 9, 66

[144] K. Vahaplar, A. M. Kalashnikova, A.V. Kimel, D. Hinzke, U. Nowak, R. Chantrell, A. Tsukamoto, A. Itoh, A. Kirilyuk, and Th. Rasing. **Ultrafast Path for Optical Magnetization Reversal via a Strongly Nonequilibrium State**. *Phys. Rev. Lett.*, **103**:117201, 2009. 1, 8, 29, 33, 34, 73, 74, 94

[145] J. P. van der Ziel, P. S. Pershan, and I. D. Malmstrom. *Appl. Phys. Lett.*, **15**:5, 1965. 8

[146] B. Van Waeyenberge, A. Puzic, H. Stoll, K. W. Chou, T. Tyliszczak, R. Hertel, M. Faehnle, H. Brueckl, K. Rott, G. Reiss, I. Neudecker, D. Weiss, C. H. Back, and G. Schuetz. **Magnetic vortex core reversal by excitation with short bursts of an alternating field**. *Nature*, **444**(7118):461–464, Nov 23 2006. 8

[147] M. Vomir, L. H. F. Andrade, L. Guidoni, E. Beaurepaire, and J.-Y. Bigot. **Real Space Trajectory of the Ultrafast Magnetization Dynamics in Ferromagnetic Metals**. *Phys. Rev. Lett.*, **94**:237601, Jun 2005. 1, 2

[148] J. Wang, Ł. Cywinski, C. Sun, J. Kono, H. Munekata, and L. J. Sham. **Femtosecond demagnetization and hot-hole relaxation in ferromagnetic $\mathbf{Ga_{1-x}Mn_xAs}$**. *Phys. Rev. B*, **77**:235308, Jun 2008. 2

[149] Marko Wietstruk, Alexey Melnikov, Christian Stamm, Torsten Kachel, Niko Pontius, Muhammad Sultan, Cornelius Gahl, Martin Weinelt, Hermann A. Dürr, and Uwe Bovensiepen. **Hot-Electron-Driven Enhancement of Spin-Lattice Coupling in Gd and Tb $4f$ Ferromagnets Observed by Femtosecond X-Ray Magnetic Circular Dichroism**. *Phys. Rev. Lett.*, **106**(12):127401, Mar 2011. 3

[150] R. Wilks, R. J. Hicken, M. Ali, B. J. Hickey J. D. R. Buchanan, A. T. G. Pym, and B. K. Tanner. *J. Appl. Phys.*, **95**:7441, 2004. 8

[151] Zhi-Hao Wu, Chih-Huang Lai, Sheng-Huang Huang, and Wei-Chi Lin. *JMMM*, **304**:93, 2006. 18

[152] L. Xu and S. Zhang. *Physica E*, **45**:72, 2012. 31, 38, 45, 48, 55, 56

[153] L. Xu and S. Zhang. *J. Appl. Phys.*, **113**:163911, 2013. 52, 54, 55, 56

[154] C. J. Yeomans. *Statistical Mechanics of Phase Transitions*. Oxford University Press, Oxford, UK, 1995. 42

[155] G. P. Zhang and W. Hübner. **Laser-Induced Ultrafast Demagnetization in Ferromagnetic Metals**. *Phys. Rev. Lett.*, **85**(14):3025–3028. 13

[156] G. P. Zhang, W. Hubner, G. Lefkidis, and Y. Bai Th. F. George. *Nature*, **5**:499, 2009. 9

List of Publications of P. Nieves

[1] U. Atxitia, **P. Nieves** and O. Chubykalo-Fesenko.
"*Landau-Lifshitz-Bloch equation for ferrimagnetic materials.*"
Phys. Rev. B, **86**, 104414 (2012).

[2] J. Mendil, **P. Nieves**, O. Chubykalo-Fesenko, J. Walowski, T. Santos, S. Pisana and M. Müzenberg.
"*Resolving the role of femtosecond heated electrons in ultrafast spin dynamics.*"
Scientific Reports, **4**, 3980 (2014).

[3] **P. Nieves**, D. Serantes, U. Atxitia and O. Chubykalo-Fesenko.
"*Quantum Landau-Lifshitz-Bloch equation and its comparison with the classical case.*"
Phys. Rev. B, **90**, 104428 (2014).

[4] **P. Nieves**, D. Serantes and O. Chubykalo-Fesenko.
"*The Landau-Lifshitz-Bloch equation for a quantum spin.*"
In "Ultrafast magnetism I", Springer, (2015), page 140.

[5] O. Chubykalo-Fesenko, U. Atxitia, **P. Nieves**, J. Barker and R. W. Chantrell.
"*Ultrafast demagnetization rates in two-component magnetic materials.*"
In "Ultrafast magnetism I", Springer, (2015), page 251.

[6] O. Suarez, **P. Nieves**, D. Laroze, D. Altbir and O. Chubykalo-Fesenko.
"*The ultra-fast relaxation rates and reversal time in disordered ferrimagnets.*"
Submitted to Phys. Rev. B.

[7] D. Hinzke, U. Atxitia, K. Carva, , **P. Nieves**, O. Chubykalo-Fesenko, P. Oppeneer, U. Nowak.
"*Multiscale modeling of ultrafast element specific magnetization dynamics of ferromagnetic alloys.*"
Submitted to Phys. Rev. B.

In preparation:

[8] **P. Nieves** and O. Chubykalo-Fesenko.
"*Modeling of ultrafast magnetization dynamics in FePt.*"
In preparation

[9] **P. Nieves**, D. Kechrakos and O. Chubykalo-Fesenko.
"*Modeling of core-shell nanoparticles with exchange bias.*"
In preparation

[10] **P. Nieves**, U. Atxitia, U. Nowak and O. Chubykalo-Fesenko.
"*Free energy for two-component magnets.*"
In preparation

[11] **P. Nieves**, U. Atxitia and O. Chubykalo-Fesenko.
"*Quantum Landau-Lifshitz-Bloch equation for two-component magnets.*"
In preparation

Agradecimientos

Me gustaría agradecer a Oxana Fesenko la ayuda y el apoyo que me ha dado durante el desarrollo de esta tesis. También me gustaría agradecer al profesor Uli Nowak, Unai Atxitia y Rocío Yanes por su ayuda durante mi estancia en Konstanz. También agradezco la ayuda dada por todos mis compañeros del ICMM, especialmente a David Serantes, Juan Manuel Rodríguez, Javier Pérez Carvajal, Jorge Cayao, Roberto Moreno e Iurii Ivanov. Finalmente, quisiera también agradecer a mi familia su apoyo desde la distancia durante estos años.